

A Thesis Submitted for the Degree of PhD at the University of Warwick

Permanent WRAP URL:

<http://wrap.warwick.ac.uk/109866>

Copyright and reuse:

This thesis is made available online and is protected by original copyright.

Please scroll down to view the document itself.

Please refer to the repository record for this item for information to help you to cite it.

Our policy information is available from the repository home page.

For more information, please contact the WRAP Team at: wrap@warwick.ac.uk

**Nucleophilic Thiol-yne Addition
Chemistry for the Synthesis of
Tuneable and Cytocompatible
Poly(ethylene glycol) Hydrogel
Materials**

Laura Jane Macdougall

Submitted for the degree of Doctor of Philosophy



Department of Chemistry

May 2018

Table of Contents

Table of Contents	i
List of Figures	xiv
List of Schemes	xxvii
List of Equations	xxix
List of Tables.....	xxx
Acknowledgements	xxxii
Declaration of Authorship.....	xxxiii
Publications	xxxiv
Abstract	xxxv
Abbreviations	xxxvii
Chapter 1. Introduction.....	1
1.1. Hydrogels: Theory and Application.....	2
1.2. Hydrogel Synthesis	7
1.2.1. Polymer Precursors for Hydrogel Synthesis	7
1.2.2. Crosslinking Chemistries for Hydrogel Synthesis	11
1.3. Alkyne Crosslinking Chemistries.....	21
1.3.1. Azide-Alkyne Click Cycloaddition Reactions for Hydrogel Synthesis	21
1.3.2. Thiol-yne Click Reactions.....	24

1.3.2.1. Radical-Initiated Thiol-yne Click Reaction	26
1.3.2.2. Nucleophilic Thiol-yne Click Reaction	32
1.3.3. Emerging Alkyne Click Reactions.....	37
1.4. Conclusions	39
1.5. References	40
Chapter 2. Synthesis and Characterisation of Efficient Nucleophilic Thiol-yne Hydrogel Materials with Tuneable Properties	57
2.1. Introduction	58
2.1. Results and Discussion.....	61
2.1.1. Synthesis of Alkyne and Thiol PEG Precursors	61
2.1.2. Synthesis of Thiol-yne PEG Hydrogels	66
2.1.3. General Characterisation of the Thiol-yne PEG Hydrogels.....	70
2.1.4. Mechanical Characterisation of the Thiol-yne PEG Precursors	73
2.1.5. Tuning the Mechanical Properties of Thiol-yne PEG Hydrogels	76
2.3. Conclusions	80
2.4. References	81
Chapter 3. Nonswelling Thiol-yne Crosslinked Hydrogel Materials as Cytocompatible Soft Tissue Scaffolds	87
3.1. Introduction	88
3.2. Results and Discussion.....	93

3.2.1.	Synthesis of Alkyne- and Thiol-Terminated PEG Precursors.....	93
3.2.2.	Characterisation of Swellable Thiol-yne PEG Hydrogels.....	96
3.2.3.	Characterisation of Nonswellable Thiol-yne PEG Hydrogels.....	99
3.2.3.1.	Gelation Time.....	100
3.2.3.2.	Morphology.....	102
3.2.3.3.	Rheological Characterisation	103
3.2.3.4.	Swelling Profile.....	104
3.2.3.5.	Mechanical Characterisation in the Swollen State.....	107
3.2.4	Cytocompatibility Studies on Nonswellable Thiol-yne Hydrogels.....	112
3.3.	Conclusions	115
3.4.	References	116
Chapter 4.	Stereochemically Controlled Hydrogels by Utilising Nucleophilic Thiol-yne	
	Addition Chemistry.....	120
4.1.	Introduction	121
4.2.	Results and Discussion.....	126
4.2.1.	Determining the Stereochemistry in Nucleophilic Thiol-yne PEG Hydrogels	
	126
4.2.2.	Determining the stereochemistry of the Nucleophilic Thiol-yne Hydrogels	
	through ¹ H NMR spectroscopy	130
4.2.3.	Characterisation of the Stereocontrolled Thiol-yne PEG Hydrogels	136

4.2.3.1. Gelation Time.....	136
4.2.3.2. Swelling and Structure Characterisation of the Stereocontrolled Thiol-yne Hydrogels	137
4.2.4. Mechanical Properties of the Stereocontrolled Thiol-yne Hydrogels.....	141
4.2.4.1. Rheological Characterisation of Stereocontrolled Thiol-yne Hydrogels	141
4.2.5.2. Compression Testing of the Stereocontrolled Thiol-yne Hydrogels.....	143
4.3. Conclusions	145
4.4. References	146
Chapter 5. Self-healing, Stretchable and Robust Thiol-yne Interpenetrating Networks through Utilising the Properties of Natural Polymers.....	149
5.1. Introduction	150
5.2. Results and Discussion.....	152
5.2.1. Synthesis of Thiol-yne Interpenetrating Networks (IPNs).....	152
5.2.2. Control Reaction for the Synthesis of PEG/Natural Polymer IPNs	157
5.2.3. Characterisation of the Thiol-yne IPNs	160
5.2.3.1. Swelling Kinetics of the Thiol-yne IPNs	160
5.2.3.2. Swelling and Degradation Profile of the Thiol-yne IPNs	163
5.2.3.3. Cryogenic Scanning Electron Microscopy Analysis of the Thiol-yne IPNs	165

5.2.4. Tensile characterisation of the thiol-yne IPNs	167
5.2.5. Rheological Characterisation of the Thiol-yne IPNs	169
5.2.6. Compression Testing of the thiol-yne IPNs	171
5.2.7. Self-healing characterisation of the thiol-yne IPNs	173
5.2.8. Cytocompatibility testing of the thiol-yne IPN.....	177
5.3. Conclusions	180
5.4. References	181
Chapter 6. Design of Synthetic Extracellular Matrices for Probing Breast Cancer Cell Growth Using Robust Cytocompatible Nucleophilic Thiol-yne Addition Chemistry	185
6.1. Introduction	186
6.2. Results and Discussion.....	189
6.2.1. Design of Nucleophilic Thiol-yne PEG Hydrogel-Based ECM Mimics	189
6.2.2. Characterisation of Thiol-yne PEG Hydrogels as ECM Mimics	196
6.2.2.1. Swelling Kinetics of the Thiol-yne PEG Hydrogels	196
6.2.2.2. Mechanical Properties of the Thiol-yne PEG Hydrogels.....	198
6.2.3. 2D Cell Culture of Breast Cancer Cells in Hydrogel Formation-Mimetic Conditions	202
6.2.4. 3D Encapsulation of Breast Cancer Cells in Thiol-yne PEG Hydrogels	206
6.2.5. MCF-7 Cell Proliferation in Degradable ECM Mimetic Thiol-yne PEG Hydrogels	210

6.3. Conclusions	215
6.4. References	217
Chapter 7. A Kinetic Study of the Nucleophilic Thiol-yne Addition Reaction and its Application in Hydrogel Synthesis	223
7.1. Introduction	224
7.2. Results and Discussion	227
7.2.1. Nucleophilic Thiol-yne Kinetic Study	227
7.2.1.1. The Effect of Activating Carbonyl Groups on the Rate of the Nucleophilic Thiol-yne Reaction	228
7.2.1.2. The Effect of Methyl-Terminated Alkynes on the Rate of the Nucleophilic Thiol-yne Reaction	241
7.2.2. Methyl-Terminated Alkyne Ketone PEG Thiol-yne Hydrogels	247
7.2.2.1. Synthesis of Methyl-Terminated Alkyne PEG Ketone Precursor via a Succinic Anhydride Grignard Reaction	248
7.2.2.2. Synthesis of Methyl-Terminated Alkyne PEG ketone Precursor via Friedel-Crafts Acylation	251
7.2.2.3. Synthesis of Methyl-Terminated Alkyne PEG Ketone Precursor through a Weinreb Amide Synthetic Route.....	253
7.2.2.4. Synthesis and Characterisation of Thiol-yne PEG Hydrogels Synthesised using a Methyl-Terminate Alkyne PEG Ketone.	259
7.2.3. Methyl-Terminated Alkyne Ester-PEG Thiol-yne Hydrogels	261

7.2.3.1. Synthesis of Methyl-Terminated Alkyne Ester-PEG Precursors	261
7.2.3.2. Characterisation of Methyl-Terminated Alkyne Thiol-yne PEG Hydrogels	262
7.3. Conclusions	265
7.4. References	267
Chapter 8. Conclusions and Future Work.....	272
8.1. Conclusions	273
8.2. Future work	277
Chapter 9. Experimental	279
9.1. Materials	280
9.2. General Considerations	280
9.2.1. Small Molecule Characterisation	280
9.2.2. Polymer Characterisation	281
9.2.3. General Characterisation Techniques for Hydrogels	282
9.2.3.1. Gel Fraction and Equilibrium Water Content (EWC).....	282
9.2.3.2. Mesh Size Calculations	282
9.2.3.3. Swelling and Degradation Procedure.....	284
9.2.3.4. Cryogenic Scanning Electron Microscopy.....	285
9.2.4. Mechanical Characterisation of Hydrogels.....	285
9.2.4.1. Rheological Testing	285

9.2.4.1.1. The Evolution of Storage (G') and Loss (G'') Moduli as a Function of Time Measurements	286
9.2.4.1.2. Frequency Sweep Measurements	286
9.2.4.1.3. Amplitude Sweep Measurements.....	287
9.2.4.1.4. Young's Modulus Calculations from Rheological data (Chapter 6). 287	
9.2.4.2. Uniaxial Mechanical Testing	287
9.2.4.2.1. Compression Testing.....	287
9.2.4.2.2. Tensile Testing.....	288
9.3. Experimental Procedures for Alkyne- and Thiol-Functionalised PEG Precursors ..	
.....	288
9.3.1. Synthesis of 4-Arm Alkyne-Functionalised PEG (2 kg mol^{-1}).....	288
9.3.2. Synthesis of 3-Arm Alkyne-Functionalised PEG (1 kg mol^{-1})	288
9.3.3. Synthesis of 2-Arm Alkyne-Functionalised PEG (1 kg mol^{-1})	288
9.3.4. Synthesis of 3-Arm-Thiol-Functionalised PEG (1 kg mol^{-1}).....	290
9.3.5. Synthesis of 4-Arm Thiol-Functionalised PEG (2 kg mol^{-1})	290
9.3.6. Synthesis of 2-Arm Thiol-Functionalised PEG (1 kg mol^{-1})	291
9.3.7. Synthesis of 2-Arm Thiol-Functionalised PEG (2 kg mol^{-1})	291
9.3.8. Synthesis of 2-Arm Thiol-Functionalised PEG (3 kg mol^{-1})	291
9.3.9. Synthesis of 2-Arm Thiol-Functionalised PEG (4 kg mol^{-1})	292
9.4. Experimental Procedures for Chapter 2	292

9.4.1. Control Thiol-yne Reaction between Ethyl Propiolate and 2-Hydroxyethyl Disulfide	292
9.4.2. Control Thiol-yne Reaction between PEG _{1k} (C≡CH) ₂ and 2-Mercaptoethanol.....	293
9.4.3. General Procedure for the Fabrication of PEG Hydrogels by Nucleophilic Thiol-yne Addition.....	293
9.4.4. General Procedure for the Blended Thiol-yne Hydrogels.....	294
9.5. Experimental Procedure for Chapter 3	294
9.5.1. Preparation of Nonswelling Thiol-yne Hydrogels	294
9.5.2. Characterisation and Mechanical Testing of the Nonswelling Thiol-yne Hydrogels	294
9.5.3. Cytocompatibility Studies and 3D Cell Encapsulation.....	294
9.5.3.1. Cytocompatibility Studies (2D culture)	295
9.5.3.2. Cell Encapsulation Studies (3D culture)	295
9.6. Experimental Procedures for Chapter 4	296
9.6.1. Fabrication of Stereocontrolled Thiol-yne Organogels.....	296
9.6.1.1. 4_{2A}4_{2S} Thiol-yne Gel Synthesised with CHCl ₃	296
9.6.1.2. 4_{2A}4_{2S} Thiol-yne Gel Synthesised with Acetone:CHCl ₃ (60:40)	297
9.6.1.3. 4_{2A}4_{2S} Thiol-yne Gel Synthesised with Acetone:H ₂ O (90:10).....	297
9.6.1.4. 4_{2A}4_{2S} Thiol-yne Gel Synthesised with Acetone: H ₂ O (65:35).....	297

9.6.1.5. 4_{2A}4_{2S} Thiol-yne Gel Synthesised with H ₂ O	298
9.6.2. Synthesis of Methyl-Ether Alkyne-Functionalised PEG (550 g mol ⁻¹)	298
9.6.3. Synthesis of Methyl-Ether Thiol-Functionalised PEG (550 g mol ⁻¹)	298
9.6.4. General Experimental Procedure for the Nucleophilic Thiol-yne Reaction between Monofunctionalised Alkyne and Thiol PEG Precursors.....	299
9.6.4.1. Model PEG Thiol-yne Reaction in CHCl ₃	300
9.6.4.2. Model PEG Thiol-yne Reaction in Acetone:CHCl ₃ (60:40).....	300
9.6.4.3. Model PEG Thiol-yne Reaction in Acetone:H ₂ O (90:10).....	300
9.6.4.4. Model PEG Thiol-yne Reaction in Acetone:H ₂ O (65:35).....	301
9.6.4.5. Model PEG Thiol-yne Reaction in H ₂ O (100%).....	301
9.6.5. Characterisation of the Stereocontrolled Thiol-yne PEG Hydrogels.....	302
9.6.6. Rheological Characterisation of the Stereocontrolled Hydrogels.....	302
9.7. Experimental Procedure for Chapter 5	303
9.7.1. PEG/Natural Polymer Hydrogel Fabrication	303
9.7.1.1. Fabrication of PEG/Alginate Interpenetrating Networks (IPNs).....	303
9.7.1.2. Fabrication of PEG/Chitosan IPNs	303
9.7.1.3. Fabrication of PEG/Gelatin Hydrogels	304
9.7.1.4. Fabrication of PEG/Hyaluronic Acid Hydrogels	304
9.7.1.5. Fabrication of PEG/Heparin Hydrogels.....	304
9.7.2. Cytocompatibility Studies and 3D Cell Encapsulation Studies	305

9.7.2.1. Cell Metabolic Activity (3D culture)	305
9.7.2.2. Cell Viability Assay (3D culture)	305
9.8. Experimental Procedure for Chapter 6	306
9.8.1. Synthesis of Hydrogel Precursors	306
9.8.1.1. Thiol-Functionalised Peptide Synthesis	306
9.8.1.2. Synthesis of Thiol-ene Hydrogel Precursors	307
9.8.2. Hydrogel Fabrication	307
9.8.2.1. Thiol-yne Hydrogel Synthesis	307
9.8.2.2. Thiol-ene Hydrogel Synthesis	307
9.8.3. Validation of Pendant Peptide Incorporation	308
9.8.4 Mechanical Characterisation of the Thiol-yne PEG Hydrogels	308
9.8.4.1. Rheological Characterisation of the Thiol-yne PEG Hydrogels	308
9.8.5. 2D cell Metabolic Activity and 3D Cell Encapsulation	308
9.8.5.1. Cell Encapsulation in 3D Thiol-yne and Radically-Initiated Thiol-ene Hydrogels	309
9.8.5.2. Cell metabolic activity (2D culture)	309
9.8.5.3. Cell metabolic activity (3D culture)	310
9.8.5.4. Cell viability assay (3D culture)	311
9.8.5.5. Immunostaining of Cells in 3D Culture	312
9.9. Experimental Procedure for Chapter 7	313

9.9.1. Synthesis of Phenyl Propiolate	313
9.9.2. Synthesis of Ethyl Propiolamide	314
9.9.3. Synthesis of 1-Phenylbut-2-yn-1-one	314
9.9.4. Synthesis of Non-2-yn-4-one	315
9.9.5. General Experimental Procedure for the Nucleophilic Thiol-yne Kinetic Study	317
9.9.5.1 Thiol-yne Kinetic Study for Ethyl Propiolate (EP) with DT	318
9.9.5.2. Thiol-yne Kinetic Study for Phenyl-2-propyn-1-one (PPO) with DT .	318
9.9.5.3. Thiol-yne Kinetic Study for 3-Butyn-2-one with DT	319
9.9.5.4. Thiol-yne Kinetic Study for Phenyl Propiolate with DT	319
9.9.5.5. Thiol-yne Kinetic Study for Ethyl Propiolamide with DT.....	320
9.9.5.6. Thiol-yne Kinetic Study for Ethyl Butynoate with DT.....	320
9.9.5.7. Thiol-yne Kinetic Study for 1-Phenylbut-2-yn-1-one with DT	321
9.9.5.8. Thiol-yne Kinetic Study for Non-2-yn-4-one with DT.....	321
9.9.6. Synthesis of Methyl-Terminated Alkyne PEG Ketone Precursor via Succinic Anhydride Grignard Reaction	322
9.9.6.1. Functionalisation of 3-arm PEG _{1k} (OH) ₃ with Succinic Anhydride ¹⁷ ...	322
9.9.6.2. Functionalisation of 3-arm PEG _{1k} (COOH) ₃ with Thionyl Chloride	323
9.9.6.3. Functionalisation of 3-arm PEG _{1k} (COC≡CCH ₃) ₃	323

9.9.7. Synthesis of Methyl-Terminated Alkyne PEG ketone Precursor through a Friedel-Crafts Acylation.....	324
9.9.7.1. Oxidation of PEG _{2k} (OH) ₂ using Jones' Reagent	324
9.9.7.2. Functionalisation of PEG _{2k} (COOH) ₂ with Thionyl Chloride	325
9.9.7.3. Functionalisation of PEG _{2k} (COCl) ₂ via Friedel-Crafts Acylation	325
9.9.8. Synthesis of Methyl-Terminated Alkyne PEG Ketone Precursor through a Weinreb Amide Synthetic Route.....	326
9.9.8.1. Synthesis of 2-arm PEG (2 kg mol ⁻¹) Weinreb Amide	326
9.9.8.2. Synthesis of Methyl-Terminated Alkyne 2-arm PEG ketone (2 kg mol ⁻¹) from a Weinreb Amide.....	327
9.9.9. Synthesis and Characterisation of Thiol-yne PEG Hydrogels Fabricated from a Methyl Terminate Alkyne PEG Ketone.	328
9.9.10. Synthesis of 2-arm PEG ester methyl terminate alkyne.....	328
9.9.11. Synthesis and Characterisation of Thiol-yne PEG Hydrogels Fabricated using a Methyl-Terminate Alkyne PEG Ester	329
9.10. References	330

List of Figures

Figure 1.1.	a) Schematic of a hydrated polymer network, adapted from ref. 1, b) The components of a hydrogel adapted from ref. 3.	2
Figure 1.2.	Ideal chemical structure of natural polymers which have been used in hydrogel synthesis a) alginate, b) agarose, c) DNA, d) peptide structure adapted from ref 58.	8
Figure 1.3.	Structures of a range of synthetic polymers used in hydrogel synthesis	9
Figure 1.4.	a) Concept of light-controlled enzymatic biomolecule patterning of hydrogels. b) ProteinA tethering results in patterns of Fc-chimaeric proteins (here: IgG), c) The laser-scanning technique allows the generation of precisely defined patterns of any arbitrary shape d) Confocal micrograph showing enzymatic patterning of the fluorescent adhesion peptide RGD in precisely defined cuboidal patterns ($\sim 900 \times 450 \mu\text{m}$) touching half of a microtissue. Figure modified from ref 100.	11
Figure 1.5.	Click reactions used in hydrogel synthesis.	13
Figure 1.6.	Schematic of covalently crosslinked hydrogels using furan-maleimide Diels-Alder chemistry, Adapted from ref. 125	15
Figure 1.7.	Examples of alkenes and thiols used to synthesise thiol-ene hydrogels	16
Figure 1.8.	The mechanism for the thiol-ene reaction via a base catalysed (blue arrows) or radical-initiated (red arrows) pathway	17
Figure 1.9.	Stress relaxation of thioester hydrogels. Figure modified from ref 154	18
Figure 1.10.	Structures of cyclooctynes used in the synthesis of hydrogels through SPAAC	22
Figure 1.11.	Schematic for neurogenic click hydrogel network formation. Adapted from ref. 172	23
Figure 1.12.	Reaction scheme for the thiol-yne reaction	24

- Figure 1.13.** The two reaction mechanisms radical initiated, (red arrows) and base catalysed, (blue arrows) for the thiol-yne reaction demonstrating the ability to added two thiols to one alkyne molecule **25**
- Figure 1.14.** a) Schematic representation of the synthesis of thiol-yne and POx based hyperstar copolymers, b) Confocal images of A2780 human ovarian carcinoma cells treated with Nile red loaded hyperstars. Figure modified from ref 188 **29**
- Figure 1.15.** a) Thiol-yne photopolymerisation of alkyne functionalised polyester, synthesised from lactide, b) topography image of crossing lines generated by direct laser writing, c) cell cultured on substrates with different widths of polylactide microstructures after 48 h. Modified from reference 189 **30**
- Figure 1.16.** Fabrication of bio/synthetic interpenetrating network. Figure adapted from ref 190 **31**
- Figure 1.17.** Reaction scheme of the thiol-yne experiment carried out by Truce and Simms demonstrating the stereocontrol of the thiol alkene product. Ref 194. **33**
- Figure 1.18.** Mechanism for the stereochemical control over the nucleophilic thiol-yne reaction. a) Non polar solvent and/or weak base to form the trans isomer (1); b) polar solvent and/or strong base to form the cis isomer (2). Adapted from ref 196. **34**
- Figure 1.19.** a) Synthesis of thiol-yne elastomer materials from dialkyne and dithiol precursors, b) Wide-angle X-ray diffraction of the elastomers demonstrating the effect stereochemistry has on the crystallinity of the material, c) Change in mechanical properties of thiol-yne elastomers with different stereochemsitries. Adapted from ref 198 **35**

- Figure 1.20.** Schematic of tetrazine-norbornene and nucleophilic thiol-yne addition chemistries used for double network (DN) hydrogel fabrication, Figures adapted for ref 199. **36**
- Figure 1.21.** Schematic of the PEG/Chitosan amino-yne hydrogels under physiological conditions. Modified from ref 204 **38**
- Figure 2.1.** Effects of substrate stiffness on cell morphology. Image modified from ref 24 **59**
- Figure 2.2.** ^1H NMR spectrum of alkyne-terminated 3-arm PEG ($(\text{CD}_3)_2\text{CO}$, 300 MHz, 298 K). **62**
- Figure 2.3.** ^1H NMR spectrum of thiol-terminated 2-arm PEG (1 kg mol^{-1}) (CDCl_3 , 300 MHz, 298 K) **63**
- Figure 2.4.** Size Exclusion chromatograms of a) 3-arm PEG alkyne precursors (1 kg mol^{-1}). Molecular weight determined against PMMA using DMF (5 mM NH_4BF_4) as eluent. b) 2-arm PEG thiol precursor (1 kg mol^{-1}). Molecular weight determined against polystyrene standards using CHCl_3 (0.5% NEt_3) as eluent. **63**
- Figure 2.5.** ^1H NMR spectrum of the reaction between ethyl propiolate and 2-hydroxyethyl disulfide to form a vinyl thioether product (CDCl_3 , 300 MHz, 298 K). **66**
- Figure 2.6.** ^1H NMR spectrum of the reaction between alkyne-terminated 2-arm PEG (1 kg mol^{-1}) and 2-mercaptoethanol at pH 7.8 after 10 min ($\text{D}_2\text{O}/\text{PBS}$, 400 MHz, 298 K). * = *trans* product **67**
- Figure 2.7.** a-b) Evolution of the storage (G' dotted line) and loss (G'' solid line) moduli as a function of time for the a) 3-arm alkyne and b) 4-arm alkyne nucleophilic thiol-yne PEG hydrogels. c-d) Frequency sweep chart at 298 K and a constrain strain of 0.5% for the c) 3-arm alkyne and b) 4-arm alkyne nucleophilic thiol-yne PEG hydrogels **70**

Figure 2.8.	Cryo-SEM images of the thiol-yne PEG hydrogels, scale bar = 2 μm	72
Figure 2.9.	Amplitude sweep chart at 293 K and a constant frequency of 10 rad s^{-1} for a) 3_{1A}2_S and b) 4_{2A}2_S hydrogel	73
Figure 2.10.	Representative stress/strain compression curves for the nucleophilic thiol-yne PEG hydrogels at 10 wt%.	75
Figure 2.11.	Freeze frames from the cyclic compression video for the 3_{1A}2_{1S} hydrogel demonstrating the repeatable compression of the hydrogels, scale bar = 5 mm.	76
Figure 2.12.	a) Amplitude sweep charts of the 3_{1A}2_S hydrogels synthesised from different molar ratios blends of 1 and 4 kg mol^{-1} 2-arm PEG thiol (ratio stated as 1 kg mol^{-1} :4 kg mol^{-1} precursor). b) The graphical representation of the correlation between G' of the blended 3_{1A}2_S hydrogels and the percentage of 4 kg mol^{-1} thiol-terminated PEG precursor used	77
Figure 2.13.	The correlation between the percentage of 2_S and the effect on the compressive stress and G' at 0.1% strain and 10 rad s^{-1} .	79
Figure 3.1.	^1H NMR spectrum of thiol-terminated 3-arm PEG (1 kg mol^{-1}), (CDCl_3 , 300 MHz, 298 K).	94
Figure 3.2.	^1H NMR spectrum of thiol-terminated 4-arm PEG (2 kg mol^{-1}) (CDCl_3 , 300 MHz, 298 K).	94
Figure 3.3.	SEC chromatograms of a) 3-arm PEG thiol precursor (1 kg mol^{-1}), b) 4-arm PEG thiol precursor (2 kg mol^{-1}). Molecular weights determined against polystyrene standards using CHCl_3 (0.5% NEt_3) as eluent.	95
Figure 3.4.	Swellable hydrogels characterisation (3_{1A}2_{1S} = red; 3_{1A}2_{2S} = green; 3_{1A}2_{3S} = blue): a) SF (%) as a function of time in PBS at 37 °C and b) evolution of stress at break with swelling time.	98
Figure 3.5.	Cryo SEM images of nonswellable thiol-yne PEG hydrogels, scale bar = 2 μM .	102

- Figure 3.6.** Representative curves of storage (G' ; solid line) and loss (G'' ; dashed line) modulus as a function of a) time and b) strain for nonswellable PEG hydrogels. **104**
- Figure 3.7.** Thiol-yne hydrogels response when immersed in PBS solution at 37 °C, scale bar = 1 cm. **106**
- Figure 3.8.** The swelling profile for the nonswellable nucleophilic thiol-yne PEG hydrogels displaying multi-arm architecture: a) **3_{1A}3_{1S}** (circle) and **4_{2A}4_{2S}** (square); b) **3_{1A}4_{2S}** (diamond) and **4_{2A}3_{1S}** (triangle). **106**
- Figure 3.9.** Representative stress/strain graphs for hydrogels prepared with multi-arm PEG precursors after being immersed in PBS at 37 °C for different intervals of time, a) 24 h, b) 3 days, c) 5 days, d) 7 days, e) 10 days, f) 15 days, g) 21 days and h) 25 days. **109**
- Figure 3.10.** a-b) Evolution of the compressive mechanical properties of the nonswellable nucleophilic thiol-yne PEG hydrogels displaying multi-arm architecture: a) **3_{1A}3_{1S}** (blue) and **4_{2A}4_{2S}** (yellow); b) **3_{1A}4_{2S}** (green) and **4_{2A}3_{1S}** (red). Greek letters on the bars refer to significant differences (p -value < 0.05): α vs 1 hour. c-d) Evolution of the compressive modulus of the nonswellable thiol-yne PEG hydrogels: c) **3_{1A}3_{1S}** (blue) and **4_{2A}4_{2S}** (yellow); d) **3_{1A}4_{2S}** (green) and **4_{2A}3_{1S}** (red). **110**
- Figure 3.11.** Metabolic activity of MC3T3-E1 cells seeded on top of the thiol-yne hydrogels after 24 and 72 h. **113**
- Figure 3.12.** Cytocompatibility of nonswellable thiol-yne PEG hydrogels. Images from 3D encapsulated cells after a) 24 and b) 72 h of incubation for the **3_{1A}2_{3S}** and **3_{1A}4_{2S}** hydrogels, scale bar = 200 μm . **114**
- Figure 4.1.** a) The change in stereochemistry of the azobenzene unit with light. b) Schematic overview of cell culture experiments on photoresponsive hydrogels. Fibronectin-coated gels were **123**

- softened by exposure to UV (365 nm) irradiation for 30 min. Primary human MSCs were then seeded. After 24 h, (+) blue gels were exposed to blue (490 nm) light for 1 h, whereas (-) blue gels were kept in darkness. Figure adapted from ref 20.
- Figure 4.2.** A representative FT-IR spectrum of a dried thiol-yne PEG gel synthesised with 100% water. Highlighted peak areas used to calculate the % *cis* content in the hydrogel. **128**
- Figure 4.3.** FT-IR spectrum of the stereocontrolled **4_{2A}4_{2S}** dried gels. Expanded view between 750-1,000 cm⁻¹ to show the increased intensity at 802 cm⁻¹ correlating with increased *cis* content in the dried gel. **129**
- Figure 4.5.** ¹H NMR spectrum of the alkyne-terminal methyl ether PEG₅₅₀ ((CD₃)₂CO, 300 MHz, 298 K). **131**
- Figure 4.6.** ¹H NMR spectrum of the thiol-terminal methyl ether PEG₅₅₀ (CDCl₃, 300 MHz, 298 K). **132**
- Figure 4.7.** SEC chromatograms of a) methyl ether PEG₅₅₀(C≡CH), b) methyl ether PEG₅₅₀(SH). Molecular weight determined against polystyrene standards using CHCl₃ (0.5% NEt₃) as eluent. **132**
- Figure 4.8.** ¹H NMR spectrum of the nucleophilic thiol-yne product of the alkyne- and thiol-functionalised methyl ether PEG₅₅₀ in CHCl₃ with NEt₃ (CDCl₃, 300 MHz, 298 K), *= *cis* product **134**
- Figure 4.9.** ¹H NMR spectra of the vinyl thioether product demonstrating the dependence of solvent polarity on the *cis:trans* ratio of the vinyl thioether product, (CDCl₃, 300 MHz, 298 K), (100% H₂O reaction ¹H NMR spectrum recorded in (CD₃)₂CO, 300 MHz, 298K). **135**
- Figure 4.10.** Cryo SEM images of the stereocontrolled thiol-yne hydrogels in comparison to the original PBS thiol-yne hydrogels. **139**
- Figure 4.11.** Swelling profiles of the stereocontrolled thiol-yne PEG hydrogels. Hydrogels were immersed in PBS solution and placed **141**

in an incubator at 37 °C and weighed periodically. Swelling factor (SF) was calculated as a percentage by dividing the mass at the time point by the initial mass. Conducted in triplicate.

- Figure 4.12.** Rheological characterisation of the stereocontrolled thiol-yne PEG hydrogels, a) Average G' determined at a constant strain of 0.01% and 10 rad s⁻¹, b) Representative amplitude sweep for each stereocontrolled thiol-yne PEG hydrogel at a constant strain of 10 rad s⁻¹. **143**
- Figure 4.13.** Compression testing of the stereocontrolled thiol-yne PEG hydrogels, a) average maximum compressive strength for each condition (bars, LHS axis), b) average maximum compressive strain for each condition (dots, RHS axis). **144**
- Figure 5.1.** Representative rheological frequency sweeps for the thiol-yne IPNs to demonstrate the effect the secondary electrostatic network has on the IPN. **159**
- Figure 5.2.** Representative curves showing the evolution of G' and G'' with time for thiol-yne IPNs containing a) a secondary loose electrostatically crosslinked network (alginate, chitosan, and gelatin); and b) negatively charged polysaccharides (heparin and HA). **161**
- Figure 5.3.** Mesh Size (dots, RHS axis), EWC (dotted bars, LHS axis) and gel fraction (hashed bar, LHS axis) values for the thiol-yne IPN hydrogels. Repeated in triplicate. **163**
- Figure 5.4.** Swelling profiles of the thiol-yne IPNs immersed in PBS at 37 °C, repeated in triplicate. **165**
- Figure 5.5.** Cryo SEM images of the thiol-yne IPN hydrogels, scale bar = 10 μm. **166**
- Figure 5.6.** Strain-stress curves of a) the thiol-yne IPNs; and b) PEG/Alginate IPNs prepared with different CaCO₃ concentrations. **168**

Figure 5.7.	Image of the tensile testing conducted to demonstrate the improved stretchability PEG/Alginate IPN hydrogels compared to the PEG only system, scale bar = 0.5 cm.	168
Figure 5.8.	Representative rheological frequency sweeps for the thiol-yne IPNs: a) PEG/Gelatin and PEG/Alginate, which display improved tensile performance in comparison to the PEG only system; b) PEG/Chitosan, PEG/Heparin, and PEG/HA, which exhibits an inferior tensile performance in comparison to the PEG only system.	170
Figure 5.9.	Maximum compressive stress for the thiol-yne IPNs at 98% strain, 10 replicates for each system.	172
Figure 5.10.	Images taken during the self-healing process.	173
Figure 5.11.	Assessment of the self-healing response of thiol-yne IPNs	174
Figure 5.12.	Freeze frames of the video to demonstrate the adhesive properties of the PEG/HA hydrogels.	175
Figure 5.13.	Tensile performance of self-healed thiol-yne IPNs	176
Figure 5.14.	Images showing the self-healed PEG/Alginate hydrogel	177
Figure 5.15.	Metabolic activity of cells encapsulated in a) PEG only, b) PEG/Alginate, and c) PEG/HA hydrogels after 24, 48, and 72 h incubation times. Greek letter on bars refer to significant differences (p value < 0.05): α vs 72h.	178
Figure 5.16.	Biocompatibility of PEG only, PEG/HA, and PEG/alginate hydrogels. Representative images of 3D encapsulated cells after 24 and 72 hours of incubation. Scale bar 200 μ m.	179
Figure 6.1.	Swelling profiles of the thiol-yne PEG hydrogels	192
Figure 6.2.	Fluorescence analysis of pendant peptide (RGDS) incorporation in the $3_{1A}3_{1S}PRGDS$ hydrogel system.	193
Figure 6.3.	(a) Swelling characteristics of the thiol-yne hydrogels synthesised in PBS; Comparison of $3_{1A}3_{1S}$ (circle) (1:1 alkyne:thiol end groups), $3_{1A}3_{1S}-5mM$ with reduced amount of	198

3_{1S} (-5 mM) (square), and **3_{1A3_{1S}}** **PRGDS** (triangle). (b) Comparison of the swelling characteristics of the thiol-yne hydrogels made in serum-free DMEM with the encapsulation of MCF-7 cells over 1 week; **3_{1A3_{1S}}****PRGDS** (open triangle), **3_{1A2_{2S}3_{1S}}****PRGDS** (cross), **3_{1A2_{MMP}3_{1S}}**, 10:90 ratio of **2_{MMP}:3_{1S}** (diamond).

- Figure 6.4.** Representative rheological data for the thiol-yne hydrogels synthesised in DMEM and repeated in triplicate; a) Average G' at a constant frequency of 10 rad s^{-1} and 0.5% strain, $\alpha =$ Significantly different from **3_{1A3_{1S}}** conditions, $p < 0.05$. b) Frequency sweep at a constant strain of 0.5 %, c) Evolution of G' and G'' with time, d) Amplitude sweep at a constant frequency of 10 rad s^{-1} . **200**
- Figure 6.5.** Mechanical data for the thiol-yne hydrogels synthesised in DMEM. **201**
- Figure 6.6.** Metabolic activity of breast cancer cells in 2D hydrogel formation-mimetic environments. **204**
- Figure 6.7.** Metabolic activity of MCF-7 cells incubated with propiolic acid in 2D compared to media and PBS. After 24 h of culture, cells were exposed to each condition for 15 min. Metabolic assay was assessed by Cell-Titer 96 assay (Absorbance = 490 nm). **205**
- Figure 6.8.** The metabolic activity of a) MDA-MB-231 and T47D (5,000 cells μL^{-1}), and MCF-7 cells, (2,500 cells μL^{-1}), encapsulated in the **3_{1A3_{1S}}** (no RGDS) system formed in PBS solution (pH 7.4). **207**
- Figure 6.9.** Encapsulation of MCF-7 cells in photo-initiated thiol-ene and thiol-yne (**3_{1A3_{1S}}****PRGDS**) hydrogels formed in serum-free medium. **209**
- Figure 6.10.** The metabolic activity of MCF-7 cells in 3D degradable thiol-yne hydrogels (2,500 cells μL^{-1}) assessed through the alamarBlue assay at 1, 3, 7 and 10 days after encapsulation. **211**

Figure 6.11.	Live/Dead images of the MCF-7 cells in degradable thiol-yne hydrogels.	212
Figure 6.12.	Analysis of cell cluster diameter over time for various thiol-yne hydrogel compositions over 10 days in culture.	213
Figure 6.13.	Proliferation of MCF-7 cells in 3D cell culture.	214
Figure 7.1.	Small molecule alkynes with activating groups adjacent to the alkyne; a) ethyl propiolate (ester-functionality), b) 3-butyn-2-one (ketone-functionality), c) phenyl-2-propyn-1-one (PPO, ketone-aromaticity).	228
Figure 7.2.	a) Reaction between ethyl propiolate (ester-functionalised alkyne) and DT and ^1H NMR spectrum of the thiol-yne reaction between ethyl propiolate and DT with NEt_3 in CDCl_3 after 60 min, *= <i>cis</i> alkene product, (298 K, CDCl_3 , 400 MHz).	229
Figure 7.3.	^1H NMR spectra showing the conversion of ethyl propiolate and DT to the vinyl thioether product, * = <i>cis</i> alkene (298 K, CDCl_3 , 400 MHz).	230
Figure 7.4.	a) Plot of the concentration of ethyl propiolate (EP) with respect to time showing a logarithmic correlation; b) first order rate chart used to determine the rate constant (k) for the reaction.	231
Figure 7.5.	^1H NMR spectrum of the nucleophilic thiol-yne reaction between phenyl-2-propyn-1-one and DT in the presence of NEt_3 and CDCl_3 , *= <i>trans</i> isomer, (298 K, CDCl_3 , 300 MHz).	232
Figure 7.6.	Resonance structures of PPO reacting with DT through the favoured <i>cis</i> transition state showing charge stabilisation through the aromatic ring.	232
Figure 7.7.	^1H NMR spectrum of phenyl propiolate (298 K, $(\text{CD}_3)_2\text{SO}$, 300 MHz) with insert showing the FT-IR spectrum of phenyl propiolate.	235

- Figure 7.8.** ^1H NMR spectrum for ethyl propiolamide (298 K, CDCl_3 , 300 MHz) with insert showing the FT-IR spectrum for ethyl propiolamide. 237
- Figure 7.9.** ^{13}C NMR spectrum for ethyl propiolamide (298 K, $(\text{CD}_3)_2\text{SO}$, 300 MHz). 237
- Figure 7.10.** Postulated hydrogen bonding between ethyl propiolamide molecules. 238
- Figure 7.11.** ^1H NMR spectra of ethyl propiolamide in deuterated DMF with increasing temperature (303-333 K, 400 MHz). 239
- Figure 7.12.** High resolution ESI-MS of ethylpropiolamide. Confirmation of small molecule purity. 239
- Figure 7.13.** Resonance structure of ethyl propiolamide *cis* transition state after attack of a thiolate ion demonstrating the increased stabilisation through amide resonance structures. 240
- Figure 7.14.** Structure of ethyl butynoate. 241
- Figure 7.15.** ^1H NMR spectrum for 1-phenyl but-2-yn-1-one (298 K, CDCl_3 , 300 MHz) with insert showing the FT-IR spectrum for 1-phenyl but-2-yn-1-one. 243
- Figure 7.16.** The thiol-yne product of 1-Phenyl but-2-yn-1-one with DT in the presence of NEt_3 in CDCl_3 , *=Z isomer, (298 K, CDCl_3 , 400 MHz). 245
- Figure 7.17.** ^1H NMR spectrum of Non-2-yn-4-one (298 K, $(\text{CH}_3)_2\text{SO}$, 300 MHz) with insert showing the FT-IR spectrum of non-2-yn-4-one. 246
- Figure 7.18.** Relative rates of nucleophilic thiol-yne reaction with a range of small molecule alkynes reacted with DT in the presences of NEt_3 in CDCl_3 . 247
- Figure 7.19.** ^1H NMR of the ketone-functional 3-arm PEG with a methyl-terminated alkyne, (298 K, CDCl_3 , 300 MHz) with insert 249

- showing the FT-IR of the ketone-functional 3-arm PEG with a methyl-terminated alkyne.
- Figure 7.20.** SEC analysis of the ketone-functional 3-arm PEG with a methyl-terminated alkyne (1 kg mol^{-1}). Molecular weight was determined against polystyrene standards using CHCl_3 (0.5% NEt_3) as the eluent. **249**
- Figure 7.21.** ^1H NMR spectrum for the ketone-functional PEG with a methyl-terminated alkyne synthesised through Friedel-Crafts acylation, (298 K, CDCl_3 , 300 MHz) with insert showing the FT-IR spectrum for the ketone-functional PEG with a methyl-terminated alkyne. **252**
- Figure 7.22.** ^1H NMR spectrum of 2-arm $\text{PEG}_{2k}(\text{COOH})_2$ functionalised through Jones oxidation, (298 K, $(\text{CH}_3)_2\text{SO}$), 300 MHz) with insert showing the SEC analysis of 2-arm $\text{PEG}(\text{COOH})$ (2 kg mol^{-1}) Molecular weight was determined against PEG standards using $\text{H}_2\text{O}:\text{CH}_3\text{OH}$ (80:20 ratio) as the eluent; b) quantitative ^{13}C NMR spectrum of 2-arm $\text{PEG}_{2k}(\text{COOH})_2$ with insert showing the FT-IR spectrum of 2-arm $\text{PEG}_{2k}(\text{COOH})_2$, (298 K, $(\text{CH}_3)_2\text{SO}$), 500 MHz). **255**
- Figure 7.23.** ^1H NMR spectrum for 2-arm $\text{PEG}_{2k}(\text{COCl})_2$, (298 K, CDCl_3 , 300 MHz), with Insert showing the FT-IR spectrum of 2-arm $\text{PEG}_{2k}(\text{COOH})_2$. **256**
- Figure 7.24.** ^1H NMR spectrum of 2-arm PEG Weinreb amide, (298 K, $(\text{CH}_3)_2\text{SO}$), 300 MHz), with insert showing SEC analysis of 2-arm PEG Weinreb amide (2 kg mol^{-1}) Molecular weight determined against PEG standards using $\text{H}_2\text{O}:\text{CH}_3\text{OH}$ (80:20 ratio) as eluent, b) Quantitative ^{13}C NMR spectrum of 2-arm PEG Weinreb amide, (298 K, $(\text{CH}_3)_2\text{SO}$), 500 MHz), with insert showing FT-IR spectrum of 2-arm PEG Weinreb amide. **257**

- Figure 7.25.** a) ^1H NMR spectrum of the methyl-terminated PEG ketone, (298 K, CDCl_3 , 300 MHz) with Insert showing the FT-IR spectrum of the methyl-terminated PEG ketone, *= impurity, b) SEC analysis of the methyl-terminated PEG ketone (2 kg mol^{-1}) by CHCl_3 SEC (LHS) Molecular weight was determined against polystyrene standards using CHCl_3 (0.5% NEt_3) as the eluent, and aqueous SEC analysis (RHS) molecular weight was determined against PEG standards using $\text{H}_2\text{O}:\text{CH}_3\text{OH}$ (80:20 ratio) as the eluent. **258**
- Figure 7.26.** Quantitative ^{13}C NMR spectrum of the methyl-terminated PEG ketone precursor, *= impurities, (298 K, $(\text{CH}_3)_2\text{SO}$, 500 MHz). **259**
- Figure 7.27.** ^1H NMR spectrum of the methyl-terminated alkyne PEG ketone precursor reacting with 3-arm PEG thiol in PBS solution at 10 wt%, *= Z isomer, (298 K, CDCl_3 , 300 MHz). **260**
- Figure 7.28.** FT-IR spectrum of the vinyl thioether PEG product when the methyl-terminated alkyne PEG ketone was reacted with 4-arm PEG thiol in PBS solution (1:1 ratio, 10 wt%). **260**
- Figure 7.29.** ^1H NMR spectrum of 2-arm ester-PEG functionalised with methyl-terminated alkyne end groups, (298 K, CDCl_3 , 300MHz) with insert showing a SEC chromatogram of 2-arm PEG methyl-terminated alkyne precursors (1 kg mol^{-1}). Molecular weight was determined against PMMA using DMF (5 mM NH_4BF_4) as the eluent. **262**
- Figure 7.30.** Representative stress/strain chart of a **2_{1A}4_{2S}** hydrogel (20 wt%, trizma buffer) to demonstrate repeated compressive strength with insert showing an expanded view of the high strain values and demonstrating little hysteresis occurred with repeated compression. **263**

List of Schemes

- Scheme 2.1.** Synthesis of alkyne- and thiol-functionalised PEG through Fischer esterification where n = number of functional groups per PEG molecule (*i.e.* 2-, 3- or 4-) and $R = C\equiv CH$ or CH_2CH_2SH **61**
- Scheme 2.2.** Control reaction between ethyl propiolate and 2-hydroxyethyl disulfide to form a vinyl thioether product in the presence of NEt_3 . **64**
- Scheme 2.3.** a) Nucleophilic base-catalysed reaction between an alkyne and thiol; b) schematic of the PEG precursors synthesised for crosslinking and c) schematic of exemplar hydrogel networks. The hydrogel naming convention used (X_ZA_YZS) denotes the hydrogel structures, where X = number of arms on the alkyne precursor, Y = number of arms on the thiol precursor and Z = the molecular weight of the PEG precursor, *e.g.* $4_{2A}2_{4S}$ is a hydrogel composed of a 4-arm alkyne (2 kg mol^{-1}) crosslinked with a 2-arm thiol (4 kg mol^{-1}). **68**
- Scheme 3.1.** A route to form nonswellable thiol-yne hydrogels based on multi-arm PEG precursors. **93**
- Scheme 3.2.** Nonswellable thiol-yne hydrogels based on multi-arm PEG precursors, a) precursors used to form nonswellable hydrogels, b) Combinations of potential nonswellable networks. **99**
- Scheme 4.1.** Proposed mechanism for the stereochemical control in the nucleophilic thiol-yne reaction. Adapted from ref 23. **124**
- Scheme 4.2.** Model nucleophilic thiol-yne reaction scheme between alkyne- and thiol-functionalised methyl ether PEG_{550} **131**
- Scheme 5.1.** a) Nucleophilic thiol-yne reaction, b) Legend for the alkyne, thiol and vinyl thioether, c) reaction between 4-arm PEG alkyne (2 kg mol^{-1}) and 2 arm PEG thiol (4 kg mol^{-1}) in a 1:1 ratio (alkyne:thiol) in phosphate buffered saline (PBS) solution to **153**

- create the dense covalently crosslinked synthetic network in the thiol-yne IPNs.
- Scheme 5.2** Schematics showing the crosslinking mechanism for each natural polymer system: a) alginate hydrogel forms through the electrostatic interactions with Ca^{2+} ; b) chitosan establishes electrostatic interactions with glycerol phosphate (GP); c) gelatin chains rearrange upon cooling to form a tertiary coiled structure; d) heparin and hyaluronic acid (HA), are both negativity charged, but do not form secondary networks. **155**
- Scheme 5.3.** Schematics illustrating the procedure followed to prepare a) PEG/Natural polymer IPNs with counter ion, b) PEG/Natural polymer hydrogels with no counterion. The natural polymer was dissolved and mixed with the PEG alkyne PBS solution before being added to the PEG thiol solution. The solution was then mixed and vortexed before injected into moulds for testing. **156**
- Scheme 6.1.** Hydrogel formation: (a) Alkyne- and thiol-functionalised PEG architecture, (b) Hydrogel networks formed by thiol-yne chemistry, (c) Thiol-functional bioactive peptide (**PRGDS**) and 2-arm thiol-functional cell degradable peptide (**2MMPS**), incorporated into the hydrogel network to enable cell adhesion and some cell-driven remodelling increase ECM characteristics, (d) Hydrogel network formation with bioactive peptides at 10 wt%. **196**
- Scheme 6.2.** Alkene functionalised 2-arm peptide used in the synthesis of thiol-ene hydrogels. Adapted from ref 59. **208**
- Scheme 7.1.** Small molecule nucleophilic thiol-yne reaction scheme between an activated alkyne and 1-dodcanethiol (DT). $\text{R}_1 = \text{OCH}_2\text{CH}_3$ (ester control), C_6H_5 (aromaticity), CH_3 (ketone), OC_6H_5 (aromatic ester) or NHCH_2CH_3 and $\text{R}_2 = \text{H}$. Or $\text{R}_1 = (\text{CH}_2)_4\text{CH}_3$ (ketone) or C_6H_5 (aromaticity) and $\text{R}_2 = \text{CH}_3$. **227**

Scheme 7.2.	Reaction scheme for the synthesis of phenyl propiolate.	234
Scheme 7.3.	Reaction scheme for the synthesis of ethyl proiolamide.	236
Scheme 7.4.	Synthetic route utilised for the synthesis of 1-phenyl but-2-yn-1-one.	243
Scheme 7.5.	Reaction scheme for the synthesis of Non-2-yn-4-one.	245
Scheme 7.6.	Synthetic route utilised to synthesise a ketone-functional 3-arm PEG (1 kg mol ⁻¹) with a methyl-terminated alkyne.	248
Scheme 7.7.	Synthetic route to form the ketone-functional PEG with a methyl-terminated alkyne; a) Jones' oxidation to form PEG carboxylic acid, b) Thionyl chloride acylation followed by a Friedel-Crafts acylation reaction to form the PEG ketone-functionality.	251
Scheme 7.8.	a) Synthesis of a Weinreb amide; b) mechanism for the selective formation of a ketone from a Weinreb amide and Grignard reagent, R = alkyl group.	253
Scheme 7.9.	Synthetic route to synthesise a methyl-terminated alkyne ketone-functionalised PEG precursor <i>via</i> a Weinreb amide.	254
Scheme 7.10.	Fischer esterification reaction to functionalise PEG with butynoic acid to form an ester-activated methyl-terminated alkyne.	261
Scheme 7.11.	New synthetic route for the synthesis of a methyl-terminated alkyne PEG with ketone-functionality, a) synthesis of 1-chloropent-3-yn-2-one, b) Williamson ether reaction to functionalise a PEG hydroxyl group.	266

List of Equations

Equation 1.1.	Flory-Stockmayer equation to calculate the theoretical critical number of crosslinks needed to form a gel.	3
Equation 1.2.	Gibbs free energy equation for a polymer network immersed in a fluid	4

Equation 1.3.	Equation to determine the molecular weight between two adjacent crosslinks of a non-ionic hydrogel	4
Equation 1.4.	Equation to calculate the mesh size of a hydrogel.	4
Equation 2.1.	Equilibrium water content (EWC) equation where W_s is the equilibrium swollen mass and W_d is the dry mass of the hydrogel.	71
Equation 3.1.	Swelling factor equation where W_t is the weight measured at specific time point and W_0 is the initial wet weight before immersed (after curing for 1 h).	96
Equation 3.2.	Flory-Stockmayer equation to calculate the theoretical critical amount of crosslinks needed to form a gel	101
Equation 7.1.	First order rate equation where $\ln[A]_t$ is the concentration of alkyne at a certain time point, t , $\ln[A]_0$ is the starting concentration of alkyne and k is the rate constant for the reaction.	231

List of Tables

Table 2.1.	Characterisation data for the alkyne and thiol PEG precursors	62
Table 2.2.	Gelation times and swelling kinetics of PEG hydrogels made at 10 wt% in PBS solution	69
Table 2.3.	The mechanical properties of the thiol-yne hydrogels	74
Table 2.4.	Characterisation of the blended thiol-yne PEG hydrogels (21s:24s ratio)	79
Table 3.1.	Characterisation data for the 3- and 4-arm PEG thiol precursors.	96
Table 3.2.	Gelation time (GT) and swelling kinetics of the swellable thiol-yne hydrogels at 10 wt% in PBS solution (1:1 molar ratio of alkyne to thiol end groups).	97
Table 3.3.	Gelation time (GT), and swelling kinetics of nonswelling hydrogels at 10 wt% in PBS solution (1:1 molar ratio of alkyne to thiol end groups).	100

Table 4.1.	Different solvent conditions for targeted intermediate % <i>cis</i> contents using the PEG hydrogel system determined using FT-IR spectroscopy.	130
Table 4.2.	Difference in <i>cis:trans</i> ratio determined through FT-IR and ¹ H NMR spectroscopy	135
Table 4.3.	Conditions used to form stereocontrolled thiol-yne PEG hydrogels with the same gelation time	137
Table 4.4.	Gel data for the stereocontrolled thiol-yne hydrogels	138
Table 5.1.	Optimisation of the PEG/Alginate thiol-yne IPNs composition.	154
Table 5.2.	Synthetic details for the synthesis of the PEG/Natural polymer hydrogels	155
Table 6.1.	Optimisation of the 31A22s31s hydrogel system encapsulated with MDA-MB-231 cells for long term cell culture.	194
Table 6.2.	Gelation time and mechanical properties of the thiol-yne PEG hydrogels synthesised in DMEM	202
Table 7.1.	Effect of the functional group adjacent to the alkyne on rate of the nucleophilic thiol-yne reaction with DT (1.2 eq) with NEt ₃ in CDCl ₃ .	234
Table 7.2.	Effect of the functional group adjacent to the alkyne on rate of the nucleophilic thiol-yne reaction.	240
Table 7.3.	Effect of a methyl-terminated alkyne on rate of the nucleophilic thiol-yne reaction.	242
Table 7.4.	Effect of the adjacent functional group on rate of the nucleophilic thiol-yne reaction	244

Acknowledgements

Firstly, I would like to thank my supervisor Professor Andrew Dove, your guidance and support has been invaluable over the last four years. Throughout my PhD you have inspired and encouraged me to become the chemist I am today.

A massive thank you goes to all the Dove and O'Reilly group members, past and present. It has been a pleasure (and so much fun) to work alongside some truly talented scientists. A huge debt of gratitude goes to my proof reading team especially Mar and Chiara; the conference abstracts, papers and thesis chapters would not be the same without your skills! A special thank you goes to the coffee club: Annette, Ed, Chiara and Siobhan, your constant voice of support over a coffee (or a glass of prosecco!) has been invaluable.

Across the pond, I would like to thank the A. Kloxin group at the University of Delaware, especially to Kat Wiley who gave up a lot of her time to teach a chemist about the world of cell culture as well as the best places to eat in Newark. You all made my trip an 'awesome' experience and a true highlight of my PhD.

Finally, a huge thank you goes to my friends and family. Weekend escapes from the lab to see you all stopped me becoming a (completely) crazy scientist and reminded me there is more to life than a PhD! To my sister, Shona, thank you for the big sister chats over a pain au chocolat and always being there to put my life in perspective when I needed it! Finally, to my parents, thank you for your unconditional love and support reminding me I could do anything I wanted to do! This would not have happened without your encouragement, endless cups of tea and of course the writing room.

Declaration of Authorship

This thesis is submitted to the University of Warwick in support of my application for the degree of Doctor of Philosophy. It has been composed by myself and has not been submitted in any previous application for any degree. The work presented (including data generated and data analysis) was carried out by the author except in the case outlined below:

- Synthesis and characterisation of the **31A23S** system and Flory-Stockmayer calculation (Chapter 3) was carried out by Dr Maria M. Pérez-Madriral (University of Warwick);
- Cytocompatibility and 3D cell culture of the PEG hydrogels (Chapter 3) was carried out by Dr Maria Chiara Arno (University of Warwick);
- Cytocompatibility and 3D cell culture of the PEG/Natural polymer hydrogels (Chapter 5) was carried out by Dr Maria M. Pérez-Madriral (University of Manchester);
- Synthetic peptides and thiol-ene hydrogel precursors (Chapter 6) were synthesised by Miss Katherine L. Wiley (University of Delaware). Miss K. Wiley also synthesised the 2D and 3D thiol-ene hydrogels and conducted the fluorescence analysis of pendant peptide incorporation and the immunostaining experiments. Analysis of the cell cluster diameters was also carried out by Miss K. Wiley.
- Quantitative ^{13}C NMR spectra and 600 MHz ^1H NMR spectra (Chapter 7) were obtained by Dr Ivan Prokes and Mr Robert Perry (University of Warwick). Aqueous SEC analysis was carried out by Dr Daniel Lester.

Publications

Efficient *In-situ* Nucleophilic Thiol-yne Click Chemistry for the Synthesis of Strong Hydrogel Materials with Tunable Properties, **L. J. Macdougall**, V. X. Truong and A. P. Dove, ACS Macro Lett., 2017, **6**, 93-97 (**Chapter 2**).

Nonswelling Thiol-yne Cross-Linked Hydrogel Materials as Cytocompatible Soft Tissue Scaffolds, **L. J. Macdougall**,* M. M. Perez-Madriral,* M.C. Arno and A. P. Dove, Biomacromolecules, 2017, **19**, 1378-1388 (**Chapter 3**).

Self-healing, stretchable and robust thiol-yne interpenetrating networks through utilizing the properties of natural polymers, **L. J. Macdougall**, M. M. Pérez-Madriral, J. E. Shaw, M. Inam, R.K. O'Reilly, S. M. Richardson A. P. Dove, *Manuscript Submitted*, 2018 (**Chapter 5**).

Design of Synthetic Extracellular Matrices for Probing Breast Cancer Cell Growth Using Robust Cytocompatible Nucleophilic Thiol-yne Addition Chemistry, **L. J. Macdougall**,* K. L. Wiley,* A. M. Kloxin, A. P. Dove, Biomaterials, 2018, DOI: 10.1016/j.biomaterials.2018.04.046 (**Chapter 6**).

*denotes authors contributed equally to this work

Abstract

This thesis explores the nucleophilic thiol-yne reaction as a crosslinking method for the synthesis of hydrogel materials under biologically relevant conditions. The reaction, using simple functional groups, can be carried out without the use of an external catalyst. This thesis aims to portray the immense potential this reaction has in creating hydrated polymer networks for a wide range of biomedical applications. In the review of the literature (Chapter 1), the popularity and future of hydrogels in tissue engineering has been discussed and the advantages of using alkyne functional groups to crosslink polymers has been highlighted. The main aim of this thesis is to further develop the nucleophilic thiol-yne reaction and to prepare poly(ethylene glycol) (PEG) hydrogel materials with superior performance for application as tissue engineered scaffolds (*e.g.* extracellular matrix (ECM) mimics or injectable scaffolds). This aim has been approached through a variety of experimental pathways in this thesis demonstrating the suitability of this reaction in the biomaterials field.

In Chapter 2, the nucleophilic thiol-yne reaction has been presented as a highly efficient chemistry for producing robust, high water content hydrogels which could be repeatably compressed without hysteresis. Through a straightforward blending process of PEG thiol precursors, the material properties were easily tuned to a range of relevant biological environments. In a similar manner, using the PEG precursors to tune the resultant properties, Chapter 3 addresses the swelling profiles of the thiol-yne hydrogels. By increasing the number of hydrophobic crosslinking points within the networks, nonswelling, cytocompatible hydrogel material were created when immersed in aqueous environments.

The monoaddition product of the nucleophilic thiol-yne reaction results in a vinyl thioether bond which can favour different isomers, depending on the reaction conditions. To exploit this in hydrogel synthesis, Chapter 4 describes the formation of sterecontrolled hydrogels. Significantly, an impressive range of mechanical properties was achieved, without affecting the structure or swelling behaviour of the materials.

To achieve a structure with more advantageous properties (*e.g.* self-healing and stretchability) thiol-yne interpenetrating networks (IPNs) were synthesised through the inclusion of natural polymer hydrogels (Chapter 5). These IPNs achieved the advantageous properties required in a simple and effective manner, while retaining the characteristics already exhibited by these materials. To improve on this aim, the thiol-yne PEG hydrogels successfully encapsulated breast cancer cells with enhanced viability compared to the widely used radical thiol-ene reaction (Chapter 6). Controlled matrix degradation allowed for cell proliferation and the formation of cell clusters.

Chapter 7 investigates the kinetics of the nucleophilic thiol-yne reaction with different activating groups (*e.g.* adjacent group to the alkyne), to reduce the toxicity of the PEG alkyne precursors and degradation of the resultant thiol-yne hydrogels. This chapter highlights key requirements of the functionalisation reaction to form alkyne and thiol precursors for successful hydrogel synthesis.

Chapter 8 provides a summary of the key findings from Chapters 2-7 and Chapter 9 states the experimental procedures of this thesis.

Abbreviations

2D	2-Dimensional
3D	3-Dimensional
Ar	Aromatic
CuAAC	Copper-catalysed alkyne-azide cycloaddition
Cryo SEM	Cryogenic scanning electron microscopy
d	doublet
DBU	1,8-Diazabicyclo[5.4.0]undec-7-ene
DCC	<i>N,N'</i> -Dicyclohexylcarbodiimide
DIBO	Dibenzocyclooctyne
DIFO	Difluorinated cyclooctyne
DNA	Deoxyribonucleic acid
DMAP	4-(Dimethylamino)pyridine
DMEM	Dulbecco's Modified Eagle's Medium
DMF	<i>N,N</i> -Dimethylformamide
DT	1-Dodecanethiol
<i>E</i>	Young's modulus
ECM	Extracellular matrix
EP	Ethyl propiolate
ER+	Estrogen receptor positive
ESI MS	Electrospray ionisation mass spectrometry
EWC	Equilibrium water content

FT-IR	Fourier-transform infrared
GDL	D-(+)-Glucono-1,5-lactone
GF	Gel fraction
GP	Glycerol phosphate
GT	Gelation time
HA	Hyaluronic acid
hMSCs	Human mesenchymal stem cells
IPN	Interpenetrating networks
<i>J</i>	Coupling constant
<i>k</i>	Rate constant
Ki-67	Cellular marker for proliferation
LAP	Lithium acylphosphinate
LD	Lethal Dose
m	Multiplet
MC3T3-E1	Murine pre-osteoblast cells
MCF-7	ER+ breast cancer cells
MDA-MB-231	Invasive triple negative breast cancer cells
MMP	Cell-degradable matrix metalloproteinase (GCRDVPMS↓MRGGDRCG)
M_n	Number average molecular weight
M_w	Weight average molecular weight
NMR	Nuclear magnetic resonance
NSPCs	Neutral stem/progenitor cell cultures

PBS	Phosphate buffered saline
PCL	Poly(ϵ -caprolactone)
PEG	Poly(ethylene glycol)
PHEMA	Poly(2-hydroxyethyl methacrylate)
PLA	Poly(lactic acid)
PNIPAM	Poly(<i>N</i> -isopropyl acylamide)
PPO	Phenyl-2-propyn-1-one
q	Quartet
RT	Room temperature
RAFT	Reversible addition-fragmentation chain-transfer
RGDS	Vitronectin/fibronectin mimetic adhesion sequence (peptide sequence: Arg-Gly-Asp-Ser)
RI	Refractive Index
s	Singlet
SEC	Size exclusion chromatography
SF	Swelling factor
SPAAC	Strain-promoted alkyne-azide cycloaddition
t	Triplet
T47D	ER+ breast cancer cells
THF	Tetrahydrofuran
UV	Ultraviolet
δ	Chemical shift
<i>D</i>_M	Dispersity

Chapter 1.
Introduction

1.1. Hydrogels: Theory and Application

Hydrogels, which are defined as hydrated 3D polymer networks (Figure 1.1),¹⁻³ are characterised by their high water content and porosity.^{4,5} As a result, they have a wide range of applications, from contact lenses to food additives.⁶⁻⁸ Specifically, hydrogels are most commonly used as soft contact lenses, first introduced by Wichterle and Lím in 1954.⁹ This application clearly highlights the advantageous properties of hydrogels (*e.g.* oxygen permeability and mechanical strength) and their relevance to clinical applications.¹⁰⁻¹²

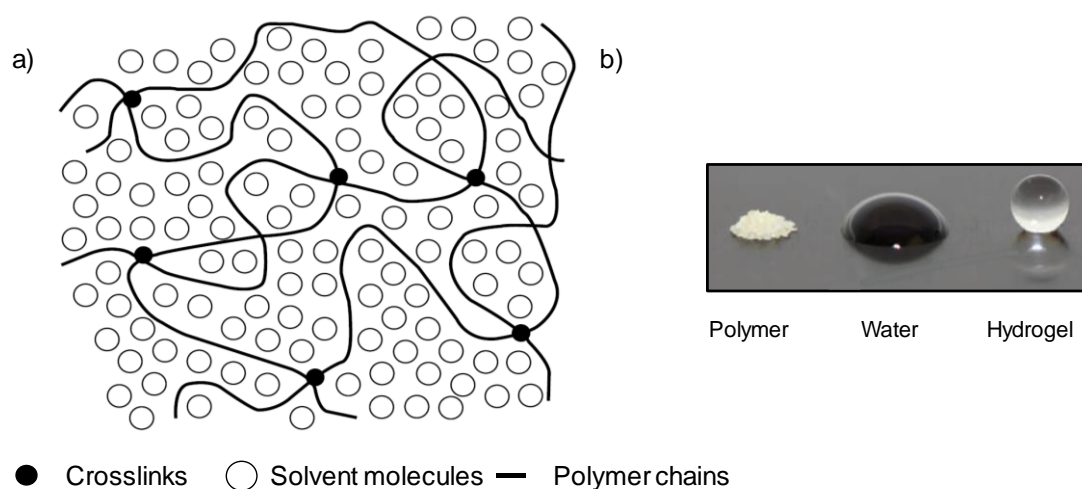


Figure 1.1. a) Schematic of a hydrated polymer network, adapted from ref. 1, b) The components of a hydrogel adapted from ref. 3.

The formation of a hydrogel occurs when the viscosity of a polyfunctional system dramatically increases, defined as the “gel point” or sol-gel transition point.¹³ Gelation can occur through many different routes and mechanisms (*e.g.* chain or step growth polymerisations, intramolecular forces, crosslinking reactions) depending on the precursors and conditions used.¹⁴ There are many different theories which can be applied to predict the gelation of a polymeric system. The most popular theory of gelation, through

the crosslinking of polymers *via* a step-growth polymerisation, is the Flory-Stockmayer theory.¹⁵⁻¹⁸ The theory predicts the point of gelation for a system of high functionality (*i.e.* more than 2 functional groups per molecule), producing a polymer network with infinite molecular weight. The theory builds on the Carothers equation, which is limited to branched stoichiometrically balanced systems, to calculate the probability of finding a crosslinked point during gelation. The Flory-Stockmayer equation can be used to calculate the theoretical critical number of crosslinks needed to form a gel (Equation 1.1). Hence, the gelation point is reached when a critical number of intermolecular linkages has been exceeded. This theory predicts the gel point of a system assuming; 1) all the functional groups are equally reactive, 2) the reaction occurs in an A-B fashion and 3) there are no intramolecular forces.

$$p_c = \frac{1}{\sqrt{(f_A - 1)(f_B - 1)/r}}$$

Equation 1.1. Flory-Stockmayer equation to calculate the theoretical critical number of crosslinks needed to form a gel, p_c , where f_A is the functionality of polymer A, f_B is the functionality polymer B, and r is the ratio between the total number of A and B groups.

Hydrogels can swell to thousands of times their dry weight, dictated through the crosslinking structure and charge density of the hydrated polymer network. Their swelling profile is defined by important parameters; 1) polymer volume fraction, the amount of water that can be absorbed and retained in the structure, 2) mesh size, the correlation distance between two adjacent crosslink points and 3) the effective molecular weight of the polymer chain between crosslink points. The Flory-Rehner theory can be used to analyse the structure of hydrogels through the combination of thermodynamic and elasticity theories. For non-ionic hydrogels it states that a crosslinked polymer gel that is immersed in a fluid and allowed to reach equilibrium with its surroundings is subject to

two opposing forces: the thermodynamic force of mixing and the retractive force of the crosslinked polymer chains.^{18, 19} At equilibrium these forces are equal and can be defined in terms of Gibbs free energy (Equation 1.2).

$$\Delta G_{total} = \Delta G_{elastic} + \Delta G_{mixing}$$

Equation 1.2. Gibbs free energy equation for the forces on a polymer network immersed in a fluid. $\Delta G_{elastic}$ = the elastic forces of the polymer network, ΔG_{mixing} = the spontaneous mixing of the fluid molecules within the polymer chains, ΔG_{total} = total Gibbs free energy change of a polymer network immersed in a fluid.

ΔG_{mixing} is typically expressed as the polymer-solvent interaction parameter (χ_1) and can be used to calculate the molecular weight between the polymer chains (Equation 1.3).²⁰

$$\frac{1}{\bar{M}_C} = \frac{2}{\bar{M}_n} - \frac{\bar{v}_1(\ln(1-v_2)+v_2 + \chi_1 v_2^2)}{v_2^{1/3} - \frac{v_2}{2}}$$

Equation 1.3. Equation to determine the molecular weight between two adjacent crosslinks of a non-ionic hydrogel (\bar{M}_C). \bar{M}_n = the number-average molecular weight of the un-crosslinked hydrogel V_1 = the molar volume of the solvent (18 cm³ mol⁻¹ for water), v_2 = the polymer volume fraction in the equilibrium swollen hydrogel, \bar{v} = the specific volume of the polymer and χ_1 = the polymer-solvent interaction parameter.

Once calculate the molecular weight between two adjacent crosslinks can be used to determine the mesh size (ξ) of the hydrogels (Equation 1.4).²¹ This parameter is important for many drug delivery applications and the flow of molecules in and out of the hydrogel structure. It also defines a hydrogel as macroporous, microporous or nonporous.

$$\xi = v_2^{-1/3} (\bar{r}_0^2)^{1/2}$$

Equation 1.4. Equation to calculate the mesh size of a hydrogel. v_2 = the polymer volume fraction in the equilibrium swollen hydrogel, $(\bar{r}_0^2)^{1/2}$ = the root-mean-square end-to-end distance of the polymer chain in the unperturbed state calculated from average bond length for the polymer, the characteristic ratio of the polymer (C_n) and the molecular weight of the repeating unit (M_r).

The ability to use these parameters to tailor the molecular structure of hydrogels results in mechanical properties with responsive and diffusive properties ideal for many biological and medical applications.²² Hence the popularity of hydrogel materials has

become very apparent in recent years, especially in the tissue engineering field. Cells are influenced by their surrounding environment, made up of extracellular matrix (ECM) proteins, soluble bioactive factors and neighbouring cells.²³ These components influence how cells grow, divide and differentiate, in response to stimuli and most importantly, how they interact through signalling with the ECM. Hence, hydrogels with highly tuneable properties can simulate *in vivo* conditions, thus creating an environment that mimics the native ECM.

The importance of accurately mimicking *in vivo* settings was highlighted by Discher and co workers²⁴⁻²⁶ through the response stem cells showed to different substrate stiffnesses. On a 2D culture configuration, cell morphology differed depending on the environment the cells were sensing (*i.e.* soft substrates resulted in fat tissue cells, while stiff substrates resulted in cartilage growth). This observation has redefined the area of tissue engineering for the culture of cells *in vitro*.²⁷⁻²⁹ It has created a drive to form hydrogels, which mimic the features of the native ECM, enabling cell culture *in vitro* but capturing the behaviour and characteristics of cells *in vivo*.^{6, 30-37} However to recreate *in vivo* environments, hydrogels require; 1) adequate porosity for the flow of nutrients in and out of the matrix, 2) degradability to allow cell proliferation and communication^{38, 39} and 3) the correct signalling factors to enable cell growth.^{3, 31, 40-43} An additional factor to address, is the ability to encapsulate cells during the crosslinking reaction to allow for a good distribution of cells within the hydrogel matrix allowing cells to sense a true representation of an *in vivo* setting.⁴⁴ Hence, it is crucial that the crosslinking chemistry is biocompatible and does not influence the viability or growth of encapsulated cells.⁴⁵⁻⁴⁷

In turn the chemistry behind hydrogels underpins their final properties and enables them to be highly versatile and synthetically flexible.^{22, 48-50}

Exploitation of this phenomena could enable further understanding into disease progression. For example by modelling the change in stiffness of tissue during the growth of a cancerous tumour or by a myocardial infarction.⁵¹ Synthetic hydrogel materials have also been used to capture different cell processes (*e.g.* differentiation of stem cells or the reorganisation of the microenvironment).⁵² These applications highlight the importance these scaffolds can have in recreating *in vivo* settings *in vitro* with the ability to encapsulate a range of different cell cultures. In this respect, hydrogel synthesis benefits from a range of chemical reactions (*e.g.* supramolecular interactions, intramolecular forces and click reactions).⁵³⁻⁵⁵ As a result, hydrogels can be prepared with tailored specifications that meet the requirements for a range of different biological environments. Additionally, the ability to control the chemistry behind these hydrated polymer networks expands the library of dynamic stimuli-responsive materials.⁵⁶

This chapter will focus on the choice of crosslinking chemistry used to prepare hydrogels for biomedical applications (*i.e.* ECM mimics or injectable robust scaffolds). It aims to highlight the use of alkyne functional groups, to synthesise dynamic hydrogels which can encapsulate cells without impacting their viability.

1.2. Hydrogel Synthesis

The synthesis of a hydrogel plays a fundamental role in determining the networks' properties and final application.²⁶ As such, the choice of polymer precursor and crosslinking chemistry to form these networks is crucial.^{27, 57} For instance, soft, flexible hydrogels needed for water sorption and injectable drug delivery require different polymer precursors and synthetic routes compared to tough, robust hydrogels used for cartilage replacement or wearable devices.^{58, 59}

1.2.1. Polymer Precursors for Hydrogel Synthesis

Many different polymers have been used to form hydrogels (*e.g.* peptides, DNA, polyacrylates and polyethers) each providing different advantages to the polymer network.^{27, 60, 61} Natural polymers (*e.g.* polysaccharides and peptides, Figure 1.2) are some of the most widely used precursors to form hydrogels because of their inherent biocompatible nature and availability.⁶²⁻⁶⁸ Alginate, first characterised in 1881,⁶⁹ has received huge attention as a natural hydrogel system as it readily forms a hydrogel through ionic interactions between the negatively charged polysaccharide chains and positively charged counterions, usually Ca^{2+} ions. These soft hydrogels form easily in aqueous conditions and have shown immense potential as robust tissue engineering scaffolds.⁷⁰⁻⁷² Chemical modifications of the functional groups present on natural polymer chains (*e.g.* addition of acrylate groups, diisocyanates and functional azides)⁷³ has further progressed the use of natural polymers in hydrogel synthesis as it has allowed them to form robust hydrogels while retaining other advantageous qualities (*e.g.* self-healing and biocompatibility).⁷⁴

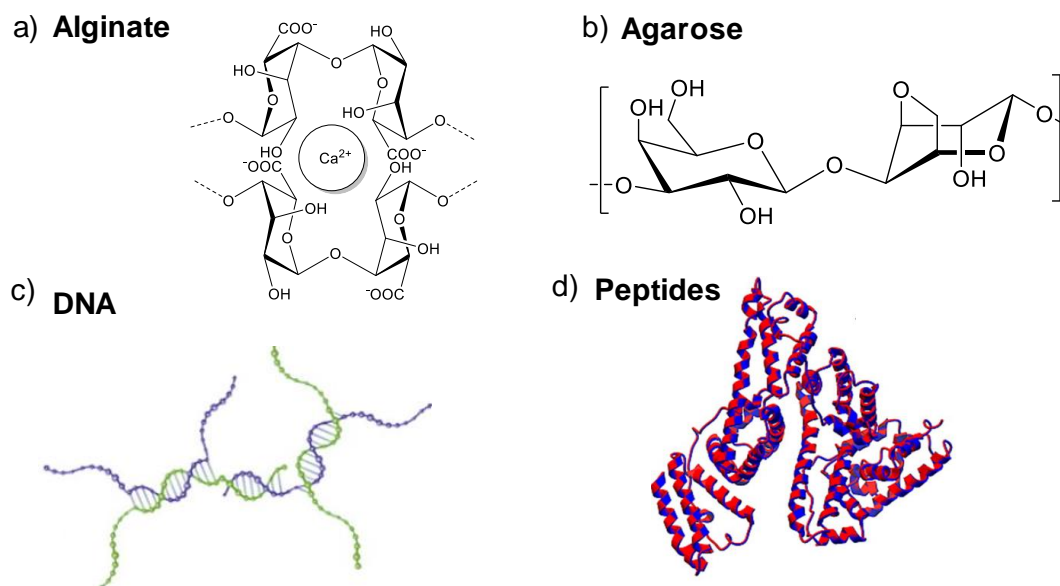
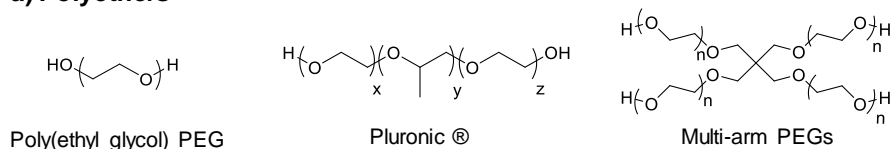


Figure 1.2. Ideal chemical structure of natural polymers which have been used in hydrogel synthesis a) alginate, b) agarose, c) DNA, d) peptide structure adapted from ref 60.

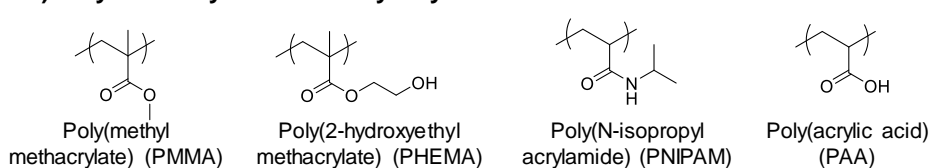
The versatility and biocompatibility of natural polymers has led to their application as adaptable biomaterials.⁷⁵ They are ideally suited for creating ECM mimics, since they are naturally abundant in the native ECM tissue, which has increased their popularity in recent times. However, unfunctionalised natural polymer hydrogels usually possess inferior mechanical properties because of the weak covalent interactions used to crosslink the polymer chains.⁷² The functionalisation reactions used to improve these properties can result in low conversions on high molecular weight polymers, which can hinder reproducibility. In addition, the limited feasibility to tune and control the hydrogels characteristics restricts the use of these materials in clinical applications. Batch-to-batch variability can also lead to irreproducible properties depending on; 1) the source of the natural polymer, 2) the molecular weight of the polymer and 3) the number of crosslinked sites on the resultant chains.⁷⁶ Hence, such variability can be problematic when hydrogels are used to assess how the mechanical properties affect cell differentiation.²⁶

Synthetic polymers overcome many of the drawbacks displayed by natural polymers for hydrogel synthesis. Through controlled polymerisation reactions, well defined and accurate molecular weight polymers can be achieved. This leads to reproducible features and enhanced control over the mechanical properties of the resultant hydrogel.⁷⁷ Many different classes of synthetic polymers have been used to form hydrogels (*e.g.* polyacrylates, polyesters and block copolymers, Figure 1.3)^{37, 49, 78} through a range of polymerisation techniques (*e.g.* step growth or controlled radical polymerisations)^{79, 80}

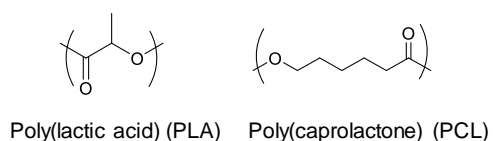
a) Polyethers



b) Polymethacrylates and Polyacrylates



c) Polyesters



d) Block copolymers

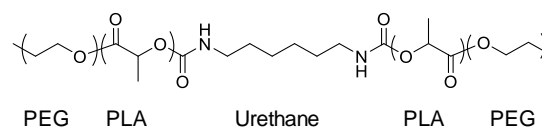


Figure 1.3. Structures of a range of synthetic polymers used in hydrogel synthesis.

Arguably, the most popular synthetic polymer for hydrogel synthesis is poly(ethylene glycol) (PEG), a commercially available, resorbable polymer (Figure 1.3 a).⁸¹ It can form robust biocompatible hydrogels and is often referred to as a ‘blank slate’,³¹ as the polymer networks do not allow protein adsorption or cell adhesion. Hence,

it can be easily manipulated to incorporate a range of biologically relevant molecules to investigate the affect biological cues have on different intracellular processes.^{78, 82, 83} The pendant hydroxyl groups offer wide synthetic flexibility,⁸⁴ and have been functionalised with numerous terminal groups including maleimides, norbornenes and thiols.⁸⁵⁻⁸⁸ These functionalities have created crosslinked PEG networks with a range of useful properties (*e.g.* controlled degradation, fluorescence and self-healing)⁸⁹⁻⁹¹ for many different applications such as cell encapsulation,^{92, 93} controlled stem cell differentiation^{74, 94, 95} and delivery vehicles.^{96, 97} PEG copolymers have also been exploited for hydrogel synthesis (Figure 1.3a). Specifically, Pluronics®, non-biodegradable triblocks of PEG and poly(propylene oxide) (PPO) (PEG-*b*-PPO-*b*-PEG), can control the swelling of PEG hydrogels at physiologically relevant temperatures through the thermoresponsive PPO unit.^{98, 99} In addition, during PEG synthesis, parameters such as the molecular weight and architecture (*i.e.* the number of pendant side chains) can be controlled. This produces a library of different commercially available PEGs which, through careful functionalisation, can result in hydrogels with a range of mechanical properties (*e.g.* compressive strength, stiffness, and tensile strain).^{96, 100, 101} The advantageous properties of PEG have been emphasised by Mosiewicz *et.al.* Through manipulating the PEG network they were able to tether fragile proteins within the structure by localised, laser-assisted uncaging for unprecedented control over photopatterning the scaffold with biomolecules (Figure 1.4).¹⁰² This work presented the role PEG networks play in providing a structure which can be functionalised with a range of model ligands and proteins with precise control. The site-specific tethering can take place in the presence of

cells creating an ECM mimic which can address questions related to spatiotemporal signalling of biomolecules *in vivo*.

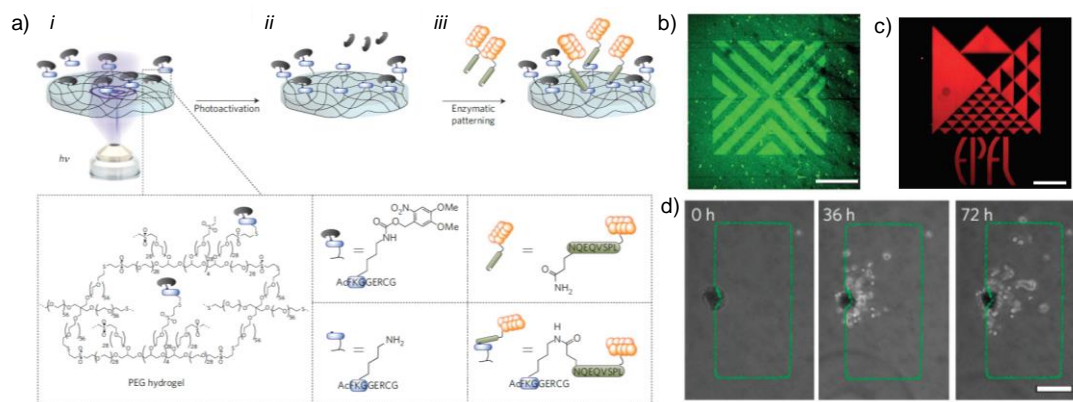


Figure 1.4. a) Concept of light-controlled enzymatic biomolecule patterning of hydrogels. i) A photolabile, caged, and therefore inactive enzymatic peptide substrate is covalently incorporated into PEG hydrogels and can be activated by light. ii) Localised cleavage of the cage by controlled light exposure from a confocal laser allows reactivation of the enzyme substrate. iii) Enzyme-catalysed (here: the transglutaminase factor XIII) reaction of the uncaged substrate with a counter-reactive substrate on a biomolecule of interest allows covalent biomolecule tethering in a highly localised, user-defined pattern; b) ProteinA tethering results in patterns of Fc-chimaeric proteins (here: IgG), c) The laser-scanning technique allows the generation of precisely defined patterns of any arbitrary shape d) Confocal micrograph showing enzymatic patterning of the fluorescent adhesion peptide RGD in precisely defined cuboidal patterns ($\sim 900 \times 450 \mu\text{m}$) touching half of a microtissue. MSCs rapidly invade the patterned gel regions as shown by time-lapse microscopy of one representative example. (scale bar, $200 \mu\text{m}$). Figure modified from ref 102.

1.2.2. Crosslinking Chemistries for Hydrogel Synthesis

Many applications require hydrogels to encapsulate cells while forming *in situ*,¹⁰³ therefore the crosslinking reaction needs to fulfil certain requirements; 1) high yielding (most polymer-polymer coupling routes lead to low conversions as a result of high molecular weight polymer chains reducing mobility of functional end groups),¹⁰⁴ 2) use of biocompatible precursors which do not generate toxic by-products and 3) can be carried out under mild or physiological conditions (*e.g.* 37°C in aqueous environment) without the use of toxic catalysts.¹⁰⁵ Fortunately, there are many different classes of reactions that

fulfil these requirements (*e.g.* electrostatic interactions, click reactions or hydrogen bonding), yielding hydrogels for a range of different applications.^{3, 23}

Non-covalent interactions to form hydrogels (*e.g.* electrostatic interactions, hydrogen bonding and host-guest interactions)^{106, 107} allows gelation to occur under physiological conditions and in the presence of cells, making these reactions ideal for tissue engineering. These routes can also result in hydrogels which possess reversible sol-gel transitions, self-healing and enhanced stretchability.^{108, 109} These advantageous qualities can be tuned through biological environmental stimuli (*e.g.* enzymes, changes in pH and redox agents)¹¹⁰ which enables the networks to respond and adapt to the surrounding conditions. The ECM is a very dynamic matrix in which its responses to external stimuli influences how cellular processes take place (*e.g.* cell-cell interactions and the presentation of adhesion ligands) therefore an essential characteristic to incorporate in synthetic mimics.⁷⁷ Although these advantageous qualities allow hydrogels to easily mimic the ECM, the interactions are often weak resulting in poor compressive strength and therefore the structures are unable to withstand external pressures. Furthermore, for these interactions to occur they often require functionalisation reactions on natural polymers which results in low conversion leading to inferior hydrogels.

The production of covalently bonded hydrogels enables the structures to withstand high compressive stress at low polymer contents. However, if cells are present during the gelation step, careful attention needs to be paid to the reaction conditions to maintain cell viability. As the popularity of hydrogels has developed, many comprehensive review articles have been published which evaluate a range of covalent reactions used for

hydrogel synthesis including; radical polymerisation, coupling reactions, click reactions and Schiff base crosslinking.^{23, 79, 103, 111, 112} However, click reactions have, by far, been the most popular route to covalently crosslink polymers into hydrated networks (Figure 1.5).^{45, 113}

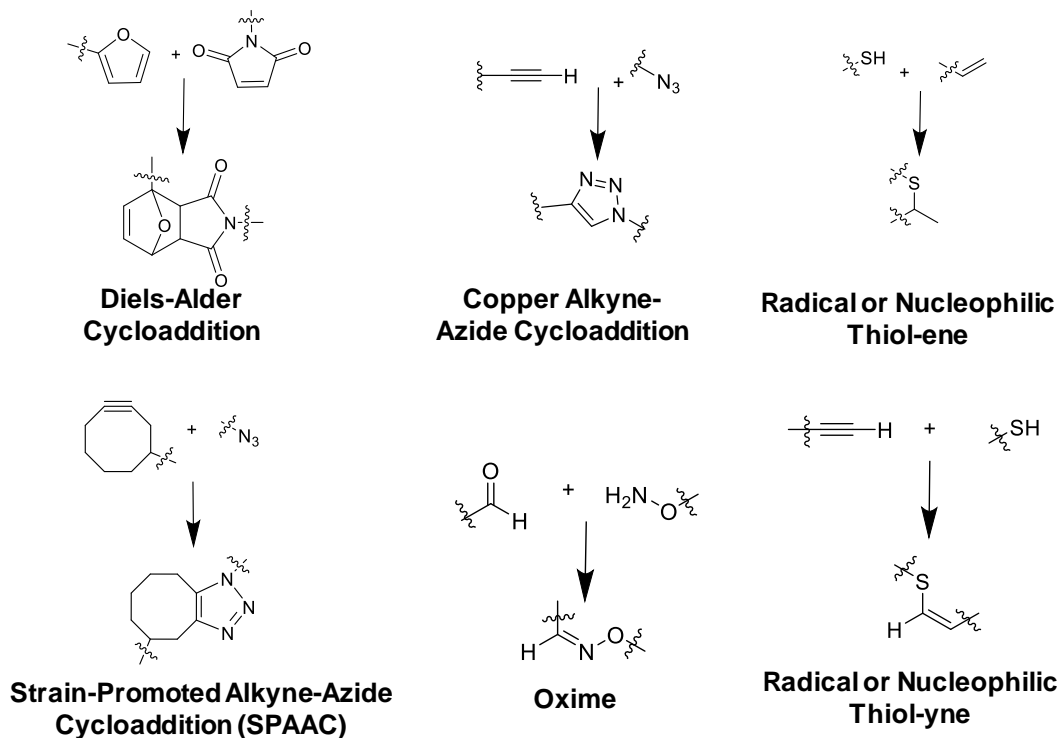


Figure 1.5. Click reactions used in hydrogel synthesis.

Click reactions were first highlighted by Sharpless and co workers,¹¹⁴ by presenting a range of high yielding reactions which could be readily carried out in water, under mild conditions and without the production of toxic by-products. These characteristics clearly demonstrate the advantageous qualities these reactions bring to the synthesis of biocompatible hydrated polymer networks.¹¹⁵ As such, click chemistry including oxime reactions, Diels-Alder reactions, thiol-ene reactions, strain-promoted azide-alkyne cycloaddition (SPAAC), and copper-catalysed azide-alkyne cycloaddition (CuAAC) have revolutionised hydrogel synthesis.¹¹⁶ The diversity of functionalities

involved in these crosslinking reactions has contributed to their versatile and biorthogonal nature. They have allowed vast progression in the field resulting in materials which are dynamic and biologically relevant to a range of different environments (*e.g.* cartilage and cancerous tumours).¹¹³

Diels-Alder reactions (*e.g.* electron-demand, intramolecular and inverse electron-demand)¹¹⁷ have been extensively used throughout the last two decades as a synthetic route for polymers^{118, 119} and hydrogels.^{120, 121} Typically for hydrogel synthesis, polymer precursors are functionalised with pendant furan and maleimide functionality through simple synthetic routes, allowing the electron-demand Diels-Alder reaction to form polymer networks.¹²² This reaction can be carried out under slightly acidic conditions at ambient temperatures without the need for a initiator.¹²³ In addition, the Diels-Alder reaction can be reversed (retro-Diels-Alder reaction) to allow hydrogels to degrade at 37 °C,¹²⁴ or for the release of peptides from the hydrogel structure.¹²⁵ The reversible nature of the reaction can also be used to create dynamic hydrogel structures. This approach was exemplified by Koehler *et.al.*¹²⁶ who exploited the reaction to post modify a PEG hydrogel structure with furan-functionalised peptides conjugated with dexamethasone. Dexamethasone could be released in a controlled manner by a retro-Diels-Alder reaction to induce osteogenic differentiation of human mesenchymal stem cells (hMSCs) in 3D. This work portrays the use of Diels-Alder reactions to sustainably deliver bioactive materials and could be especially useful for bone regeneration.

A common disadvantage of the Diels-Alder click hydrogels are the slow gelation times they possess. Recently, to address this drawback Smith *et.al.* explored the kinetics

of this reaction by increasing the electron density on the diene (methylfuran instead of furan) (Figure 1.6).¹²⁷ The reaction accelerated and occurred at pH 7.4, thus enabling cell encapsulation, demonstrating the cytocompatibility of this optimised reaction and highlighted its potential to produce hydrogels as platforms for studying tumour progression *in vivo*. Although this optimised reaction has produced robust hydrogels under physiological conditions (pH 7.4) there were ~50% furan groups left unreacted in the network which could affect the swelling profile of these systems as the crosslinking density would be reduced. Another drawback of this route is the low yield in the functionalisation reaction to form the furan-functionalised hyaluronic acid. The reaction can only reach a maximum of 60% substitution after 72 h which could potentially lead to a lower crosslinking efficiency, effecting the robust nature and swelling profile of these hydrogels.

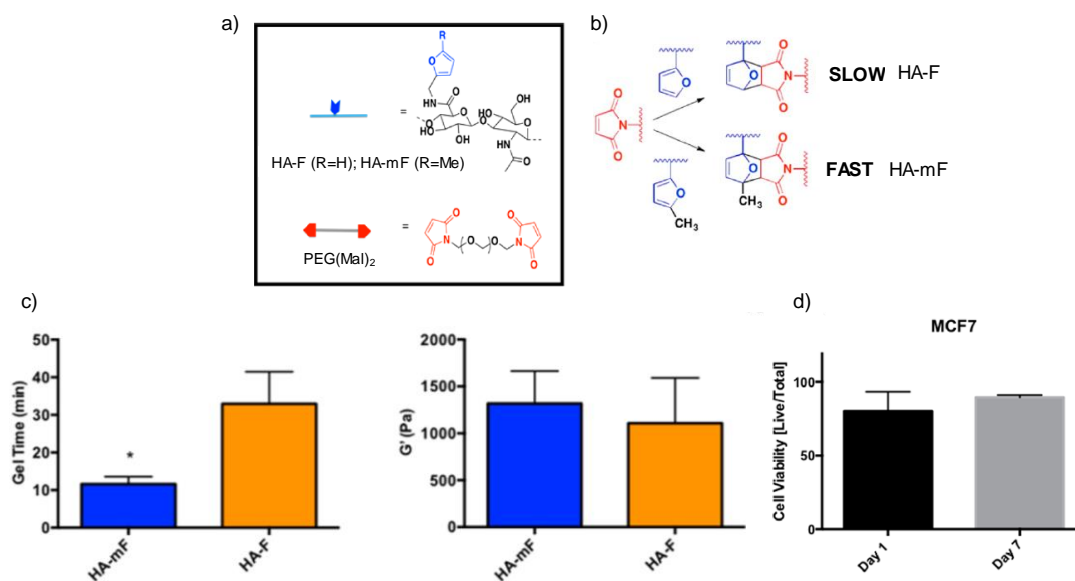


Figure 1.6. a) Schematic of covalently crosslinked hydrogels using furan-maleimide Diels-Alder chemistry, (b) Replacing furan with methylfuran accelerates the DA reaction at pH 7.4, (c) Comparison of bulk properties of HA-FA and HA-mF hydrogels cross-linked with (Mal) (LHS) rheological determination of time to gelation of HA-mF and HA-FA (RHS) Final elastic storage moduli (stiffness) of HA-mF and HA-FA, (d) Quantification of cell viability from MCF-7 breast cancer cell lines. Adapted from ref. 127.

In contrast a click reaction which owes its success to the synthetic flexibility and natural abundance of precursors, in contrast to the Diels-Alder reaction, is the thiol-ene reaction. A wide range of alkene precursors can be utilised in this reaction from acrylates to maleimides,¹²⁸⁻¹³⁰ that can react with a variety of thiols (*e.g.* cysteines, thiopropionates and aromatic thiols) (Figure 1.7).¹³¹ The reaction has been demonstrated to synthesise biocompatible, robust hydrogels,¹³²⁻¹³⁴ through two pathways (either radically-initiated or base catalysed) (Figure 1.8).^{135, 136} The scaffolds are able to be post modified,¹³⁷ exhibit controlled degradation^{86, 88, 138} and allow cell encapsulation.^{139, 140}

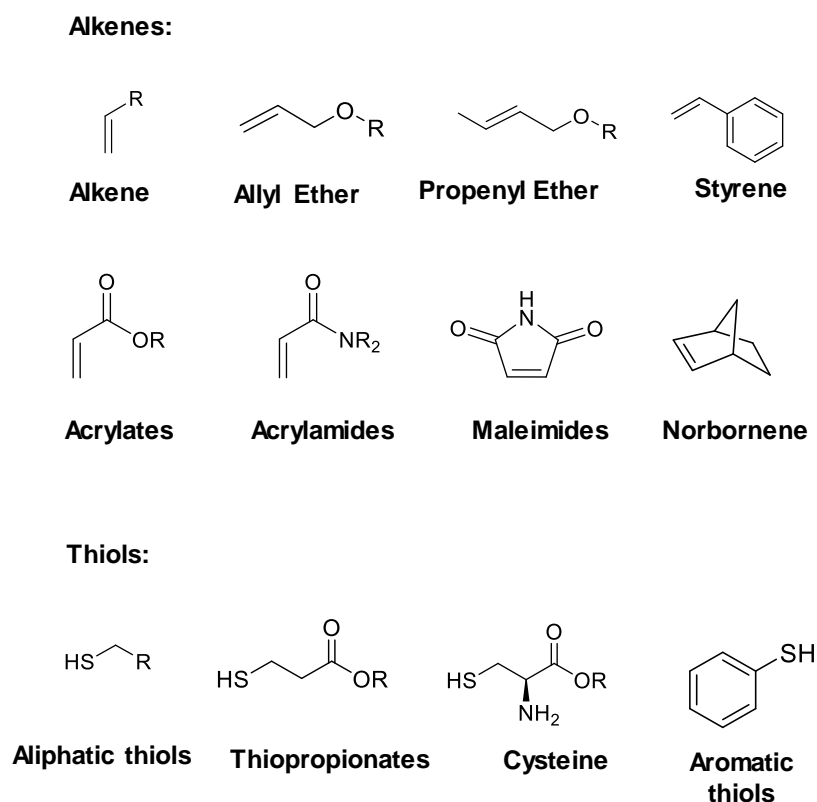


Figure 1.7. Examples of alkenes and thiols used to synthesise thiol-ene hydrogels

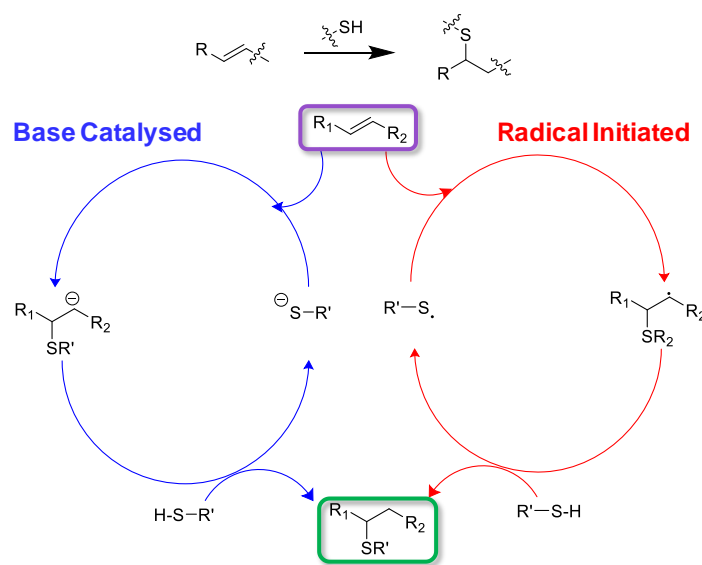


Figure 1.8. The mechanism for the thiol-ene reaction via a base catalysed (blue arrows) or radical-initiated (red arrows) pathway.

The radically-initiated pathway has been used extensively to create hydrogels on a rapid time scale using a range of polymer precursors including PEG, peptides and polymers synthesised through controlled polymerisation techniques.^{134, 141, 142} The chemistry has been used to form and post modify hydrogels for many applications (*e.g.* protein delivery, antifouling materials and cartilage regeneration)^{87, 143, 144} Through careful choice of UV light intensity and photoinitiator the scaffolds can encapsulate cells during gelation creating ideal ECM mimics.^{52, 88, 145} These thiol-ene structures can be manipulated by cells through the incorporation of cell-degradable linkages and can promote cell growth through the inclusion of cell adhesive peptides.^{82, 89, 146-153} In addition to this, the radical chemistry has been used to 3D print hydrogels for the controlled formation of patterned networks.^{142, 154} Specifically Brown *et.al.* demonstrated the use of radical thiol-ene reactions to form dynamic, viscoelastic materials for the encapsulation of hMSCs.¹⁵⁵ By incorporating a dynamic thioester unit to the PEG thiol precursor, they

were able to control the reorganisation of the network under physiological conditions (Figure 1.9). Specifically, the viscoelastic properties of the hydrogels were mediated through light exposure which could break the dynamic thioester bond, allowing stress relaxation (σ) and the controlled spread and proliferation of encapsulated hMSCs within the structure. This work demonstrates the flexibility of the thiol-ene chemistry and its vital role in creating dynamic materials.

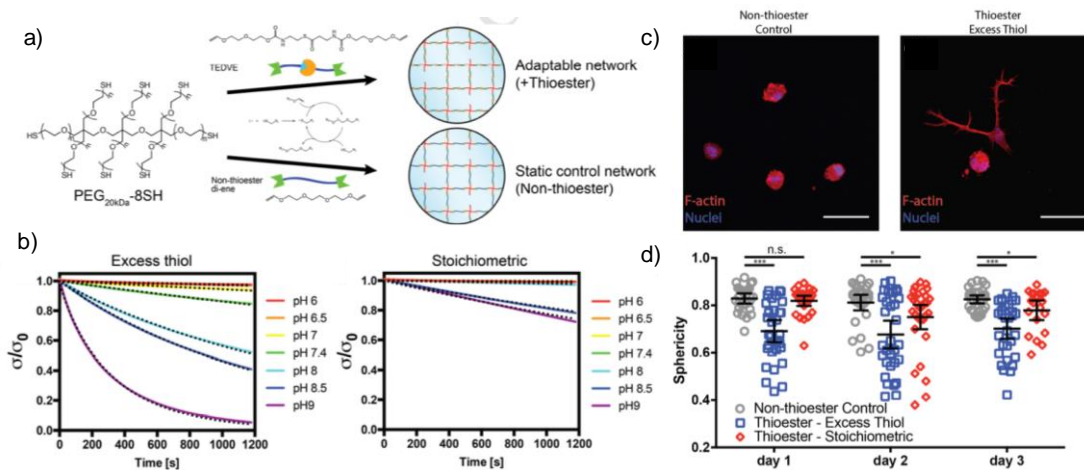


Figure 1.9. a) 8-arm PEG star macromers end-functionalised with thiols are crosslinked by divinyl molecules with and without thioesters to yield adaptable and static networks, respectively, b) Stress relaxation of thioester hydrogels with (LHS) excess network thiols at various pH, (RHS) stoichiometric thioester networks (no free network thiols) at various pH. Dotted lines represent fitted stretched exponentials, c) hMSCs encapsulated in thioester hydrogels are viable, acquire elongated morphologies and have increased proliferation relative to static networks, d) Sphericity of the three-dimensional cell shapes was analysed during culture within hydrogels. Thioester networks formed with excess thiols (blue squares) show dramatically increased spreading (i.e. lower sphericity) compared to static hydrogels within one day of encapsulation and this difference is retained throughout the experiment. Thioester networks formed with stoichiometric thiols begin to spread after one day in culture. Figure modified from ref 155.

Although the radical thiol-ene reaction offers many advantages for the synthesis of hydrogels (*e.g.* easy accessible functional groups, low polymer contents, rapid gelation). The presence of a photoinitiator and the ability to generate free radicals can affect the viability of some cell lines in these scaffolds therefore restricting the versatility

of this chemistry to encapsulate a wide range of cell lines.^{44, 156} However, the nucleophilic base-catalysed pathway (Michael addition) overcomes the drawbacks of radical thiol-ene chemistry by crosslinking polymers with pendant electron-deficient alkenes and thiols in almost quantitative yields.¹⁵⁷ The rate of the reaction is highly influenced by the reactivity of the functional groups; for alkenes, maleimides and vinyl sulfones reacts much faster than acrylamides and methacrylate while aromatic thiols react faster than aliphatic thiols. A range of catalysts can be used for the reaction (*e.g.* triethylamine, NEt_3 , triphenyl phosphine, PPh_3 , and hexylamine) however if cells are present during the reaction the choice of catalyst is restricted.¹⁵⁸⁻¹⁶¹ In specific cases the reaction conditions can be very mild, for example the nucleophilic thiol-ene reaction can proceed in phosphate buffered saline (PBS) solution under slightly basic conditions (pH 7.4) with no external catalyst utilising the activated alkene.^{162, 163, 164} As demonstrated by Darling *et.al.* who crosslinked maleimide-functional PEG with di-thiol-functionalised peptides to create a thiol-ene hydrogel in buffer solution (pH 7.4).¹⁶⁵ This pathway enabled the encapsulation of human dermal fibroblast (HDF), however the group raised the issue of inconsistency in the hydrogel as a consequence of fast gelation times with the maleimide precursor. This led to the formation of non-uniform hydrogels and a variety of cellular responses depending on where the cell resided in the structure. By slowing down the gelation time of the Michael addition thiol-ene reaction, through creating a tag sequence that could interrupt the thiol-ene reaction, allowed enhanced mixing of the polymer precursors to occur. The resultant uniform hydrogels allowed for clear, representative cellular response to the hydrogel properties at any given location within the structure. This is important for accurate conclusions to be drawn between material properties and cellular response.

However, to increase the gelation time for these hydrogels the tag system employed used a zinc ion to disrupt the thiol-ene reaction which may not be compatible for all cell lines reducing the versatility of this reaction. Furthermore, the hydrogels still formed very rapidly (1 min) therefore many practicality issues remain with this system. In the next section, alternative routes utilising alkyne-based reactions are reviewed to overcome such problems.

1.3. Alkyne Crosslinking Chemistries

1.3.1. Azide-Alkyne Click Cycloaddition Reactions for Hydrogel Synthesis

Alkyne functional groups play an important role in forming biomaterials as highlighted by the advent of click reactions.¹⁵⁰ This has been exploited through their use in copper(I) catalysed azide-alkyne cycloadditions (CuAAC)^{166, 167} and strain-promoted azide-alkyne cycloadditions (SPAAC) reactions,^{50, 168} which have both been used extensively to form click hydrogels *in situ* (Figure 1.5). However, in recent times, the CuAAC reaction has become less favoured for the synthesis of *in situ* hydrogels, because of its low biocompatibility and the inherent difficulty to remove the copper catalyst.^{169, 170} Consequently, the SPAAC reaction was seen as a suitable solution to overcome these drawbacks since the reaction occurs without the need for a toxic copper catalyst.^{171, 172} The intramolecular strain of the cyclooctyne allows it to readily react with an azide at ambient temperatures. Since the potential of the reaction was first discovered by Bertozzi,¹⁶⁹ different cyclooctynes have been developed to increase the reaction time under physiological conditions through the addition of electron-withdrawing groups in the α position of the triple bond (Figure 1.10). The use of fluoro substituents creating difluorinated cyclooctynes (DIFO) increased the reactivity of the alkyne to azides to a similar rate as the CuAAC chemistry. This rate of reactivity could also be achieved through the use of dibenzocyclooctyne (DIBO) molecules. Both these ring strained alkynes have been used for hydrogel synthesis.

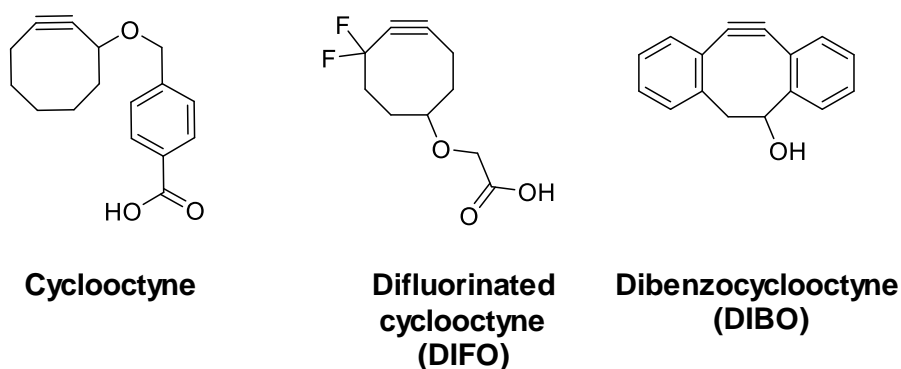


Figure 1.10. Structures of cyclooctynes used in the synthesis of hydrogels through SPAAC.

Initially DeForest *et.al.* used DIFO as a pendant group on a enzymatically-degradable peptide which could react with a 4-arm PEG azide to create a hydrogel in 1 h at 37 °C.¹³⁷ This work also demonstrated the bio-orthogonality of click reactions by employing a secondary thiol-ene click reaction to biopattern the structure. By utilising pendant vinyl functionalities present on the polymer backbone with a thiol-functionalised fluorescent RGD peptides, the structure was able to selectively promote cell attachment. This SPAAC structure could also enzymatically degrade providing an ideal platform to study cell behaviour for tissue engineering applications. In recent times, Li *et.al.* have utilised DIBO- and azide-functional PEGs to form SPAAC hydrogels (Figure 1.11a).¹⁷³ These structures were able to covalently attach a potent neurogenic factor, IFN- γ , to recapture features of the central nervous system. They successfully encapsulated neutral stem/progenitor cell cultures (NSPCs) in water at room temperature. Interestingly the group investigated the affect UV light and free radical photoinitiators had on the viability of encapsulated NSPCs after gelation (Figure 1.11c). They found that the cell metabolic activity decreased when the cells were exposed to the UV light/photoinitiator conditions suggesting that these conditions, needed for popular radical click reactions (*e.g.* thiol-ene

reactions), could be detrimental to cell proliferation (Figure 1.11d). Overall, the bio-orthogonal nature and appropriate mechanical properties of these SPAAC hydrogels provides great potential for these scaffolds in tissue engineering especially for neural regeneration (*e.g.* treatment of Parkinson's disease, spinal cord injuries and strokes).¹⁷³ Although this reaction overcomes many of the issues with CuAAC and thiol-ene click reactions, the synthesis of the ring-strained cyclooctyne has proven difficult and they are costly to purchase from commercial suppliers. This has stunted the development of SPAAC reactions to produce commercially relevant biomaterials.¹⁷⁴

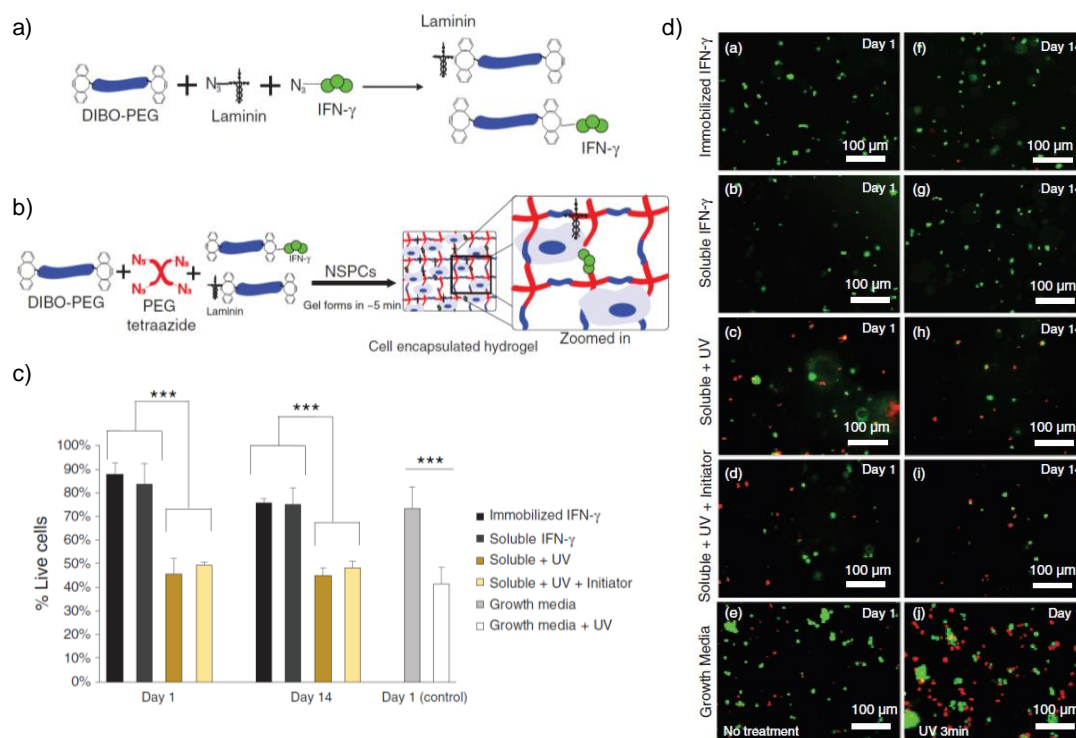


Figure 1.11. a) Schematic for neurogenic click hydrogel network formation. (a) DIBO-PEG reacted with azide-IFN-c or separately azidelamininto form DIBO-PEG-proteins for subsequent reactions, (b) DIBO-PEG-protein, PEG tetraazide plus NSPCs form a stem cell encapsulated hydrogel able to specify neuronal differentiation in 3D, c) Cell viability assayed by Live/Dead tested at day 1 and day 14 for NSPCs exposed to the listed treatments. d) Live/Dead assay results indicate cell viability differences when ultraviolet light exposure occurred (3 min, 2.7 mW/cm²) at day 1 and day 14. Live cells stain green, dead cells stain red. Adapted from ref. 172.

1.3.2. Thiol-yne Click Reactions

An alkyne reaction which has received less attention since the introduction of click reactions to hydrogel synthesis is the thiol-yne addition reaction (Figure 1.12).¹⁷⁵ Similar to other click reactions, it does not produce any by-products and occurs under mild reaction conditions, resulting in high yields which highlights its potential as a method to synthesise biomaterials.¹⁷⁶⁻¹⁷⁸ Analogous to the thiol-ene reaction, the thiol-yne addition reaction can follow two pathways; 1) the radical-initiated pathway using UV light and an initiator or 2) through the nucleophilic pathway (Michael addition) using a base to catalyse the reaction (Figure 1.13).¹⁷⁸ However, unlike the thiol-ene reaction, the thiol-yne can add two thiol molecules to one alkyne, increasing its potential for polymer coupling and the formation of hyperbranched structures.¹⁷⁹

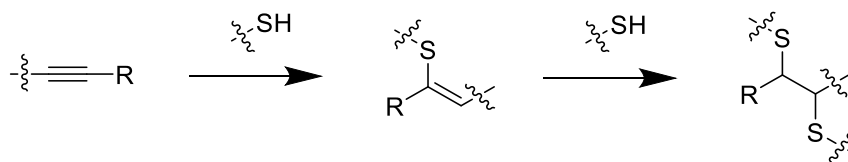


Figure 1.12. Reaction scheme for the thiol-yne reaction

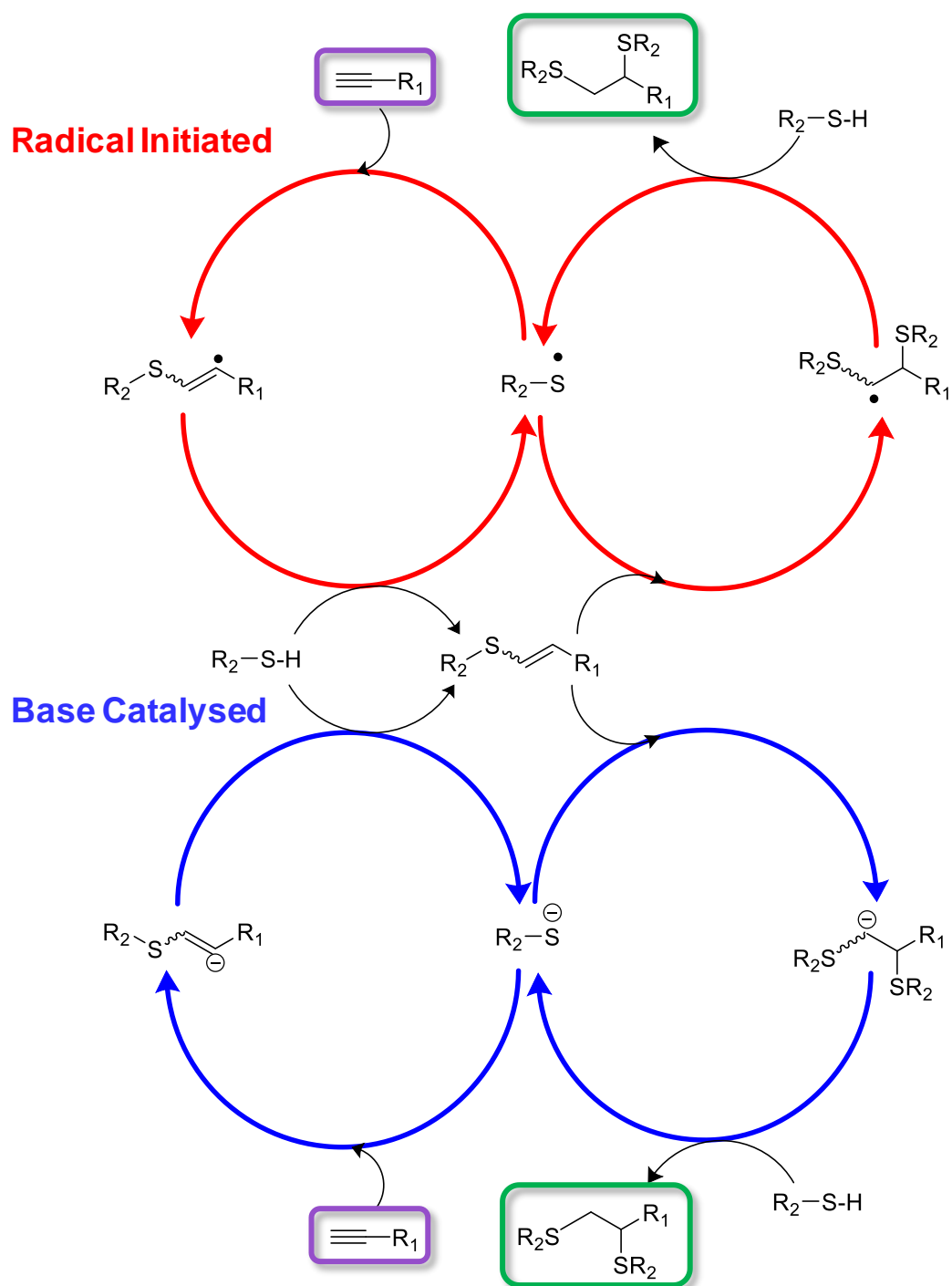


Figure 1.13. The two reaction mechanisms radical initiated, (red arrows) and base catalysed, (blue arrows) for the thiol-yne reaction demonstrating the ability to add two thiols to one alkyne molecule.

Although first noted in 1935,¹⁸⁰ when the properties of unsaturated sulfur compounds were investigated, the thiol-yne addition reaction was only sporadically used through the 20th century; Kohler and Potter¹⁸⁰ reported the rapid formation of vinyl thioethers in both stereochemical forms by adding thiocresol to phenylacetylene. This was further noted by Bader *et.al.* in 1949, when hex-1-yne was reacted with a variety of thiols, and the vinyl thioether product was formed.¹⁸¹ Both the mono and di adducts were observed when using thioacetic acid, albeit the yields were low (53%). Interestingly, in this early work, it was noted that the reaction proceeded in high yields without the use of a radical initiator through the use of *p*-methoxyphenylacetylene, an activated alkyne. This allowed the formation of the mono-addition product highlighting the reactivity of activated alkynes towards thiols in the thiol-yne reaction. This indicated an alternative pathway could be used instead of the radical route to form vinyl thioethers. Although stated in these early papers, the reaction has only received a small amount of use in recent decades.^{182, 183} However, since it combines two of the most widely used functional groups in click chemistry, alkynes and thiols, its popularity in polymer chemistry and materials science is increasing, and its true potential as a crosslinking reaction is starting to be unveiled.¹⁷⁹

1.3.2.1. Radical-Initiated Thiol-yne Click Reaction

The radical thiol-yne reaction, like its counterpart thiol-ene reaction, has been more popular than the alternative base-catalysed route. It has been used for a range of different applications in polymer science (*e.g.* modification of peptides and proteins, polymer-polymer coupling and post modification reaction) owing to its mild reaction conditions and the natural abundance of functional groups.¹⁷⁵ The radical pathway adopts

a similar mechanism to the radical thiol-ene reaction (Figure 1.13). Briefly, a thiyl radical, generated thermally or photochemically, attacks the alkyne to form a vinyl thioether radical. This forms a vinyl thioether through the chain transfer reaction of another thiol. Under certain conditions, the vinyl thioether is quickly attacked again by a thiyl radical resulting in a 1,2 bis-addition dithioether product.¹⁷⁵

Established by Bowman and co workers in 2008 as a photopolymerisation reaction to synthesise highly cross-linked networks, the group also investigated the kinetics of the reaction in comparison to its thiol-ene analogy.¹⁷⁷ By utilising different alkynes, they were able to highly crosslink polymers to create networks with improved homogeneity, which were also over six times the density of the thiol-ene equivalent polymers as a result of two thiols adding to one alkyne molecule. These enabled the production of a new class of functional and structurally tailored materials. Further to this, the rate of the radical thiol-yne reaction was independent of the alkyne concentration and instead dependent on the thiol concentration, which dictated the mechanism of polymer coupling. Hence, the mechanism deviated from the step growth characteristics to homo- or copolymerisation, as the reaction becomes thiol limited. The increased crosslinked density resulted in materials with higher glass transition temperature, which could be post modified when polymerisation was off-stoichiometry. This work highlighted the use of the radical thiol-yne reaction to synthesise functional polymer networks, with unique physical and chemical properties.

An established field for radical thiol-yne chemistry is in the preparation of hyperbranched polymers pioneered by Perrier and co workers in 2009.¹⁸⁴ They

synthesised functional hyperbranched polymers at room temperature in high yields and in a short time scale (*e.g.* 2 h). Polymers with both alkyne and thiol functionalities were synthesised through radical addition-fragmentation chain transfer (RAFT) polymerisations of styrene, mediated by an alkyne-functional chain transfer agent.¹⁸⁵ The resultant polymer then underwent thiol-yne photopolymerisation with UV irradiation to yield a range of hyperbranched polymers. The molecular weight and branching of these materials was assessed to reveal the dependency of the molecular weight of the RAFT polymer, on the resultant size of the hyperbranched structure.¹⁸⁶ This was further explored to create functional hyperbranched structures¹⁸⁷ and to synthesise networks with well-controlled molecular weights and distributions, while maintaining very high degrees of branching through a monomer feeding approach.¹⁸⁸ Recently, through the use of poly(2-oxazoline) (POx), to create a shell around the hyperbranched structures, the group synthesised well defined ‘hyperstar’ copolymers (Figure 1.14a)¹⁸⁹ that could encapsulate Nile red into the core of the structure. Furthermore, the hyperstars were cytocompatible and able to pass through the cellular membrane into the cytoplasm of human ovarian carcinoma cells, but not in the mitochondria, demonstrating an energy dependent uptake into cells, as expected for a structure of that size (Figure 1.14b). Hence, the synthesis of functional, well-defined thiol-yne hyperbranched polymers demonstrates the favourable characteristics of the thiol-yne reaction; high efficiency, mild reaction conditions and fast reaction times.

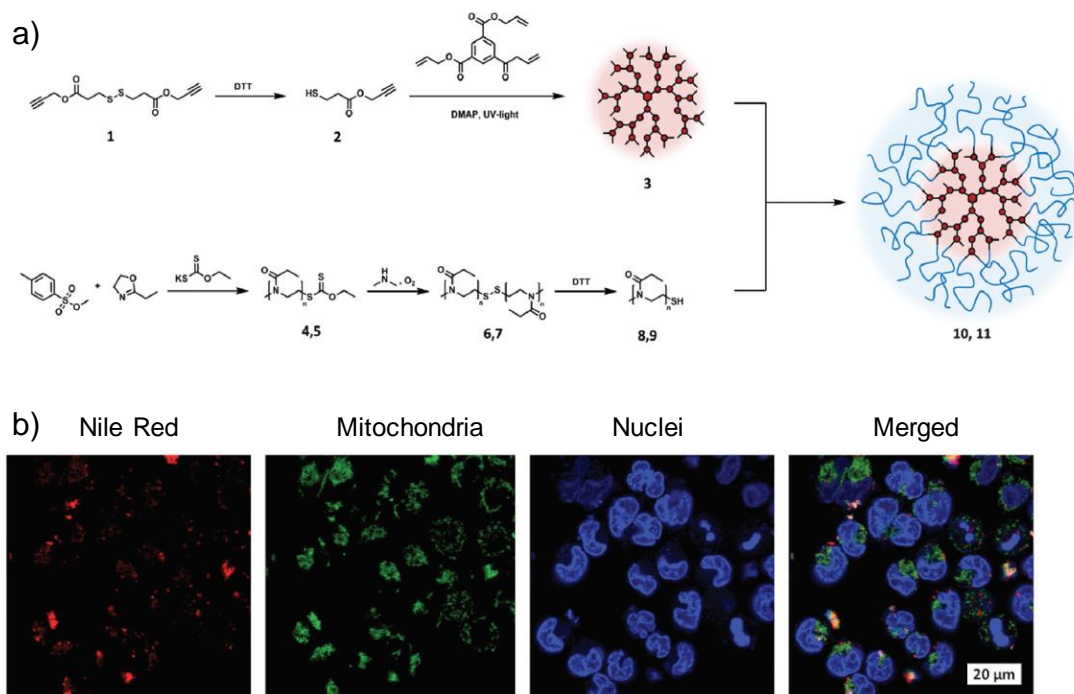


Figure 1.14. a) Schematic representation of the synthesis of thiol-yne and POx based hyperstar copolymers, b) Confocal images of A2780 human ovarian carcinoma cells treated with Nile red loaded hyperstars. Figure modified from ref 189.

To expand the use of the radical thiol-yne chemistry, it has further been applied to the preparation of networks from polyesters. Concellón *et.al.*¹⁹⁰ reported the synthesis of degradable thiol-yne polylactide (PLA) networks by crosslinking alkyne-functional PLA with pentaerythritol tetrakis (3-mercaptopropionate) in the presence of a photoinitiator in dichloromethane (CH_2Cl_2 , Figure 1.15a). Interestingly, for cell patterning applications, they generated microstructures with this material through direct laser writing (Figure 1.15c).

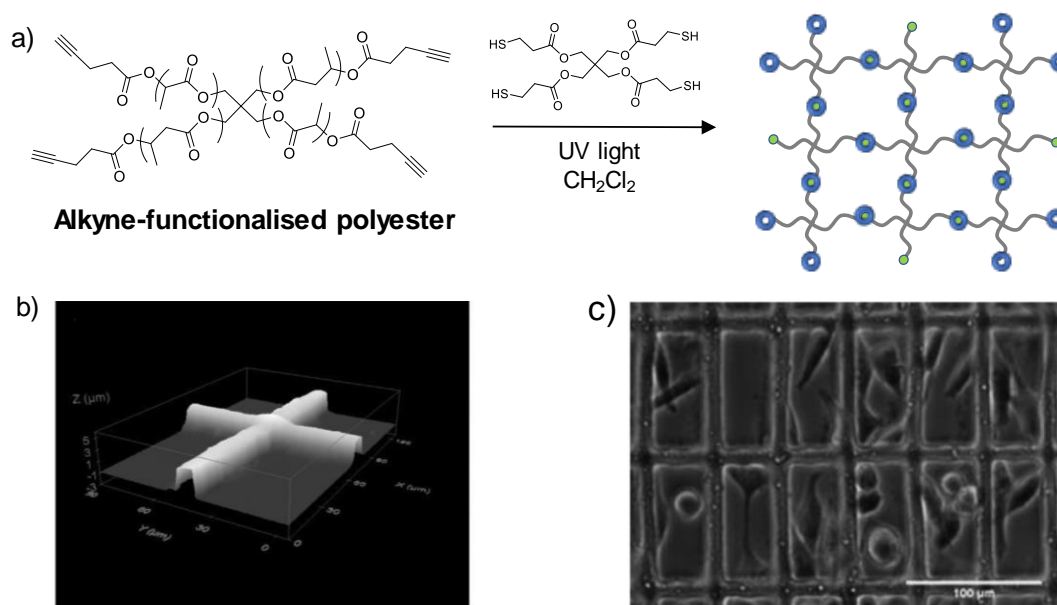


Figure 1.15. a) Thiol-yne photopolymerisation of alkyne functionalised polyester, synthesised from lactide, b) topography image of crossing lines generated by direct laser writing, c) cell cultured on substrates with different widths of polylactide microstructures after 48 h. Modified from reference 190.

This thiol-yne chemistry has also been applied to crosslinking polymers in water to create hydrogels. Daniele *et.al.* synthesised interpenetrating networks (IPNs) as tissue scaffolds,¹⁹¹ utilising both the thiol-yne and thiol-ene reactions through simultaneous radical pathways to create intertwined hydrogel networks (Figure 1.16). 4-arm PEG thiol precursors reacted with both; 4-arm PEG alkyne, to create a well-defined PEG thiol-yne network and Gelatin methacrylamide, to create a secondary thiol-ene network. The resultant scaffold exhibited robust mechanical properties, which influenced the extent of adhesion and proliferation of encapsulated cells. Furthermore, ECM proteins were covalently attached into the matrix, allowing for the long-term study of cells in a 3D environment.

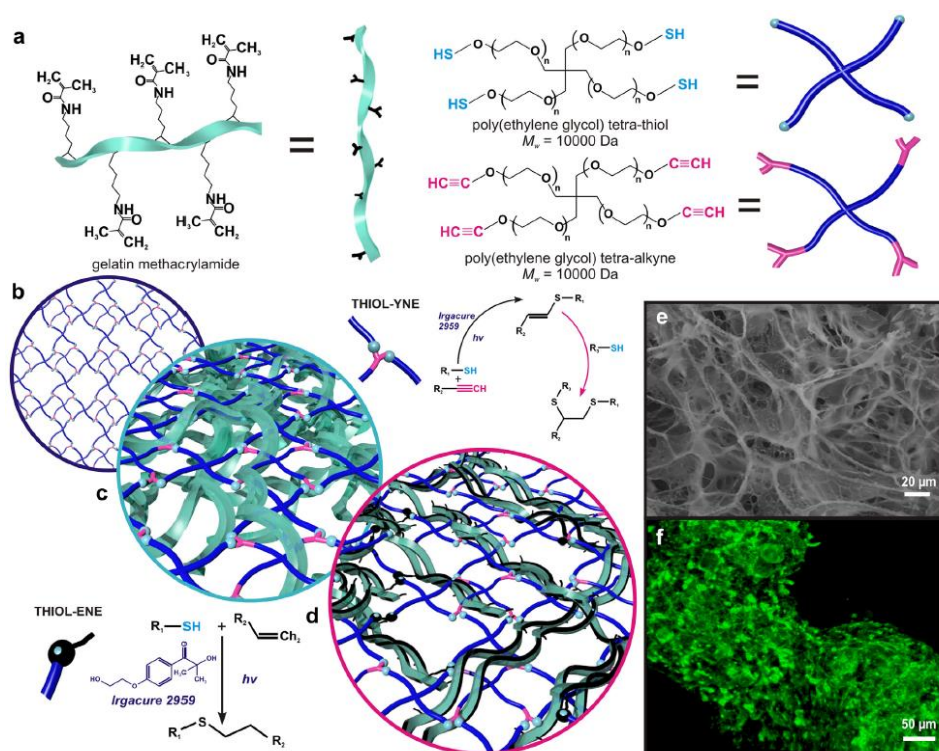


Figure 1.16. Fabrication of bio/synthetic interpenetrating network (BioSIN) of (a) gelatin methacrylamide and PEG *via* concurrent photoinitiation of thiol-ene and thiol-yne coupling. The click-functionalised macromer precursors undergo multi-mode crosslinking to form an interlocking 3D hydrogel, (b) The well-defined network architecture of TYC-formed PEG hydrogels were intertwined with either, (c) physically-incorporated gelatin (BioSIN), or (d) covalently crosslinked gelatin methacrylamide (BioSIN.) in which the gelatin methacrylamide reacts with both itself and the PEG network. (e) The architectural heterogeneity emulated native extracellular matrix, and (f) superior physiochemical properties were able to support the continued proliferation of encapsulated cells, where cytoskeletal F-actin fibre staining illustrates the density and interaction of encapsulated cells. Figure adapted from ref 191.

The radical thiol-yne reaction has also been used to postmodify a range of hydrogels because of its robust and efficient nature. Glutathione was used to post modified thiol-yne hydrogels through residual pendant alkyne groups in hydrogel networks,¹⁹² while β -cyclodextrin has been ‘clicked’ on to pHEMA hydrogels through this chemistry to increase the hydrogels performance as a drug delivery vehicle.¹⁹³ These works emphasise the benefits of the radical thiol-yne reaction as a route to synthesise polymeric networks and the ability to post modify materials in a simple and efficient manner.

1.3.2.2. Nucleophilic Thiol-yne Click Reaction

The addition of thiols to alkynes following a nucleophilic mechanism does not require an initiator or the use of UV light, therefore exhibiting a reaction with a lot of potential.¹⁷⁵ The nucleophilic pathway was first investigated by Cristol *et.al.*¹⁹⁴ and Truce and Simms,¹⁹⁵ who studied in depth the stereochemistry of the resultant vinyl thioether product. Through the base catalysed route, they investigated three alkynes (phenylacetylene, 2-butyne and 1-hexyne), which all formed the mono-addition product when reacted with *p*-toluenethiol in ethanol. The stereochemistry of the resultant products was investigated, and they concluded that the stereochemistry of the product was dictated by the starting alkyne used. Phenylacetylene produced exclusively the *cis* product, while 2-butyne gave high *trans* product and 1-hexyne yielded both isomers (Figure 1.17). The rationale for this reactivity was attributed to the stability of the intermediate carbanion. If the carbanion was stabilised (*e.g.* through the aromatic group in phenylacetylene) then the *cis* isomer was favoured. This work highlighted a unique characteristic of the nucleophilic thiol-yne addition reaction, the stereochemical control of the vinyl thioether product through the properties of the starting alkyne.¹⁹⁶

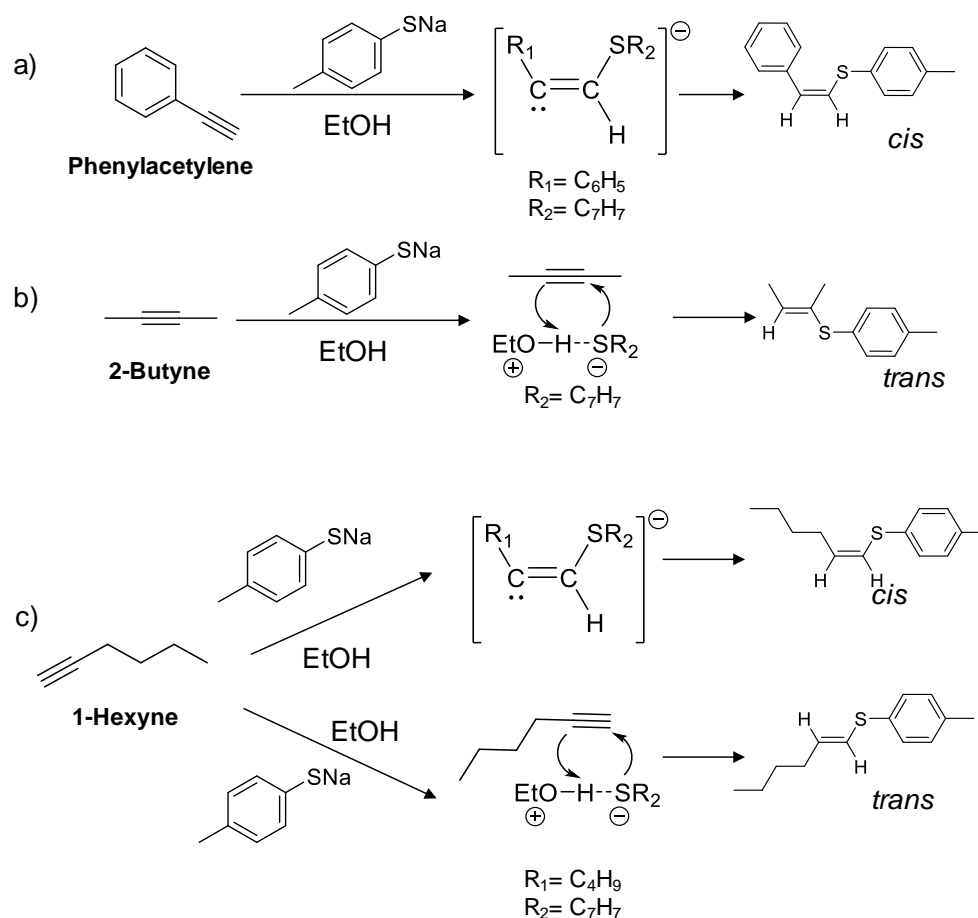


Figure 1.17. Reaction scheme of the thiol-yne experiment carried out by Truce and Simms demonstrating the stereocontrol of the thiol alkene product. Ref 195.

Furthermore, the polarity of the solvent and the strength of the base used to catalyse the reaction can also play an important role in dictating the stereochemistry of the resultant monoaddition product.^{196, 197} Through the use of a polar solvent and/or a strong base the *cis* vinyl thioether is favoured, as a result of a stable carbocation formation after the addition of a thiolate ion (Figure 1.18). The carbocation can then be protonated to form the *cis* isomer. In contrast, when the reaction takes place in non polar solvents with or without a weak base, the *trans* isomer is obtained, primarily as the conditions cause a thiol-base pair to form through hydrogen bonding. This arrangement then favours the attack of the alkyne by the hydrogen bonded pair from the same side, resulting in the

production of the *trans* isomer. Hence, this characteristic can be easily exploited to fabricate stereocontrolled vinyl thioethers through the careful choice of the catalyst and solvent system. For example, products with high *cis* content (94%) can be obtained by conducting the reaction in water, whereas high *trans* content (97%) dominate when CHCl_3 and NEt_3 are used instead.

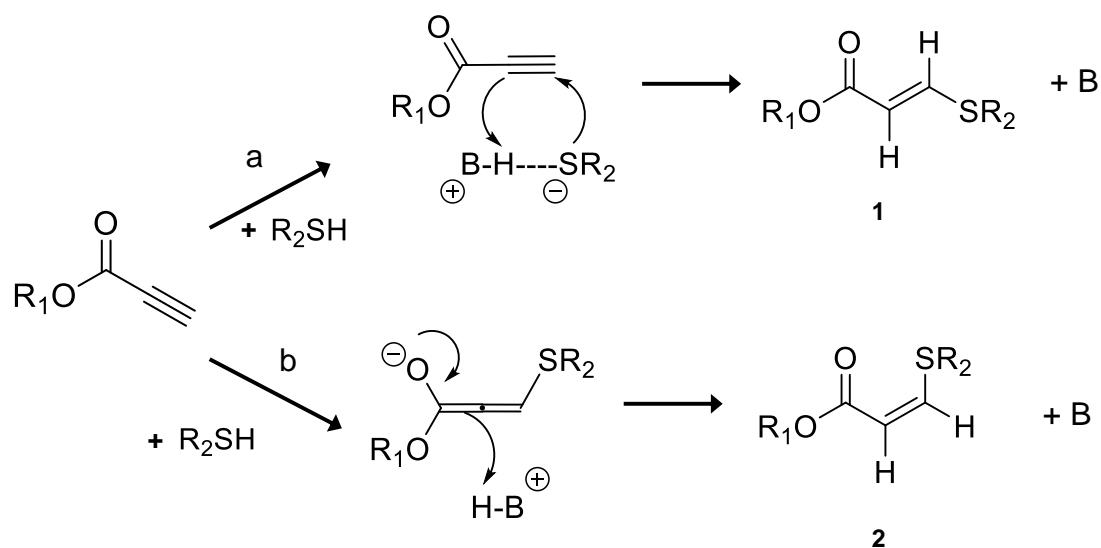


Figure 1.18. Mechanism for the stereochemical control over the nucleophilic thiol-yne reaction. a) Non polar solvent and/or weak base to form the *trans* isomer (1); b) polar solvent and/or strong base to form the *cis* isomer (2). Adapted from ref 197.

Applying the nucleophilic thiol-yne reaction to material synthesis, Yao *et.al.*¹⁹⁸ described the formation of linear poly(vinylene sulfide)s without the use of a catalyst in THF at 30 °C, highlighting the speed and mild conditions needed for the thiol-yne reaction. Bell *et.al.* utilised the stereochemical control property of the thiol-yne reaction to synthesise step-growth elastomers in different solvent/catalyst systems to create a range of materials with different mechanical properties (Figure 1.19).¹⁹⁹ Specifically, highly stretchable elastomers contained a high *trans* content, whereas high *cis* vinyl thioether

bonds led to an increased crystallinity and higher Young's moduli, which resulted in more rigid and brittle materials (Figure 1.19b). This work highlighted the potential of the stereocontrolled nucleophilic thiol-yne reaction to the formation of stereospecific materials with a range of mechanical properties.

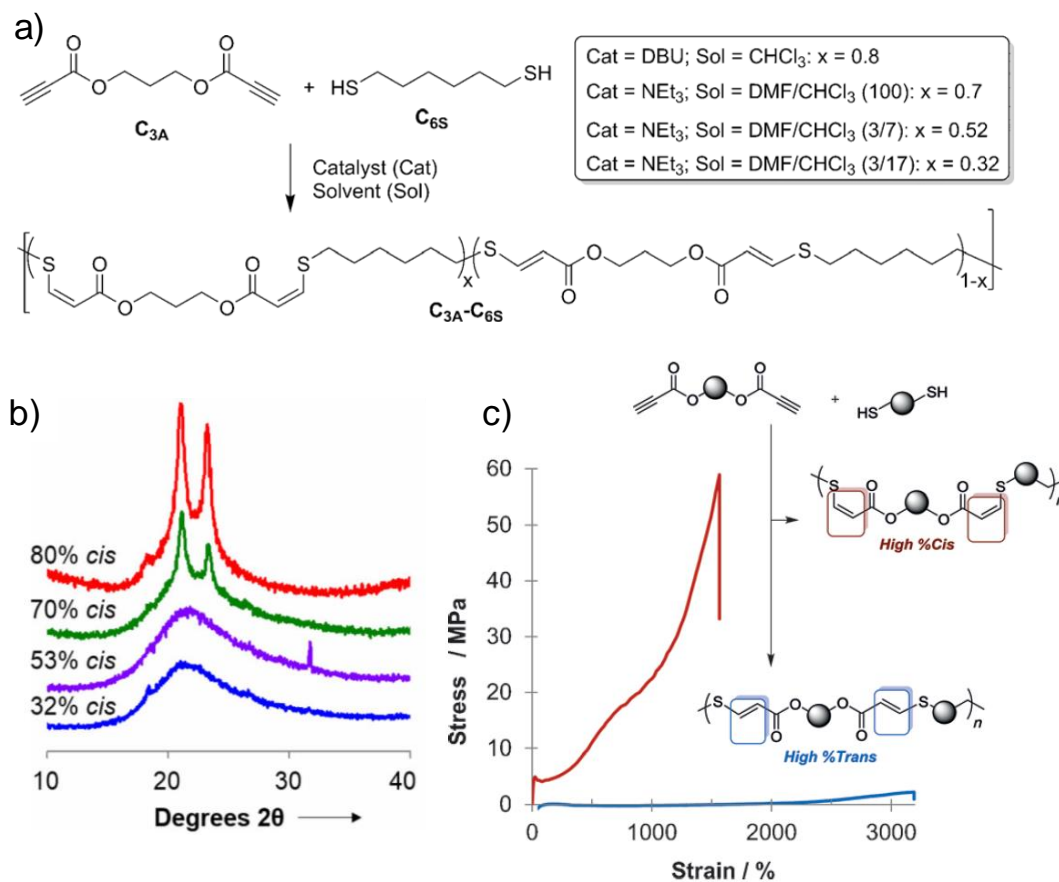


Figure 1.19. a) Synthesis of thiol-yne elastomer materials from dialkyne and dithiol precursors, b) Wide-angle X-ray diffraction of the elastomers demonstrating the effect stereochemistry has on the crystallinity of the material, c) Change in mechanical properties of thiol-yne elastomers with different stereochemistries. Adapted from ref 199.

In hydrogel synthesis, the nucleophilic thiol-yne reaction has been employed to form dense PEG networks as part of a double network (DN) hydrogel for cartilage regeneration.²⁰⁰ Through the functionalisation of commercially available multi-arm PEG

with electron-deficient alkyne and thiol end groups, the nucleophilic thiol-yne reaction occurred in PBS solution (pH 7.4) without the need of an external base catalyst. The slightly basic pH of the PBS solution catalysed the reaction and allowed these networks to form simultaneously with an inverse electron-demand Diels-Alder reaction between a norbornene-functionalised chitosan with a tetrazine-functionalised PEG (Figure 1.20a). The resultant double network hydrogel (10 wt%) reached up to 15 MPa compressive stress at 98% strain and was repeatedly compressed up to 10 times without hysteresis. Furthermore, hMSCs were easily encapsulated within the double network with excellent cell viability and distribution (Figure 1.20d). Therefore, the nucleophilic thiol-yne reaction is cytocompatible and shows immense potential as a platform for hydrogel production.

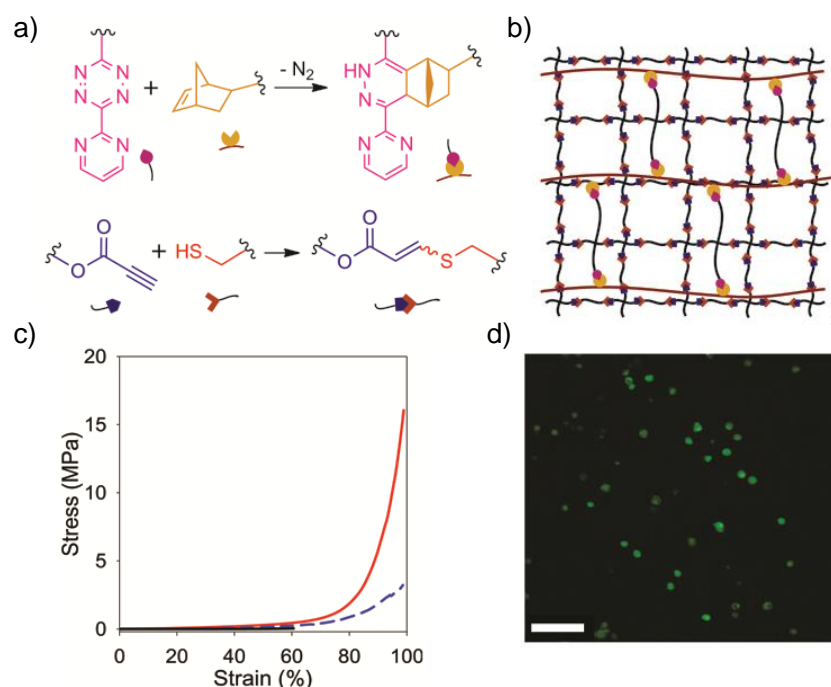


Figure 1.20. a) Schematic of tetrazine-norbornene and nucleophilic thiol-yne addition chemistries used for double network (DN) hydrogel fabrication, b) Schematic of the DN, c) Representative compression curves of dense SN gel (dash blue line), loose SN gel (black line), and DN gel (red line), d) Representative live/dead image of hMSCs 48 h post encapsulation (green cell = alive, red cell = dead); scale bar = 100 μ m. Figures adapted for ref 200.

Moreover, the nucleophilic thiol-yne reaction has also been used to form hydrogel scaffolds with antibacterial properties. Cai *et.al.*²⁰¹ synthesised nucleophilic thiol-yne PEG hydrogels with different stoichiometric ratios of alkyne to thiol end groups. The network was then post modified with a thiol-functionalised antimicrobial peptide *via* a second nucleophilic thiol-yne reaction, resulting in a thiol-yne PEG network which was effective against bacterial growth. The group confirmed the cytocompatibility of the thiol-yne hydrogel with 3T3 fibroblast cells, and further demonstrated the material as a wound dressing. In summary, although still in its infancy, the potential of the nucleophilic thiol-yne reaction to render functional and dynamic materials for biomedical and tissue engineering applications is vast.

1.3.3. Emerging Alkyne Click Reactions

It is evident in recent literature the popularity of click reactions and the development and progression they have made in material synthesis.²⁰² For instance, amino-yne and phenol-yne have both been presented as new click reactions for the formation of biomaterials,²⁰³ each with their own advantages over previous click chemistries. In detail, the amino-yne click reaction was applied by He *et.al.* to form poly(β -aminoacrylates) by reacting dipropiolates with diamines in CH₂Cl₂ at room temperature.²⁰⁴ Interestingly, the reactivity of the ester-alkynes was high enough that an external catalyst was not required. Using the amino-yne reaction, the group prepared regio- and stereospecific polymers with high molecular weights. Through further optimisation, the amino-yne reaction has also been implemented in hydrogel synthesis²⁰⁵ to crosslink ester-alkyne functionalised PEG with amine groups naturally found in

chitosan (Figure 1.21). These cytocompatible hydrogels, which were injectable and formed under physiological condition, degraded through changes in pH.

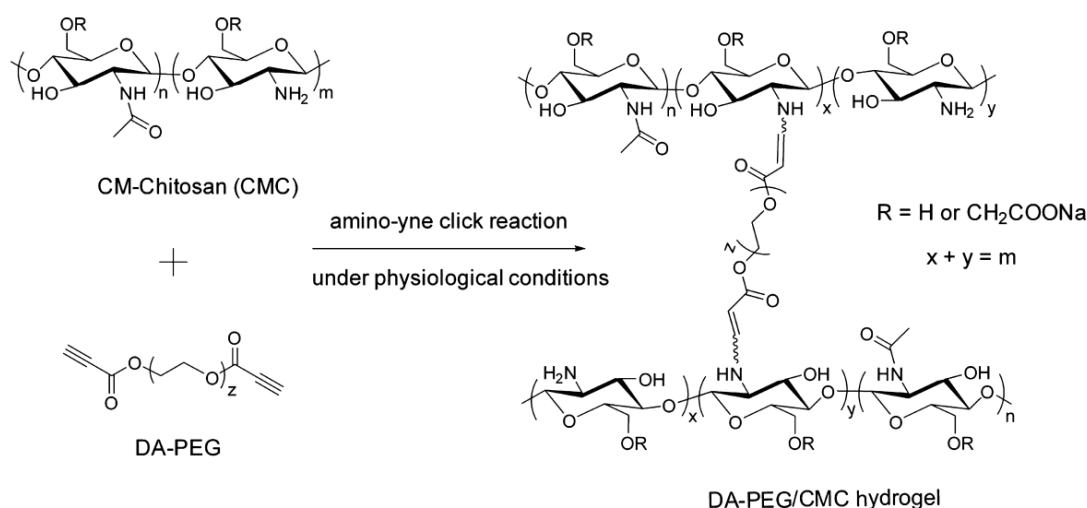


Figure 1.21. Schematic of the PEG/Chitosan amino-yne hydrogels under physiological conditions. Modified from ref 205.

Recently, phenyl-yne click reactions between ester-activated alkynes and phenols have been shown to form regio- and stereoregular poly(vinylene ether ketone)s.²⁰⁶ In a similar manner to the thiol-yne and amino-yne reactions, these polymerisation reactions result in high molecular weight polymers in high yields. These polymers, which easily degrade through acidic conditions, are conceived as a promising platform for the design of biomedical devices. However, to expand the application of this route, the reaction conditions need further optimisation. Currently, strong Lewis bases catalyse the reaction, a route that is incompatible with cells, preventing its use in clinical settings. However, exploring this reaction is still in its early stages but this initial study demonstrates its huge potential for the synthesis of biomaterials.

1.4. Conclusions

In the last decade, the scientific community and, especially, material scientists have witnessed the explosion of research into hydrogel-based biomaterials as their true potential has emerged; from mimicking a range of biological environments to their use as drug delivery vehicles and wound dressings. Undeniably, this success is down to their versatile nature based on the possibility of using many different polymers, with a range of different properties, and synthetic routes to prepare them. This chapter has summarised the key advances made in the hydrogel field, focusing on the crosslinking chemistry used to form these structures. Among them, the thiol-yne reaction has been highlighted as an advantageous crosslinking chemistry for the synthesis of biomaterials which still has significant potential to form dynamic materials for a range of applications. Overall, this chapter has highlighted the important role chemistry plays in the formation of dynamic and responsive hydrogels. These materials have the potential to advance our understanding on a range of complex biological process and the use of hydrogels as devices to screen and develop new drugs and biomedical devices.

1.5. References

1. F. Horkay and G. B. McKenna, in *Physical Properties of Polymers Handbook*, ed. J. E. Mark, Springer New York, New York, NY, 2007, pp. 497-523.
2. A. S. Hoffman, *Adv. Drug Delivery Rev.*, 2002, **54**, 3-12.
3. D. Seliktar, *Science*, 2012, **336**, 1124-1128.
4. Y. Li, J. Rodrigues and H. Tomas, *Chem. Soc. Rev.*, 2012, **41**, 2193-2221.
5. K. Y. Lee and D. J. Mooney, *Chem. Rev.*, 2001, **101**, 1869-1879.
6. J. A. Burdick and W. L. Murphy, *Nat. Commun.*, 2012, **3**, 1269.
7. X. Chen, B. D. Martin, T. K. Neubauer, R. J. Linhardt, J. S. Dordick and D. G. Rethwisch, *Carbohydr. Polym.*, 1995, **28**, 15-21.
8. P. C. Nicolson and J. Vogt, *Biomaterials*, 2001, **22**, 3273-3283.
9. O. Wichterle and D. LÍM, *Nature*, 1960, **185**, 117.
10. B. D. Ratner, A. S. Hoffman, F. J. Schoen and J. E. Lemons, *Biomaterials Science: An Introduction to Materials in Medicine*, Elsevier Science, 2004.
11. J. C. Bray and E. W. Merrill, *J. Appl. Polym. Sci.*, 1973, **17**, 3779-3794.
12. C. M. Kirschner and K. S. Anseth, *Acta Mater.*, 2013, **61**, 931-944.
13. F. Redaelli, M. Sorbona and F. Rossi, in *Bioresorbable Polymers for Biomedical Applications*, Woodhead Publishing, 2017, pp. 205-228.
14. Z. Ahmad and R. F. T. Stepto, *Colloid. Polym. Sci.*, 1980, **258**, 663-674.

15. W. H. Stockmayer, *J. Chem. Phys.*, 1943, **11**, 45-55.
16. W. H. Stockmayer, *The Journal of Chemical Physics*, 1944, **12**, 125-131.
17. P. J. Flory, *J. Phys. Chem.*, 1942, **46**, 132-140.
18. P. J. Flory, *J. Am. Chem. Soc.*, 1941, **63**, 3083-3090.
19. P. J. Flory and J. R. Jr., *The Journal of Chemical Physics*, 1943, **11**, 521-526.
20. M. C. Koetting, J. T. Peters, S. D. Steichen and N. A. Peppas, *Mater. Sci. Eng. R-Rep.*, 2015, **93**, 1-49.
21. S. P. Zustiak and J. B. Leach, *Biomacromolecules*, 2010, **11**, 1348-1357.
22. N. A. Peppas, J. Z. Hilt, A. Khademhosseini and R. Langer, *Adv. Mater.*, 2006, **18**, 1345-1360.
23. P. M. Kharkar, K. L. Kiick and A. M. Kloxin, *Chem. Soc. Rev.*, 2013, **42**, 7335-7372.
24. A. J. Engler, S. Sen, H. L. Sweeney and D. E. Discher, *Cell*, 2006, **126**, 677-689.
25. A. J. Engler, M. A. Griffin, S. Sen, C. G. Bönnemann, H. L. Sweeney and D. E. Discher, *J. Cell Biol.*, 2004, **166**, 877-887.
26. D. E. Discher, P. Janmey and Y.-l. Wang, *Science*, 2005, **310**, 1139-1143.
27. J. Zhu and R. E. Marchant, *Expert Rev. Med. Devices*, 2011, **8**, 607-626.
28. E. L. S. Fong, S.-E. Lamhamedi-Cherradi, E. Burdett, V. Ramamoorthy, A. J. Lazar, F. K. Kasper, M. C. Farach-Carson, D. Vishwamitra, E. G. Demicco, B. A.

- Menegaz, H. M. Amin, A. G. Mikos and J. A. Ludwig, *Proc. Natl. Acad. Sci. USA*, 2013, **110**, 6500-6505.
29. S. C. Owen and M. S. Shoichet, *J. Biomed. Mater. Res., Part A*, 2010, **94A**, 1321-1331.
30. Y. Luo and M. S. Shoichet, *Nat. Mater.*, 2004, **3**, 249.
31. B. K. Mann, A. S. Gobin, A. T. Tsai, R. H. Schmedlen and J. L. West, *Biomaterials*, 2001, **22**, 3045-3051.
32. M. Guvendiren and J. A. Burdick, *Curr. Opin. Biotechnol.*, 2013, **24**, 841-846.
33. D. Antoni, H. Burckel, E. Josset and G. Noel, *Int. J. Mol. Sci.*, 2015, **16**, 5517.
34. W. L. Murphy, T. C. McDevitt and A. J. Engler, *Nat. Mater.*, 2014, **13**, 547-557.
35. O. Chaudhuri, S. T. Koshy, C. Branco da Cunha, J.-W. Shin, C. S. Verbeke, K. H. Allison and D. J. Mooney, *Nat. Mater.*, 2014, **13**, 970.
36. O. Chaudhuri, L. Gu, D. Klumpers, M. Darnell, S. A. Bencherif, J. C. Weaver, N. Huebsch, H.-p. Lee, E. Lippens, G. N. Duda and D. J. Mooney, *Nat. Mater.*, 2015, **15**, 326.
37. Z. Gong, S. E. Szczesny, S. R. Caliri, E. E. Charrier, O. Chaudhuri, X. Cao, Y. Lin, R. L. Mauck, P. A. Janmey, J. A. Burdick and V. B. Shenoy, *Proc. Natl. Acad. Sci. USA*, 2018, **115**, E2686-E2695.
38. J. A. Burdick, C. Chung, X. Jia, M. A. Randolph and R. Langer, *Biomacromolecules*, 2005, **6**, 386-391.

39. B. Trappmann, B. M. Baker, W. J. Polacheck, C. K. Choi, J. A. Burdick and C. S. Chen, *Nat. Commun.*, 2017, **8**, 371.
40. M. P. Lutolf and H. M. Blau, *Adv. Mater.*, 2009, **21**, 3255-3268.
41. N. Gjorevski and C. M. Nelson, *Cytokine Growth Factor Rev.*, 2009, **20**, 459-465.
42. M. C. Regier, S. I. Montanez-Sauri, M. P. Schwartz, W. L. Murphy, D. J. Beebe and K. E. Sung, *Biomacromolecules*, 2017, **18**, 709-718.
43. F. M. Watt and W. T. S. Huck, *Nat. Rev. Mol. Cell Biol.*, 2013, **14**, 467.
44. C. G. Williams, A. N. Malik, T. K. Kim, P. N. Manson and J. H. Elisseeff, *Biomaterials*, 2005, **26**, 1211-1218.
45. Y. Jiang, J. Chen, C. Deng, E. J. Suuronen and Z. Zhong, *Biomaterials*, 2014, **35**, 4969-4985.
46. D. L. Alge, M. A. Azagarsamy, D. F. Donohue and K. S. Anseth, *Biomacromolecules*, 2013, **14**, 949-953.
47. M. A. Azagarsamy and K. S. Anseth, *ACS Macro Lett.*, 2013, **2**, 5-9.
48. B. V. Slaughter, S. S. Khurshid, O. Z. Fisher, A. Khademhosseini and N. A. Peppas, *Adv. Mater.*, 2009, **21**, 3307-3329.
49. E. S. Place, J. H. George, C. K. Williams and M. M. Stevens, *Chem. Soc. Rev.*, 2009, **38**, 1139-1151.
50. C. A. DeForest, E. A. Sims and K. S. Anseth, *Chem. Mater.*, 2010, **22**, 4783-4790.

51. R. S. Stowers, S. C. Allen and L. J. Suggs, *Proc. Natl. Acad. Sci. USA*, 2015, **112**, 1953-1958.
52. M. W. Tibbitt and K. S. Anseth, *Biotechnol. Bioeng.*, 2009, **103**, 655-663.
53. E. A. Appel, J. del Barrio, X. J. Loh and O. A. Scherman, *Chem. Soc. Rev.*, 2012, **41**, 6195-6214.
54. N. A. Peppas and A. R. Khare, *Adv. Drug Delivery Rev.*, 1993, **11**, 1-35.
55. K. S. Anseth and H. A. Klok, *Biomacromolecules*, 2016, **17**, 1-3.
56. J. L. Drury and D. J. Mooney, *Biomaterials*, 2003, **24**, 4337-4351.
57. D. Puppi, F. Chiellini, A. M. Piras and E. Chiellini, *Prog. Polym. Sci.*, 2010, **35**, 403-440.
58. Y. Qiu and K. Park, *Adv. Drug Deliv. Rev.*, 2001, **53**, 321-339.
59. E. Caló and V. V. Khutoryanskiy, *Eur. Polym. J.*, 2015, **65**, 252-267.
60. Y. Nishida, S. Ohtsuki, Y. Araie, Y. Umeki, M. Endo, T. Emura, K. Hidaka, H. Sugiyama, Y. Takahashi, Y. Takakura and M. Nishikawa, *Nanomed. Nanotechnol. Biol. Med.*, 2016, **12**, 123-130.
61. A. Dasgupta, J. H. Mondal and D. Das, *RSC Advances*, 2013, **3**, 9117-9149.
62. W. Zhao, X. Jin, Y. Cong, Y. Liu and J. Fu, *J. Chem. Technol. Biotechnol.*, 2013, **88**, 327-339.
63. T. Coviello, P. Matricardi, C. Marianecchi and F. Alhaique, *J. Control. Release*, 2007, **119**, 5-24.

64. E. E. Antoine, P. P. Vlachos and M. N. Rylander, *Tissue Eng., Part B*, 2014, **20**, 683-696.
65. P. B. Malafaya, G. A. Silva and R. L. Reis, *Adv. Drug Delivery Rev.*, 2007, **59**, 207-233.
66. F. Ahmadi, Z. Oveisi, S. M. Samani and Z. Amoozgar, *Res. Pharm. Sci.*, 2015, **10**, 1-16.
67. R. Ahmadi and J. D. d. Bruijn, *J. Biomed. Mater. Res., Part A*, 2008, **86A**, 824-832.
68. H. T. Ta, H. Han, I. Larson, C. R. Dass and D. E. Dunstan, *Int. J. Pharm.*, 2009, **371**, 134-141.
69. A. D. Augst, H. J. Kong and D. J. Mooney, *Macromol. Biosci.*, 2006, **6**, 623-633.
70. J. A. Rowley, G. Madlambayan and D. J. Mooney, *Biomaterials*, 1999, **20**, 45-53.
71. K. Y. Lee and D. J. Mooney, *Prog. Polym. Sci.*, 2012, **37**, 106-126.
72. J. L. Drury, R. G. Dennis and D. J. Mooney, *Biomaterials*, 2004, **25**, 3187-3199.
73. N. Bhattarai, J. Gunn and M. Zhang, *Adv. Drug Delivery Rev.*, 2010, **62**, 83-99.
74. R. A. Marklein and J. A. Burdick, *Soft Matter*, 2010, **6**, 136-143.
75. N. M. Alves and J. F. Mano, *Int. J. Biol. Macromol.*, 2008, **43**, 401-414.
76. S. Bhatia, in *Natural Polymer Drug Delivery Systems: Nanoparticles, Plants, and Algae*, Springer International Publishing, Cham, 2016, pp. 95-118.
77. M. P. Lutolf and J. A. Hubbell, *Nat. Biotechnol.*, 2005, **23**, 47.

78. K. M. Schultz and K. S. Anseth, *Soft Matter*, 2013, **9**, 1570-1579.
79. T. R. Hoare and D. S. Kohane, *Polymer*, 2008, **49**, 1993-2007.
80. J. Kopeček, *Biomaterials*, 2007, **28**, 5185-5192.
81. E. Jain, L. Hill, E. Canning, S. A. Sell and S. P. Zustiak, *J. Mater. Chem. B*, 2017, **5**, 2679-2691.
82. C. N. Salinas and K. S. Anseth, *J. Tissue Eng. Regener. Med.*, 2008, **2**, 296-304.
83. S. P. Singh, M. P. Schwartz, J. Y. Lee, B. D. Fairbanks and K. S. Anseth, *Biomater. Sci.*, 2014, **2**, 1024-1034.
84. J. Li and W. J. Kao, *Biomacromolecules*, 2003, **4**, 1055-1067.
85. A. J. García, *Ann. Biomed. Eng.*, 2014, **42**, 312-322.
86. A. M. Kloxin, A. M. Kasko, C. N. Salinas and K. S. Anseth, *Science*, 2009, **324**, 59-63.
87. J. J. Roberts and S. J. Bryant, *Biomaterials*, 2013, **34**, 9969-9979.
88. A. A. Aimetti, A. J. Machen and K. S. Anseth, *Biomaterials*, 2009, **30**, 6048-6054.
89. P. M. Kharkar, A. M. Kloxin and K. L. Kiick, *J. Mater. Chem. B*, 2014, **2**, 5511-5521.
90. S.-H. Lee, J. J. Moon and J. L. West, *Biomaterials*, 2008, **29**, 2962-2968.
91. C. Shao, M. Wang, H. Chang, F. Xu and J. Yang, *ACS Sustainable Chem. Eng.*, 2017, **5**, 6167-6174.

92. E. A. Phelps, N. O. Enemchukwu, V. F. Fiore, J. C. Sy, N. Murthy, T. A. Sulchek, T. H. Barker and A. J. García, *Adv. Mater.*, 2012, **24**, 64-70.
93. S. R. Caliyari and J. A. Burdick, *Nat. Methods*, 2016, **13**, 405.
94. D. S. W. Benoit, A. R. Durney and K. S. Anseth, *Biomaterials*, 2007, **28**, 66-77.
95. M. P. Lutolf, P. M. Gilbert and H. M. Blau, *Nature*, 2009, **462**, 433.
96. C.-C. Lin and K. S. Anseth, *Pharm. Res.*, 2009, **26**, 631-643.
97. N. A. Peppas, K. B. Keys, M. Torres-Lugo and A. M. Lowman, *J. Controlled Release*, 1999, **62**, 81-87.
98. V. X. Truong, K. M. Tsang and J. S. Forsythe, *Biomacromolecules*, 2017, **18**, 757-766.
99. L. Klouda, *Eur. J. Pharm. Biopharm.*, 2015, **97**, 338-349.
100. S. R. Hynes, M. F. Rauch, J. P. Bertram and E. B. Lavik, *J. Biomed. Mater. Res., Part A*, 2009, **89A**, 499-509.
101. K. T. Nguyen and J. L. West, *Biomaterials*, 2002, **23**, 4307-4314.
102. K. A. Mosiewicz, L. Kolb, A. J. van der Vlies, M. M. Martino, P. S. Lienemann, J. A. Hubbell, M. Ehrbar and M. P. Lutolf, *Nat. Mater.*, 2013, **12**, 1072.
103. W. E. Hennink and C. F. van Nostrum, *Adv. Drug Delivery Rev.*, 2012, **64**, 223-236.
104. C. F. Hansell, P. Espeel, M. M. Stamenovic, I. A. Barker, A. P. Dove, F. E. Du Prez and R. K. O'Reilly, *J. Am. Chem. Soc.*, 2011, **133**, 13828-13831.

105. D. F. Williams, *Biomaterials*, 2008, **29**, 2941-2953.
106. A. Phadke, C. Zhang, B. Arman, C.-C. Hsu, R. A. Mashelkar, A. K. Lele, M. J. Tauber, G. Arya and S. Varghese, *Proc. Natl. Acad. Sci. USA*, 2012, **109**, 4383-4388.
107. M. Mihajlovic, M. Staropoli, M.-S. Appavou, H. M. Wyss, W. Pyckhout-Hintzen and R. P. Sijbesma, *Macromolecules*, 2017, **50**, 3333-3346.
108. X. Ding and Y. Wang, *J. Mater. Chem. B*, 2017, **5**, 887-906.
109. M. Nakahata, Y. Takashima, H. Yamaguchi and A. Harada, *Nat. Commun.*, 2011, **2**, 511.
110. R. Dong, Y. Pang, Y. Su and X. Zhu, *Biomater. Sci.*, 2015, **3**, 937-954.
111. D. Y. Ko, U. P. Shinde, B. Yeon and B. Jeong, *Prog. Polym. Sci.*, 2013, **38**, 672-701.
112. K. R. Kamath and K. Park, *Adv. Drug Delivery Rev.*, 1993, **11**, 59-84.
113. C. M. Nimmo and M. S. Shoichet, *Bioconjugate Chem.*, 2011, **22**, 2199-2209.
114. H. C. Kolb, M. G. Finn and K. B. Sharpless, *Angew. Chem., Int. Ed.*, 2001, **40**, 2004-2021.
115. J. E. Moses and A. D. Moorhouse, *Chem. Soc. Rev.*, 2007, **36**, 1249-1262.
116. M. Malkoch, R. Vestberg, N. Gupta, L. Mespouille, P. Dubois, A. F. Mason, J. L. Hedrick, Q. Liao, C. W. Frank, K. Kingsbury and C. J. Hawker, *Chem. Commun.*, 2006, 2774-2776.

117. M. Gregoritzza and F. P. Brandl, *Eur. J. Pharm. Biopharm.*, 2015, **97**, 438-453.
118. C. Goussé, A. Gandini and P. Hodge, *Macromolecules*, 1998, **31**, 314-321.
119. K. Kamahori, S. Tada, K. Ito and S. Itsuno, *Macromolecules*, 1999, **32**, 541-547.
120. C. M. Nimmo, S. C. Owen and M. S. Shoichet, *Biomacromolecules*, 2011, **12**, 824-830.
121. H.-L. Wei, Z. Yang, L.-M. Zheng and Y.-M. Shen, *Polymer*, 2009, **50**, 2836-2840.
122. M. A. Tasdelen, *Polym. Chem.*, 2011, **2**, 2133-2145.
123. A. Gandini, *Prog. Polym. Sci.*, 2013, **38**, 1-29.
124. S. Kirchhof, A. Strasser, H.-J. Wittmann, V. Messmann, N. Hammer, A. M. Goepferich and F. P. Brandl, *J. Mater. Chem. B*, 2015, **3**, 449-457.
125. K. C. Koehler, K. S. Anseth and C. N. Bowman, *Biomacromolecules*, 2013, **14**, 538-547.
126. K. C. Koehler, D. L. Alge, K. S. Anseth and C. N. Bowman, *Biomaterials*, 2013, **34**, 4150-4158.
127. L. J. Smith, S. M. Taimoory, R. Y. Tam, A. E. G. Baker, N. Bintah Mohammad, J. F. Trant and M. S. Shoichet, *Biomacromolecules*, 2018, **19**, 926-935.
128. M. P. Lutolf, N. Tirelli, S. Cerritelli, L. Cavalli and J. A. Hubbell, *Bioconjugate Chem.*, 2001, **12**, 1051-1056.
129. H. Shih and C.-C. Lin, *Biomacromolecules*, 2012, **13**, 2003-2012.

130. J. Mergy, A. Fournier, E. Hachet and R. Auzély-Velty, *J. Polym. Sci., Part A: Polym. Chem.*, 2012, **50**, 4019-4028.
131. A. B. Lowe, *Polym. Chem.*, 2010, **1**, 17-36.
132. C. E. Hoyle, A. B. Lowe and C. N. Bowman, *Chem. Soc. Rev.*, 2010, **39**, 1355-1387.
133. C. E. Hoyle, T. Y. Lee and T. Roper, *J. Polym. Sci., Part A: Polym. Chem.*, 2004, **42**, 5301-5338.
134. M. J. Kade, D. J. Burke and C. J. Hawker, *J. Polym. Sci., Part A: Polym. Chem.*, 2010, **48**, 743-750.
135. C. A. DeForest and K. S. Anseth, *Nat. Chem.*, 2011, **3**, 925-931.
136. A. Dondoni, *Angew. Chem. Int. Ed.*, 2008, **47**, 8995-8997.
137. C. A. DeForest, B. D. Polizzotti and K. S. Anseth, *Nat. Mater.*, 2009, **8**, 659-664.
138. A. E. Rydholm, S. K. Reddy, K. S. Anseth and C. N. Bowman, *Biomacromolecules*, 2006, **7**, 2827-2836.
139. C.-C. Lin, A. Raza and H. Shih, *Biomaterials*, 2011, **32**, 9685-9695.
140. C. E. Hoyle and C. N. Bowman, *Angew. Chem., Int. Ed.*, 2010, **49**, 1540-1573.
141. L. A. Sawicki and A. M. Kloxin, *J. Visualized Exp.*, 2016, 54462.
142. N. Cengiz, T. N. Gevrek, R. Sanyal and A. Sanyal, *Chem. Commun.*, 2017, **53**, 8894-8897.

143. P. Lundberg, A. Bruin, J. W. Klijnstra, A. M. Nyström, M. Johansson, M. Malkoch and A. Hult, *ACS Appl. Mater. Interfaces*, 2010, **2**, 903-912.
144. N. Gupta, B. F. Lin, L. M. Campos, M. D. Dimitriou, S. T. Hikita, N. D. Treat, M. V. Tirrell, D. O. Clegg, E. J. Kramer and C. J. Hawker, *Nat. Chem.*, 2010, **2**, 138-145.
145. J. C. Grim, I. A. Marozas and K. S. Anseth, *J. Controlled Release*, 2015, **219**, 95-106.
146. P. M. Kharkar, K. L. Kiick and A. M. Kloxin, *Polym. Chem.*, 2015, **6**, 5565-5574.
147. J. M. Zhu, *Biomaterials*, 2010, **31**, 4639-4656.
148. K. S. Straley and S. C. Heilshorn, *Soft Matter*, 2009, **5**, 114-124.
149. S. T. Gould, N. J. Darling and K. S. Anseth, *Acta Biomater.*, 2012, **8**, 3201-3209.
150. N. D. Gallant, K. A. Lavery, E. J. Amis and M. L. Becker, *Adv. Mater.*, 2007, **19**, 965-969.
151. M. S. Rehmann, A. C. Garibian and A. M. Kloxin, *Macromol. Symp.*, 2013, **329**, 58-65.
152. P. M. Kharkar, M. S. Rehmann, K. M. Skeens, E. Maverakis and A. M. Kloxin, *ACS Biomater. Sci. Eng.*, 2016, **2**, 165-179.
153. M. S. Rehmann and A. M. Kloxin, *Soft Matter*, 2013, **9**, 6737-6746.
154. S. Bertlein, G. Brown, K. S. Lim, T. Jungst, T. Boeck, T. Blunk, J. Tessmar, G. J. Hooper, T. B. F. Woodfield and J. Groll, *Adv. Mater.*, 2017, **29**, 1703404.

155. T. E. Brown, B. J. Carberry, B. T. Worrel, O. Y. Dudaryeva, M. K. McBride, C. N. Bowman and K. S. Anseth, *Biomaterials*, 2018, DOI: <https://doi.org/10.1016/j.biomaterials.2018.03.060>.
156. L. Xu, N. Sheybani, W. A. Yeudall and H. Yang, *Biomater. Sci.*, 2015, **3**, 250-255.
157. D. P. Nair, M. Podgórski, S. Chatani, T. Gong, W. Xi, C. R. Fenoli and C. N. Bowman, *Chem. Mater.*, 2014, **26**, 724-744.
158. Y. Dong, A. O. Saeed, W. Hassan, C. Keigher, Y. Zheng, H. Tai, A. Pandit and W. Wang, *Macromol. Rapid Commun.*, 2012, **33**, 120-126.
159. Z. Liu, Q. Lin, Y. Sun, T. Liu, C. Bao, F. Li and L. Zhu, *Adv. Mater.*, 2014, **26**, 3912-3917.
160. T. M. O'Shea, A. A. Aimetti, E. Kim, V. Yesilyurt and R. Langer, *Adv. Mater.*, 2015, **27**, 65-72.
161. L. He, D. Szopinski, Y. Wu, G. A. Luinstra and P. Theato, *ACS Macro Lett.*, 2015, **4**, 673-678.
162. Z. Q. Liu, Z. Wei, X. L. Zhu, G. Y. Huang, F. Xu, J. H. Yang, Y. Osada, M. Zrínyi, J. H. Li and Y. M. Chen, *Colloids Surf. B. Biointerfaces*, 2015, **128**, 140-148.
163. D. J. Hall, H. M. V. D. Berghe and A. P. Dove, *Polym. Int.*, 2011, **60**, 1149-1157.
164. M. Li, P. De, H. Li and B. S. Sumerlin, *Polym. Chem.*, 2010, **1**, 854-859.
165. N. J. Darling, Y.-S. Hung, S. Sharma and T. Segura, *Biomaterials*, 2016, **101**, 199-206.

166. B. J. Adzima, Y. Tao, C. J. Kloxin, C. A. DeForest, K. S. Anseth and C. N. Bowman, *Nat. Chem.*, 2011, **3**, 256-259.
167. J.-F. Lutz and Z. Zarafshani, *Adv. Drug Delivery Rev.*, 2008, **60**, 958-970.
168. J.-F. Lutz, *Angew. Chem., Int. Ed.*, 2008, **47**, 2182-2184.
169. J. M. Baskin, J. A. Prescher, S. T. Laughlin, N. J. Agard, P. V. Chang, I. A. Miller, A. Lo, J. A. Codelli and C. R. Bertozzi, *Proc. Natl. Acad. Sci. USA*, 2007, **104**, 16793-16797.
170. K. Lava, B. Verbraeken and R. Hoogenboom, *Eur. Polym. J.*, 2015, **65**, 98-111.
171. D. Steinhilber, T. Rossow, S. Wedepohl, F. Paulus, S. Seiffert and R. Haag, *Angew. Chem., Int. Ed.*, 2013, **52**, 13538-13543.
172. N. J. Agard, J. A. Prescher and C. R. Bertozzi, *J. Am. Chem. Soc.*, 2004, **126**, 15046-15047.
173. H. Li, J. Zheng, H. Wang, M. L. Becker and N. D. Leipzig, *J. Biomater. Appl.*, 2018, **32**, 1222-1230.
174. W. Tang and M. L. Becker, *Chem. Soc. Rev.*, 2014, **43**, 7013-7039.
175. A. B. Lowe, *Polymer*, 2014, **55**, 5517-5549.
176. J. W. Chan, C. E. Hoyle and A. B. Lowe, *J. Am. Chem. Soc.*, 2009, **131**, 5751-5753.
177. B. D. Fairbanks, T. F. Scott, C. J. Kloxin, K. S. Anseth and C. N. Bowman, *Macromolecules*, 2009, **42**, 211-217.
178. A. Massi and D. Nanni, *Org. Biomol. Chem.*, 2012, **10**, 3791-3807.

179. R. Hoogenboom, *Angew. Chem. Int. Ed.*, 2010, **49**, 3415-3417.
180. E. P. Kohler and H. Potter, *J. Am. Chem. Soc.*, 1935, **57**, 1316-1321.
181. H. Bader, L. C. Cross, I. Heilbron and E. R. H. Jones, *J. Chem. Soc.*, 1949, 619-623.
182. D. M. Graham and J. F. Soltys, *Can. J. Chem.*, 1969, **47**, 2529-2533.
183. I. Yoshifumi, W. Kuni, N. Kyoko, B. Jean-Luc, O. Koichiro and U. Kiitiro, *Chem. Lett.*, 1987, **16**, 1647-1650.
184. D. Konkolewicz, A. Gray-Weale and S. Perrier, *J. Am. Chem. Soc.*, 2009, **131**, 18075-18077.
185. D. Konkolewicz, C. K. Poon, A. Gray-Weale and S. Perrier, *Chem. Commun.*, 2011, **47**, 239-241.
186. R. Barbey and S. Perrier, *Macromolecules*, 2014, **47**, 6697-6705.
187. R. Barbey and S. Perrier, *ACS Macro Lett.*, 2013, **2**, 366-370.
188. A. B. Cook, R. Barbey, J. A. Burns and S. Perrier, *Macromolecules*, 2016, **49**, 1296-1304.
189. M. Hartlieb, T. Floyd, A. B. Cook, C. Sanchez-Cano, S. Catrouillet, J. A. Burns and S. Perrier, *Polym. Chem.*, 2017, **8**, 2041-2054.
190. A. Concellón, L. Asín, S. González-Lana, J. M. de la Fuente, C. Sánchez-Somolinos, M. Piñol and L. Oriol, *Polymer*, 2017, **117**, 259-267.

191. M. A. Daniele, A. A. Adams, J. Naciri, S. H. North and F. S. Ligler, *Biomaterials*, 2014, **35**, 1845-1856.
192. Y. Xu, H. Xu, X. Jiang and J. Yin, *Adv. Funct. Mater.*, 2014, **24**, 1679-1686.
193. X. Hu, H. Tan, X. Wang and P. Chen, *Colloids Surf. Physicochem. Eng. Aspects*, 2016, **489**, 297-304.
194. S. J. Cristol, A. Begoon, W. P. Norris and P. S. Ramey, *J. Am. Chem. Soc.*, 1954, **76**, 4558-4561.
195. W. E. Truce and J. A. Simms, *J. Am. Chem. Soc.*, 1956, **78**, 2756-2759.
196. W. E. Truce and G. J. W. Tichenor, *J. Org. Chem.*, 1972, **37**, 2391-2396.
197. V. X. Truong and A. P. Dove, *Angew. Chem., Int. Ed.*, 2013, **52**, 4132-4136.
198. B. Yao, J. Mei, J. Li, J. Wang, H. Wu, J. Z. Sun, A. Qin and B. Z. Tang, *Macromolecules*, 2014, **47**, 1325-1333.
199. C. A. Bell, J. Yu, I. A. Barker, V. X. Truong, Z. Cao, A. V. Dobrinyin, M. L. Becker and A. P. Dove, *Angew. Chem.*, 2016, **128**, 13270-13274.
200. V. X. Truong, M. P. Ablett, S. M. Richardson, J. A. Hoyland and A. P. Dove, *J. Am. Chem. Soc.*, 2015, **137**, 1618-1622.
201. X. Y. Cai, J. Z. Li, N. N. Li, J. C. Chen, E.-T. Kang and L. Q. Xu, *Biomater. Sci.*, 2016, **4**, 1663-1672.
202. Y. Zou, L. Zhang, L. Yang, F. Zhu, M. Ding, F. Lin, Z. Wang and Y. Li, *J. Controlled Release*, 2018, **273**, 160-179.

203. L. Yu, Z. Zhang, Y.-Z. You and C.-Y. Hong, *Eur. Polym. J.*, 2018, **103**, 80-87.
204. B. He, H. Su, T. Bai, Y. Wu, S. Li, M. Gao, R. Hu, Z. Zhao, A. Qin, J. Ling and B. Z. Tang, *J. Am. Chem. Soc.*, 2017, **139**, 5437-5443.
205. J. Huang and X. Jiang, *ACS Appl. Mater. Interfaces*, 2018, **10**, 361-370.
206. Y. Shi, T. Bai, W. Bai, Z. Wang, M. Chen, B. Yao, J. Z. Sun, A. Qin, J. Ling and B. Z. Tang, *Chem. - Eur. J.*, 2017, **23**, 10725-10731.

Chapter 2.

Synthesis and Characterisation of Efficient Nucleophilic Thiol-yne Hydrogel Materials with Tuneable Properties

2.1. Introduction

Tailoring the characteristics of a material to meet the needs of a biological environment is a key objective in biomaterials science.¹⁻³ Hydrogels, with their high water content and synthetic flexibility, are promising candidates to fulfil this goal.⁴⁻⁷ Over the last decade, research into hydrogels has expanded, revealing their true potential as synthetic biological materials,⁸⁻¹⁰ enabling their use for a broad array of applications such as scaffolds for tissue engineering¹¹⁻¹³ or carriers for drug delivery.^{14, 15} Nevertheless, the design of hydrogels with pre-defined and specific properties that respond to the demands of a particular biological environment or elicit a desired cellular response remains challenging.¹⁸⁻²³ The fabrication of tuneable hydrogels has the potential to allow us to broaden our understanding on the influence material properties have on cellular response. This in turn will provide an insight into how cells grow and replicate depending on their surrounding environment. Ultimately, cell differentiation is guided by mechanical signalling (Figure 2.1), as demonstrated by Janmey and Discher *et.al.*,^{18, 26} who showed that the mechanical properties of a new tissue, is influenced by the substrate's stiffness (typically, the Young's moduli can vary from 17 Pa for human fat tissue to 950 kPa for articular cartilage).²⁸ Therefore, hydrogels that are capable of mimicking a wide range of stiffness, in a simple and efficient manner, applicable to biological tissue will render them ideal materials to produce commercially viable candidates to advance the area of biomaterials.

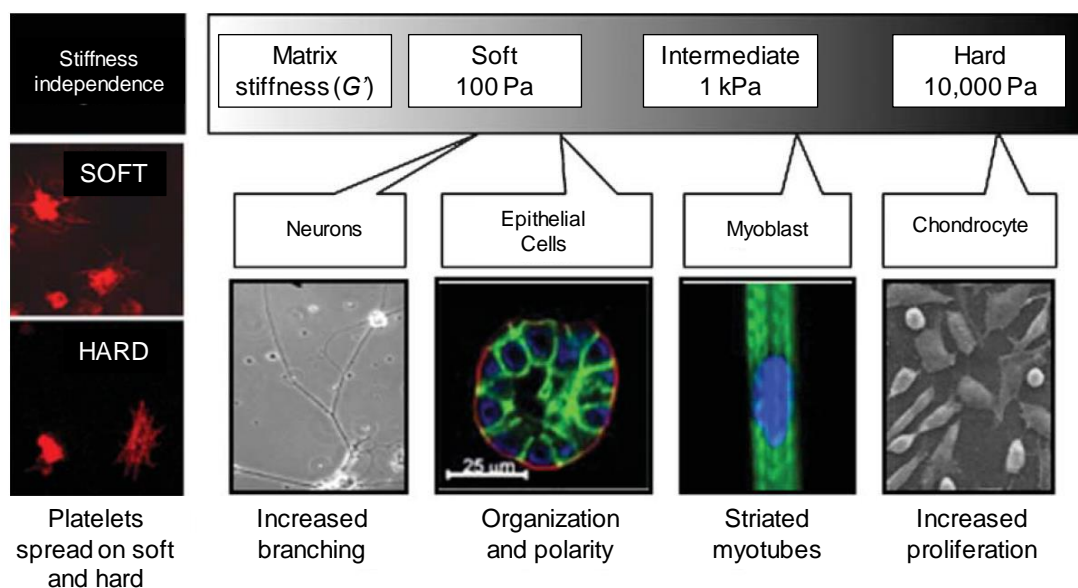


Figure 2.1. Effects of substrate stiffness on cell morphology. Cell types grown on polyacrylamide gel substrates display *in vivo* like morphological and functional properties on compliance similar to that of the particular tissue from which they are derived. Platelets, which circulate through the blood and are normally nonadherent, do not respond to substrate mechanics.²⁴ Neurons, mammary epithelial cells, and other epithelial cells isolated from soft tissue thrive on soft materials (shear modulus $G' = 100$ Pa).²⁵ Myoblasts of the muscle display actomyosin striations only on intermediate compliance substrates ($G' = 4$ kPa).²⁷ Chondrocytes exhibit increased growth and proliferation markers on hard gels with compliance similar to hard cartilage ($G' = 10$ kPa). Image modified from ref 24.

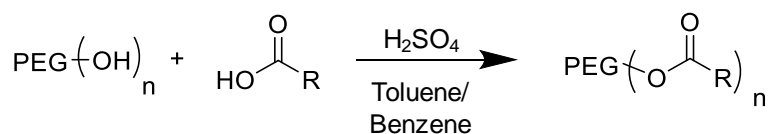
The introduction of metal-free bioorthogonal click reactions to hydrogel synthesis,^{10, 29-31} including the strain- or electron withdrawing group-promoted azide-alkyne [3+2] cycloaddition (SPAAC),³²⁻³⁶ inverse electron-demand Diels-Alder,³⁷⁻³⁹ oxime³⁹⁻⁴³ or the thiol-ene coupling reactions,^{30, 44-46} has greatly enhanced the formation of synthetic hydrogels, enabling their synthetic production under physiological conditions. The biorthogonality of these click crosslinking methods, in addition to their easily accessible functional groups, results in suitable approaches for biomaterial applications.⁴⁷ Recently the nucleophilic thiol-yne click reaction has been demonstrated as an attractive reaction for the synthesis of biomaterials.^{48, 49} Similarly to the thiol-ene reaction,⁴⁸ the thiol-yne mechanism can be carried out *via* both radical and nucleophilic pathways. The radical

pathway has been adopted to form biomaterials from linear⁵⁰ and multifunctional brush polymers,⁵¹ as well as from block copolymers.⁵² In recent years the nucleophilic pathway has received increasing attention as a consequence of its high speed and efficiency, both in the synthesis of elastomer⁵³ and hydrogel materials.⁵⁴ In particular, Truong *et al.* reported the synthesis of a double network hydrogel, prepared *via* two orthogonal click reactions; a dense nucleophilic thiol-yne poly(ethylene glycol) (PEG) network which was simultaneously crosslinked with a loose chitosan functionalised norbornene-tetrazine network (Chapter 1, Figure 1.20).⁵⁵ This work showed the excellent mechanical properties exhibited by the hydrogel, which included repeatable compression, this was attributed to the high efficiency and rapid nature of the nucleophilic thiol-yne addition reaction, to form the dense single network. It is postulated that further investigation into this synthetic approach would enable the synthesis of robust hydrogel materials with excellent and tuneable mechanical properties in a simple and bioorthogonal manner. For this reason, this chapter explores how the mechanical properties of nucleophilic thiol-yne PEG hydrogels can be readily varied across a wide range of stiffness and compressive strength values *via* a simple blending procedure. It can be foreseen that this feature, which leads to versatile and tailored hydrogels, could be exploited in many areas within the biomedical field, such as understanding the role mechanical stiffness plays on cell differentiation and other processes.

2.1. Results and Discussion

2.1.1. Synthesis of Alkyne and Thiol PEG Precursors

Nucleophilic thiol-yne hydrogels were formed from alkyne- and thiol-terminated poly(ethylene glycol) (PEG) precursors displaying different architectures (*i.e.* 2-, 3- or 4-arm) and molecular weights (ranging from 1 to 4 kg mol⁻¹). Following a modified version of a previously reported procedure,⁵⁵ the PEG precursors were functionalised through simple Fischer esterification in a toluene/benzene (50:50) solution, with either propiolic or 3-mercaptopropionic acid, to produce the alkyne- or thiol-terminated precursors respectively (Scheme 2.1).



Scheme 2.1. Synthesis of alkyne- and thiol-functionalised PEG through Fischer esterification where *n*= number of functional groups per PEG molecule (*i.e.* 2-, 3- or 4-) and R = C≡CH or CH₂CH₂SH.

After the work up procedure, the resultant crude PEG alkyne was stirred with charcoal and passed through a celite column to remove the colouration of the product, in order to form colourless hydrogel materials. Although this is a simple and highly efficient end group modification, a significant reduction in yield was observed during the final synthetic step for the alkyne precursors (61-70%) compared to the synthesised thiol PEG precursors (96-99%). Nevertheless, ¹H NMR spectroscopy and SEC analysis confirmed high end group functionalisation (92-99%) for all the PEG precursors (Table 2.1), as shown for the 3-arm PEG alkyne (1 kg mol⁻¹) and the 2-arm PEG thiol (1 kg mol⁻¹) (Figure 2.2, 2.3 and 2.4, respectively).

Table 2.1. Characterisation data for the alkyne and thiol PEG precursors.

PEG precursor	End group conversion ^a (%)	M_n theory (kg mol ⁻¹)	M_n NMR (kg mol ⁻¹)	M_n SEC (kg mol ⁻¹)	\bar{D}_M
3-arm alkyne (1 kg mol ⁻¹)	92	1.2	1.2 ^a	3.3 ^b	1.04 ^b
4-arm alkyne (2 kg mol ⁻¹)	93	2.2	2.4 ^a	5.9 ^b	1.08 ^b
2-arm thiol (1 kg mol ⁻¹)	96	1.2	1.2 ^c	1.1 ^d	1.24 ^d
2-arm thiol (2 kg mol ⁻¹)	>99	2.2	2.2 ^c	2.7 ^d	1.26 ^d
2-arm thiol (4 kg mol ⁻¹)	>99	4.2	4.3 ^c	6.9 ^d	1.10 ^d

^a Determined by ¹H NMR spectroscopy in deuterated acetone. ^b Determined by SEC analysis in DMF against poly(methyl methacrylate). ^c Determined by ¹H NMR spectroscopy in deuterated chloroform. ^d Determined by SEC analysis in chloroform against polystyrene standards

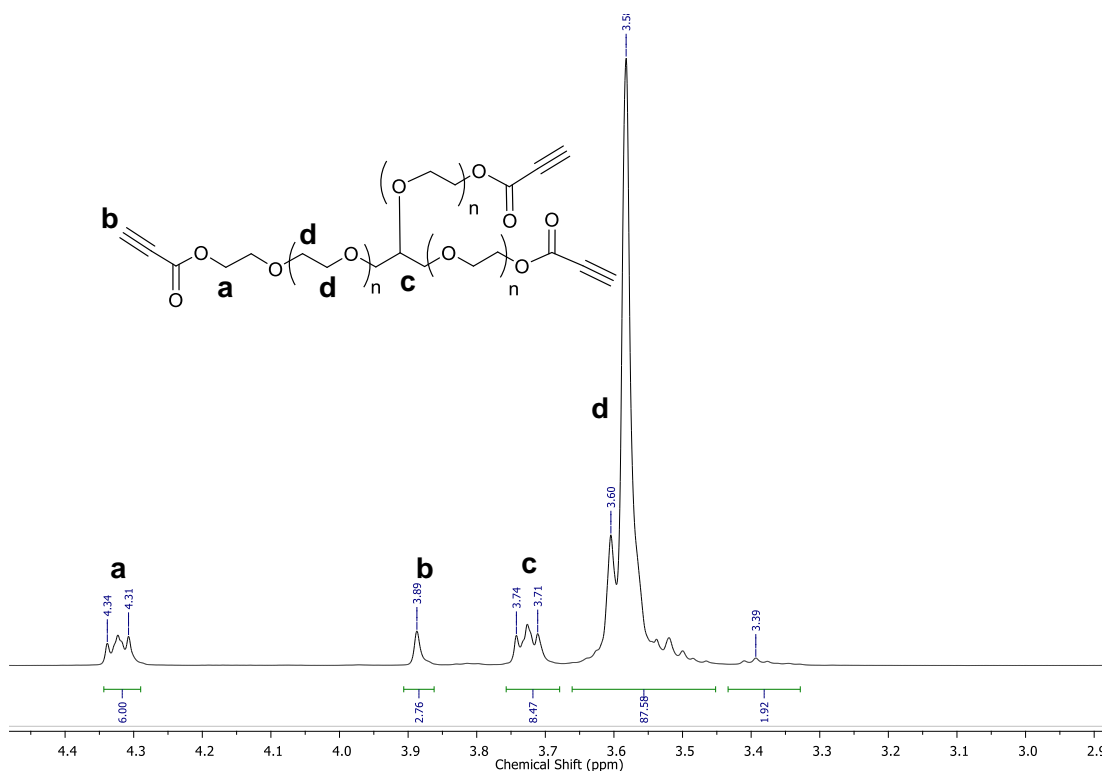


Figure 2.2. ¹H NMR spectrum of alkyne-terminated 3-arm PEG ((CD₃)₂CO, 300 MHz, 298 K).

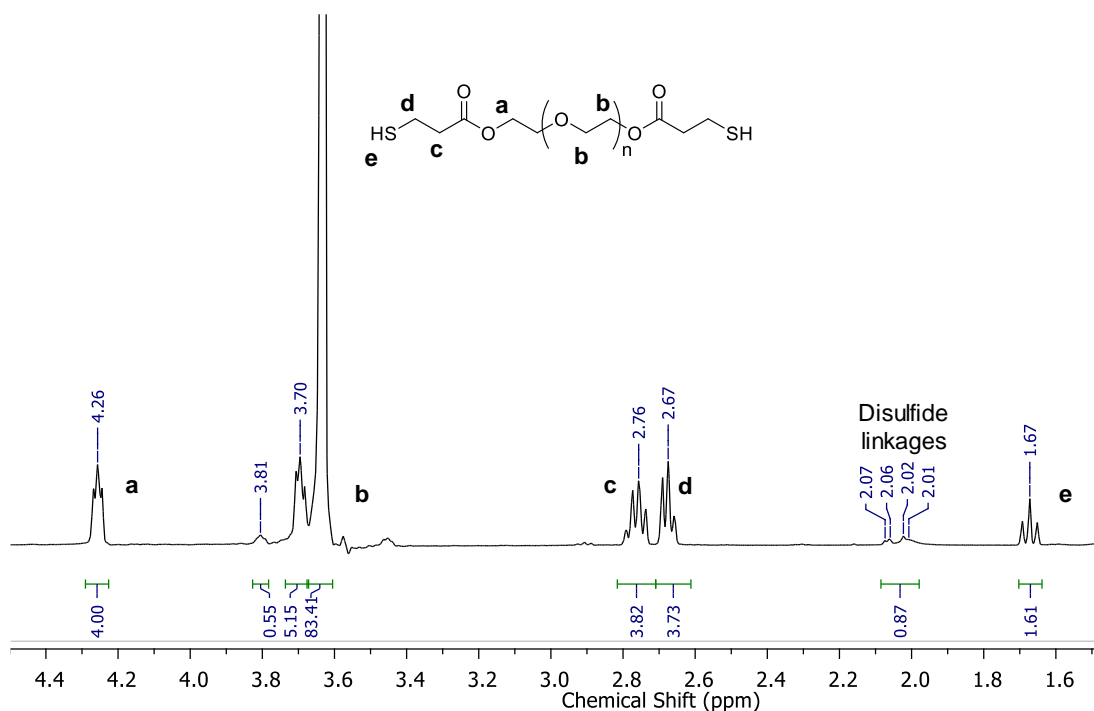


Figure 2.3. ^1H NMR spectrum of thiol-terminated 2-arm PEG (1 kg mol^{-1}) (CDCl_3 , 300 MHz, 298 K).

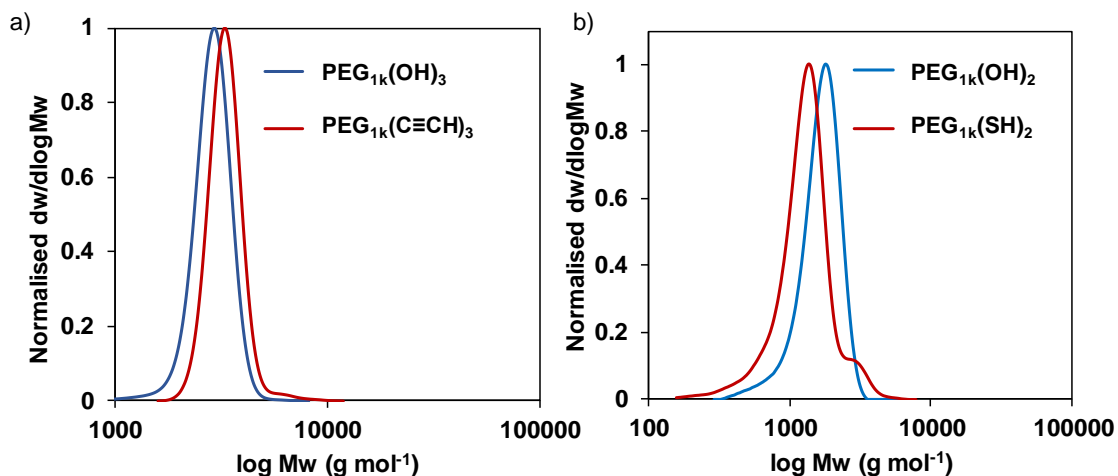
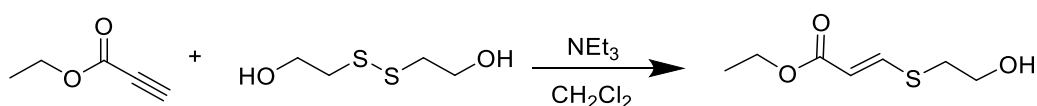


Figure 2.4. Size Exclusion chromatograms of a) 3-arm PEG alkyne precursors (1 kg mol^{-1}). Molecular weight determined against PMMA using DMF ($5 \text{ mM NH}_4\text{BF}_4$) as eluent. b) 2-arm PEG thiol precursor (1 kg mol^{-1}). Molecular weight determined against polystyrene standards using CHCl_3 ($0.5\% \text{ NEt}_3$) as eluent.

The ^1H NMR spectrum for the 2-arm PEG thiol (Figure 2.3) presents additional low intensity shifts between $\delta = 2.01$ and 2.06 ppm. These shifts were very broad with multiplet splitting characteristics which suggested that a small amount (11% calculated through integration of the multiplet) of a high molecular weight product had formed possibly through disulfide linkages between thiol end groups. The presence of a high molecular weight impurity was further confirmed by a small high molecular weight peak *via* SEC analysis.

To determine if disulfide linkages would hinder the nucleophilic thiol-yne reaction from taking place, a control reaction was carried out between an ester-activated alkyne, ethyl propiolate, and a disulfide small molecule, 2-hydroxyethyl disulfide, in the presence of triethylamine (NEt_3) in dichloromethane, (CH_2Cl_2), (Scheme 2.2). If the vinyl thioether product was formed, it would confirm that the disulfide linkage could break under the reaction conditions needed for the synthesis of nucleophilic thiol-yne hydrogels and therefore it could be concluded that the disulfide linkages in the thiol PEG precursors would have no effect on the hydrogel network formation and crosslinking efficiency in the hydrogel synthesis.



Scheme 2.2 Control reaction between ethyl propiolate and 2-hydroxyethyl disulfide to form a vinyl thioether product in the presence of NEt_3 .

The reaction was left to stir for 4 h, before characterising the product by ^1H NMR spectroscopy. Characterisation of the reaction revealed that the major product obtained

in the control reaction was the *trans* vinyl thioether product, thus demonstrating that the presence of disulfide linkages has no effect on the thiol-yne reaction (Figure 2.5). This was attributed to the high reactivity of the ester-activated alkyne, which could act to break the disulfide linkages, allowing the thiol-yne reaction to proceed. Consequently, as a result of the high efficiency, observed between the disulfide linkages and the alkyne PEG precursor in the presence of a base, no further purification was required to break the disulfide bonds in the PEG thiol precursors prior to the hydrogel network formation. As previously reported in the literature by Truong *et al.*, the reaction conditions have been shown to dictate the regioselectivity of the nucleophilic thiol-yne mechanism.⁴⁸ Specifically, the polarity of the solvent and the strength of the base used in the reaction, can be varied to control the transition state pathway and as such can be used to predict the stereochemistry of the vinyl thioether product. Accordingly, the observed *trans* stereochemistry of the vinyl thioether product obtained in this reaction is a consequence of the applied combination of a non polar solvent (CH_2Cl_2), used in combination with a weak base, NEt_3 .

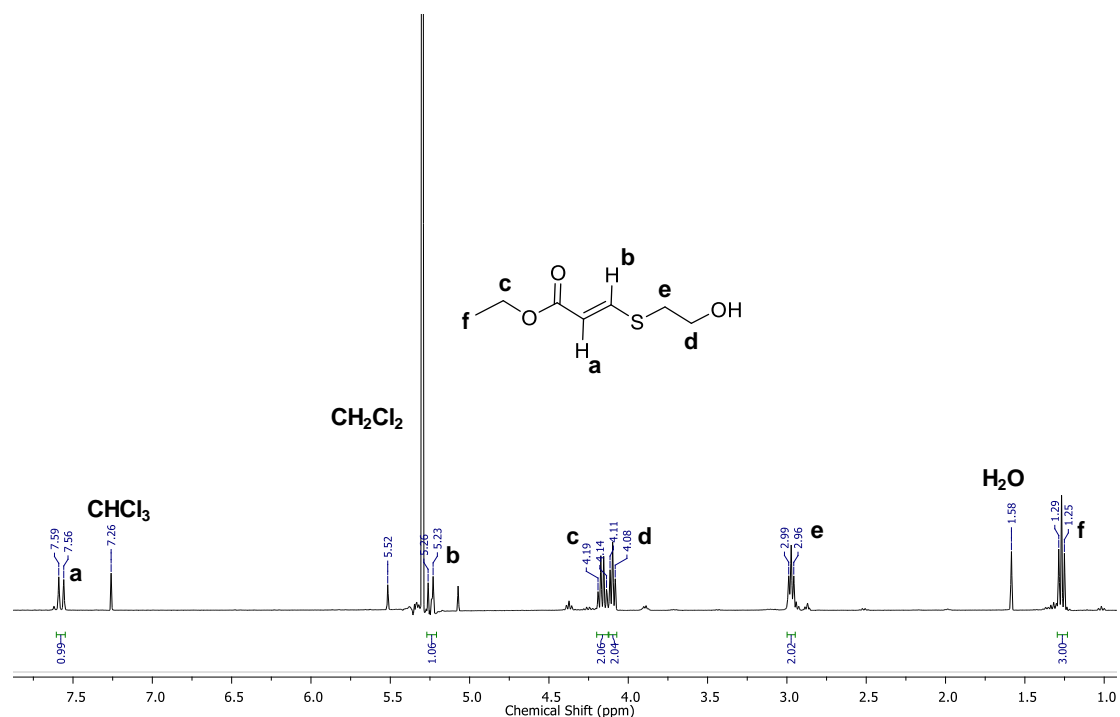


Figure 2.5. ^1H NMR spectrum of the reaction between ethyl propiolate and 2-hydroxyethyl disulfide to form a vinyl thioether product (CDCl_3 , 300 MHz, 298 K).

2.1.2. Synthesis of Thiol-yne PEG Hydrogels

To confirm that the nucleophilic thiol-yne reaction takes place in an aqueous environment, required for hydrogel synthesis, a small molecule model nucleophilic thiol-yne reaction was carried out. Specifically, 2-mercaptoethanol was added in excess to the 2-arm PEG alkyne (**2_{1A}**) in deuterated phosphate buffered saline (PBS) solution and the product was characterised *via* ^1H NMR spectroscopy. In accordance with previous literature,^{48, 53} the weakly basic polar reaction conditions favoured the formation of the mono addition *cis* vinyl thioether as the major product (Figure 2.6). The monoaddition product demonstrates the stability of the product, preventing the reaction from undergoing any further reactions to the double addition product. This demonstrates

the click like nature of the reaction following a single reaction pathway and forming a stable product in high yields (>99%).⁴⁸

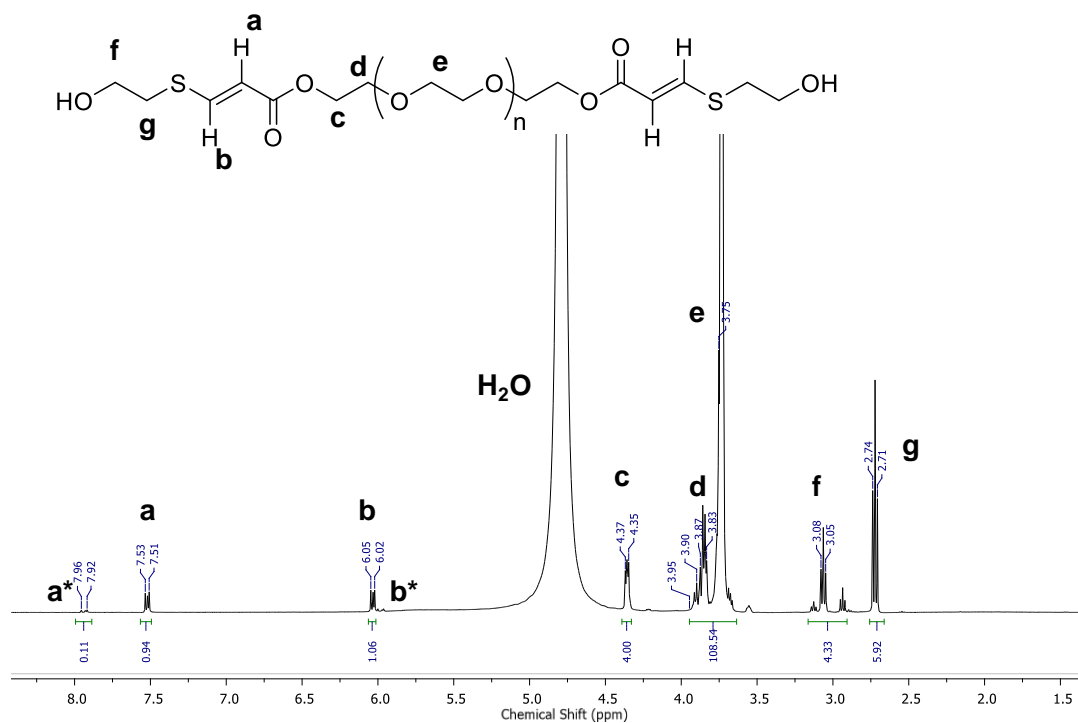
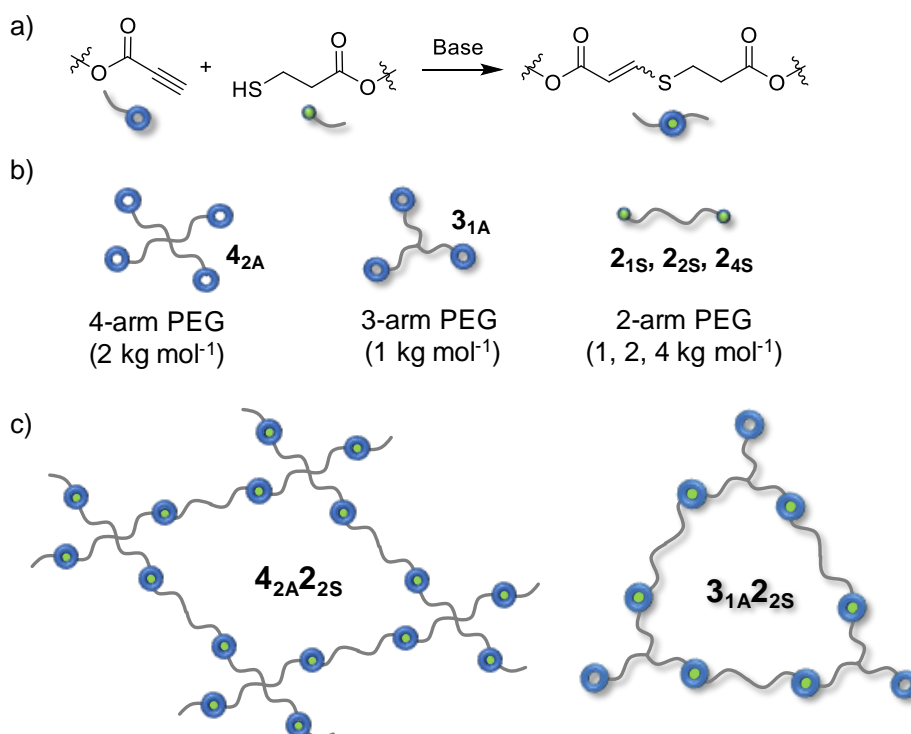


Figure 2.6. ¹H NMR spectrum of the reaction between alkyne-terminated 2-arm PEG (1 kg mol⁻¹) and 2-mercaptoethanol at pH 7.8 after 10 min (D₂O/PBS, 400 MHz, 298 K). * = *trans* product.

Thiol-yne PEG hydrogels were subsequently prepared by mixing solutions containing a 1:1 molar ratio of alkyne to thiol polymer precursors in PBS solution at pH 7.4. The polymer content was kept at 10 wt% and injected into suitable moulds to create materials for testing. All the hydrogels were formed in 2 mL plastic syringe mould (dimensions 4 mm × 9 mm), allowing uniform cylindrical samples to form without a meniscus which could be easily removed from the mould after curing. A range of different PEG precursors were combined, and the resulting hydrogel and its features were fully characterised *via* swelling kinetics, cryogenic scanning electron microscopy (cryo SEM), compression and rheology. The nomenclature for each hydrogel was

determined by the structure and molecular weight of the PEG alkyne and thiol precursor. Each hydrogel was named in relation to the number of arms on the alkyne (A) and thiol (S) precursors. The subscript denoted the molecular weight of the polymer and functional group, *e.g.* **4_{2A}2_{4S}** was a hydrogel composed of a 4-arm alkyne (2 kg mol⁻¹) crosslinked with a 2-arm thiol (4 kg mol⁻¹, Scheme 2.3).



Scheme 2.3. a) Nucleophilic base-catalysed reaction between an alkyne and thiol; b) schematic of the PEG precursors synthesised for crosslinking and c) schematic of exemplar hydrogel networks. The hydrogel naming convention used (**X_{ZA}Y_{ZS}**) denotes the hydrogel structures, where X = number of arms on the alkyne precursor, Y = number of arms on the thiol precursor and Z = the molecular weight of the PEG precursor, *e.g.* **4_{2A}2_{4S}** is a hydrogel composed of a 4-arm alkyne (2 kg mol⁻¹) crosslinked with a 2-arm thiol (4 kg mol⁻¹).

As determined by the vial tilt method, all the hydrogels formed within 10 min after mixing the alkyne- and thiol-terminated PEG solutions (Table 2.2). The gelation time increased with the molecular weight of the PEG precursors, most likely as a result of the decreased end-group concentration in the final pre-network (Table 2.2).

Table 2.2. Gelation times and swelling kinetics of PEG hydrogels made at 10 wt% in PBS solution.

Hydrogel ^a	Molar Conc. of End Group (mM)	Gelation Time ^c (s)	Gel Fraction (%)	Equilibrium Water Content (%)	Mesh Size ^d (nm)
3 _{1A} 2 _{1S}	2.69	210 ± 7	73.9 ± 2.6	95.2 ± 0.9	5.80 ± 0.49
3 _{1A} 2 _{2S}	1.38	290 ± 10	80.2 ± 1.9	94.2 ± 0.8	6.36 ± 0.16
3 _{1A} 2 _{4S}	0.51	600 ± 12	71.8 ± 0.2	95.1 ± 2.4	9.74 ± 0.93
4 _{2A} 2 _{1S}	1.75	87 ± 5	94.8 ± 0.6	91.9 ± 0.5	5.55 ± 0.17
4 _{2A} 2 _{2S}	0.95	125 ± 6	98.8 ± 0.7	92.4 ± 0.2	6.38 ± 0.07
4 _{2A} 2 _{4S}	0.40	238 ± 10	99.3 ± 0.7	94.2 ± 0.1	8.53 ± 0.06

^aThe hydrogel naming convention used (X_{ZA}Y_{ZS}) denotes the hydrogel structures, where X = number of arms on the alkyne precursor, Y = number of arms on the thiol precursor and Z = the molecular weight of the PEG precursor, *e.g.* 4_{2A}2_{4S} is a hydrogel formed from a 4-arm alkyne at 2 kg.mol⁻¹ crosslinked with a 2-arm thiol at 4 kg.mol⁻¹. ^bHydrogels prepared in a 1:1 molar ratio of alkyne to thiol end groups. ^cMeasured *via* the vial tilt method. ^dCalculated from the Flory-Rehner equation.^{16, 17}

The kinetics of the gelation process were further investigated through rheological experiments. By monitoring the evolution of storage (G') and loss (G'') moduli of the mixture with time (Figure 2.7), the gelation times were defined by the crossover point between G' and G'' and were in good agreement with the vial tilt data, (Table 2.2). The G' and G'' values for the hydrogels were observed to reach a plateau after 30 min, thus indicating the hydrogels had reached stabilisation (Figure 2.7). To confirm that the thiol-yne hydrogels were viscoelastically stable and independent of frequency, rheological frequency sweep tests were conducted. Indeed, G' and G'' values remain constant throughout the frequency range (from 0 to 100 rad s⁻¹), thus confirming that the hydrogels were fully crosslinked (Figure 2.8).

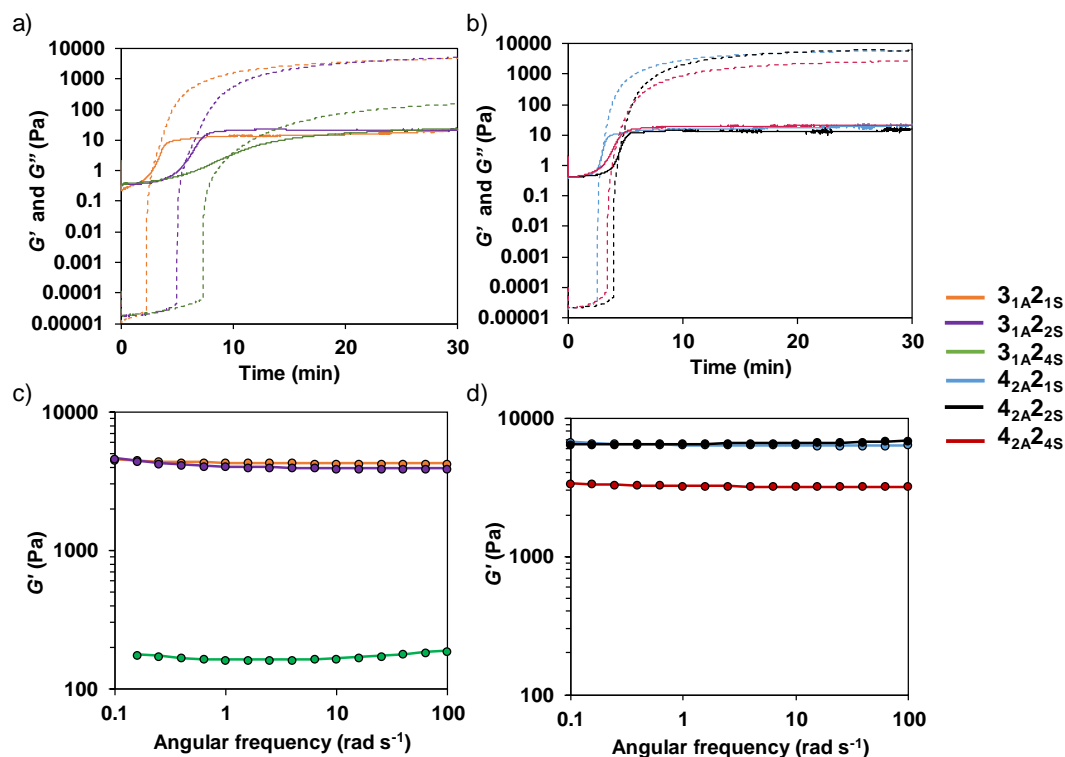


Figure 2.7. a-b) Evolution of the storage (G' dotted line) and loss (G'' solid line) moduli as a function of time for the a) 3-arm alkyne and b) 4-arm alkyne nucleophilic thiol-yne PEG hydrogels. c-d) Frequency sweep chart at 298 K and a constrain strain of 0.5% for the c) 3-arm alkyne and b) 4-arm alkyne nucleophilic thiol-yne PEG hydrogels.

2.1.3. General Characterisation of the Thiol-yne PEG Hydrogels

The gel fraction (GF) of a hydrogel, can be used to measure of the efficiency of the crosslinking reaction. To assess the efficiency of the thiol-yne hydrogels the prepared hydrogels were lyophilised, and weights recorded. The hydrogels were then allowed to swell in water for 3 days with frequent changes of water to remove unreacted precursors. The hydrogels were then lyophilised and weights recorded again. The percentage difference between the weights determined the amount of unreacted precursors present in the system and therefore the efficiency of the reaction. For these systems, GF was high for all the synthesised hydrogels (>74%, Table 2.2) thus

illustrating the high efficiency of the nucleophilic thiol-yne reaction as a polymer crosslinking reaction in aqueous conditions, suitable for preparing hydrogels as biomaterials. In particular, the GF was higher for the hydrogels crosslinked with a 4-arm alkyne precursor compared to those primarily composed from a 3-arm alkyne precursor (99% and 80%, respectively), which revealed that a more efficient thiol-yne addition reaction takes place with the 4-arm alkyne precursor. This observation is attributed to the greater number of functional groups per molecule which leads to an increased probability of crosslinking, thus lowering the amount of unreacted precursor in the hydrogel and increasing the GF values. However, direct comparisons should be avoided because of the difference in molecular weight between the two alkyne precursors (*i.e.* 3-arm alkyne at 1 kg mol⁻¹ compared to 4-arm alkyne at 2 kg mol⁻¹).

To determine the water permeability and surface properties of the hydrogels, their equilibrium water content (EWC) was measured. The prepared hydrogels were swollen in water for 24 h so that swelling could reach equilibrium and the hydrogels were weighed (W_s). The samples were then lyophilised, and the dried weights (W_d) were recorded. The EWC equation (Equation 2.1) was applied to calculate the EWC for each system.

$$EWC (\%) = \frac{W_s - W_d}{W_s} \times 100 \%$$

Equation 2.1. Equilibrium water content (EWC) equation where W_s is the equilibrium swollen mass and W_d is the dry mass of the hydrogel.

Regardless of the PEG precursor used, all the synthesised hydrogels displayed high EWC percentages (>92%, Table 2.2), which is indicative of a porous structure able to hold large amounts of water. The average mesh size of the thiol-yne hydrogels,

calculated using the Flory-Rehner equation,^{16, 17} calculates the mesh size of a hydrogel based on the volume swelling ratio for each system and the molecular weight of the polymer precursors. For the nucleophilic thiol-yne reaction the mesh size ranged from 5.6-9.7 nm and followed the same trend as the gelation time and EWC data. Indeed, the longer, more flexible 2-arm PEG thiol precursors form hydrogel networks with large pore structures owing to the increased chain length between crosslinking sites.

Cryo SEM was undertaken to further study the structure of the prepared hydrogels. As a consequence of the limitations of this technique, the images are indicative of the growth of the ice crystals formed during the freezing and drying process, and therefore it cannot be conclusively ascertained if there is a trend between the geometry and molecular weight of the functionalised PEG precursors and the resultant mesh size. Nevertheless, the images suggest that all the hydrogels have a porous structure and the ice crystal growth is not affected by the molecular weight or the number of crosslinking points on the PEG precursor (Figure 2.8).

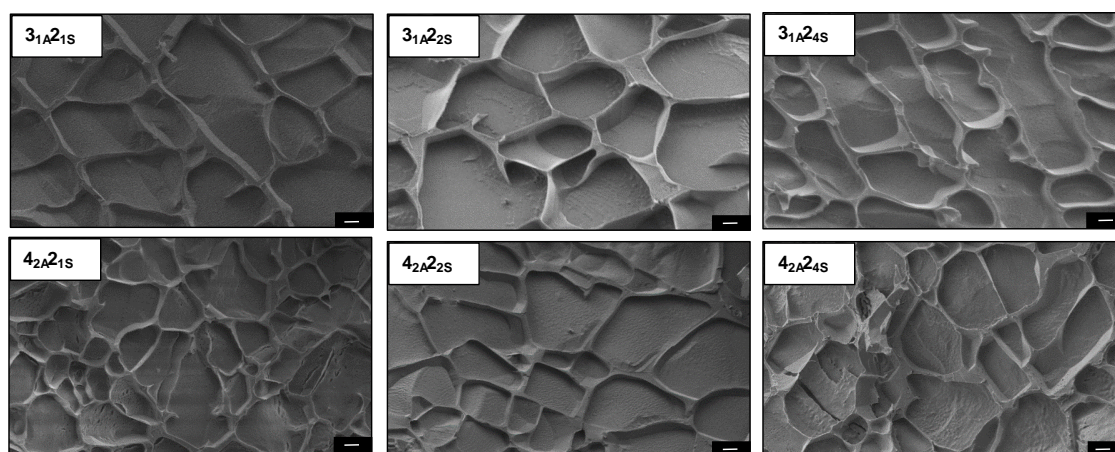


Figure 2.8. Cryo-SEM images of the thiol-yne PEG hydrogels, scale bar = 2 μm .

2.1.4. Mechanical Characterisation of the Thiol-yne PEG Precursors

Within the context of designing hydrogels for biomedical applications, controlling their mechanical properties (*e.g.* Young's modulus, ultimate compressive strength and G') to suit a given biological environment or to guide cell differentiation, has attracted much attention.⁵⁶ Hence, the mechanical performance of the click hydrogels was fully assessed through rheological and compressive testing to determine their capabilities to mimic different biological environments. Amplitude sweep tests were performed on the thiol-yne hydrogels at a constant frequency of 10 rad s^{-1} with G' and G'' measured as the strain was ramped logarithmically from 0.01 to 100% (Figure 2.9). Negligible change was observed in the G' values for each hydrogel system, even after applying 100% strain, which demonstrates that these materials can withstand high strain without releasing any stored energy. This results in flexible hydrogels capable of withstanding large amounts of strain without breaking the internal crosslinked network.

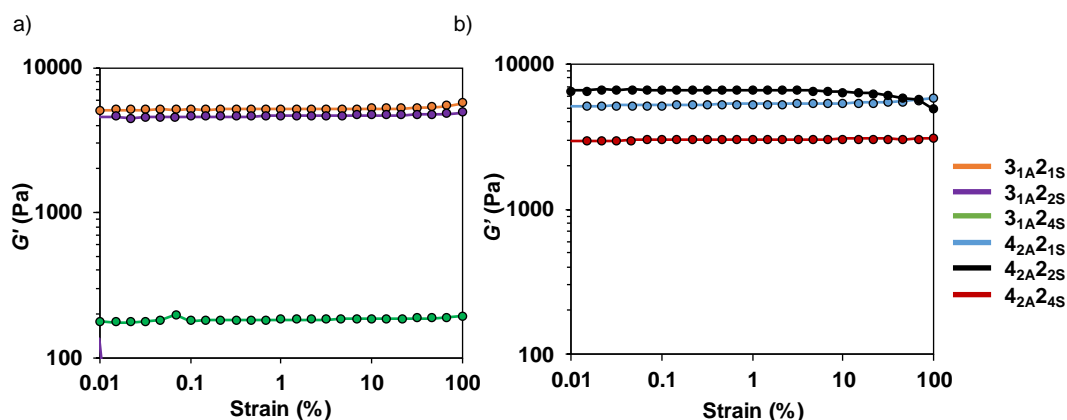


Figure 2.9. Amplitude sweep chart at 293 K and a constant frequency of 10 rad s^{-1} for a) $3_{1A}2_{2S}$ and b) $4_{2A}2_{2S}$ hydrogels.

Most notably, the moderation in length of the 2-arm PEG thiol precursors led to a remarkable range of accessible G' values of almost three orders of magnitude, from

180 to 7000 Pa, when cross linked with the 3-arm PEG alkyne precursor (Table 2.3). This range of G' correlated with an increase in the calculated mesh size (Table 2.2) revealing as the mesh size increased the hydrogel structure became less rigid. This correlates with literature values confirming longer polymer chains between crosslink points increasing the mesh size, allowing increased movement between polymer chains and therefore a decrease in G' .^{40, 57} Hence, considering that a wider range of precursors would no doubt enable the selection of specific gel stiffness, it was postulated that by a simple blending approach of the thiol precursors, hydrogels with highly tuneable stiffness could be prepared from the same chemistry (Section 2.2.5).

Table 2.3. The mechanical properties of the thiol-yne hydrogels

Hydrogel	Compressive Strain (%)	Compressive Stress (kPa)	Young's Modulus (kPa)	G' (Pa) ^a
3 _{1A} 2 _{1S}	95 ± 0	673 ± 18	0.11 ± 0.01	5562 ± 599
3 _{1A} 2 _{2S}	95 ± 0	1397 ± 279	0.22 ± 0.06	5497 ± 1119
3 _{1A} 2 _{4S}	95 ± 0	1670 ± 261	0.21 ± 0.02	168 ± 49
4 _{2A} 2 _{1S}	80 ± 3.5	429 ± 111	0.46 ± 0.16	5234 ± 1123
4 _{2A} 2 _{2S}	82 ± 1.3	735 ± 115	0.47 ± 0.07	6925 ± 913
4 _{2A} 2 _{4S}	95 ± 0.5	2373 ± 137	0.26 ± 0.04	2866 ± 543

^aAverage of G' at 10 rad s⁻¹ and 0.1% strain

To further evaluate the mechanical response of the thiol-yne PEG hydrogels, uniaxial compressive tests were conducted to determine the ultimate compressive strength and Young's modulus of each hydrogel. The hydrogels were left to gel in moulds of specific dimensions (9 × 4 mm) for 1 h, before a known force was applied to

the hydrogel, the resultant stress and strain were then measured. Similar to the rheological properties, depending on the PEG precursors combined, the thiol-yne hydrogels show a wide range of compressive strengths, from 0.6 to 2.4 MPa (Figure 2.10 and Table 2.3). Interestingly, only **4_{2A}2_{1S}** and **4_{1A}2_{2S}** hydrogels, which contained low molecular weight PEG thiol precursors, ruptured at *ca.* 80% strain, whereas all the other systems (*i.e.* **3_{1A}2_{1S}**, **3_{1A}2_{2S}**, **3_{1A}2_{4S}** and **4_{2A}2_{4S}**) were able to withstand the full 95% strain. Moreover, for those hydrogels that did not rupture, a clear trend can be observed: the maximum compressive strength increases with the molecular weight of the thiol PEG precursor. This is a consequence of the longer chains between crosslink points which are able to accommodate the increased force applied on the hydrogels. For instance, **4_{2A}2_{4S}** displayed the highest compressive strain (2.4 MPa), followed by **3_{1A}2_{4S}** (1.7 MPa).

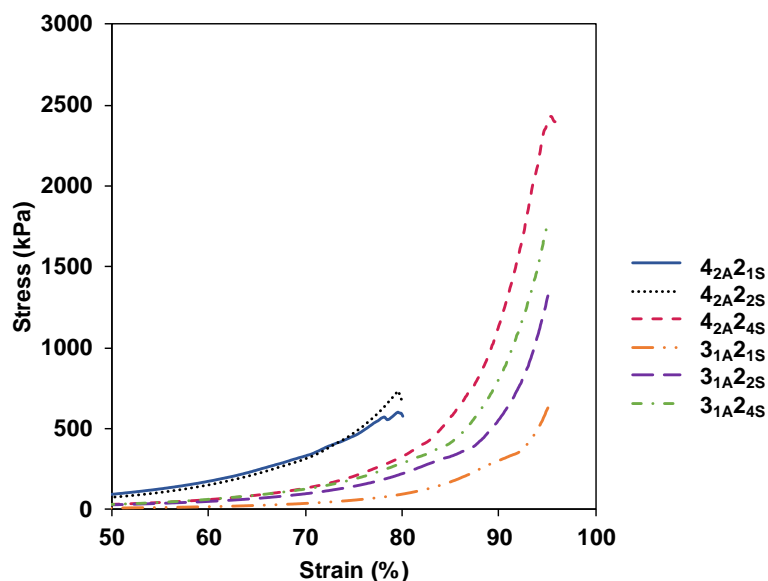


Figure 2.10. Representative stress/strain compression curves for the nucleophilic thiol-yne PEG hydrogels at 10 wt%.

Further mechanical testing revealed that, in a similar manner to the double network hydrogels, in which these systems are the dense single network,⁵⁵ the **3A2s series** and **4A2As** hydrogels could be compressed repeatedly to 90% strain, with the **3A2s** systems able to withstand 95% strain, up to 10 times without breaking (Figure 2.11). The ability for the **3A2s** hydrogels to tolerate higher strain could be a result of the geometry and molecular weight of the 3-arm PEG alkyne. Specifically, with fewer and

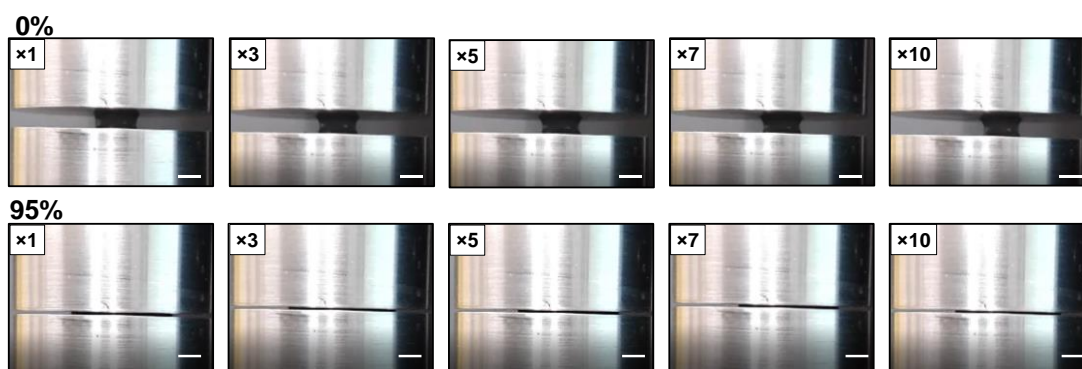


Figure 2.11. Freeze frames from the cyclic compression video for the **3A2s** hydrogel demonstrating the repeatable compression of the hydrogels, scale bar = 5 mm.

shorter chain ends, the 3-arm PEG precursor is less likely than the 4-arm precursor to form loops or leave unreacted chain ends, which are not taken into account in the GF measurement. Hence, it is postulated that the **3A2s** system forms a more perfect network,⁵⁸⁻⁶⁰ in which less elastic defects (*e.g.* loops or catenanes) are present, thus resulting in enhanced mechanical performance.

2.1.5. Tuning the Mechanical Properties of Thiol-yne PEG Hydrogels

Designing hydrogels with tuneable properties (*e.g.* gelation time, stiffness or Young's modulus) that allows facile mimicking of a range of biological environment, diversifies a hydrogel's application. The large range of G' values accessible *via* combining different PEG precursors in this system enabled a detailed investigation into the other

effects the blending process has on the thiol-yne hydrogel properties (Figure 2.9). Specifically, hydrogels were prepared by blending **2_{1S}** and **2_{4S}** in 3 different molar ratio (*i.e.* 25:75, 50:50, and 75:25 **2_{1S}**:**2_{4S}** respectively), and crosslinked the network with the 3-arm PEG alkyne precursor, **3_{1A}**. As expected, the blending approach produced hydrogels with intermediate values of G' (250, 1000, and 2000 Pa, respectively) between those previously observed for **3_{1A}2_{1S}** and **3_{1A}2_{4S}** systems (Figure 2.12a). The range of stiffness achieved correlated well with that displayed by different biological substrates. Indeed, the low G' values (180-250 Pa) correspond to ‘soft’ tissue, ideal for the growth of neurons and epithelial cells,²⁴ whereas intermediate values ($G' = 1-2$ kPa)

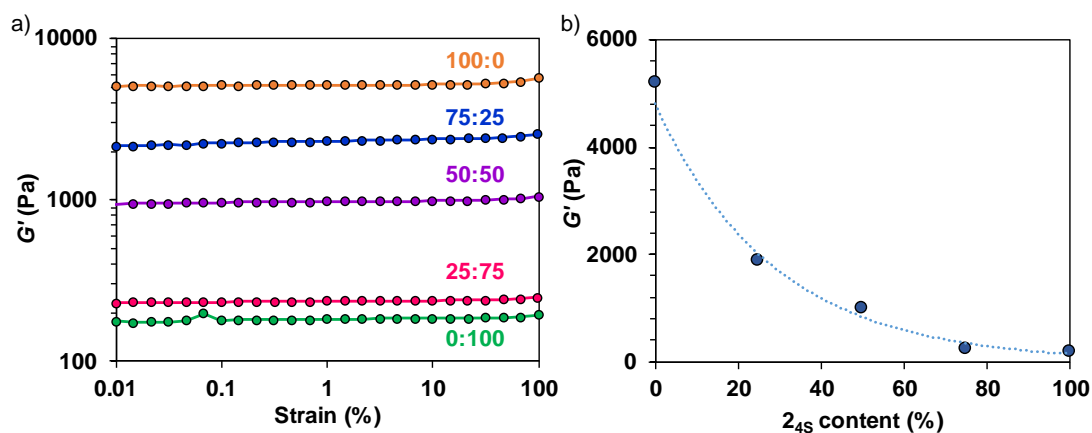


Figure 2.12. a) Amplitude sweep charts of the **3_{1A}2_s** hydrogels synthesised from different molar ratios blends of 1 and 4 kg mol⁻¹ 2-arm PEG thiol (ratio stated as 1 kg mol⁻¹:4 kg mol⁻¹ precursor). b) The graphical representation of the correlation between G' of the blended **3_{1A}2_s** hydrogels and the percentage of 4 kg mol⁻¹ thiol-terminated PEG precursor used.

are similar to an environment suitable for muscle formation.²⁷ Conversely, the stiffest hydrogels could provide a more suitable substrate for promoting the growth of cartilage.²⁸ Hence, our blended hydrogels result in robust biomaterials with a highly tuneable nature that mimicked a range of biological environments in terms of stiffness in a predictable manner (Figure 2.12b).

Further characterisation of the hydrogel networks formed *via* the blending process, not only tuned the stiffness of the thiol-yne hydrogels, but also enabled the modification of other features, such as the mesh size and the compressive strength (Table 2.4). The blended hydrogels showed high GF (71-81 %) and EWC (95-97 %) values, thus confirming that the blending process did not affect the efficiency of the reaction and therefore both PEG thiol precursors were incorporated into the networks and thus contributed to the mechanical properties of the resultant materials. Interestingly, the mesh size of the networks resembled that shown by **3_{1A}2_{4S}** network compared to **3_{1A}2_{1S}** network, which was attributed to the swelling process (*i.e.* the more hydrophilic nature of **2_{4S}** causes the hydrogel to swell more, thus increasing the mesh size).

Moreover, there was an excellent correlation between the compressive strength of the blended hydrogels and the content of **2_{4S}** (Figure 2.13); the compressive strength of the hydrogels increased with the percentage of **2_{4S}**, while the stiffness of the material decreased. This in turn, further confirms the feasibility of the blending strategy to produce hydrogels with tuneable mechanical properties suitable for a wide range of biomedical applications.

Table 2.4 Characterisation of the blended thiol-yne PEG hydrogels ($2_{1s}:2_{4s}$ ratio)

Hydrogel	Gel Fraction (%)	Equilibrium Water Content (%)	Mesh Size ^a (nm)	Compressive Stress (kPa)	G' (Pa) ^b	Young's Modulus (kPa)
$3_{1A}2_{1S}$	73.9 ± 2.6	95.2 ± 0.9	5.80 ± 0.49	670 ± 14	5562 ± 599	0.11 ± 0.01
$3_{1A}2_{75:25}$	73.7 ± 2.5	97.6 ± 0.3	8.85 ± 0.44	1188 ± 481	2192 ± 385	0.23 ± 0.05
$3_{1A}2_{50:50}$	80.8 ± 0.5	97.0 ± 0.5	9.84 ± 1.04	2074 ± 415	1459 ± 354	0.19 ± 0.05
$3_{1A}2_{25:75}$	75.3 ± 2.1	97.9 ± 0.1	10.89 ± 0.37	2165 ± 571	233 ± 4.3	0.18 ± 0.06
$3_{1A}2_{4S}$	71.8 ± 0.2	95.1 ± 2.4	9.74 ± 0.93	2339 ± 179	168 ± 49	0.21 ± 0.02

^aCalculated from the Flory-Rehner equation. ^bAverage of G' at 10 rad s^{-1} and 0.1% strain

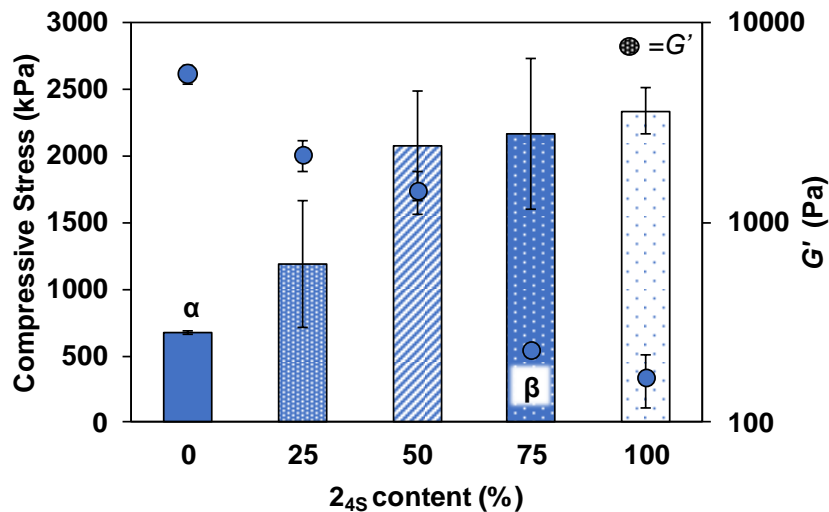


Figure 2.13. The correlation between the percentage of 2_{4s} and the effect on the compressive stress and G' at 0.1% strain and 10 rad s^{-1} . α = Compressive stress significantly different from 100% 2_{4s} condition $p < 0.05$. β = G' not significantly different from 100% 2_{4s} condition $p < 0.05$.

2.3. Conclusions

New and adaptable biomaterials are necessary to aid our understanding of different biological environments (*e.g.* cancer metastasis and cell differentiation). To address this need, we have designed hydrogels with a range of biologically relevant properties. After functionalising a range of PEG precursors that differ in architecture and molecular weight with alkyne or thiol end groups, we have demonstrated that the nucleophilic thiol-yne click reaction is highly suitable for preparing robust hydrogels under physiological relevant conditions, without the need of an external catalyst or any further purification steps. Most importantly, with suitable molecular geometry, these hydrogels display high mechanical strength with repeatable compression without rupture, revealing their ability to mimic a variety of biological environments. Furthermore, by judicious choice of the PEG precursor, the mechanical properties of these materials can be tuned over almost three orders of magnitude, accessing material properties similar to soft, medium, and high load-bearing tissues. Overall, the potential of the nucleophilic thiol-yne reaction to form tuneable robust hydrogels that can be adapted to a range of bioapplications allows future work to build on this fundamental study, thus improving the properties of biomaterials to better mimic different *in vivo* conditions.

2.4. References

1. R. Langer and D. A. Tirrell, *Nature*, 2004, **428**, 487-492.
2. D. W. Hutmacher, *Biomaterials*, 2000, **21**, 2529-2543.
3. M. Elsbahy and K. L. Wooley, *Chem. Soc. Rev.*, 2012, **41**, 2545-2561.
4. E. A. Appel, J. del Barrio, X. J. Loh and O. A. Scherman, *Chem. Soc. Rev.*, 2012, **41**, 6195-6214.
5. A. S. Hoffman, *Adv. Drug Deliv. Rev.*, 2002, **54**, 3-12.
6. J. Y. Sun, X. H. Zhao, W. R. K. Illeperuma, O. Chaudhuri, K. H. Oh, D. J. Mooney, J. J. Vlassak and Z. G. Suo, *Nature*, 2012, **489**, 133-136.
7. K. Y. Lee and D. J. Mooney, *Chem. Rev.*, 2001, **101**, 1869-1879.
8. S. Pina, J. M. Oliveira and R. L. Reis, *Adv. Mater.*, 2015, **27**, 1143-1169.
9. N. Annabi, A. Tamayol, J. A. Uquillas, M. Akbari, L. E. Bertassoni, C. Cha, G. Camci-Unal, M. R. Dokmeci, N. A. Peppas and A. Khademhosseini, *Adv. Mater.*, 2014, **26**, 85-124.
10. P. M. Kharkar, K. L. Kiick and A. M. Kloxin, *Chem. Soc. Rev.*, 2013, **42**, 7335-7372.
11. S. Van Vlierberghe, P. Dubruel and E. Schacht, *Biomacromolecules*, 2011, **12**, 1387-1408.
12. J. M. Zhu, *Biomaterials*, 2010, **31**, 4639-4656.

13. J. L. Drury and D. J. Mooney, *Biomaterials*, 2003, **24**, 4337-4351.
14. B. V. Slaughter, S. S. Khurshid, O. Z. Fisher, A. Khademhosseini and N. A. Peppas, *Adv. Mater.*, 2009, **21**, 3307-3329.
15. Y. Qiu and K. Park, *Adv. Drug Deliv. Rev.*, 2001, **53**, 321-339.
16. S. P. Zustiak and J. B. Leach, *Biomacromolecules*, 2010, **11**, 1348-1357.
17. T. Canal and N. A. Peppas, *J. Biomed. Mater. Res.*, 1989, **23**, 1183-1193.
18. A. J. Engler, S. Sen, H. L. Sweeney and D. E. Discher, *Cell*, 2006, **126**, 677-689.
19. E. Bellas and C. S. Chen, *Curr. Opin. Cell Biol.*, 2014, **31**, 92-97.
20. Enateri V. Alakpa, V. Jayawarna, A. Lampel, Karl V. Burgess, Christopher C. West, Sanne C. J. Bakker, S. Roy, N. Javid, S. Fleming, Dimitris A. Lamprou, J. Yang, A. Miller, Andrew J. Urquhart, Pim W. J. M. Frederix, Neil T. Hunt, B. Péault, Rein V. Ulijn and Matthew J. Dalby, *Chem*, 2016, **1**, 298-319.
21. S. Khetan, M. Guvendiren, W. R. Legant, D. M. Cohen, C. S. Chen and J. A. Burdick, *Nat. Mater.*, 2013, **12**, 458-465.
22. D. A. Young, Y. S. Choi, A. J. Engler and K. L. Christman, *Biomaterials*, 2013, **34**, 8581-8588.
23. W. L. Murphy, T. C. McDevitt and A. J. Engler, *Nat. Mater.*, 2014, **13**, 547-557.
24. P. C. Georges and P. A. Janmey, *J. Appl. Physiol.*, 2005, **98**, 1547-1553.

25. M. J. Paszek, N. Zahir, K. R. Johnson, J. N. Lakins, G. I. Rozenberg, A. Gefen, C. A. Reinhart-King, S. S. Margulies, M. Dembo, D. Boettiger, D. A. Hammer and V. M. Weaver, *Cancer Cell*, 2005, **8**, 241-254.
26. D. E. Discher, P. Janmey and Y.-I. Wang, *Science*, 2005, **310**, 1139-1143.
27. A. J. Engler, M. A. Griffin, S. Sen, C. G. Bönnemann, H. L. Sweeney and D. E. Discher, *J. Cell Biol.*, 2004, **166**, 877-887.
28. I. Levental, P. C. Georges and P. A. Janmey, *Soft Matter*, 2007, **3**, 299-306.
29. E. M. Sletten and C. R. Bertozzi, *Acc. Chem. Res.*, 2011, **44**, 666-676.
30. C. E. Hoyle and C. N. Bowman, *Angew. Chem., Int. Ed.*, 2010, **49**, 1540-1573.
31. M. A. Azagarsamy and K. S. Anseth, *ACS Macro Lett.*, 2013, **2**, 5-9.
32. N. J. Agard, J. A. Prescher and C. R. Bertozzi, *J. Am. Chem. Soc.*, 2004, **126**, 15046-15047.
33. C. A. DeForest, B. D. Polizzotti and K. S. Anseth, *Nat. Mater.*, 2009, **8**, 659-664.
34. C. A. DeForest, E. A. Sims and K. S. Anseth, *Chem. Mater.*, 2010, **22**, 4783-4790.
35. D. Steinhilber, T. Rossow, S. Wedepohl, F. Paulus, S. Seiffert and R. Haag, *Angew. Chem., Int. Ed.*, 2013, **52**, 13538-13543.
36. V. X. Truong, M. P. Ablett, H. T. J. Gilbert, J. Bowen, S. M. Richardson, J. A. Hoyland and A. P. Dove, *Biomater. Sci.*, 2014, **2**, 167-175.

37. M. L. Blackman, M. Royzen and J. M. Fox, *J. Am. Chem. Soc.*, 2008, **130**, 13518-13519.
38. C. F. Hansell, P. Espeel, M. M. Stamenovic, I. A. Barker, A. P. Dove, F. E. Du Prez and R. K. O'Reilly, *J. Am. Chem. Soc.*, 2011, **133**, 13828-13831.
39. D. L. Alge, M. A. Azagarsamy, D. F. Donohue and K. S. Anseth, *Biomacromolecules*, 2013, **14**, 949-953.
40. Z. K. Zander, G. Hua, C. G. Wiener, B. D. Vogt and M. L. Becker, *Adv. Mater.*, 2015, **27**, 6283-6288.
41. G. N. Grover, J. Lam, T. H. Nguyen, T. Segura and H. D. Maynard, *Biomacromolecules*, 2012, **13**, 3013-3017.
42. G. N. Grover, R. L. Braden and K. L. Christman, *Adv. Mater.*, 2013, **25**, 2937-2942.
43. F. Lin, J. Yu, W. Tang, J. Zheng, A. Defante, K. Guo, C. Wesdemiotis and M. L. Becker, *Biomacromolecules*, 2013, **14**, 3749-3758.
44. P. van de Wetering, A. T. Metters, R. G. Schoenmakers and J. A. Hubbell, *J. Control. Release*, 2005, **102**, 619-627.
45. A. E. Rydholm, S. K. Reddy, K. S. Anseth and C. N. Bowman, *Biomacromolecules*, 2006, **7**, 2827-2836.
46. P. M. Kharkar, M. S. Rehmman, K. M. Skeens, E. Maverakis and A. M. Kloxin, *ACS Biomater. Sci. Eng.*, 2016, **2**, 165-179.

47. M. A. Haque, T. Kurokawa and J. P. Gong, *Polymer*, 2012, **53**, 1805-1822.
48. V. X. Truong and A. P. Dove, *Angew. Chem., Int. Ed.*, 2013, **52**, 4132-4136.
49. B. Yao, J. Mei, J. Li, J. Wang, H. Wu, J. Z. Sun, A. Qin and B. Z. Tang, *Macromolecules*, 2014, **47**, 1325-1333.
50. O. u. Türünç and M. A. R. Meier, *J. Polym. Sci., Part A: Polym. Chem.*, 2012, **50**, 1689-1695.
51. R. M. Hensarling, V. A. Doughty, J. W. Chan and D. L. Patton, *J. Am. Chem. Soc.*, 2009, **131**, 14673-14675.
52. L. Sun, W. Liu and C.-M. Dong, *Chem. Comm.*, 2011, **47**, 11282-11284.
53. C. A. Bell, J. Yu, I. A. Barker, V. X. Truong, Z. Cao, A. V. Dobrinyin, M. L. Becker and A. P. Dove, *Angew. Chem.*, 2016, **128**, 13270-13274.
54. X. Y. Cai, J. Z. Li, N. N. Li, J. C. Chen, E.-T. Kang and L. Q. Xu, *Biomater. Sci.*, 2016, **4**, 1663-1672.
55. V. X. Truong, M. P. Ablett, S. M. Richardson, J. A. Hoyland and A. P. Dove, *J. Am. Chem. Soc.*, 2015, **137**, 1618-1622.
56. Y. S. Zhang and A. Khademhosseini, *Science*, 2017, **356**, eaaf3627.
57. M. S. Hahn, H. Liao, D. Munoz-Pinto, X. Qu, Y. Hou and M. A. Grunlan, *Acta Biomater.*, 2008, **4**, 1161-1171.
58. H. X. Zhou, E. M. Schon, M. Z. Wang, M. J. Glassman, J. Liu, M. J. Zhong, D. D. Diaz, B. D. Olsen and J. A. Johnson, *J. Am. Chem. Soc.*, 2014, **136**, 9464-9470.

59. H. X. Zhou, J. Woo, A. M. Cok, M. Z. Wang, B. D. Olsen and J. A. Johnson, *J. A. Proc. Nat. Acad. Sci. U. S. A.*, 2012, **109**, 19119-19124.
60. K. Kawamoto, M. J. Zhong, R. Wang, B. D. Olsen and J. A. Johnson, *Macromolecules*, 2015, **48**, 8980-8988.

Chapter 3.

Nonswelling Thiol-yne Crosslinked Hydrogel Materials as Cytocompatible Soft Tissue Scaffolds

3.1. Introduction

Hydrogels have become a powerful platform as tissue engineering scaffolds as a consequence of their unique features (high water content, suitable porosity, synthetic versatility, and biocompatibility), however they suffer from swelling-induced behaviour which can limit their applications in this field.¹⁻³ Furthermore, these materials must mimic unique biological environments by displaying specific mechanical strength, robustness, and stability. Therefore, the design of hydrogels with finely tuned properties for a specific bio application is still a challenging task.⁴⁻⁶

To address this issue, biorthogonal click hydrogels that form rapidly under physiological conditions by covalently bonding non-toxic polymeric chains through easily accessible functional groups, have been synthesised.⁷⁻⁹ As previously mentioned, these materials, which are envisaged as promising soft tissue scaffolds, can be prepared using a wide range of click reactions for example thiol-ene, oxime, inverse electron demand Diels Alder, strain promoted azide-alkyne cycloaddition (SPAAC) and copper-catalysed azide-alkyne cycloaddition (CuAAC).^{7, 8} Although these chemistries form efficient networks that are biocompatible, some of the functional groups can be difficult to synthesise onto polymer backbones *e.g.* strained alkynes. Furthermore, some click reactions follow a UV initiated radical pathway, using a photoinitiator to conduct the crosslinking reaction releasing free radicals during the crosslinking process. It has been demonstrated in the literature, that the release of free radicals during the network formation can be cytotoxic to some cell lines *e.g.* human mesenchymal stem cells (hMSCs) and can cause more toxicity issues than the presence of the photoinitiator.¹⁰⁻¹² Therefore by using a radical pathway the cytotoxicity of the crosslinking reaction can

limit the number of different cell lines which can be encapsulated into the network, reducing the number of cell lines which are able to be cultured in these systems. In particular, hMSC are commonly encapsulated in tissue engineering applications (*e.g.* scaffolds) as they provide a useful and relevant cell line which has the potential to differentiate into a wide range of cell types.¹³ In contrast, the nucleophilic thiol-yne addition reaction¹⁴ is highly suitable for hydrogel synthesis as a consequence of its efficient and rapid nature, through the use of easily accessible functional end groups (activated alkyne- and thiol-functionalities). This allows for the design of unique hydrogels with pre-defined and robust features.¹⁵⁻¹⁸

In Chapter 2,¹⁷ the synthesis of robust poly(ethylene glycol) (PEG) thiol-yne hydrogels with tuneable properties was described. To exploit the nucleophilic pathway, PEG precursors were easily functionalised with either an activated alkyne (carbonyl adjacent to the alkyne) or thiol end groups allowing the reaction to take place under physiological conditions (37 °C in phosphate buffered saline (PBS) solution, pH 7.4) without the need of an external catalyst. Through the optimisation of the molecular weight, architecture, and composition of the alkyne- and thiol-terminated PEG precursors, the resulting hydrogels displayed a wide range of tuneable compressive strengths (up to 2.4 MPa) and stiffness. These tuneable properties demonstrated how the materials could be tuned to a range of applicable mechanical properties making them ideal to mimic different biological environments (*e.g.* muscle or cartilage).

To further develop the thiol-yne PEG system, the hydrogel materials need to maintain their robust mechanical properties in an environment which resembles the

relevant *in vivo* settings (e.g. immersed in an aqueous environment). This will allow understanding into how the polymer network behaves in water including its swelling and degradation rate. Although some hydrogel systems remain unaltered when immersed in aqueous solutions,^{19, 20} in general most swell in aqueous environments at 37 °C, which not only expands and deforms the polymeric network isotropically, but also has a major impact on their mechanical performance. Swelling induced effects include loss of mechanical performance,²¹ changes in hydrogel stiffness,²² enhanced hydrolytic degradation,¹ or when used *in vivo*, compromised patient health by excessive compression to the surrounding tissue, thus greatly limiting their biomedical application. Consequently, research into the mechanical response of our thiol-yne PEG hydrogels in the swollen state over time is an important and relevant study for these materials to further progress them as biomaterials.²³

Attempts in the literature to overcome this drawback rely on synthesising nonswellable hydrogels which are able to retain their high compressive modulus and strength despite being immersed in aqueous media.²⁴⁻²⁷ Specifically, the swelling induced by the hydrophilic segments of the polymer backbone has been shown to be counterbalanced by either; 1) exploiting the thermoresponsive properties of polymers that collapse above a certain temperature, ideally body temperature,^{18, 25, 28} or 2) modulating the architecture of the polymeric precursors.^{1, 24, 29} Both approaches have been shown to effectivity reduce the swelling characteristics of different hydrogel systems. Recently, the former approach (1) was exemplified by Truong *et al.*¹⁸ who applied this method to the preparation of nucleophilic thiol-yne hydrogels with a commercially available thermoresponsive triblock copolymer, Pluronic®, made from PEG and poly(propylene

oxide) (PPO), PEG-PPG-PEG. The Pluronic unit is thermoresponsive around body temperature therefore they were able to utilise it to reduce water uptake at a physiologically relevant temperature. The viscoelastic properties of the resulting hydrogels were characterised by rheology. Notably however, the authors found that these systems were not suitable for 3D cell encapsulation, instead the system led to high levels of cell death as a consequence of a pluronic linker in the PEG hydrogel backbone. Furthermore, the effect of swelling suppression on the compressive strength of thiol-yne hydrogels was not assessed.

Alternatively, by modulating the architecture of the polymer precursor using multi-arm precursors results in dense hydrogel networks with high crosslinking densities and reduced hydrophilicity. This has been shown by Kamata and co workers^{1, 24, 29} who have demonstrated how the control over swelling and shrinking of PEG networks produces hydrogels with robust mechanical properties (up to 60 MPa) without hysteresis thus demonstrating an effective route for creating nonswelling hydrogel materials.

Herein, the performance of thiol-yne PEG hydrogels has been improved,¹⁷ by rendering them nonswellable and thus controlling their degradation profiles and mechanical performance in aqueous environments. To do this, the thiol-functionalised PEG precursor was altered to effectively suppress swelling by increasing the hydrophobic nature of the PEG hydrogels by increasing the number of crosslinking sites in the network, using alkyne- and thiol-functionalised PEG precursors displaying a 3- or 4-arm architecture. This system has been compared to the thiol-yne hydrogels described in Chapter 2 where a 2-arm thiol-functionalised PEG precursor was used.^{17, 18}

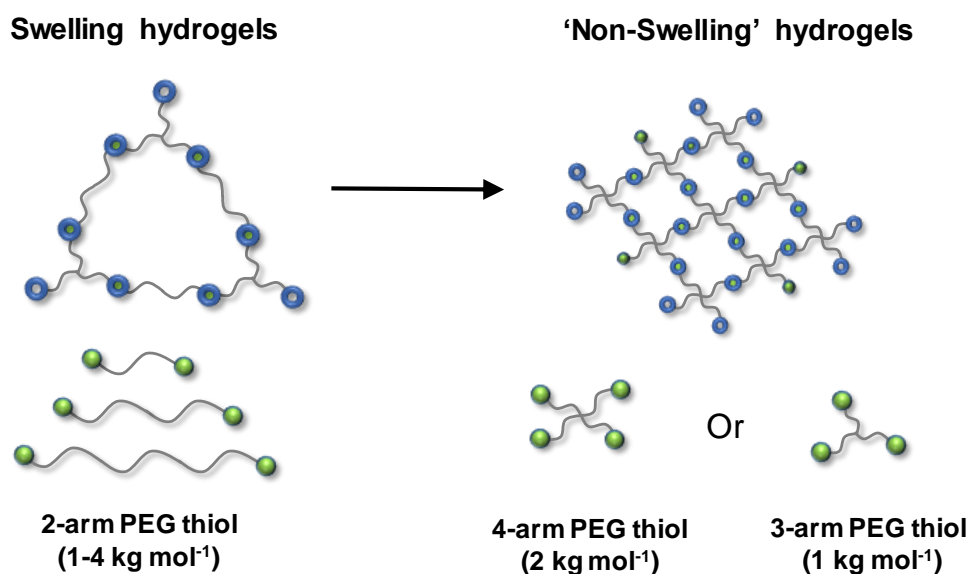
The characterisation of the resulting hydrogels was monitored through the evolution of their compressive strength with time after being immersed in PBS solution at 37 °C while also capturing their degradation profiles. Most importantly, their potential as soft tissue scaffolds was assessed through the encapsulation of MC3T3-E1 (murine pre-osteoblasts) cells over a 72 h period.

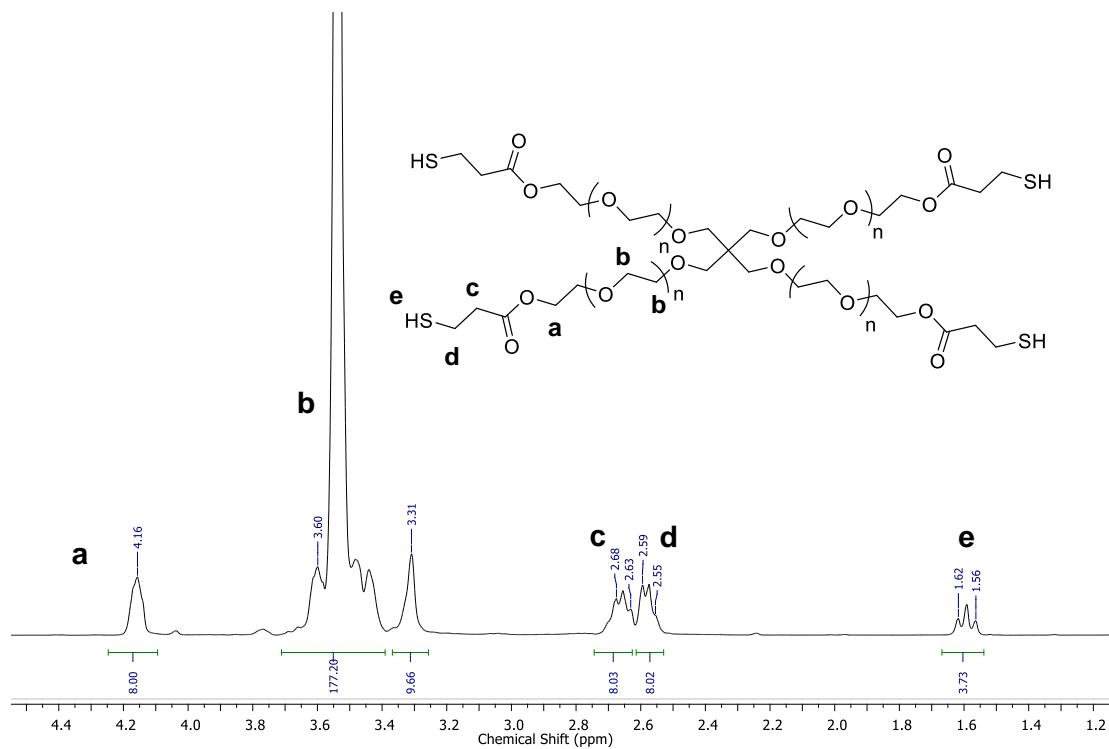
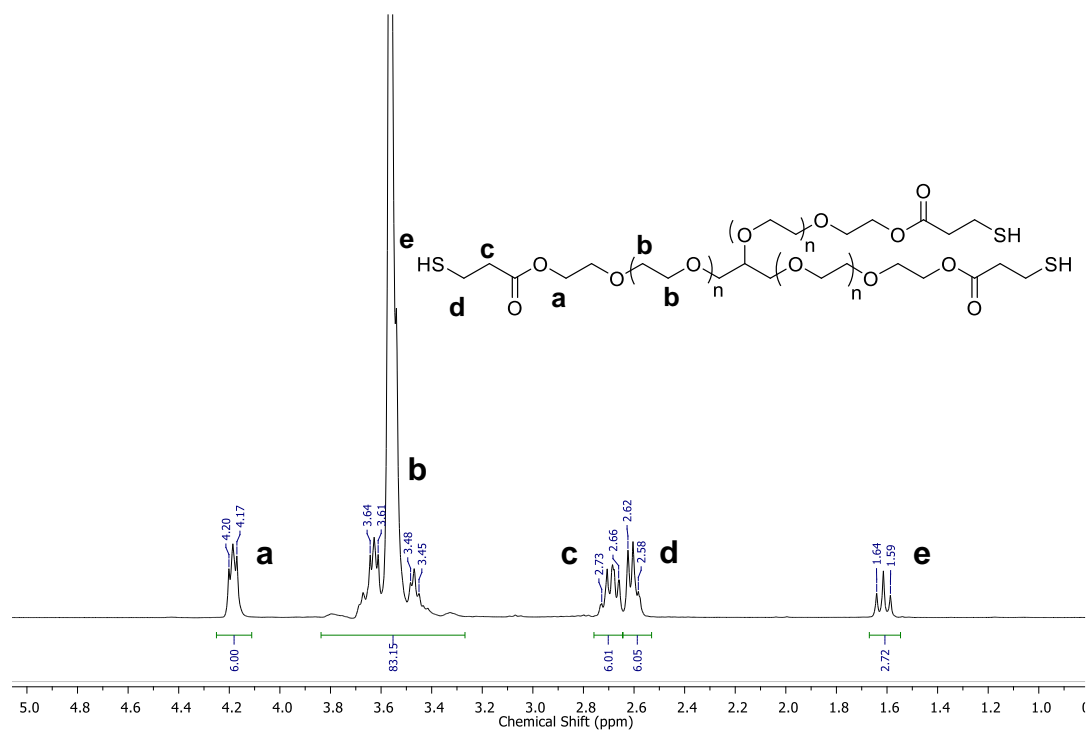
3.2. Results and Discussion

3.2.1. Synthesis of Alkyne- and Thiol-Terminated PEG Precursors

The design of nonswellable hydrogels has been achieved by increasing the crosslinking density of the thiol-yne hydrogel network described in Chapter 2, an accessible strategy that alters the swelling characteristics of our previous robust PEG hydrogels prepared through the nucleophilic thiol-yne addition reaction (Scheme 3.1).¹⁷ This route reduces the hydrophilicity of the system, by incorporating in 3 and 4-arm thiol-functionalised PEG precursors using Fischer esterification reactions. These reactions are highly efficient, with end group conversion values up to 99%, determined through ¹H NMR spectroscopy and SEC analyses (Table 3.1, Figures 3.1-3.3). The PEG thiol precursors were then reacted with the 3- and 4-arm PEG alkyne precursors (synthesis described in Chapter 2).

Scheme 3.1. A route to form nonswellable thiol-yne hydrogels based on multi-arm PEG precursors.





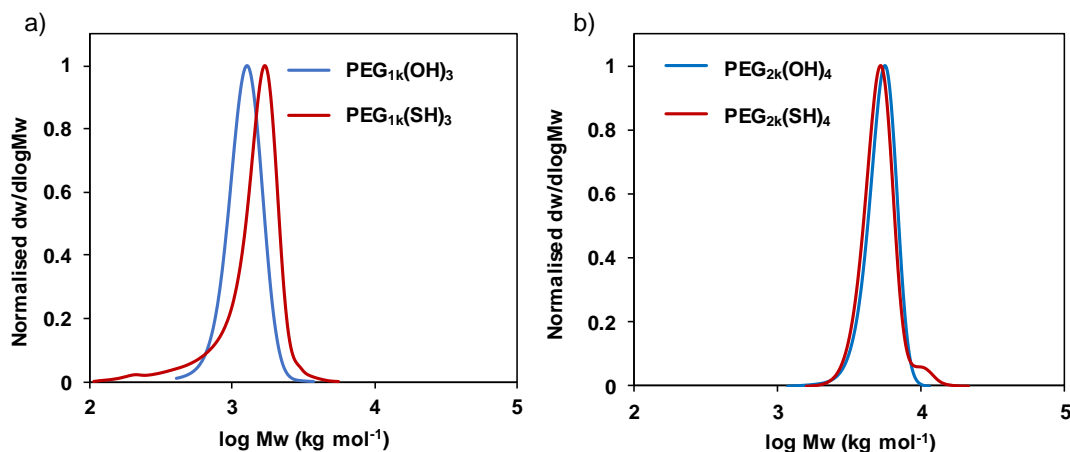


Figure 3.3. SEC chromatograms of a) 3-arm PEG thiol precursor (1 kg mol⁻¹), b) 4-arm PEG thiol precursor (2 kg mol⁻¹). Molecular weights determined against polystyrene standards using CHCl₃ (0.5% NEt₃) as eluent.

Once the modified PEG thiol precursors were synthesised, hydrogels with 10 wt% polymer content were subsequently prepared by mixing solutions containing a 1:1 molar ratio of alkyne to thiol end groups in PBS solution at pH 7.4. The same hydrogel nomenclature from Chapter 2 has been expanded here to include the additional PEG precursors. The system is dependent on the PEG precursors, each precursor is denoted considering the number of arms, molecular weight, and the incorporated functionality, **S** for thiol or **A** for alkyne. Hence, **3_{1S}** refers to the 3-arm thiol-terminated PEG precursor (1 kg mol⁻¹). For comparison, the original 3-arm PEG alkyne hydrogel system designed in Chapter 2 has also been fully characterised to assess its degradation and mechanical properties over time.

Table 3.1. Characterisation data for the 3- and 4-arm PEG thiol precursors

Thiol PEG precursor	End group conversion (%) ^a	M_n NMR ^a (kg mol ⁻¹)	M_n SEC ^b (kg mol ⁻¹)	D_M^b
PEG _{1k} (SH) ₃	96	1.3	1.2	1.08
PEG _{2k} (SH) ₄	>99	1.9	4.7	1.06

^aDetermined by ¹H NMR spectroscopy in deuterated chloroform. ^bDetermined by SEC analysis in chloroform against polystyrene standards.

3.2.2. Characterisation of Swellable Thiol-yne PEG Hydrogels

In general, most hydrogels swell when placed in aqueous solution; consequently, their volume increases, and severe alterations of their mechanical properties occur.²⁴ In order to characterise the swelling behaviour of the previously related system (Chapter 2), thiol-yne PEG hydrogels were prepared using 2-arm thiol-terminated PEG precursors (**31A21S**, **31A22S**, and **31A23S**) to provide control measurements. To assess their swelling profile the swelling factor (SF) for each system was calculated (Equation 3.1).

$$\text{Swelling Factor (\%)} = \frac{W_t}{W_0} \times 100\%$$

Equation 3.1. Swelling factor equation where W_t is the weight measured at specific time point and W_0 is the initial wet weight before immersed (after curing for 1 h).

As expected, these hydrogels undergo swelling up to $179.9 \pm 29.4\%$, $443.0 \pm 7.4\%$, and $408.0 \pm 9.0\%$, respectively, before degrading completely in the aqueous solution within 3 and 4 days (Figure 3.4a). For thiol-yne hydrogels, bulk hydrolytic degradation occurs, which results from the combination of the diffusion of water into a polymer network and the subsequent random cleavage of hydrolysable bonds.³⁰⁻³² In addition, carboxylic acid groups, from the ester cleavage, display an autocatalytic effect, decreasing the density of the network which contributes to the loss of structural and mechanical stability. Ultimately, as observed, the hydrogel network swelled and then

dissolves into the PBS solution.³³ Additionally, swelling experiments also reveal information on the equilibrium water content (EWC) and mesh size of the hydrogel networks. Both features are key factors for tissue engineering scaffolds: cells require high water content, as well as an adequate diffusion of nutrients, oxygen, and growth factors in order to grow and proliferate. Data for the **31A21S** and **31A22S** systems, collected in Chapter 2, have been repeated here for easier comparison with the **31A23S** system and nonswelling systems. High EWC percentages (94-95%, Table 3.2) confirmed that the swellable hydrogels contain porous structures with the ability to hold large amounts of water. The average mesh size of these thiol-yne networks, calculated using the Flory-Rehner equation, explained in Chapter 2,³⁴ ranged between 5.8 and 6.4 nm (Table 3.2), demonstrating there was little difference in mesh size when the molecular weight of the PEG thiol precursor increased to 3 kg mol⁻¹.

Table 3.2. Gelation time (GT) and swelling kinetics of the swellable thiol-yne hydrogels at 10 wt% in PBS solution (1:1 molar ratio of alkyne to thiol end groups).

Hydrogel	GT ^a (s)	GF (%)	EWC (%)	Mesh Size ^b (nm)
31A21S	210 ± 7	74 ± 2.6	95 ± 0.9	5.8 ± 0.49
31A22S	290 ± 10	80 ± 1.9	94 ± 0.8	6.4 ± 0.16
31A23S	438 ± 5	78 ± 4.9	95 ± 0.1	5.9 ± 0.03

The hydrogel naming (**X_ZA_YZ_S**) denotes its structure, where X = number of arms of the alkyne precursor, Y = number of arms of the thiol precursor, and Z = molecular weight of the PEG precursor. a) Measured via the vial tilt methods. b) Calculated from the Flory-Rehner equation.

As expected, the swelling response of the control hydrogels (**31A21S**, **31A22S**, and **31A23S**) had a significant negative effect on their mechanical performance (Figure 3.4). The compressive strength decreased with immersion time (Figure 3.4b), which became

more evident with increasing molecular weight of the thiol-terminated PEG precursor, for instance, for the $3_{1A}2_{3S}$ system, the compressive strength decreased from 2.4 ± 0.3 MPa to 1.0 ± 0.05 MPa. These hydrogels had long, flexible PEG thiol chains which could withstand large amounts of strain. However, these PEG chains also displayed a hydrophilic character, thus attracting more water molecules into the network, which in turn accelerated degradation rates and impaired the mechanical performance. Hence, to counteract this effect, specific modifications of the PEG precursors were targeted to render the hydrogels nonswellable (Scheme 3.2). The resulting nonswellable hydrogels were immersed in PBS solution at 37°C for 30 days or until degradation, and their swelling response and mechanical properties in the swollen state were assessed periodically.

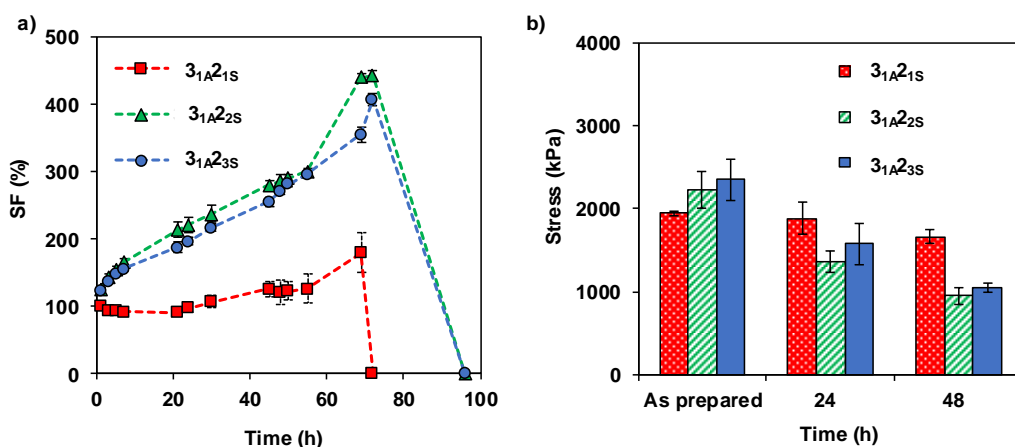
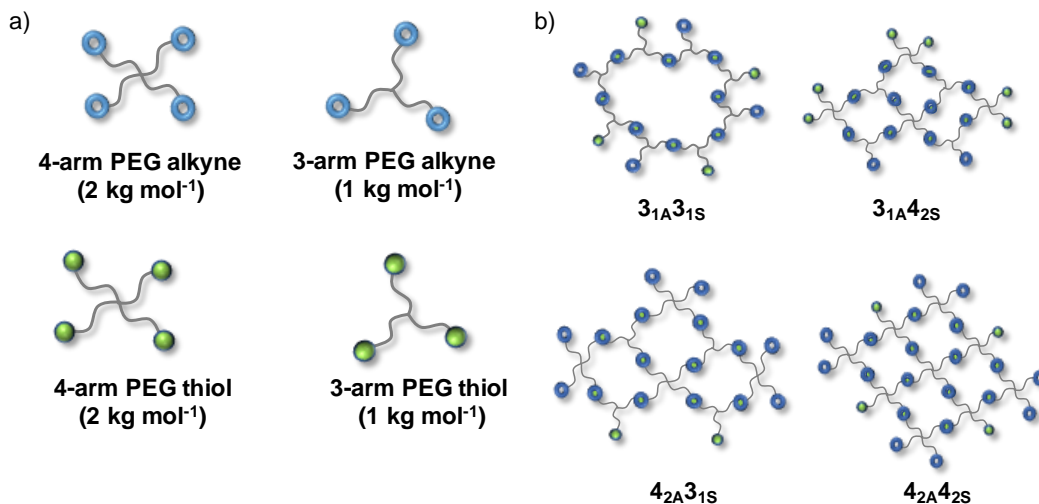


Figure 3.4. Swellable hydrogels characterisation ($3_{1A}2_{1S}$ = red; $3_{1A}2_{2S}$ = green; $3_{1A}2_{3S}$ = blue): a) SF (%) as a function of time in PBS at 37°C and b) evolution of stress at break with swelling time.

Scheme 3.2. Nonswellable thiol-yne hydrogels based on multi-arm PEG precursors, a) precursors used to form nonswellable hydrogels, b) Combinations of potential nonswellable networks.



3.2.3. Characterisation of Nonswellable Thiol-yne PEG Hydrogels

The water uptake of thiol-yne hydrogels immersed in PBS solution at 37 °C was effectively regulated by applying a straightforward approach based on rendering the polymeric networks less hydrophilic. By increasing the number of crosslinking sites and reducing the molecular weight of the hydrophilic polymer backbone increases the density of the network,²⁴ preventing water to be drawn into the system creating a nonswelling multi-arm thiol-yne hydrogel system. In the multi-arm thiol-yne hydrogel systems, the 2-arm thiol-functionalised PEG precursors were replaced with either a 3- or 4-arm precursor (Scheme 3.2). Four multi-arm PEG precursors were synthesised (**3_{1S}**, **3_{1A}**, **4_{2S}**, **4_{2A}**), as described in section 3.2.1, and accordingly four different hydrogel systems were prepared as a result of different combinations: **3_{1A}3_{1S}**, **3_{1A}4_{2S}**, **4_{2A}3_{1S}**, and **4_{2A}4_{2S}**.

3.2.3.1 Gelation Time

All the multi-arm hydrogels formed almost immediately after mixing the alkyne and thiol containing solutions. Gelation times for these systems, which were firstly determined by the vial tilt method and ranged between 11 and 26 s (Table 3.3). The fast gelation times were attributed to the elevated number of crosslinking points that were also spatially closer to each other, thus resulting in rapid gelation. This effect is more pronounced for the **4_{2A}4_{2S}** hydrogel, formed with the 4-arm PEG precursors, which displays the highest number of reactive groups per molecule. In contrast, all the control systems, which are formed with 2-arm thiol PEG precursors, (section 3.2.2), displayed higher gelation times that increase with molecular weight (GT= 210-438 s).

Table 3.3. Gelation time (GT), and swelling kinetics of nonswelling hydrogels at 10 wt% in PBS solution (1:1 molar ratio of alkyne to thiol end groups).

Hydrogel	GT ^a (s)	GF (%)	EWC (%)	Mesh Size ^b (nm)
3_{1A}3_{1S}	26 ± 3	78 ± 1.2	90 ± 0.2	4.2 ± 0.07
3_{1A}4_{2S}	25 ± 9	75 ± 1.3	90 ± 0.5	4.7 ± 0.14
4_{2A}3_{1S}	15 ± 5	92 ± 0.7	87 ± 1.7	4.4 ± 0.47
4_{2A}4_{2S}	11 ± 2	89 ± 1.8	86 ± 0.9	4.4 ± 0.24

a) Measured via the vial tilt methods. b) Calculated from the Flory-Rehner equation.

Among the different theories applied to the gelation of polymers, the Flory-Stockmayer theory states that gelation occurs when systems of high functionality produce an infinite molecular weight network through crosslinking provided that the reaction is carried out far enough, thus shifting the system from the liquid to the gel phase.³⁵⁻³⁷ This definition is derived from the probability of finding a crosslinking point during gelation.

Hence, the gelation point, is reached when a critical number of intermolecular linkages have been exceeded. More specifically, this theory states that the theoretical critical amount of crosslinks needed to form a gel, p_c , can be calculated (Equation 3.2).

$$p_c = \frac{1}{\sqrt{(f_A - 1)(f_B - 1)/r}}$$

Equation 3.2. Flory-Stockmayer equation to calculate the theoretical critical amount of crosslinks needed to form a gel, p_c , where f_A is the functionality of the alkyne PEG precursors, f_B is the functionality of the thiol PEG precursors, and r is the ratio between the total number of alkyne and thiol groups (*i.e.* $r = 1$ as the thiol-yne hydrogels are synthesised under stoichiometric conditions).³⁸

For the control systems with a 3-arm alkyne precursor and a 2-arm thiol precursor (*i.e.* **3_{1A}2_{1S}**, **3_{1A}2_{2S}**, **3_{1A}2_{3S}**), the value that the Flory-Stockmayer theory predicts for p_c is 0.71, which means that gelation takes place when the amount of PEG alkyne precursors that have reacted is higher than 71%. In the case of the multi-arm hydrogel systems with either a 3- or 4-arm PEG precursor, the value obtained for p_c is 0.50, 0.41, and 0.33 for **3_{1A}3_{1S}**, **3_{1A}4_{2S}** or **4_{2A}3_{1S}**, and **4_{2A}4_{2S}**, respectively, thus indicating that these systems reach the gelation point with fewer intermolecular linkages. However, the reaction still continues between reactive groups after the gelation point as indicated by the high GF values (75-92%, Table 3.3). GF is an indication of the efficiency of the reaction, revealing that a high percentage of the precursors undergo the thiol-yne reaction resulting in a network with more crosslinked sites. Hence, although other factors such as molecular weight of the PEG precursors influence gelation, the gelation time values observed by the vial tilt method are in good agreement with the values predicted from the Flory-Stockmayer theory.

3.2.3.2 Morphology

The calculated mesh size for the multi-arm PEG hydrogels was between 4.2-4.7 nm, (Table 3.3) smaller than the control swellable hydrogels (5.8-6.4 nm). This confirms the prediction that increased crosslinking sites and reduced molecular weight PEG precursors results in a denser network formation when using the 3- or 4-arm PEG thiol precursors which will aid their nonswelling performance. Cryo SEM characterisation was also conducted to further understand the morphology of the networks by the ice crystal growth during the freezing process. For all systems, the structure revealed is porous with a range of different sizes that ice crystals can grow to during the freezing process (Figure 3.5).

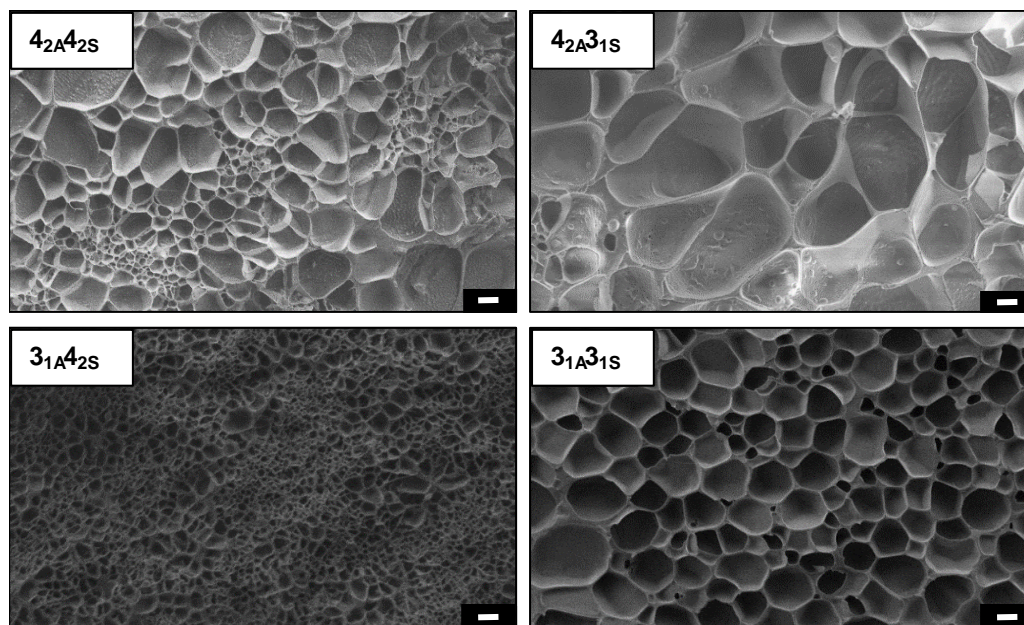


Figure 3.5. Cryo SEM images of nonswellable thiol-yne PEG hydrogels, scale bar = 2 μ M.

The hydrogels prepared with **4_{2A}** exhibited a much broader distribution of ice crystal sizes, while using **3_{1A}** resulted in hydrogels with a more homogeneous structure. Additionally, the ice crystal structure for the **3_{1A}4_{2S}** is significantly smaller in comparison

to the other multi-arm hydrogel systems, which could be an effect of the freezing process during imaging.

3.2.3.3 Rheological Characterisation

Rheological tests were carried out to fully evaluate the viscoelastic properties of the nonswellable thiol-yne hydrogels, to determine any possible drawbacks derived from this approach to suppress the swelling response. By monitoring the evolution of both the storage (G') and loss (G'') moduli of a sample with time, the gelation time, which is defined as the crossover point between G' and G'' , can be determined. The gelation time for the four multi-arm systems, was within 30 s (Figure 3.6a), which was in good agreement with the results from the vial tilt method, thus indicating that the hydrogels are fully crosslinked into stable and robust networks despite the quick gelation process (G' and G'' plateau after 2 min). As previously observed, increasing the concentration of reactive end groups in solution reduced the gelation time.

The viscoelastic properties were determined by monitoring the G' and G'' moduli as the strain on the hydrogel increased (Figure 3.6b). All the multi-arm hydrogels showed high G' (ranging from 7.3 ± 0.08 - 18.8 ± 0.8 kPa) which is indicative of highly viscoelastic materials and significantly higher than the control swelling **31A23S** system ($G' = 3 \pm 0.4$ kPa). Moreover, G' increased with the number of functional groups per molecule, thus suggesting that a more rigid structure is formed as a consequence of the higher density of crosslinking points. Consequently, the stiffer materials were unable to withstand high levels of strain. For instance, G' decreases at 32% of strain for **42A42A** and **31A42S**, whereas the hydrogels with a more elastic network (**42A31S** and **31A31S**) start to yield at higher strain

(47%, Figure 3.6b). However, the G' did not correlate with the calculated mesh size for these hydrogels indicating the swelling profile of these hydrogels had been altered. The Flory-Renher equation used to calculate mesh size assumes the structure swells when immersed in aqueous conditions therefore if these structures are nonswelling the calculated mesh size may deviate from the true value and therefore not correlate with the rheological properties.³⁴

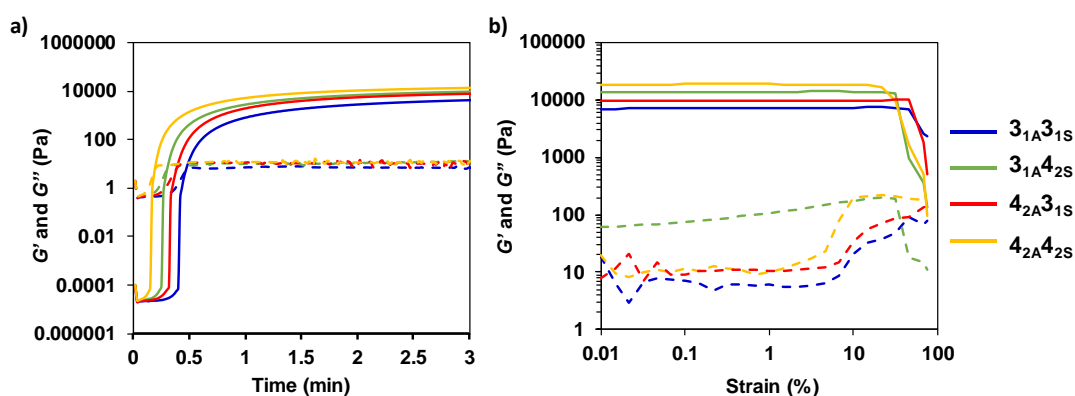


Figure 3.6. Representative curves of storage (G' ; solid line) and loss (G'' ; dashed line) modulus as a function of a) time and b) strain for nonswellable PEG hydrogels.

3.2.3.4 Swelling Profile

It is important to note a few considerations for these nonswelling hydrogels as a result of their end application, for example as injectable scaffolds for the treatment of osteoarthritis.²⁹ The degree of swelling expected for these injectable hydrogels should be close to 100%, allowing enough swelling for an “expansion fit” of the hydrogel within the joint where cartilage has been eroded. A considerable increase in volume, swelling above 100%, could potentially damage the nearby tissues, causing pain and triggering an inflammatory response. While a sudden shrinkage not only implies lower water content, but also results in a smaller hydrogel which will not fill the eroded joint and therefore not

alleviate pain. Moreover, hydrogels as tissue engineering scaffolds are required to be mechanically stable and robust for long term cell culture studies (*e.g.* from days to months), allowing cells to adhere, grow, and eventually develop new tissue while the hydrogel slowly degrades. The multi-arm strategy was successful in suppressing the swelling profile of the thiol-yne hydrogels and thus controlling the increase in volume, however, the resulting hydrogels exhibited distinct swelling behaviours (Figure 3.7). The rate at which each hydrogel expelled and attracted water was dependent on the architecture of the thiol- and alkyne-terminated PEG precursors. All four systems rapidly shrunk after the initial 24 h immersed in PBS solution at 37 °C, (Figure 3.8) postulated to be a consequence of the increased density of crosslinked sites, promoting the reduced hydrophilic nature of the hydrogel network, thus repelling water out of system. Although the hydrogels remained unchanged for 5 days with swelling factor (SF) values in the range between 46 ± 0.1 and $71 \pm 3.1\%$, they started to swell back slowly to 100% after 15 days. After 21 days, signs of hydrogel degradation appeared which allowed an increased amount of water into the network, thus accelerating the swelling rate rapidly and in turn the degradation rate. Moreover, despite the shrinkage of the polymeric network, multi-arm PEG hydrogels also displayed high EWC values (between 86% and 90%, Table 3.3) in comparison to control swellable hydrogels, which is evidence that changes in the architecture of the PEG precursor have little effect on the network's ability to hold water. In contrast, they display a reduced average mesh size (4.2-4.7 nm) as a consequence of the increased number of crosslinking sites and shorter polymeric chains.

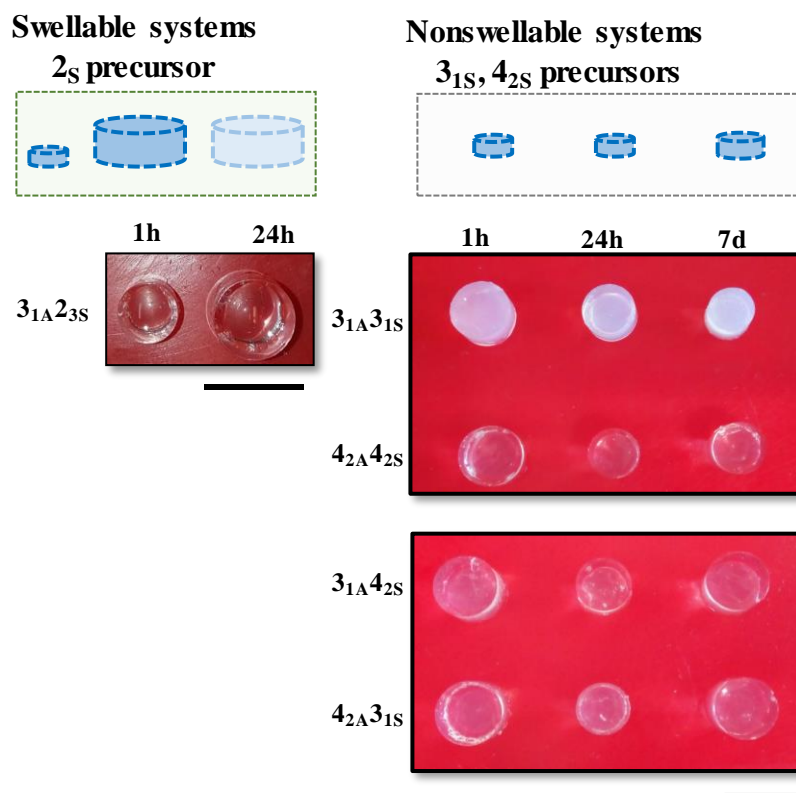


Figure 3.7. Thiol-yne hydrogels response when immersed in PBS solution at 37 °C, scale bar = 1 cm.

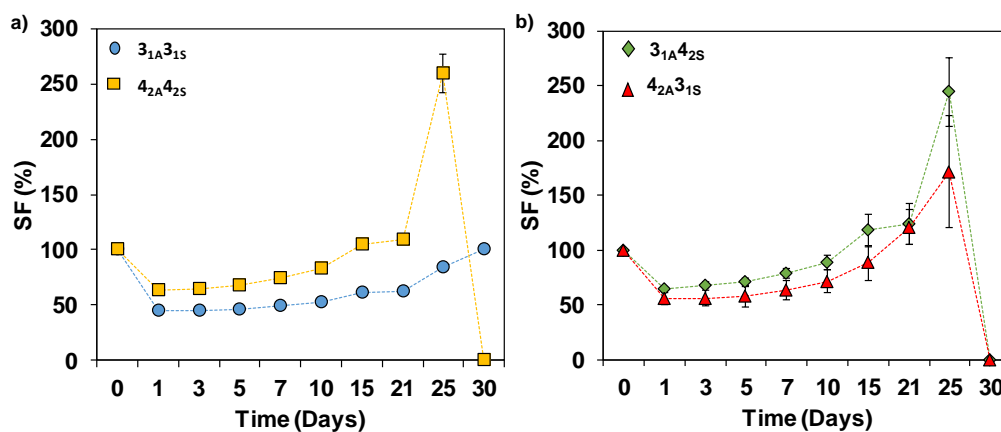


Figure 3.8. The swelling profile for the nonswellable nucleophilic thiol-yne PEG hydrogels displaying multi-arm architecture: a) 3_{1A}3_{1S} (circle) and 4_{2A}4_{2S} (square); b) 3_{1A}4_{2S} (diamond) and 4_{2A}3_{1S} (triangle).

The **4_{2A}4_{2S}**, **4_{2A}3_{1S}** and **3_{1A}4_{2S}** behaved similarly; these systems shrunk to 64% after 24 h and then recovered, swelling up to 2.5 times their original mass after 25 days in PBS solution before degrading completely. In contrast, the **3_{1A}3_{1S}** hydrogel displayed a SF of 45% after 24 h, which is maintained for 7 days before the system starts to slowly swell to 100%, with no signs of degradation after 30 days. Therefore, it was proposed that the ratio between crosslinked sites and the length of the PEG arm controls the swelling profile of multi-arm hydrogels. Indeed, the **3_{1A}3_{1S}** system, which displays the shortest average arm length between each cross-linking site (*i.e.* 0.33 kg mol⁻¹), results in a very dense system with enhanced hydrophobic nature and reduced ability to attract water. Consequently, the rate of ester hydrolysis is lower in this system, which reduces the degradation rate of the polymeric network.

3.2.3.5 Mechanical Characterisation in the Swollen State.

Uniaxial compression testing was performed over a 30 day swelling period to evaluate the mechanical performance of nonswellable PEG hydrogels in the swollen state. Specifically, hydrogels were prepared and left to cure for 1 h to allow for the hydrogels to be fully crosslinked, before immersing them in PBS solution at 37 °C, then after a set period of time, their mechanical properties were characterised. The thiol-yne multi-arm hydrogels presented a range of compressive strengths that were related to both their swelling factor (SF) and immersion time. After the initial 24 h in PBS solution at 37 °C, their compressive strength values increased (Figure 3.9 and 3.10). Specifically, for the **4_{2A}4_{2S}** system, which displayed the greatest change, the compressive strength increased from 120 ± 13 kPa to 385 ± 38 kPa in 24 h (Figure 3.9a). This response is in good

agreement with the decrease of the SF. As water molecules are expelled from the hydrogel network, the polymer content increases and the mechanical properties of the multi-arm hydrogels improve. Moreover, as long as the SF remained constant, no changes in the mechanical performance were observed. For instance, the **3_{1A}4_{2S}** system reached its maximum strength after 24 h, while the **4_{2A}4_{2S}** system displayed its highest stress values after 5 days, which further reflects the unique properties of each system, based on the architecture and molecular weight of the PEG precursors. However, when the swelling factor increased over 100% (after 15 days), the mechanical properties of the multi-arm hydrogels were severely compromised. Once swollen, the accelerated rate of ester hydrolysis promotes the degradation process, and thus weakens the hydrogel structure, which is reflected by a reduction in the compressive strength after 25 days of immersion. Finally, when SF values higher than 150% were reached, the hydrogels degraded very rapidly and dissolved into the PBS solution.

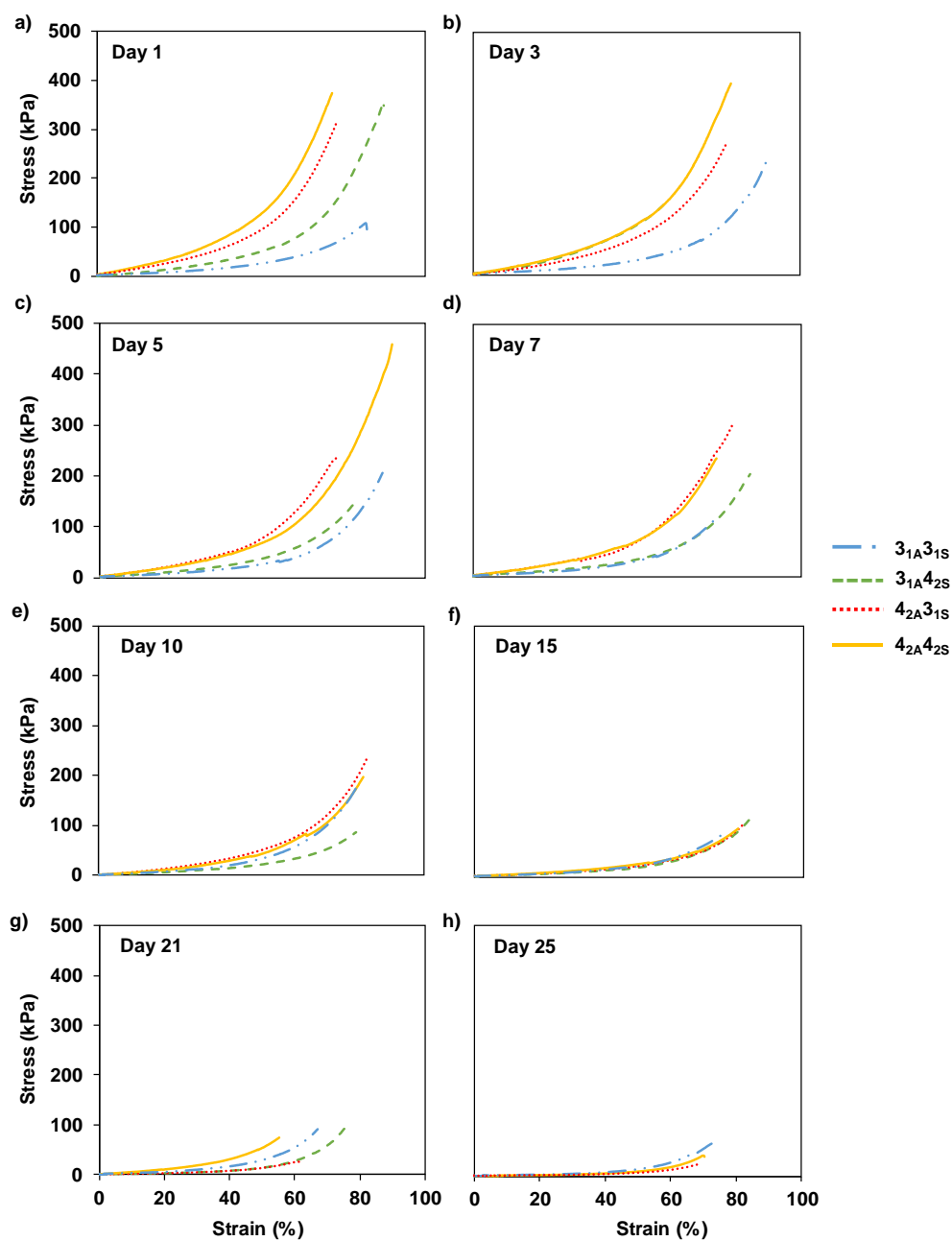


Figure 3.9. Representative stress/strain graphs for hydrogels prepared with multi-arm PEG precursors after being immersed in PBS at 37 °C for different intervals of time, a) 24 h, b) 3 days, c) 5 days, d) 7 days, e) 10 days, f) 15 days, g) 21 days and h) 25 days.

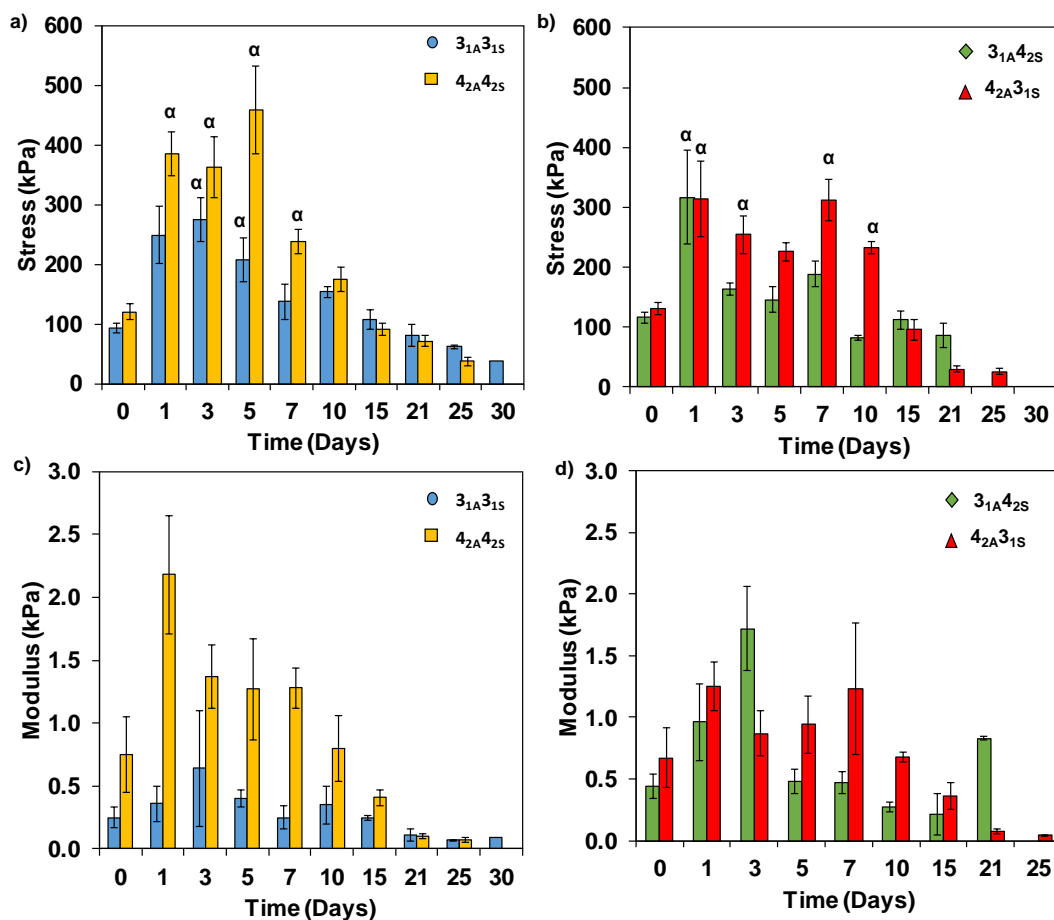


Figure 3.10. a-b) Evolution of the compressive mechanical properties of the nonswellable nucleophilic thiol-yne PEG hydrogels displaying multi-arm architecture: a) $3_{1A}3_{1S}$ (blue) and $4_{2A}4_{2S}$ (yellow); b) $3_{1A}4_{2S}$ (green) and $4_{2A}3_{1S}$ (red). Greek letters on the bars refer to significant differences (p -value < 0.05): α vs 1 hour. c-d) Evolution of the compressive modulus of the nonswellable thiol-yne PEG hydrogels: c) $3_{1A}3_{1S}$ (blue) and $4_{2A}4_{2S}$ (yellow); d) $3_{1A}4_{2S}$ (green) and $4_{2A}3_{1S}$ (red).

It is important to note that the compressive strength values exhibited by multi-arm hydrogels are not as high as those displayed by the control swellable systems, (e.g. the compressive strength of the $3_{1A}2_{3S}$ system is 1.0 ± 0.05 MPa after 3 days) mainly as a consequence of the increased stiffness of the system. The polymeric chains are highly crosslinked and unable to adapt and withstand an external stress; the multi-arm hydrogels break at lower strain values (48.2-66.4%, Figure 3.9) compared to the control system

which can reach 98% strain. Nevertheless, they are able to retain their mechanical performance over time in the swollen state for longer (Figures 3.10), and thus can be effectively applied as biodegradable scaffolds for soft tissue regeneration in a biological context where extremely robust hydrogels are not required.

Overall, the major factor influencing the thiol-yne hydrogels mechanical response is the swelling degree, and thus the condition of the polymeric matrix.²⁴ The architecture of the PEG precursors has a fundamental influence on the swelling response of the resultant multi-arm thiol-yne hydrogels, which in turn affects their compressive strength. Although the multi-arm hydrogels display lower compressive strength values in comparison to the swellable systems (but within the range of soft load bearing tissue), their enhanced stability allowed them to retain their mechanical performance for at least 15 days.

3.2.4 Cytocompatibility Studies on Nonswellable Thiol-yne Hydrogels

Injectable tissue scaffolds are a potential application of nonswelling hydrogels to alleviate joint pain for patients with osteoarthritis.^{39, 40} By injecting a nonswelling cell-laden hydrogel material into the inflamed joint allows cartilage to regrow avoiding invasive joint replacement surgery. To evaluate the thiol-yne nonswellable hydrogels as injectable tissue scaffolds, the cytocompatibility of the multi-arm **3_{1A}4_{2S}** hydrogel was compared to the swellable **3_{1A}2_{3S}** (2-arm thiol-terminated PEG (3kg mol⁻¹)) hydrogel (control system). MC3T3-E1 cells, an osteoblast precursor cell line, were used in this study as they are frequently used to model bone formation *in vitro* for osteoarthritis research.⁴¹ Cell viability tests on MC3T3-E1 cells were conducted by seeding the cells on top of the hydrogels, which had been prepared *in situ* directly on to inserts with a 0.4 μm pore PET membrane in the wells of the tissue culture plates, thus no washing steps were applied to the hydrogels. After 24 and 72 h the cell's metabolic activity was measured using PrestoBlue metabolic assay (Figure 3.11). Both systems had high metabolic activity after 72 h, suggesting high viability of the cells, however the **3_{1A}4_{2S}** system showed lower metabolic activity than the control system. This can be ascribed to the fact that after 72 h the **3_{1A}4_{2S}** system has already shrunk by 44%, demonstrating the influence the increased crosslinking density and therefore the swelling ratio has on the viability of the cells. In order for cells to grow and proliferate they need to be able to manipulate their surrounding environment, by localised degradation allowing them to spread and increase in number. In this system however, the material was very rigid and stiff, which the cells could sense even when seeded on the surface, therefore they are unable to manipulate the material, which translates to a reduction in metabolic activity. The control system, a softer material,

offered the cells more space to spread out in the hydrogel environment, enhancing their proliferation and thus their metabolic activity.

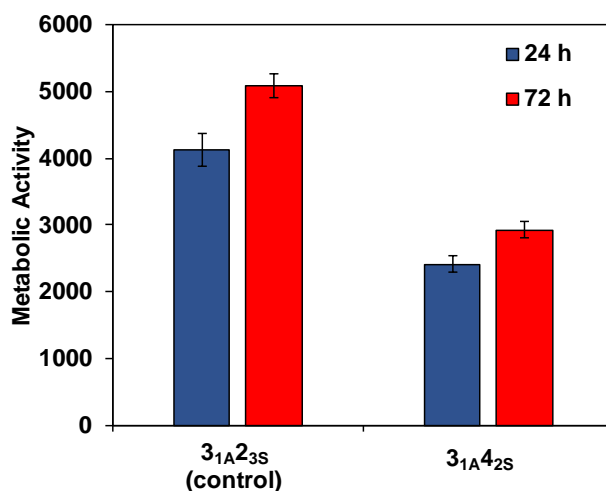


Figure 3.11. Metabolic activity of MC3T3-E1 cells seeded on top of the thiol-yne hydrogels after 24 and 72 h.

Although the 2D data shows that the cells seeded on the surface of the $3_{1A}4_{2S}$ hydrogel system have a lower metabolic activity than the control system, the values are not indicative of high cell death. Therefore, 3D cell encapsulation experiments were also undertaken, and cell viability was assessed after 24 and 72 h of incubation by live-dead fluorescent staining (Figure 3.12). After 24 h of incubation, all the hydrogels showed high cell viability with >95% live cells, which indicates that the materials are nontoxic at this stage. Both the control hydrogels and the multi-arm PEG hydrogels displayed a high percentage of live cells. Interestingly, the stiffer nature of the multi-arm $3_{1A}4_{2S}$ hydrogel did not have a negative effect on the cell viability of 3D encapsulated cells indicating nutrients and oxygen were still able to diffuse through the denser nonswelling structure.

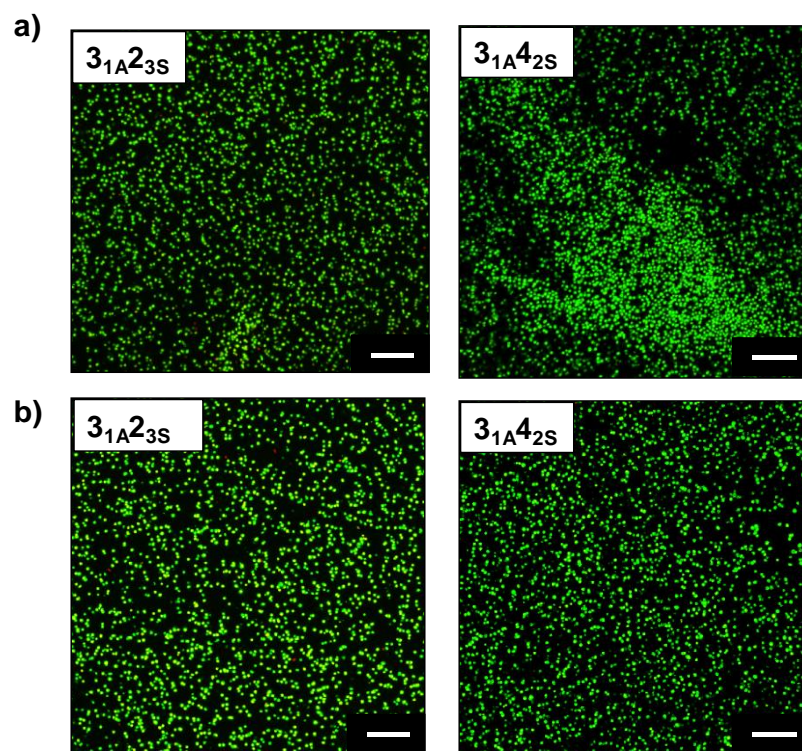


Figure 3.12. Cytocompatibility of nonswellable thiol-yne PEG hydrogels. Images from 3D encapsulated cells after a) 24 and b) 72 h of incubation for the $3_{1A}2_{3S}$ and $3_{1A}4_{2S}$ hydrogels, scale bar = 200 μm .

3.3. Conclusions

The design of a biomaterial that perfectly matches all the requirements for a specific biological context is challenging. Here, an approach to overcome the negative effect of water uptake on the mechanical properties of robust hydrogels crosslinked by thiol-yne nucleophilic addition has been presented. Through the use of multi-arm alkyne- and thiol-terminated PEG precursors, nonswellable hydrogels retain their structure with adequate mechanical performance in the swollen state over time, as well as displaying tuneable degradation rates. Most importantly, the nonswellable hydrogels are highly cytocompatible when cells are encapsulated within the polymeric network, indicating the water content and mesh size allowed for adequate diffusion of oxygen and nutrients. Therefore, this work highlights the suitability of nonswellable hydrogels prepared by efficient thiol-yne chemistry as potential candidates to address a major issue of hydrogels as biomaterials.

3.4. References

1. H. Kamata, X. Li, U.-i. Chung and T. Sakai, *Adv. Healthcare Mat.*, 2015, **4**, 2360-2374.
2. D. A. Gyles, L. D. Castro, J. O. C. Silva and R. M. Ribeiro-Costa, *Eur. Polym. J.*, 2017, **88**, 373-392.
3. R. Y. Tam, L. J. Smith and M. S. Shoichet, *Acc. Chem. Res.*, 2017, **50**, 703-713.
4. Y. Li, J. Rodrigues and H. Tomas, *Chem. Soc. Rev.*, 2012, **41**, 2193-2221.
5. B. V. Slaughter, S. S. Khurshid, O. Z. Fisher, A. Khademhosseini and N. A. Peppas, *Adv. Mater.*, 2009, **21**, 3307-3329.
6. Q. Huang, Y. Zou, M. C. Arno, S. Chen, T. Wang, J. Gao, A. P. Dove and J. Du, *Chem. Soc. Rev.*, 2017, **46**, 6255-6275.
7. P. M. Kharkar, K. L. Kiick and A. M. Kloxin, *Chem. Soc. Rev.*, 2013, **42**, 7335-7372.
8. M. A. Azagarsamy and K. S. Anseth, *ACS Macro Lett.*, 2013, **2**, 5-9.
9. D. Y. Ko, U. P. Shinde, B. Yeon and B. Jeong, *Prog. Polym. Sci.*, 2013, **38**, 672-701.
10. L. Xu, N. Sheybani, W. A. Yeudall and H. Yang, *Biomater. Sci.*, 2015, **3**, 250-255.
11. C. G. Williams, A. N. Malik, T. K. Kim, P. N. Manson and J. H. Elisseeff, *Biomaterials*, 2005, **26**, 1211-1218.
12. D. Macaya and M. Spector, *Biomed. Mater.*, 2012, **7**, 012001.

13. A.-M. Yousefi, P. F. James, R. Akbarzadeh, A. Subramanian, C. Flavin and H. Oudadesse, *Stem Cells Int.*, 2016, **2016**, 13.
14. V. X. Truong and A. P. Dove, *Angew. Chem., Int. Ed.*, 2013, **52**, 4132-4136.
15. V. X. Truong, M. P. Ablett, S. M. Richardson, J. A. Hoyland and A. P. Dove, *J. Am. Chem. Soc.*, 2015, **137**, 1618-1622.
16. X. Y. Cai, J. Z. Li, N. N. Li, J. C. Chen, E.-T. Kang and L. Q. Xu, *Biomater. Sci.*, 2016, **4**, 1663-1672.
17. L. J. Macdougall, V. X. Truong and A. P. Dove, *ACS Macro. Lett.*, 2017, **6**, 93-97.
18. V. X. Truong, K. M. Tsang and J. S. Forsythe, *Biomacromolecules*, 2017, **18**, 757-766.
19. X. Dai, Y. Zhang, L. Gao, T. Bai, W. Wang, Y. Cui and W. Liu, *Adv. Mater.*, 2015, **27**, 3566-3571.
20. F. Luo, T. L. Sun, T. Nakajima, T. Kurokawa, Y. Zhao, K. Sato, A. B. Ihsan, X. Li, H. Guo and J. P. Gong, *Adv. Mater.*, 2015, **27**, 2722-2727.
21. H. Itagaki, T. Kurokawa, H. Furukawa, T. Nakajima, Y. Katsumoto and J. P. Gong, *Macromolecules*, 2010, **43**, 9495-9500.
22. T. Wang, D. Liu, C. Lian, S. Zheng, X. Liu and Z. Tong, *Soft Matter*, 2012, **8**, 774-783.
23. H. Chen, F. Yang, R. Hu, M. Zhang, B. Ren, X. Gong, J. Ma, B. Jiang, Q. Chen and J. Zheng, *J. Mater. Chem. B*, 2016, **4**, 5814-5824.

24. H. Kamata, Y. Akagi, Y. Kayasuga-Kariya, U.-i. Chung and T. Sakai, *Science*, 2014, **343**, 873.
25. L. Klouda, *Eur. J. Pharm. Biopharm.*, 2015, **97**, 338-349.
26. T. M. O'Shea, A. A. Aimetti, E. Kim, V. Yesilyurt and R. Langer, *Adv. Mater.*, 2015, **27**, 65-72.
27. H. He, J. Guan and J. L. Lee, *J. Controlled Release*, 2006, **110**, 339-346.
28. M. C. Koetting, J. T. Peters, S. D. Steichen and N. A. Peppas, *Mater. Sci. Eng. R-Rep.*, 2015, **93**, 1-49.
29. H. Kamata, K. Kushiro, M. Takai, U.-i. Chung and T. Sakai, *Angew. Chem., Int. Ed.*, 2016, **128**, 9428-9432.
30. K. E. Uhrich, S. M. Cannizzaro, R. S. Langer and K. M. Shakesheff, *Chem. Rev.*, 1999, **99**, 3181-3198.
31. R. P. Brannigan and A. P. Dove, *Biomater. Sci.*, 2017, **5**, 9-21.
32. L. S. Nair and C. T. Laurencin, *Prog. Polym. Sci.*, 2007, **32**, 762-798.
33. S. Lyu and D. Untereker, *Int. J. Mol. Sci.*, 2009, **10**, 4033.
34. T. Canal and N. A. Peppas, *J. Biomed. Mater. Res.*, 1989, **23**, 1183-1193.
35. P. J. Flory, *J. Am. Chem. Soc.*, 1941, **63**, 3083-3090.
36. P. J. Flory, *J. Phys. Chem.*, 1942, **46**, 132-140.
37. W. H. Stockmayer, *J. Chem. Phys.*, 1943, **11**, 45-55.

38. K. M. Schultz and K. S. Anseth, *Soft Matter*, 2013, **9**, 1570-1579.
39. M. Liu, X. Zeng, C. Ma, H. Yi, Z. Ali, X. Mou, S. Li, Y. Deng and N. He, *Bone Res.*, 2017, **5**, 17014.
40. A. A. Pitsillides and F. Beier, *Nat Rev Rheumatol*, 2011, **7**, 654-663.
41. J. Ni, Yuan, X.M., Yao, Q., & Peng, L.B. , *Int. J. Mol. Med.*, 2015, **35**, 1755-1760.

Chapter 4.

Stereochemically Controlled Hydrogels by Utilising Nucleophilic Thiol-yne Addition Chemistry

4.1. Introduction

Stereochemistry concerns the three-dimensional (3D) spatial arrangements of molecular bonds and is vitally important in many areas of chemistry. Specifically, the function or activity of a molecule can be greatly influenced by the respective stereochemistry. A striking example is the small molecule drug, thalidomide, where one enantiomer is therapeutic and the other is a teratogenic.^{1,2} Stereochemistry is also critically important in relation to macromolecules as it is known to affect bulk material properties such as hardness or elasticity. The natural polymers of polyisoprene (natural rubber and gutta percha) differ only in their double bond stereochemistry (*cis* or *trans*), but poly(*cis*-isoprene) is elastic and amorphous, while poly(*trans*-isoprene) is comparatively brittle and crystalline.³ The ability to rationally tune the mechanical properties of a material is a fundamental aim of materials science. This is especially significant in the area of biomaterials, where there is the potential to take a foundational material and alter the stereochemistry, to afford new structures that mimic different biological environments.⁴ ⁶ Hydrogels are increasingly being exploited as biomaterial scaffolds since they fit the requirements for a synthetic biomaterial (*e.g.* high water content, appropriate mechanical properties and low toxicity).⁷⁻⁹ As highlighted in the literature, some fundamental properties of hydrogels (*e.g.* stiffness, strength and tensile properties) can be tuned which enables efficient mimicry of various biological environments.¹⁰⁻¹⁴

The stereochemistry of hydrogels, as it relates to bulk material properties, has only recently been examined and is an emerging topic in biomaterials research. Early reports used the stereochemistry of the pendent group on the polymer backbone (*e.g.*

poly(lactide)^{15, 16} or poly(hydroxyethyl methacrylate) (PHEMA)¹⁷) to control the stiffness and swelling behaviour of hydrogels, thus creating tuneable mimics of extracellular matrices (ECM). Anseth and co-workers investigated a dynamic hydrogel where the stereochemistry was modulated *in situ*, to change the storage modulus (G') over a 5 kPa range by leveraging the photo-isomerisable azobenzene moiety.^{18, 19} This gave a handle to control the differentiation of stem cells encapsulated in the materials. Lee *et. al.* have also used an azobenzene unit as a photo-switchable, crosslinking unit to adjust the stiffness of polyacrylamide hydrogels (Figure 4.1a) thereby creating a scaffold to study the mechano-signalling in human mesenchymal stem cells (hMSCs).²⁰ The change in hydrogel stiffness ($E = 5-10$ kPa, Figure 4.1b) resulted in an altered cell morphology and thus was an important advancement in regenerative medicine and tissue engineering (Figure 4.1c). Although the azobenzene unit provided a dynamic platform for tuning hydrogel stiffness, changes in the stiffness of the materials was relatively modest and the azobenzene moiety ultimately relaxes back to the more thermodynamically stable *trans* conformation after photo-excitation. This limits access to materials with higher G' values (*e.g.* cartilage) and precludes “locking” the material to a defined stereochemistry for long term cell studies.

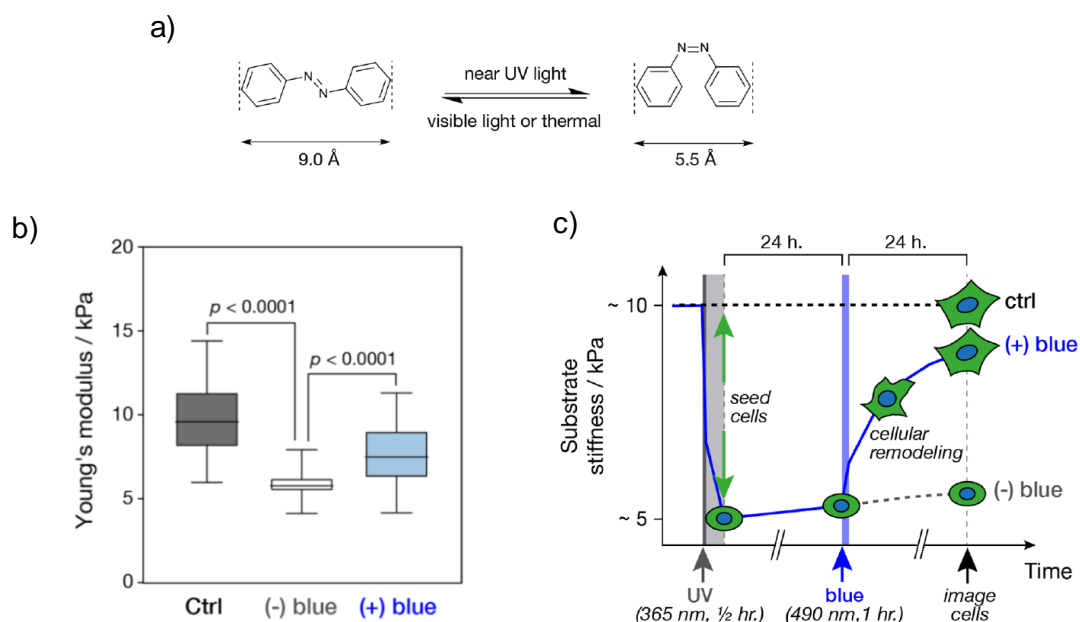
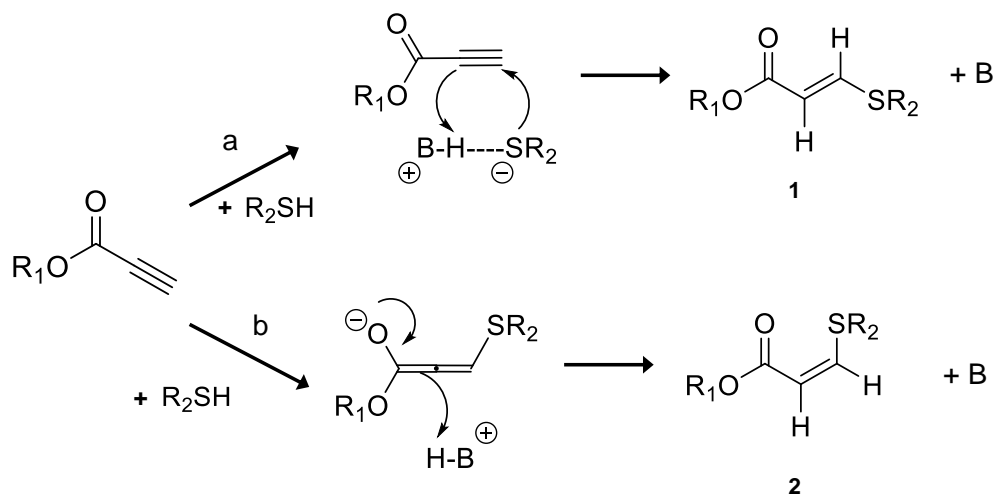


Figure 4.1. a) The change in stereochemistry of the azobenzene unit with light. b) Schematic overview of cell culture experiments on photoresponsive hydrogels. Fibronectin-coated gels were softened by exposure to UV (365 nm) irradiation for 30 min. Primary human MSCs were then seeded. After 24 h, (+) blue gels were exposed to blue (490 nm) light for 1 h, whereas (-) blue gels were kept in darkness. Figure adapted from ref 20.

To address the problems of dynamic bonds, the stereochemistry can be permanently set during the formation of the hydrogel, by targeting precise *cis:trans* ratios to tune the mechanical properties. The nucleophilic thiol-yne reaction is a promising method as it is a suitable crosslinking reaction in hydrogel synthesis^{21, 22} and the stereochemistry of the vinyl thioether product can also be manipulated.²³ When the reaction is conducted under weakly basic conditions, the mono-addition product (vinyl thioether) is formed exclusively and the stereochemistry can be manipulated by the choice of solvent and base. By utilising a non polar solvent and/or a weak base the *trans* product is favoured (Scheme 4.1a). This is likely a result of the thiol and base acting as a hydrogen-bonded pair to attack the alkyne from the same face. When a polar solvent is used, regardless of base, the thiolate anion attacks first (obeying the anti-addition rule) and the

transition state species is then protonated by the base to favour the *cis* isomer (Scheme 4.1b).²⁴ By tuning the polarity of the solvent or base, a range of *cis:trans* ratios can be targeted.



Scheme 4.1. Proposed mechanism for the stereochemical control in the nucleophilic thiol-yne reaction. a) Non polar solvent and/or weak base to form the *trans* isomer (1); b) polar solvent and/or strong base to form the *cis* isomer (2). Adapted from ref 23.

This characteristic of the nucleophilic thiol-yne addition reaction has been previously employed to synthesise elastomeric materials. The materials had controlled mechanical properties dependent on the stereochemistry of the vinyl thioether moiety in the polymer backbone. Through judicious choice of solvent (*e.g.* chloroform (CHCl₃) or *N,N*-dimethylformamide, (DMF)) and base (*e.g.* triethylamine, (NEt₃) or 1,8-diazabicyclo[5.4.0]undec-7-ene (DBU)) a set of materials were synthesised with different *cis* contents. The elastomeric materials with low *cis* contents were elastic and soft (Young's modulus (*E*) = 2.7 MPa). In contrast, high *cis* content materials were less elastic and tougher (*E* = 59.8 MPa).²⁵

In this chapter the effect of the stereochemistry on the mechanical properties of thiol-yne hydrogels was examined. The stereochemistry of the vinyl thioether unit was characterised using Fourier transform infrared (FT-IR) and ^1H NMR spectroscopy. Rheological and compression testing were then conducted to obtain mechanical information of the hydrogels and this was correlated to the overall stereochemistry.

4.2. Results and Discussion

4.2.1. Determining the Stereochemistry in Nucleophilic Thiol-yne PEG Hydrogels

Stereochemical control during synthesis, can lead to materials with different properties. In the context of the nucleophilic thiol-yne addition reaction, the use of a polar solvent and a strong base (DBU) favours the vinyl thioether product with a high *cis* content.²⁶ In contrast, using a non polar solvent with a weak base (NEt₃) results in a high *trans* content product. If this phenomenon was applied to the thiol-yne hydrogel system, it was hypothesised that stereocontrolled hydrated networks with a range of different properties could be created. In previous chapters, the thiol-yne gels have been synthesised in water and therefore it is assumed that these materials have a high *cis* content. Thus, to target higher *trans* content materials with potentially different mechanical properties, it was postulated that the PEG networks could be synthesised using a range of solvents with different polarity to produce organogels (*i.e.* polymeric networks hydrated in organic solvents). To determine new solvent conditions for stereocontrolled hydrogels three solvents (*i.e.* non polar, moderately polar, and polar) were chosen with NEt₃ to catalyse the reaction. The study utilised a nonpolar solvent, CHCl₃, a polar solvent, H₂O and acetone as a solvent with intermediate polarity, which had all previously shown good control over the stereochemistry of the vinyl thioether product.²⁶ The PEG hydrogel system, **4_{2A}4_{2S}** was used as the model system to study the stereochemistry in the thiol-yne hydrogels, synthesised using 4-arm alkyne- and thiol-functionalised PEG (2 kg mol⁻¹), previously characterised as a nonswelling system (Chapter 3, Section 3.2.3.4). The thiol-yne **4_{2A}4_{2S}** hydrogel system was chosen as it exhibited the highest compressive strength over time in previous analysis, (459 ± 74 kPa after 5 days, Chapter 3, Section 3.2.3.5).

Additionally, as a consequence of the hydrophobic nature of this system, there is no appreciable bulk degradation in 15 days after immersion in an aqueous environment.

FT-IR spectroscopy was used to obtain the *cis:trans* ratio in the gels as the characterisation could be carried out in the solid state and the signals corresponding to the vinyl thioether product were sensitive to the stereochemistry of the double bond. To conduct the analysis, the samples were dried to remove the solvent and base, used in the synthesis of the hydrogel, then sliced into thin discs. For each system, 10 measurements were performed on different areas of the gel to confirm the stereochemistry was uniform. In addition to the stereochemistry, FT-IR spectroscopy gave an insight into reaction conversion by the disappearance of the diagnostic alkyne stretch at 2100 cm^{-1} (Figure 4.2). The percentage *cis* in the organogel was determined by normalising the area of the *cis* alkene bending signal at 802 cm^{-1} with the area of the signal for the C-H stretch at 2866 cm^{-1} . As previous studies demonstrated (Chapter 2, Section 2.2.1), using H_2O as the solvent with a PEG precursor, resulted in a product with 94% *cis* content. Therefore, the *cis* content of the organogels was determined by dividing the normalised peak area by the area for the materials synthesised using aqueous conditions (94% *cis*).

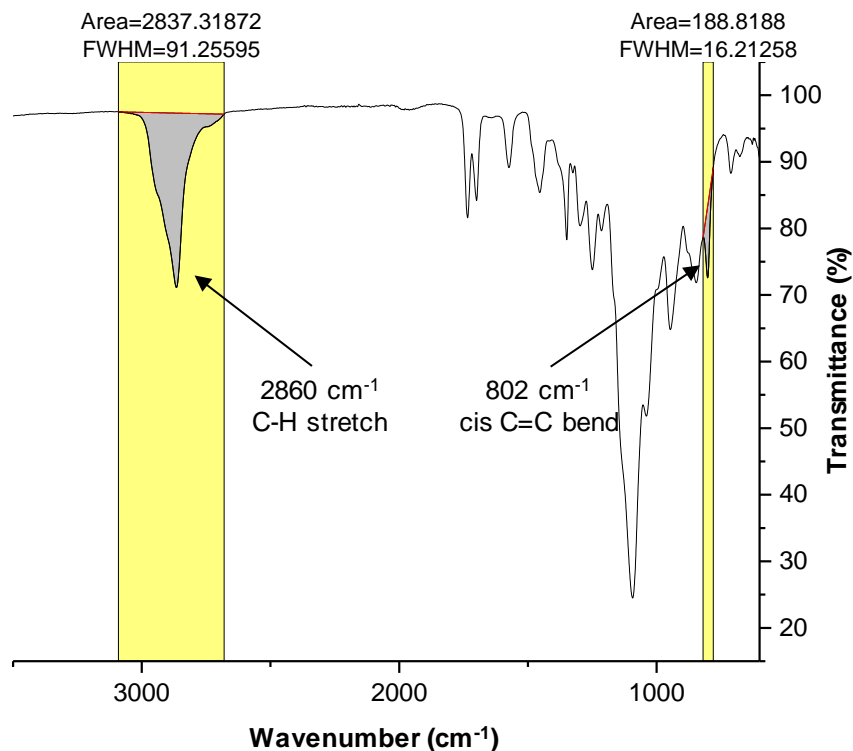


Figure 4.2. A representative FT-IR spectrum of a dried thiol-yne PEG gel synthesised with 100% water. Highlighted peak areas used to calculate the % *cis* content in the hydrogel.

A series of gels were synthesised using different solvent blends resulting in a range of different *cis:trans* ratios (10 ± 3.5 , 23 ± 2.8 , 51 ± 4.3 and $81 \pm 28\%$ *cis*) as characterised through FT-IR spectroscopy (Figure 4.3 and Table 4.1). The standard error on these measurements were low highlighting the stereochemistry was uniform throughout the sample. These solvent conditions demonstrated the effect the PEG chain and gel synthesis had on the stereochemistry of the vinyl thioether product. Interestingly, even in highly non polar conditions (CHCl_3), $10 \pm 3.5\%$ *cis* content was present compared to none detected in the reaction between ethyl propiolate and 1-dodecanethiol, (determined by ^1H NMR spectroscopy, Chapter 2, Section 2.2.1) and shown by Truong *et.al.*²⁶ This demonstrates the influence the PEG chains had on the overall reaction's polarity, increasing the polarity of the system to favour a small amount of the *cis* product. The

difference in *cis* content could also highlight discrepancies between FT-IR and NMR spectroscopy methods. The *cis* bending signal is in the fingerprint region of the FT-IR spectrum, therefore other modes of vibrations in the sample could also contribute to the signal area, thus artificially elevating the measured *cis* content. Nevertheless, this experiment demonstrated the precise control of stereochemistry in the hydrogel system. Moreover, it showed that the stereochemistry in gels could be easily determined through FT-IR spectroscopy which is a simple, effective and cheap method of analyses.

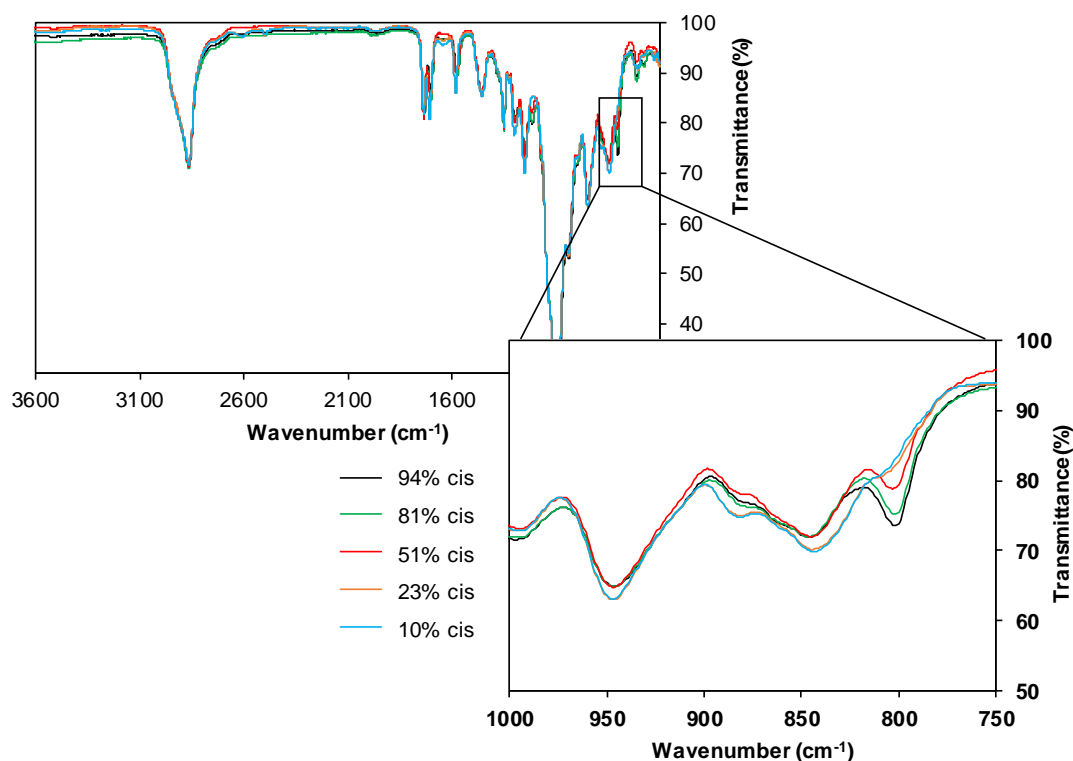


Figure 4.3. FT-IR spectrum of the stereocontrolled **4_{2A}4_{2S}** dried gels. Expanded view between 750-1,000 cm⁻¹ to show the increased intensity at 802 cm⁻¹ correlating with increased *cis* content in the dried gel.

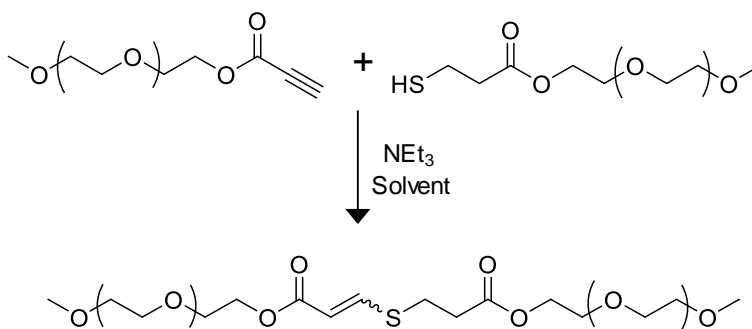
Table 4.1. Different solvent conditions for targeted intermediate % *cis* contents using the PEG hydrogel system determined using FT-IR spectroscopy.

Target % <i>cis</i> content	Solvent conditions (%)			Actual % <i>cis</i> content determined by FT-IR spectroscopy
	CHCl ₃	Acetone	H ₂ O	
94	-	-	100	94 ± 2
75	-	65	35	82 ± 28
50	-	90	10	51 ± 4.3
25	40	60	-	23 ± 2.8
0	100	-	-	10 ± 3.5

Although FT-IR spectroscopy is a useful tool to determine the stereochemistry in the thiol-yne PEG gels, a more quantitative method (¹H NMR spectroscopy) was employed to elucidate the relative stereochemistry by examining a small molecule study.

4.2.2. Determining the stereochemistry of the Nucleophilic Thiol-yne Hydrogels through ¹H NMR spectroscopy

A small molecule reaction scheme was designed to reflect the characteristics and polarity of the PEG precursors used in the thiol-yne hydrogels synthesis. A low molecular weight methyl ether (monofunctionalised) PEG ($M_w = 550 \text{ g mol}^{-1}$) was chosen (Scheme 4.2) and functionalised with alkyne and thiol end groups in the same Fisher esterification procedure as previously described (Chapter 2, Section 2.2). Resulting in products with high conversion (> 92%) as determined by ¹H NMR spectroscopy and SEC analysis (Figures 4.5-4.7).



Scheme 4.2. Model nucleophilic thiol-yne reaction scheme between alkyne- and thiol-functionalised methyl ether PEG₅₅₀.

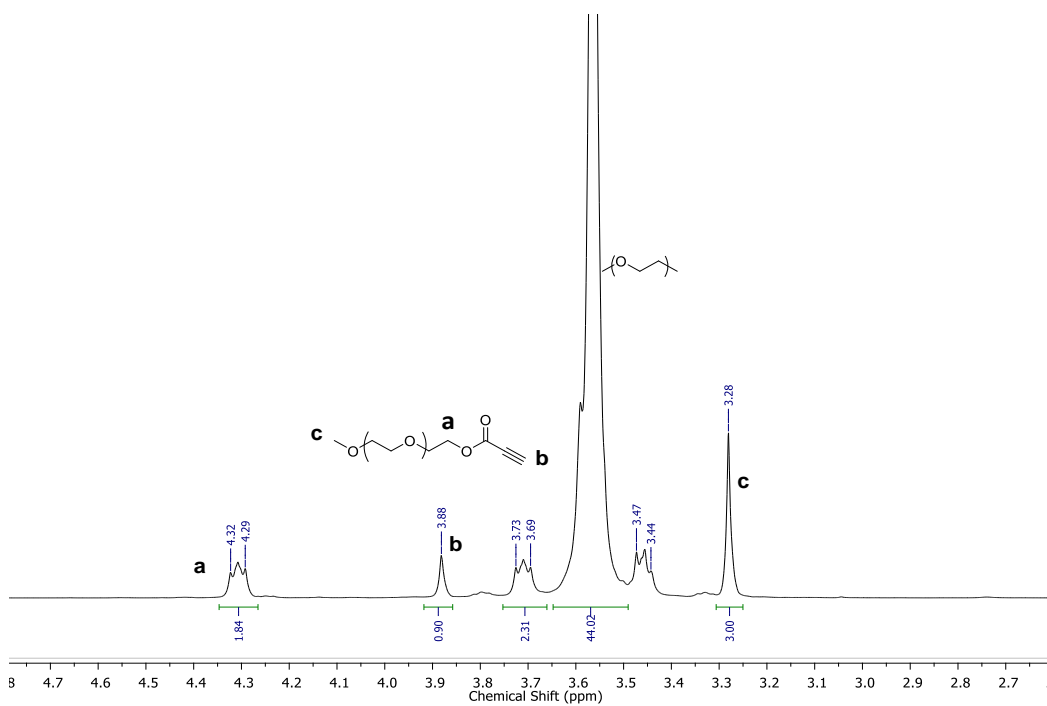


Figure 4.5. ¹H NMR spectrum of the alkyne-terminal methyl ether PEG₅₅₀ ($(\text{CD}_3)_2\text{CO}$, 300 MHz, 298 K).

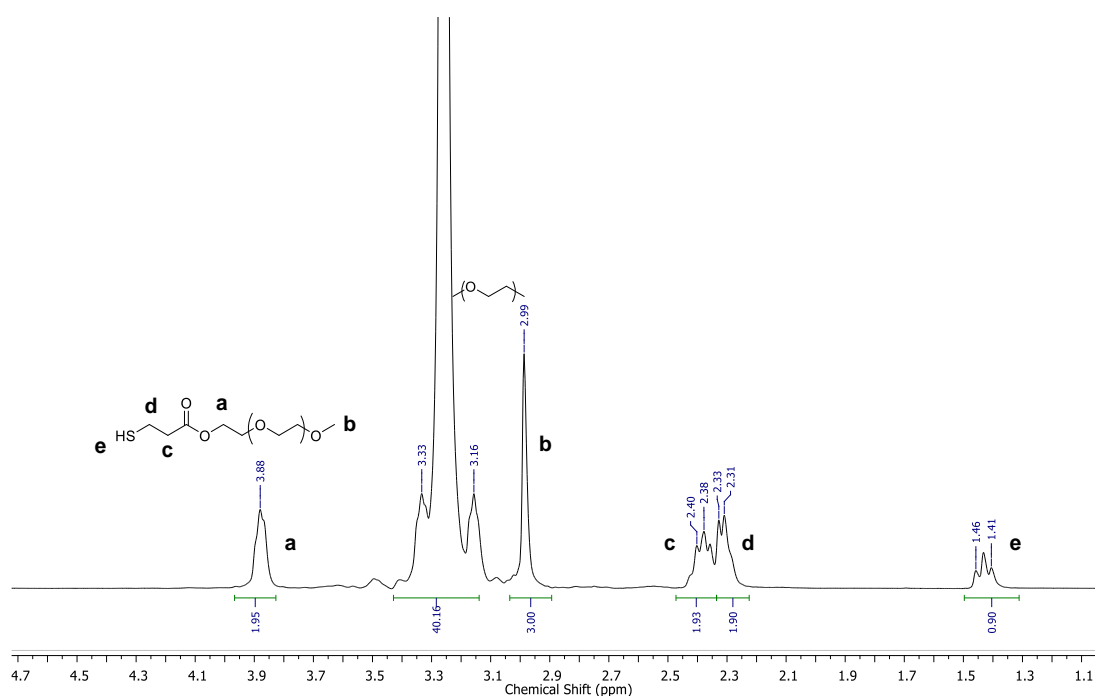


Figure 4.6. ¹H NMR spectrum of the thiol-terminal methyl ether PEG₅₅₀ ((CDCl₃, 300 MHz, 298 K).

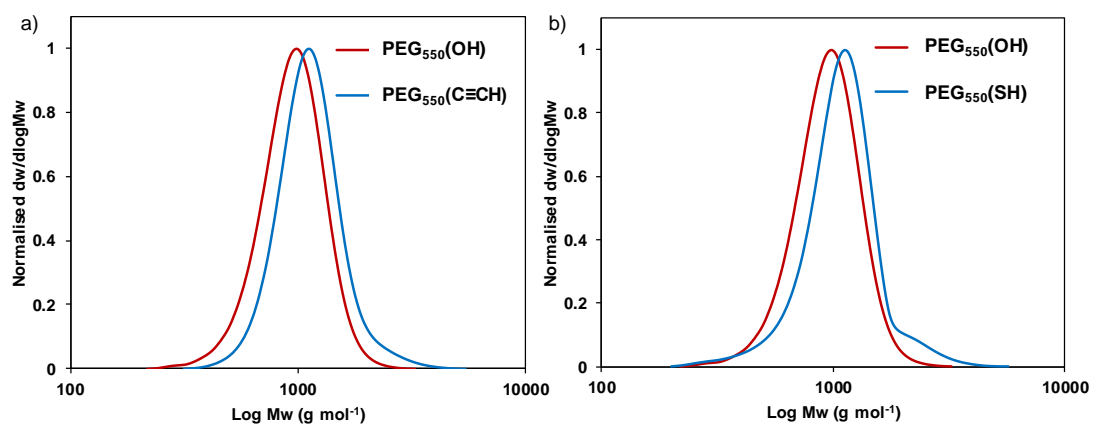


Figure 4.7. SEC chromatograms of a) methyl ether PEG₅₅₀(C≡CH), b) methyl ether PEG₅₅₀(SH). Molecular weight determined against polystyrene standards using CHCl₃ (0.5% NEt₃) as eluent.

The model alkyne- and thiol-functionalised methyl ether PEG₅₅₀ precursors were dissolved in the appropriate solvent system, used to synthesise the range of stereocontrolled thiol-yne hydrogels (Section 4.2.2). NEt₃ was added to the PEG thiol solution followed by the solution containing the PEG alkyne. The reaction was then sealed

and stirred for 1 h before concentrating *in vacuo*. In accordance with previous studies, the increase in polarity of the reaction solvent led to a higher overall *cis* content. The respective isomers were distinguishable and well resolved in the ^1H NMR spectrum (Figure 4.8). The signals corresponding to the *cis* and *trans* protons were assigned using the three bond coupling constants ($^3J_{\text{HH}}$) which differ depending on the stereochemistry of the alkene bond. *Trans* $^3J_{\text{HH}}$ values range between 11-19 Hz whereas *cis* $^3J_{\text{HH}}$ values range between 5-14 Hz.²⁷ For the vinyl thioether compound, that was afforded by the reaction between the alkyne- and thiol-functional monofunctionalised PEG₅₅₀, the two doublets at $\delta = 6.95$ and 5.65 ppm were assigned as the *cis* isomer ($^3J_{\text{HH}} = 9$ Hz). The signals at $\delta = 7.42$ and 5.55 ppm were assigned to the *trans* isomer since the coupling constant was greater ($^3J_{\text{HH}} = 15$ Hz). For all the thiol-yne PEG₅₅₀ reactions the %*cis* was higher than the values obtained through FT-IR spectroscopy, for example 100% CHCl_3 (%*cis* by FT-IR = $10 \pm 3.5\%$), resulted in a vinyl thioether product with $23 \pm 0.5\%$ *cis* (Figure 4.8). This discrepancy can be attributed to the polarity of the thiol-yne overall reaction mixture. It is probable the PEG reactants increase the polarity and thus the %*cis* content of the products (Figure 4.9, Table 4.2).²⁸ In addition to polarity considerations, other factors (*e.g.* proximity of chain ends and gel formation) may have also affected the stereochemical outcomes. Since ^1H NMR spectroscopy is a more quantitative technique than FT-IR spectroscopy and the error on the %*cis* values are lower, the results from the small molecule experiment are more likely to be representative of the actual *cis* content in the gels. Furthermore, the signals are distinct and do not overlap with other signals in the spectrum, unlike in FT-IR where the *cis* alkene bending peak (802 cm^{-1}) is in the fingerprint region and therefore the area of the peak could be influenced by vibrations

from other bonds. Therefore, the relative abundances determined by ^1H NMR spectroscopy were used for subsequent analysis.

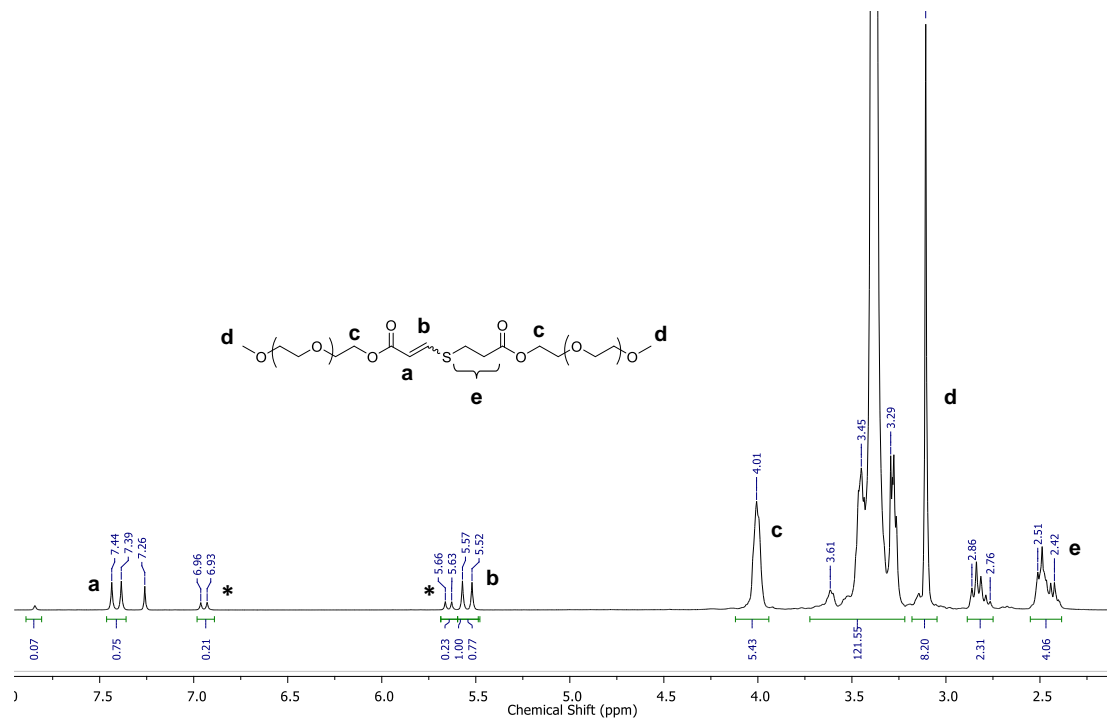


Figure 4.8. ^1H NMR spectrum of the nucleophilic thiol-yne product of the alkyne- and thiol-functionalised methyl ether PEG₅₅₀ in CHCl_3 with NEt_3 (CDCl_3 , 300 MHz, 298 K), *= *cis* product.

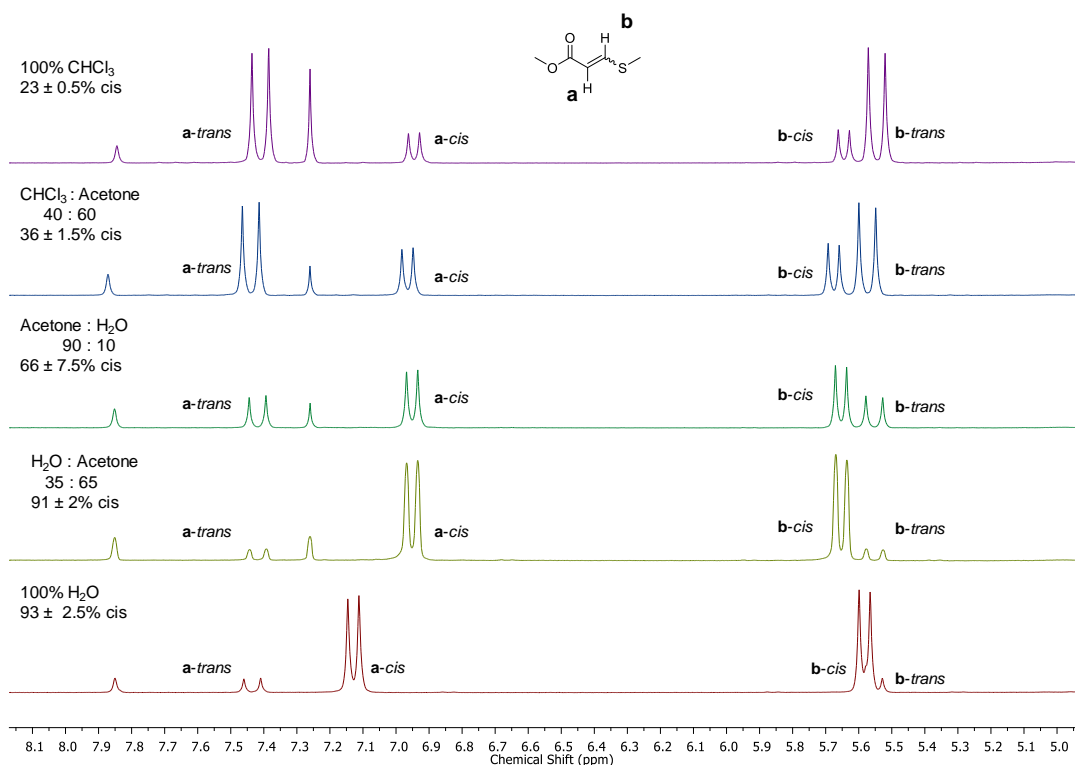


Figure 4.9. ¹H NMR spectra of the vinyl thioether product demonstrating the dependence of solvent polarity on the *cis:trans* ratio of the vinyl thioether product, (CDCl₃, 300 MHz, 298 K), (100% H₂O reaction ¹H NMR spectrum recorded in (CD₃)₂CO, 300 MHz, 298K).

Table 4.2. Difference in *cis:trans* ratio determined through FT-IR and ¹H NMR spectroscopy

% <i>cis</i> content determined by FT-IR spectroscopy	Solvent conditions	% <i>cis</i> content determined by ¹ H NMR spectroscopy
94 ± 2	100% H ₂ O	93 ± 2.5
82 ± 28	35:65 H ₂ O:Acetone	91 ± 2
51 ± 4.3	90:10 Acetone:H ₂ O	66 ± 7.5
23 ± 2.8	60:40 Acetone:CHCl ₃	36 ± 1.5
10 ± 3.5	100% CHCl ₃	23 ± 0.5

4.2.3. Characterisation of the Stereocontrolled Thiol-yne PEG Hydrogels

4.2.3.1. Gelation Time

After optimising the solvent system for the gel synthesis, characterisation of the mechanical properties of the materials were conducted through swelling, rheology and compression testing. For comparisons to be valid, between the % *cis* content in the hydrogel and the resultant mechanical properties of the hydrogels, other factors in the formation of the hydrogels were maintained (*e.g.* gelation time and water content) as these factors could alter the bulk material properties.²⁹ To keep the gelation time consistent throughout all the gel systems, the amount of base, NEt₃ was changed accordingly (Table 4.3). The original nonswelling hydrogel, formed in phosphate buffered saline (PBS) solution, formed hydrogels very rapidly (*i.e.* less than 30 s). Nevertheless, they had a high gel fraction (GF), suggesting the efficiency of the reaction was not affected. As a result, to make this system comparable to the previously analysed system, plus allowing practical handling of the gels, the target gelation time was chosen to be 1 min. This afforded suitable time for precursors to mix and for the materials to be injected into suitable moulds without premature gelation. The calculated amount of base to tune gelation times to approximately 1 min was dependent on the polarity of the solvent. The rate of reaction increased as the polarity of the reaction mixture increased. When high *trans* materials were targeted by using a non polar reaction medium, more NEt₃ was required to catalyse the organogel formation in a suitable timeframe (Table 4.3). FT-IR spectroscopy was conducted on the resultant materials to confirm that the amount of base did not affect the resultant stereochemistry.

Table 4.3. Conditions used to form stereocontrolled thiol-yne PEG hydrogels with the same gelation time.

% <i>cis</i> content	Solvent conditions	Amount of NEt₃ ($\mu\text{L mL}^{-1}$)
93 \pm 2.5	100% H ₂ O	0.7
91 \pm 2	H ₂ O : Acetone 35 : 65	1.66
66 \pm 7.5	Acetone : H ₂ O 90 : 10	10
36 \pm 1.5	Acetone : CHCl ₃ 60 : 40	20
23 \pm 0.5	100% CHCl ₃	34

4.2.3.2. Swelling and Structure Characterisation of the Stereocontrolled Thiol-yne Hydrogels

After synthesising the organogels, the materials were left to cure for 1 h to ensure the reaction had gone to completion. They were then immersed into acetone for 5 days with frequent solvent changes. Acetone was chosen since it is miscible with both CHCl₃ and H₂O, as well as the NEt₃ catalyst. In addition, minimal hydrolysis could take place during this washing step since conditions as only a small amount of water was present; this is important as it maintains structural integrity for mechanical testing. After 5 days, water was gradually introduced into the organogels to form hydrogels. Once the hydrogels had started to swell (2 days) it was determined that the solvent exchange was complete. After this process, the dimensions of the hydrogels were measured to confirm that that they were the same size and swelling factor. The samples were then ready to fully

characterise through swelling kinetics, rheology and compression studies. All characterisation of the hydrogels was carried out after the 7 day solvent exchange process, apart from the gel fraction (GF) study as this procedure analysed the amount of unreacted precursor in the gel after formation which would be removed during the solvent exchange process. To determine gel fraction (GF), the ‘as prepared’ organogels were cured for 1 h then lyophilised to remove the solvent and base. The samples were then weighed according to the normal gel fraction procedure (Chapter 2, Section 2.2.2) and swollen in water for 3 days. The gels were then lyophilised again and weighed to calculate the efficiency of the reaction. The GF was high for all the systems (> 92%, Table 4.4), suggesting that neither the polarity of the solvent nor the amount of base affected the overall efficiency of the reaction.

Table 4.4. Gel data for the stereocontrolled thiol-yne hydrogels

% cis	Gel Fraction (%)	EWC (%)	Mesh Size (nm)
93 ± 2.5	97 ± 1	92.1 ± 0.6	6.69 ± 0.2
91 ± 2.0	92 ± 2	88.0 ± 0.4	5.36 ± 0.1
66 ± 7.5	95 ± 1.5	89.3 ± 0.2	5.55 ± 0.2
36 ± 1.5	94 ± 1	87.4 ± 0.1	5.19 ± 0.02
23 ± 0.5	96 ± 1	84.5 ± 0.3	4.48 ± 0.08

To confirm the stereochemically-controlled thiol-yne hydrogels had similar swelling kinetics profiles, their swelling characteristics, mesh size and structure were investigated. Regardless of their *cis* content, the equilibrium swelling content (EWC) was high (>84%) for all the systems (Table 4.4) suggesting that the stereochemistry did not

affect the hydrogels ability to hold water. In addition, the EWC values were similar to the thiol-yne hydrogels formed in PBS solution (Chapter 3, Section 3.2.3), further confirming that stereochemistry and synthetic conditions did not affect the swelling ability. Final confirmation was attained from the mesh size of the hydrogels ($4.5 \pm 0.08 - 6.7 \pm 0.2$ nm), calculated by the Flory-Rehner equation (described in chapter 2, section 2.2.3), which suggests little correlation between mesh size and stereochemistry (Table 4.4). Cryogenic scanning electron microscopy (cryo SEM) analysis also showed that the ice crystal growth during the freezing process of this technique was not dependent on stereochemistry since results are similar to the previously made PBS hydrogels (Figure 4.10).

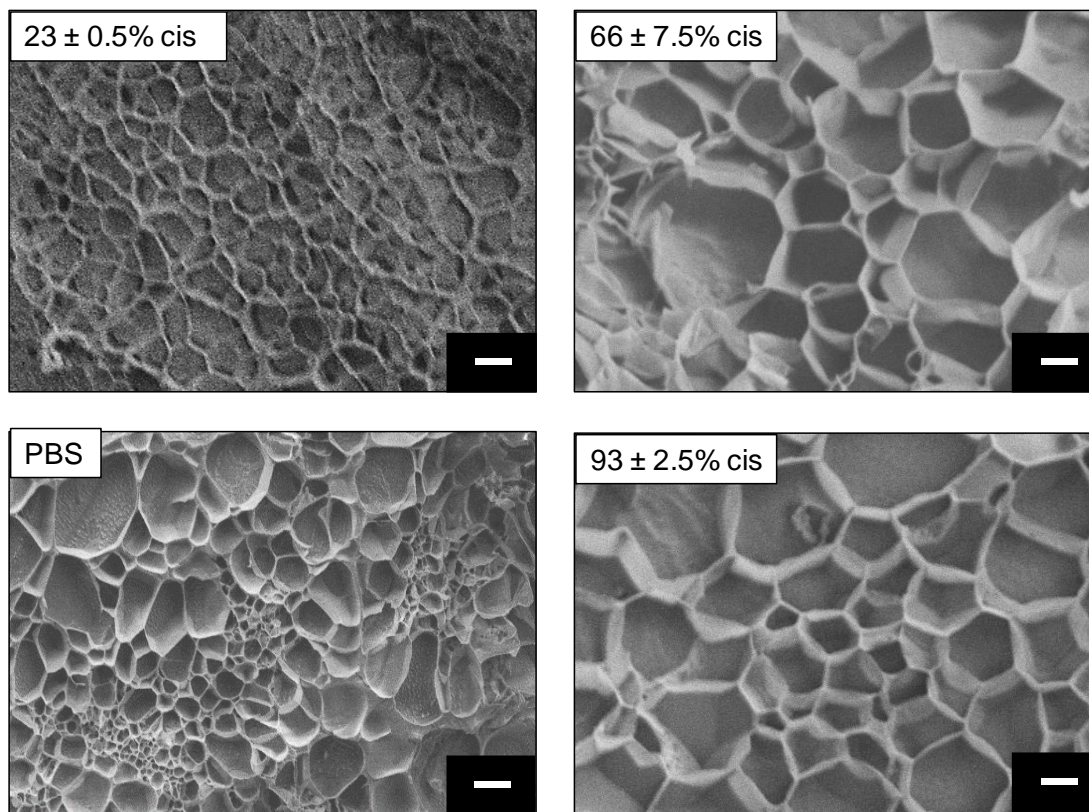


Figure 4.10. Cryo SEM images of the stereocontrolled thiol-yne hydrogels in comparison to the original PBS thiol-yne hydrogels.

It is important for these systems to resist complete bulk degradation in aqueous environments so that they retain robust mechanical properties for cell culture studies. To evaluate this requirement, a swelling study experiment was conducted to monitor the swelling profile over time. The hydrogels were weighed after the solvent exchange process was complete (7 days after synthesis), immersed in PBS solution, then placed in an incubator at 37 °C. The hydrogels were then weighed periodically for 28 days to calculate the swelling factor (SF). These materials show a similar profile to the PBS **4_{2A}4_{2S}** hydrogels (Chapter 3, Section 3.2.3.3). The stereocontrolled gels initially shrank when placed in PBS solution at 37 °C, then swelled back to their original dimensions within 15 days (Figure 4.11). After 15 days, hydrolysis of the ester units began to deteriorate the structural integrity of the material as evidenced by the increased SF. This degradation profile is also similar to PBS hydrogels, demonstrating that the thiol-yne system is highly adaptable, forming virtually the same networks regardless of the solvent or catalyst used. This result is particularly important since it was predicted that increased amount of base would increase the subsequent hydrolysis rate of the hydrogel, however this was not seen. All samples had similar swelling rates, suggesting the density for all the samples were comparable and thus a similar amount of water could be absorbed. Therefore, it was concluded that the stereochemistry of the vinyl thioether bond was not influenced by the amount of NEt₃ used in the organogel synthesis. In addition, degradation of the networks displayed similar characteristics, confirming this was not a contributing factor for differences between the mechanical properties of the stereocontrolled hydrogels.

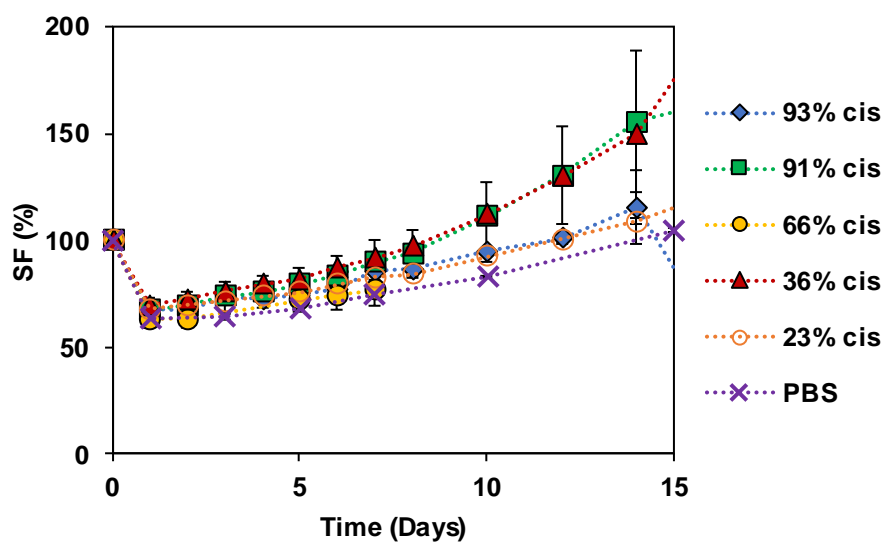


Figure 4.11. Swelling profiles of the stereocontrolled thiol-yne PEG hydrogels. Hydrogels were immersed in PBS solution and placed in an incubator at 37 °C and weighed periodically. Swelling factor (SF) was calculated as a percentage by dividing the mass at the time point by the initial mass. Conducted in triplicate.

4.2.4. Mechanical Properties of the Stereocontrolled Thiol-yne Hydrogels

Once the structural characteristics of the hydrogels were confirmed the mechanical properties were assessed through rheological and compression testing. The dimensions of the hydrogels were kept the same to make sure that the results were not a consequence of swelling and were a direct result of the different stereochemistry contents in the hydrogels.

4.2.4.1. Rheological Characterisation of Stereocontrolled Thiol-yne Hydrogels

Rheological oscillation testing was performed after the solvent exchange process. Excess water was removed from the pre-formed hydrogels (after the 7 day solvent exchange process) and tested in parallel plate configuration. The normal force was kept constant (0.04 N) throughout testing to ensure there was contact between the sample and the plates and to confirm that the sample did not dehydrate during testing. Each sample was then subjected to an amplitude sweep test and the storage (G') and loss (G'') moduli

were recorded as the amount of strain was increased from 0.01–10%. The results of the amplitude sweep tests demonstrated that stereochemistry of the vinyl thioether bond did influence the viscoelastic properties of the thiol-yne hydrogels. As the *cis* content increased, the G' values decreased, suggesting the hydrogels were getting softer (Figure 4.12). This trend also correlated with an increase in the calculated mesh size (Table 4.4) which revealed that as the *cis* content increased the mesh size also increased. This is a result of larger distances between crosslinked sites resulting in a less rigid structure and therefore contributes to a lower G' . However the dominant factor of a decrease in G' is the conformation arrangement of the vinyl thioether crosslink where the *trans* conformation is more planar than the bent *cis* conformation, allowing better chain packing and therefore less elasticity as the *trans* content increased.¹⁸ G' values ranged from 25 ± 0.02 kPa to 10 ± 2.7 kPa as the *cis* content increased. The difference in G' (15 kPa) is larger than other reports using azobenzene hydrogels,^{18, 20, 30} thus highlighting an advantage of the nucleophilic thiol-yne addition reaction. Nevertheless, the recorded range of G' values (10 ± 2.7 - 25 ± 0.02 kPa) for these hydrogels implied that these materials were very stiff and rigid, which limits their suitability to mimic a range of different biological environments. Nevertheless, these systems display mechanical properties that could make them suitable as cartilage mimics where development and proliferation markers of chondrocytes could be monitored *in vitro* for osteoarthritis research.^{31, 32} To access a larger range of viscoelastic properties and more effectively mimic different biological materials, different PEG precursors, in combination with tuning the stereochemistry, could be used to lower G' values.

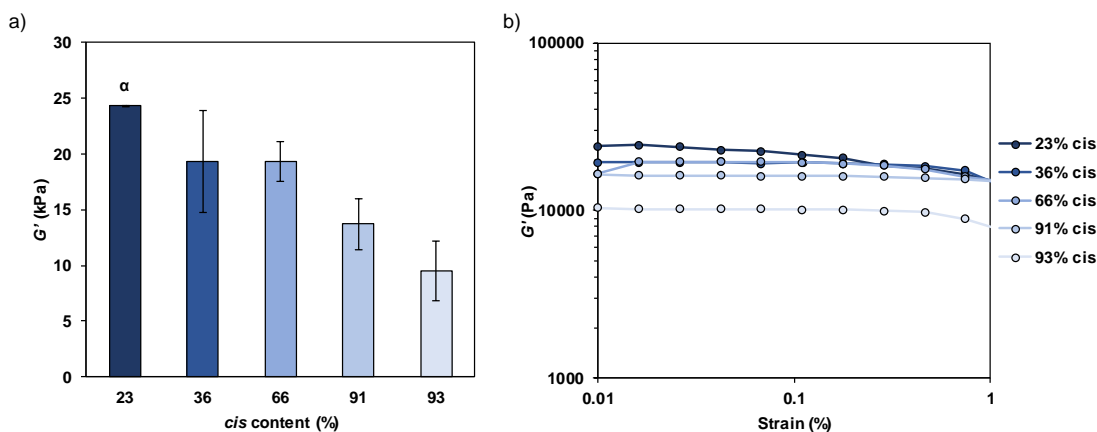


Figure 4.12. Rheological characterisation of the stereocontrolled thiol-yne PEG hydrogels, a) Average G' determined at a constant strain of 0.01% and 10 rad s^{-1} , b) Representative amplitude sweep for each stereocontrolled thiol-yne PEG hydrogel at a constant strain of 10 rad s^{-1} . α = Significantly different from 93% cis content hydrogel condition $p < 0.05$.

4.2.5.2. Compression Testing of the Stereocontrolled Thiol-yne Hydrogels

For compression testing, cylindrical organogels (4×9 mm) with different *cis* contents were synthesised in the same manner as previously described. The samples were then subjected to the solvent exchange process for 7 days before testing. Compression testing was conducted using a uniaxial tensiometer with compression grips and samples were subjected to a force of 5 kN and 98% strain. All the hydrogels failed at a similar strain (50%), however the respective stress at break varied according to their *cis* content (Figure 4.13). It was found that high *cis* content hydrogels were weaker (maximum compression stress = 126 ± 15 kPa) in comparison to high *trans* content hydrogels which could withstand higher amounts of load (325 ± 16 kPa). These results suggest that the stereochemistry influenced how the hydrogels withstood load which can be correlated to the molecular properties (*i.e.* conformation of the resultant *cis* and *trans* vinyl thioether units) within the bulk material. The organised, planar *trans* conformation provided a more suitable environment for chain packing and for crosslink points to attract.¹⁸ This allowed

larger amounts of load to be dissipated within the structure, in comparison to the more amorphous, bent *cis* confirmation. Undoubtedly, the stereochemistry of the vinyl thioether bond is critical to the strength of resultant hydrogel material which therefore dictates the external pressures the material can withstand.

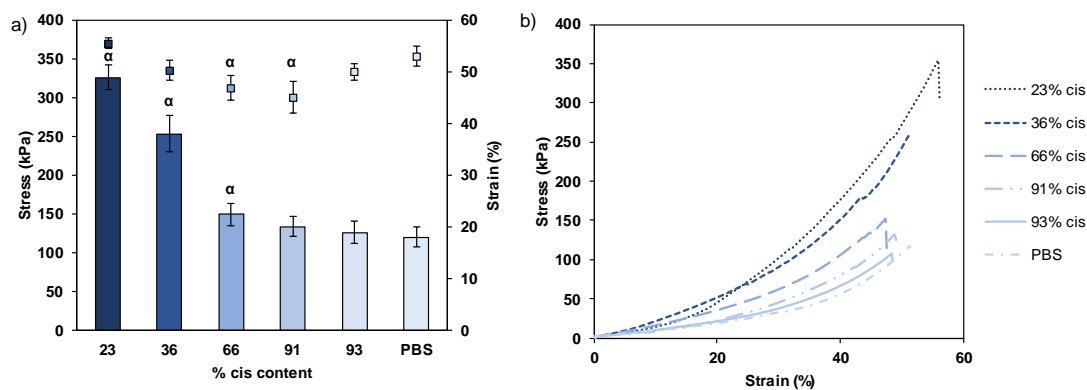


Figure 4.13. Compression testing of the stereocontrolled thiol-yne PEG hydrogels, a) average maximum compressive strength for each condition (bars, LHS axis), b) average maximum compressive strain for each condition (dots, RHS axis). α = Significantly different from PBS condition, $p < 0.05$.

4.3. Conclusions

An important aim in biomaterials research is to be able to mimic a wide range of biological properties using the same material. To fulfil this requirement, the material needs to be synthesised using the same precursors and reaction conditions. This ensures that the resultant toxicity and basic structure of the material is consistent between material batches. Stereochemistry lends itself to this requirement, since isomeric materials with different mechanical properties can be synthesised using the same precursors. The ability to control the stereochemistry of the thiol-yne PEG hydrogel system afforded materials with diverse mechanical properties while maintaining consistent swelling and structure profiles. Although these materials are stiffer than other related stereocontrolled hydrogel systems, they grant access to a wider range of G' , suitable biological environments. Furthermore, the hydrogels in this study feature stereochemistry which is irreversible (*i.e.* “locked”), allowing the effect of the stereochemistry to be monitored over long periods of time. This is an attractive property for studying long term effects of stereochemistry. Future work seeks to establish a correlation between stereochemistry and stem cell differentiation to assess their suitability as biomaterials for regenerative medicine.

4.4. References

1. C. Wolf, *Dynamic Stereochemistry of Chiral Compounds: Principles and Applications*, Royal Society of Chemistry, 2007.
2. W. G. McBride, *Lancet*, 1961, **278**, 1358.
3. C. W. Bunn, *Trans. Faraday Soc.*, 1942, **38**, 372-376.
4. S. Lv, D. M. Dudek, Y. Cao, M. M. Balamurali, J. Gosline and H. Li, *Nature*, 2010, **465**, 69.
5. K. S. Straley and S. C. Heilshorn, *Soft Matter*, 2009, **5**, 114-124.
6. S. K. Bhatia, *Engineering Biomaterials for Regenerative Medicine: Novel Technologies for Clinical Applications*, Springer New York, 2011.
7. A. S. Hoffman, *Adv. Drug Delivery Rev.*, 2002, **54**, 3-12.
8. H. Geckil, F. Xu, X. Zhang, S. Moon and U. Demirci, *Nanomedicine (London, U. K.)*, 2010, **5**, 469-484.
9. R. Langer and N. A. Peppas, *AIChE J.*, 2003, **49**, 2990-3006.
10. A. M. Kloxin, A. M. Kasko, C. N. Salinas and K. S. Anseth, *Science*, 2009, **324**, 59-63.
11. D. Seliktar, *Science*, 2012, **336**, 1124-1128.
12. I. L. Kim, R. L. Mauck and J. A. Burdick, *Biomaterials*, 2011, **32**, 8771-8782.
13. M. W. Tibbitt and K. S. Anseth, *Biotechnol. Bioeng.*, 2009, **103**, 655-663.

14. M. S. Rehmann and A. M. Kloxin, *Soft Matter*, 2013, **9**, 6737-6746.
15. N. Sanabria-DeLong, S. K. Agrawal, S. R. Bhatia and G. N. Tew, *Macromolecules*, 2006, **39**, 1308-1310.
16. G. N. Tew, N. Sanabria-DeLong, S. K. Agrawal and S. R. Bhatia, *Soft Matter*, 2005, **1**, 253-258.
17. D. E. Gregonis, G. A. Russell, J. D. Andrade and A. C. deVisser, *Polymer*, 1978, **19**, 1279-1284.
18. A. M. Rosales, K. M. Mabry, E. M. Nehls and K. S. Anseth, *Biomacromolecules*, 2015, **16**, 798-806.
19. A. M. Rosales, C. B. Rodell, M. H. Chen, M. G. Morrow, K. S. Anseth and J. A. Burdick, *Bioconjugate Chem.*, 2018, **29**, 905-913.
20. I. N. Lee, O. Dobre, D. Richards, C. Ballestrem, J. M. Curran, J. A. Hunt, S. M. Richardson, J. Swift and L. S. Wong, *ACS Appl. Mater. Interfaces*, 2018, **10**, 7765-7776.
21. X. Y. Cai, J. Z. Li, N. N. Li, J. C. Chen, E.-T. Kang and L. Q. Xu, *Biomater. Sci.*, 2016, **4**, 1663-1672.
22. V. X. Truong, M. P. Ablett, S. M. Richardson, J. A. Hoyland and A. P. Dove, *J. Am. Chem. Soc.*, 2015, **137**, 1618-1622.
23. V. X. Truong and A. P. Dove, *Angew. Chem., Int. Ed.*, 2013, **52**, 4132-4136.
24. W. E. Truce and G. J. W. Tichenor, *J. Org. Chem.*, 1972, **37**, 2391-2396.

25. C. A. Bell, J. Yu, I. A. Barker, V. X. Truong, Z. Cao, A. V. Dobrinyin, M. L. Becker and A. P. Dove, *Angew. Chem.*, 2016, **128**, 13270-13274.
26. V. X. Truong and A. P. Dove, *Angew. Chem., Int. Ed.*, 2013, **52**, 4132-4136.
27. D. H. Williams and I. Fleming, *Spectroscopic Methods in Organic Chemistry*, McGraw-Hill, 1995.
28. A. Herrmann, L. Pratsch, K. Arnold and G. Lassmann, *Biochim. Biophys. Acta*, 1983, **733**, 87-94.
29. Y. Li, J. Rodrigues and H. Tomas, *Chem. Soc. Rev.*, 2012, **41**, 2193-2221.
30. A. M. Rosales, C. B. Rodell, M. H. Chen, M. G. Morrow, K. S. Anseth and J. A. Burdick, *Bioconjugate Chem.*, 2018, DOI: 10.1021/acs.bioconjchem.7b00802.
31. I. Levental, P. C. Georges and P. A. Janmey, *Soft Matter*, 2007, **3**, 299-306.
32. N. G. Genes, J. A. Rowley, D. J. Mooney and L. J. Bonassar, *Arch. Biochem. Biophys.*, 2004, **422**, 161-167.

Chapter 5.

Self-healing, Stretchable and Robust Thiol-yne Interpenetrating Networks through Utilising the Properties of Natural Polymers

5.1. Introduction

For hydrogels to be competitive biomaterials in clinical applications, they need to be prepared by straightforward synthetic routes using commercially available precursors, thus ensuring the route followed is the most attractive and cost effective.¹⁻⁵ There is currently a huge interest in hydrogels since their ability to mimic the features of the native extracellular matrix (ECM) (*i.e.* porous structure, adequate stiffness, controlled mechanical properties) allowing cell growth and proliferation to be studied *in vitro* in a 3D environment.⁶⁻⁸ However, to further improve their properties as ECM mimics, the design of hydrogels should also target other requirements, which include: (1) gelation *in situ* at the defect site (*i.e.* injectability), (2) self-healing, and (3) enhanced mechanical properties (*i.e.* stretchability).⁹⁻¹¹

Self-healing is defined as a materials ability to self-mend repairing any damage automatically,¹²⁻¹⁵ hence, hydrogels designed to exhibit this property are able to repair after failure *in situ*, thus adapting to their surrounding environment.^{16, 17} There are several methods to render hydrogels self-healing: the use of supramolecular interactions using a guest-host route,^{18, 19} hydrogen bonding,^{20, 21} or ionic interactions.²²⁻²⁴ In addition to self-healing properties, a hydrogel with improved stretching properties better mimics the elastic qualities of native tissue, creating materials with promising characteristics.²⁵ Bearing both concepts in mind, nature provides us with a wide range of biocompatible natural polymers (*e.g.* alginate and gelatin) that are cheap to produce and can easily form hydrogels with good self-healing and tensile properties,²⁶⁻²⁸ however, they cannot be

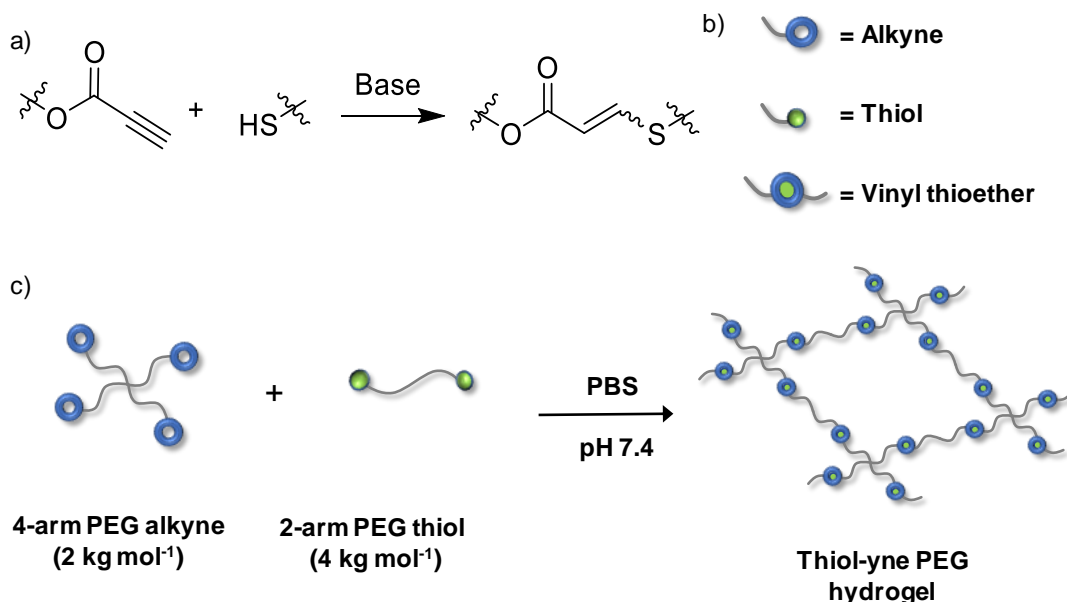
tuned to different biological environments, display weak compressive strengths,²⁹⁻³¹ and can lack reproducibility.^{32, 33} In this regard, many attempts have been made to overcome these drawbacks by including dynamic crosslinking systems³⁴, slide-ring connections,³⁵ and synthesising interpenetrating networks (IPNs).³⁶

Thus, it was hypothesised that blending a natural polymer with the robust synthetic thiol-yne PEG hydrogel system (characterised in Chapter 2) would result in a thiol-yne IPN hydrogel that possesses the advantages of both the natural hydrogel system (*i.e.* self-healing and stretchability) and the synthetic system (*i.e.* tuneable stiffness, reproducibility and robust compressive strength), which are ideal characteristics of a ECM mimic. To synthesis these networks, five commercially available unfunctionalised natural polymers (*i.e.* alginate, chitosan, gelatin, heparin, or hyaluronic acid (HA)) were blended within the thiol-yne hydrogel system,³⁷ and their self-healing response, swelling profile, and mechanical properties were characterised.

5.2. Results and Discussion

5.2.1. Synthesis of Thiol-yne Interpenetrating Networks (IPNs)

Although it remains a challenging task, developing hydrogels with superior features, by following strategies as simple and affordable as possible, renders these biomaterials competitive products open to commercialisation. With this mindset, to expand the range of properties displayed by the thiol-yne PEG hydrogels without compromising those already optimised (*i.e.* robustness and cytocompatibility),³⁷ the 42A24S thiol-yne PEG system (nomenclature described in Chapter 2) was chosen as the covalently crosslinked hydrogel network as it displayed the highest compressive strength (2.4 MPa) in the series characterised (Chapter 2). As previously described (Chapter 2, Section 2.2.1), 2-arm (4 kg mol⁻¹) and 4-arm (2 kg mol⁻¹) PEG precursors were functionalised through simple Fischer esterification reactions with 3-mercaptopropionic acid and propiolic acid, respectively, to yield highly functionalised thiol- and alkyne-precursors (end-group conversion >99% and 93%, respectively) in high yield (83% and 61%, respectively). Dense covalent thiol-yne hydrogels readily formed in PBS solution (pH 7.4) and hereafter referred to as the control or PEG only hydrogels (Scheme 5.1).



Scheme 5.1. a) Nucleophilic thiol-yne reaction, b) Legend for the alkyne, thiol and vinyl thioether, c) reaction between 4-arm PEG alkyne (2 kg mol⁻¹) and 2 arm PEG thiol (4 kg mol⁻¹) in a 1:1 ratio (alkyne:thiol) in phosphate buffered saline (PBS) solution to create the dense covalently crosslinked synthetic network in the thiol-yne IPNs.

Five different natural polymers (alginate, chitosan, gelatin, hyaluronic acid (HA) and heparin) were blended with the PEG precursors before gelation without further purification or functionalisation. To create thiol-yne IPNs with superior properties, a range of optimisation reactions were carried out to investigate the required amount of natural polymer to be added ensuring that; (1) the natural polymer was homogeneously distributed within the dense hydrogel network, avoiding phase separation, and (2) the resulting IPN benefited from the advantages of all the components. Initial experiments were carried out using the PEG/Alginate system and found that adding 0.5-2 wt% of alginate to a 10-11 wt% thiol-yne polymer network prevented the IPN from self-healing (Table 5.1). It was thought that this could be a consequence of the PEG content preventing the alginate chains from moving to form electrostatic interactions allowing self-healing to

occur. Or the concentration of alginate is too low in these systems and therefore it was unable to spread around the PEG network allowing new electrostatic bonds to form. Conversely, when a lower thiol-yne PEG content was used (5.3-7.5 wt%), gel formation did not occur or the two-systems phase separated; however, IPNs prepared with intermediate PEG wt% values displayed the beneficial characteristics of both systems. Therefore, according to these observations, all the thiol-yne IPN hydrogels were prepared with 8 wt% thiol-yne PEG and 1 wt% natural polymer content (overall 9 wt% solid content, Table 5.1).

Table 5.1. Optimisation of the PEG/Alginate thiol-yne IPNs composition.

Gel #	Alginate (%)	PEG (%)	Total % solids	Characterisation of the IPN
1	1.5	11	12.5	No self healing
2	2	10	12	No self healing
3	0.5	10	10.5	No self healing
4	0.7	5.3	6	No gel
5	1	7	8	Weak gel
6	2.25	6.75	9	Phase separation
7	1.5	7.5	9	Phase separation
8	1	8	9	Homogeneous gel, self healing
9	0.5	8.5	9	Gel weaker in compression testing than 8 wt% gel

Once the composition of the hydrogels was optimised, IPNs were prepared for testing. For all the systems two solutions were prepared by dissolving the alkyne and thiol precursors in phosphate buffered saline (PBS) solution respectively. The natural polymer and additional components, if required, were added to the solutions (see Table 5.2 and

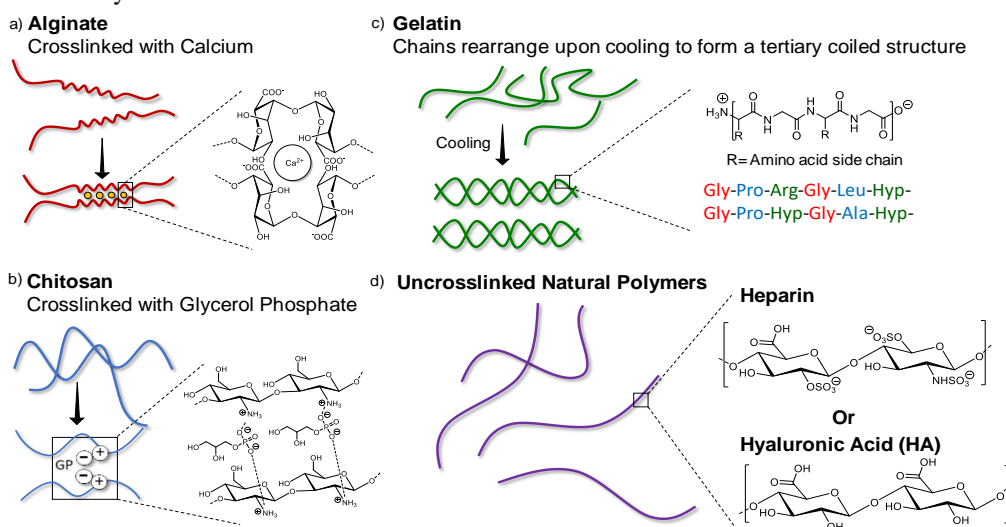
Scheme 5.2 for more details) before both solutions were mixed, vortexed and then injected into suitable moulds ready for testing (Scheme 5.3). The PEG/HA and PEG/Heparin systems were prepared to evaluate the effect adding an uncrosslinked single polysaccharide chain had on the thiol-yne network.

Table 5.2. Synthetic details for the synthesis of the PEG/Natural polymer hydrogels

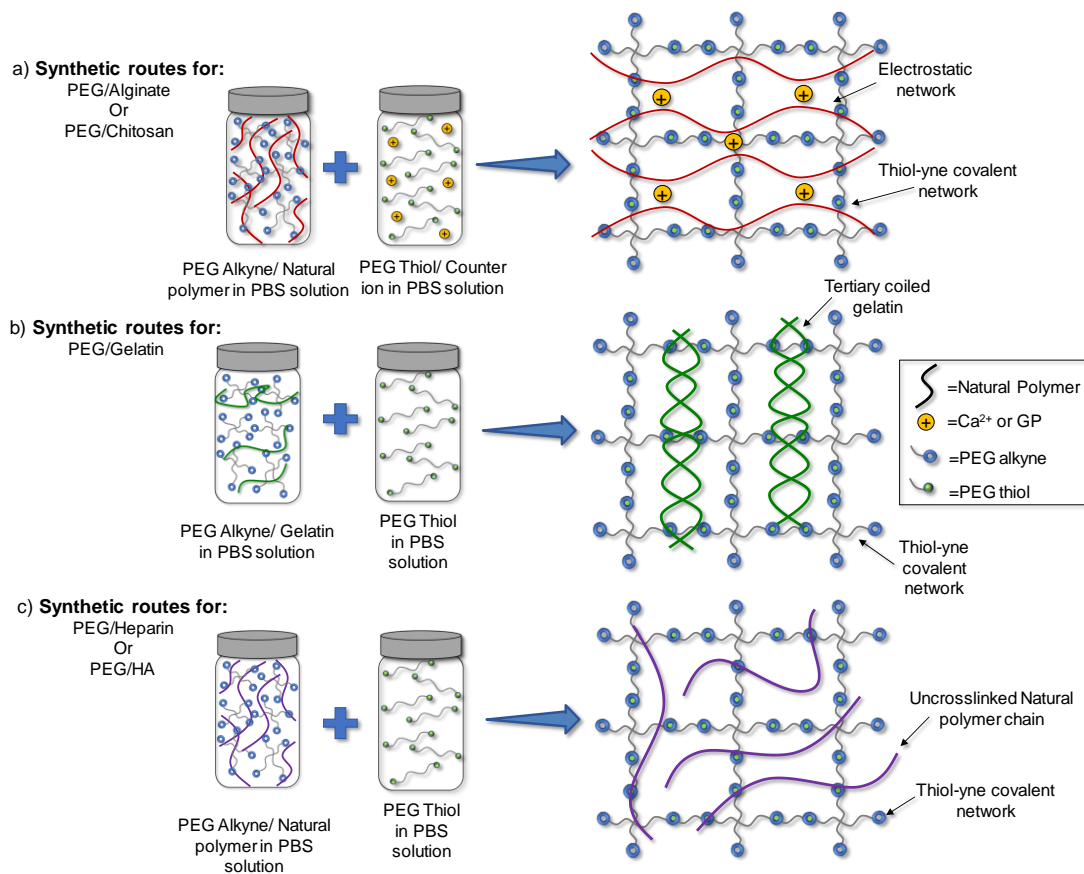
PEG/Natural Polymer ^a	Alkyne PBS solution	Thiol PBS solution	Synthetic details
PEG/Alginate	Alginate CaCO ₃ (0.2 wt%)	D-(+)-glucono-1,5-lactone (GDL) (1 wt%)	Alginate in PBS solution and heated to 70 °C to dissolved then added to PEG alkyne solution
PEG/Chitosan	Chitosan	Glycerol Phosphate (GP) (5 wt%)	Chitosan dissolved in 0.1 M HCl before addition to PEG alkyne solution
PEG/Gelatin	Gelatin	-	Gelatin heated to 70 °C to dissolve before addition to PEG alkyne solution
PEG/Heparin	Heparin	-	No additional required
PEG/HA	HA	-	No additional required

^a All PEG/Natural polymer networks were made at 8 wt%:1 wt% (PEG:Natural polymer) ratio.

Scheme 5.2. Schematics showing the crosslinking mechanism for each natural polymer system: a) alginate hydrogel forms through the electrostatic interactions with Ca²⁺; b) chitosan establishes electrostatic interactions with glycerol phosphate (GP); c) gelatin chains rearrange upon cooling to form a tertiary coiled structure; d) heparin and hyaluronic acid (HA), are both negativity charged, but do not form secondary networks.



Scheme 5.3. Schematics illustrating the procedure followed to prepare a) PEG/Natural polymer IPNs with counter ion, b) PEG/Natural polymer hydrogels with no counterion. The natural polymer was dissolved and mixed with the PEG alkyne PBS solution before being added to the PEG thiol solution. The solution was then mixed and vortexed before injected into moulds for testing.



5.2.2. Control Reaction for the Synthesis of PEG/Natural Polymer IPNs

Control reactions were carried out for the PEG/Alginate, PEG/Chitosan, and PEG/Gelatin systems to assess the effect of the loose secondary electrostatic network on the rheological properties of the resulting IPNs (Figure 5.1). For all three systems, the thiol-yne IPNs (8 wt% PEG, 1 wt% natural polymer) decreased in stiffness compared to the PEG only hydrogel (dark blue data vs. red data), which could be a result of the secondary network disrupting the covalent reaction proceeding, reducing the number of crosslinked sites and therefore reducing the stiffness. However, the IPNs increased the stiffness of the single natural polymer hydrogels as expected (light blue data vs. red data); the solid content increased in these systems and the stronger covalent bonds present from the thiol-yne crosslinking reaction increased the elastic properties of the hydrogels. The control experiments further showed the influence the addition of the PEG alkyne precursor had on the elastic properties of the natural polymer hydrogels (green vs. light blue data); for alginate and chitosan, the electrostatic interactions within the networks are strong enough not to be affected by the addition of PEG alkyne, whereas for the gelatin system, G' decreases dramatically demonstrating that the interactions between the gelatin chains are disrupted and weaker than the alginate and chitosan interactions. Furthermore, the rheological data confirms the ratio between the two systems (8 wt%:1 wt%) effects the elastic properties of both systems which could translate to improved properties for both systems.

For the alginate and chitosan systems, control reactions were also carried out to confirm the affect the concentration of the counterions (CaCO_3 and GP, respectively) had

on the formation of the resultant IPN. In the case of the PEG/Alginate the formation of the IPN without CaCO_3 (*i.e.* no secondary electrostatic networks can form) shows an increase in G' (Figure 5.1a), indicating an increase in the stiffness of the system more similar to the single thiol-yne network (Figure 5.1a). This suggests the formation of a secondary electrostatic interaction disrupts the thiol-yne reaction from occurring, lowering G' . With an increased amount of CaCO_3 (0.2 wt% to 1 wt%) improved tensile properties are seen (Figure 5.6, Section 5.2.4) however, this increase prevented the formation of transparent hydrogels which is not suitable for cell encapsulation as cells cannot be imaged through the opaque hydrogel. Therefore, the addition of 0.2 wt% CaCO_3 was confirmed as an appropriate amount of counterion needed to form PEG/Alginate hydrogels.

For PEG/Chitosan hydrogels the amount of GP added directly affected the crosslinking reaction and, consequently, the formation of the IPN. None or weak gelation occurred with low amounts of GP (0-3 wt%) as a result of the chitosan solution acidic nature, preventing the thiol-yne reaction occurring *via* the nucleophilic pathway. Chitosan was dissolved in 0.1 M HCl before addition to the PEG alkyne solution, since it is only soluble in water under acidic conditions, GP works as a counterion in the formation of the chitosan hydrogels but also importantly increases the pH of the solution needed for the thiol-yne reaction to occur. Accordingly, if the amount of GP is not high enough, the pH of the solution remains low, and the nucleophilic thiol-yne reaction cannot proceed, resulting in poor gel formation. Consequently, the addition of 5 wt% GP was found to increase the pH of the solution, to allow the thiol-yne reaction to occur *via* a nucleophilic

pathway and to form single chitosan hydrogel therefore successful IPN formation, while also preventing phase separation of the GP crashing out of solution. Once the composition of the thiol-yne IPNs was complete, the properties of the thiol-yne IPNs were characterised through swelling, rheological, compression and tensile testing.

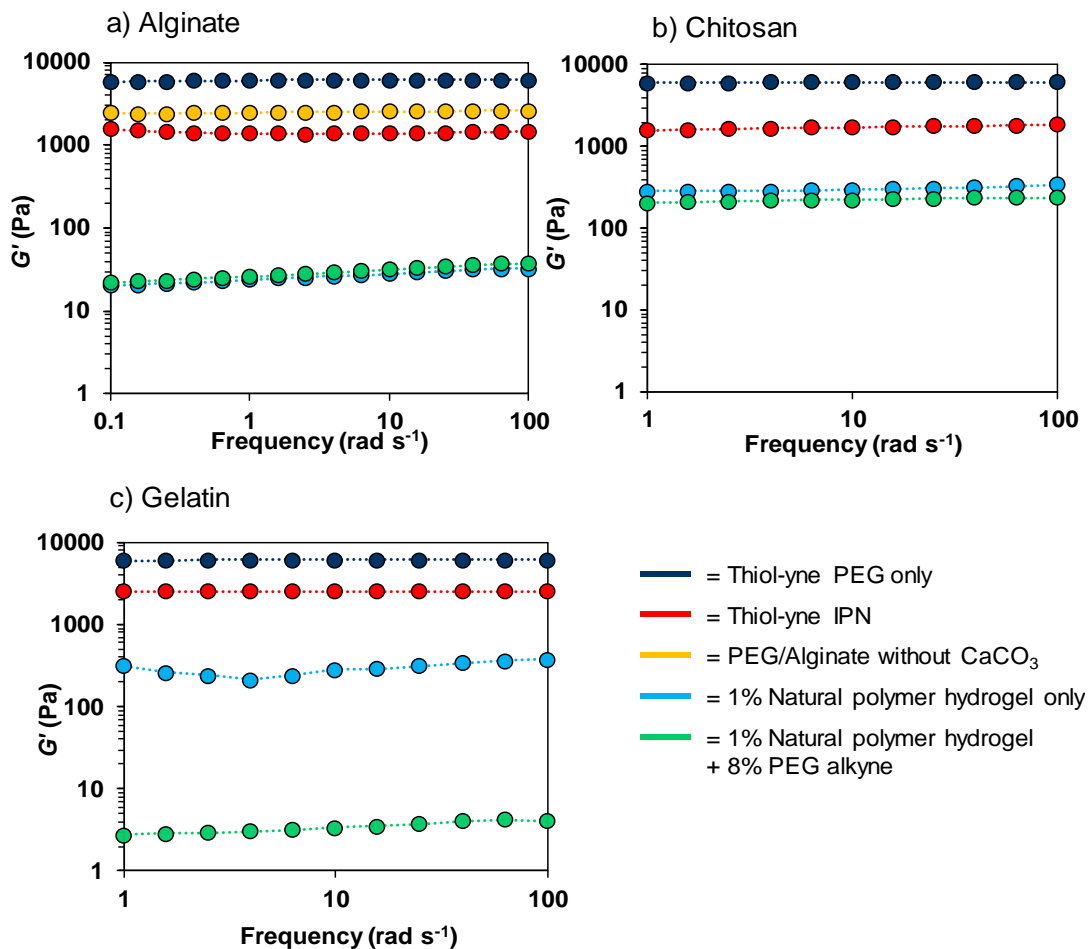


Figure 5.1. Representative rheological frequency sweeps for the thiol-yne IPNs to demonstrate the effect the secondary electrostatic network has on the IPN.

5.2.3. Characterisation of the Thiol-yne IPNs

5.2.3.1. Swelling Kinetics of the Thiol-yne IPNs

PEG only thiol-yne hydrogels were formed in PBS solution (pH 7.4) at 8 wt% PEG content within 3 min owing to the high efficiency and fast reaction rate of the nucleophilic thiol-yne click reaction. The gelation time of hydrogels containing natural polymers increases slightly in comparison to the control PEG only system (3 min), albeit they all still form very quickly within 10 min as measured through rheological experiments (Figure 5.2), thus confirming the hydrogels formed rapidly as a result of the efficient thiol-yne crosslinking reaction. By monitoring G' and G'' with time, it was observed that most of the hydrogels were stable 40 min after gel formation. However, the PEG/Alginate system did not rapidly reach a plateau, suggesting the formation of the secondary electrostatic network affected the rate of the thiol-yne reaction. The addition of the alginate chains prevented the mobility of the alkyne and thiol end groups which therefore delayed the time it took for the hydrogel to reach stabilisation. As such this slow gelation and stabilisation time could contribute to the final mechanical properties displayed by the PEG/Alginate IPNs.

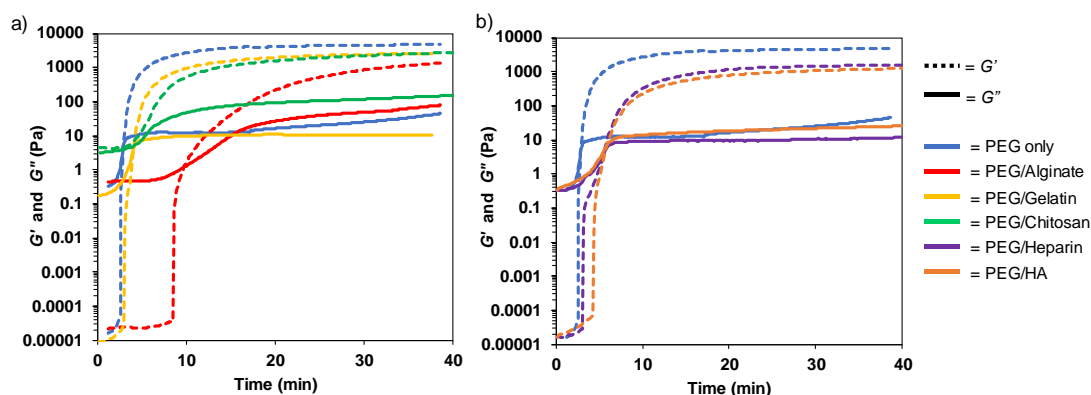


Figure 5.2. Representative curves showing the evolution of G' and G'' with time for thiol-yne IPNs containing a) a secondary loose electrostatically crosslinked network (alginate, chitosan, and gelatin); and b) negatively charged polysaccharides (heparin and HA).

Gel fraction (GF) values, which are indicative of the efficiency of the crosslinking reaction, decreased for all the blended systems (Figure 5.3, hashed bar), as a consequence of the presence of the natural polymers, which possessed higher molecular weights compared to the PEG precursors, and thus inhibited the crosslinking of the reactive PEG chain ends. The unreacted chains were washed out during the GF process, which resulted in lowering the GF % value. Furthermore, uncrosslinked polysaccharides, which did not form a secondary network (*i.e.* HA and Heparin), could also be easily washed out, thus explaining the very low value obtained for PEG/HA ($32 \pm 0.3\%$). Interestingly, PEG/Chitosan GF values were lower than expected ($GF = 56 \pm 1\%$). In this case, the low pH of the solution affected the thiol-yne reaction during gel formation, as previously mentioned, acidic conditions are required for dissolving chitosan in water, but these conditions decreased the efficiency of the thiol-yne reaction, which resulted in lower GF values for this system. However, regardless of the natural polymer blended, the equilibrium water content (EWC) values remained high (95-98%) for all the systems, thus

indicating that the polysaccharide had little effect on the ability of the hydrogel to hold water (Figure 5.3, dotted bars).

The mesh size of the PEG/Natural polymer hydrogels were calculated using the Flory-Rehner equation based on the volume swelling ratio for each system. However, precaution should be taken when using this method for IPN systems as the model does not take into account natural ionic hydrogel systems. The mesh sizes ranged from 9.7 ± 0.2 - 13.6 ± 0.3 nm (Figure 5.3, dots) and reflected the affect the addition of a secondary network had on the thiol-yne network. For the systems where a counterion was introduced and the secondary networks were electrostatically crosslinked (*i.e.* PEG/Alginate and PEG/Chitosan) the mesh sizes were smaller than the single PEG only system (*i.e.* 9.92 ± 0.13 and 9.73 ± 0.16 nm respectively compared to 10.9 ± 0.2 nm), as a result of more crosslinking in the IPNs. In contrast the PEG/Gelatin, PEG/HA and PEG/Heparin systems displayed higher mesh sizes (11.8 ± 0.2 , 13.6 ± 0.3 and 12.4 ± 0.1 nm respectively) than the PEG only systems, demonstrating the disruption the addition of a uncrosslinked polymer chain had caused to the thiol-yne network and resultant crosslinking density.

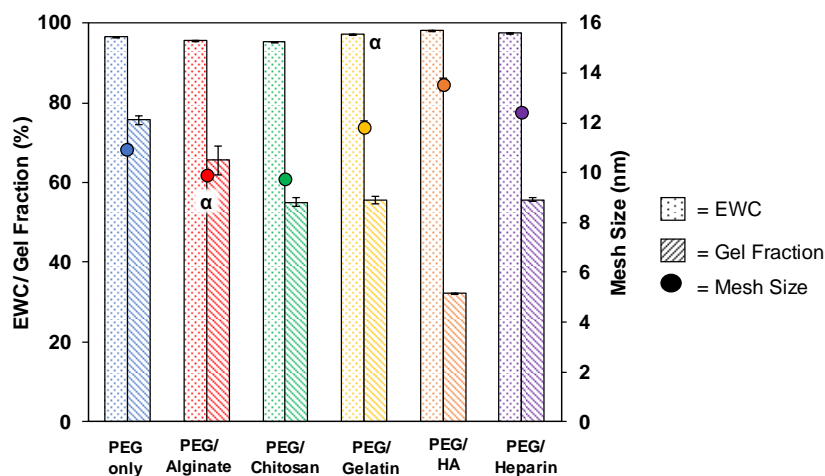


Figure 5.3. Mesh Size (dots, RHS axis), EWC (dotted bars, LHS axis) and gel fraction (hashed bar, LHS axis) values for the thiol-yne IPN hydrogels. Repeated in triplicate. α = Data is not significantly different from PEG only condition ($p < 0.05$).

5.2.3.2. Swelling and Degradation Profile of the Thiol-yne IPNs

To assess the long term swelling and degradation profiles of the thiol-yne IPNs, samples were placed in PBS solution at 37 °C (pH 7.4), and their weights were recorded daily. The hydrogels started to swell immediately after they were immersed in the solution, reaching a maximum swelling factor (SF, method described in Chapter 3) before completely dissolving (Figure 5.4). As a reference, PEG only hydrogels reached a maximum SF of $564 \pm 27\%$ in 6 days and then degraded after 7 days of immersion in PBS solution. In the case of the PEG/Natural polymer hydrogels, although the swelling profiles were unique for each thiol-yne IPN system, they followed some general patterns. For PEG/Gelatin, PEG/HA, and PEG/Heparin hydrogels, where the natural polymer is not crosslinked, the degradation rate increases in comparison to the control PEG only system (Figure 5.4), as a consequence of the natural polymer disrupting the thiol-yne reaction and

reducing the number of hydrophobic crosslinking sites. In addition, the natural polymer chains are inherently hydrophilic elevating this effect. Hence, the hydrophilicity of the polymeric thiol-yne network increases, allowing more water to infiltrate into the polymeric network, accelerating the degradation of the networks through ester hydrolysis of the alkyne and thiol PEG precursors. Specifically, the SF reached values of $493 \pm 2\%$, $455 \pm 8\%$, and $433 \pm 46\%$ for PEG/Gelatin, PEG/HA, and PEG/Heparin, respectively, before degrading in 3-5 days.

In contrast, the presence of a second electrostatic crosslinked network, based on alginate or chitosan, slows down the degradation of the single thiol-yne network (*i.e.* hydrogels are stable for up to 8 and 11 days, respectively). This is an important factor of the materials for their use as biomaterials to mimic an *in vivo* setting, where hydrogels need to retain their robust mechanical stability over time to support cell growth and proliferation. With the addition of a secondary electrostatic crosslinked network, the degradation time of the thiol-yne network increases resulting in IPNs which retain their structure for up to 12 days, allowing cells to be cultured and studied within the 3D hydrogel matrix.

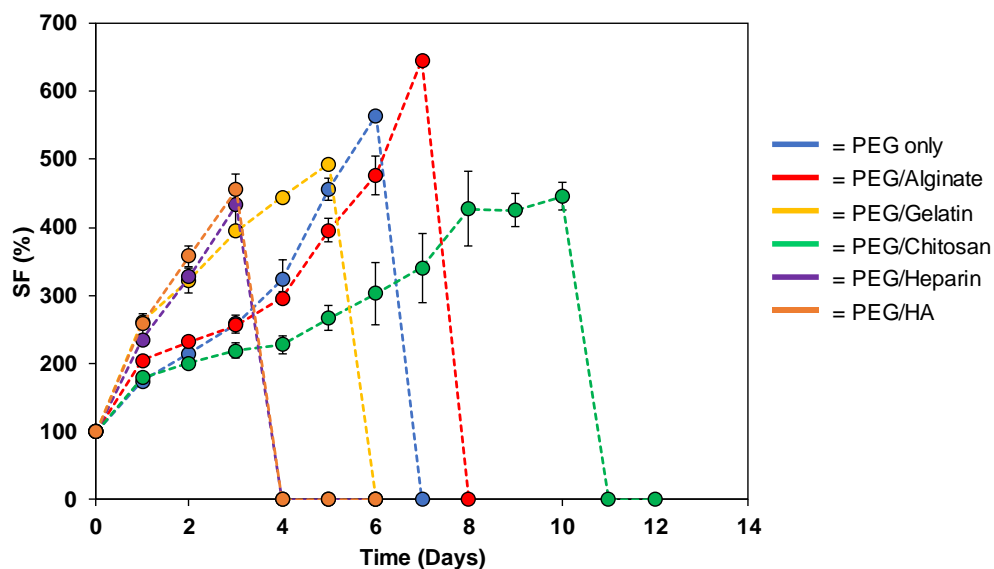


Figure 5.4. Swelling profiles of the thiol-yne IPNs immersed in PBS at 37 °C, repeated in triplicate.

5.2.3.3. Cryogenic Scanning Electron Microscopy Analysis of the Thiol-yne IPNs

Introducing a natural polymer within the densely crosslinked thiol-yne network also affects how ice crystals grow within the structures when observed by cryogenic scanning electron microscopy (cryo SEM). PEG/HA and PEG/Chitosan thiol-yne systems displayed smaller ice crystals than those observed for PEG only and PEG/Alginate systems (Figure 5.5). Interestingly this does not correlate with the mesh sizes calculated by the Flory-Rehner equation (Figure 5.3), where smaller mesh sizes were calculated for the PEG/Alginate and PEG/Chitosan systems compared to the PEG only systems and system with heparin, HA and gelatin. However, these results do correlate with the maximum SF values the systems can reach, both the PEG/HA and PEG/Chitosan systems have lower maximum SF values ($455 \pm 8\%$ and $445.1 \pm 20\%$ respectively, Figure 5.4)

than PEG only and PEG/Alginate SF= $564 \pm 27\%$ and $476 \pm 29\%$ respectively, Figure 5.4) indicating less water is introduced into the system. These cryo SEM images suggest that the secondary electrostatic networks influenced the internal structure of the thiol-yne IPNs which could affect the mechanical properties of these systems.

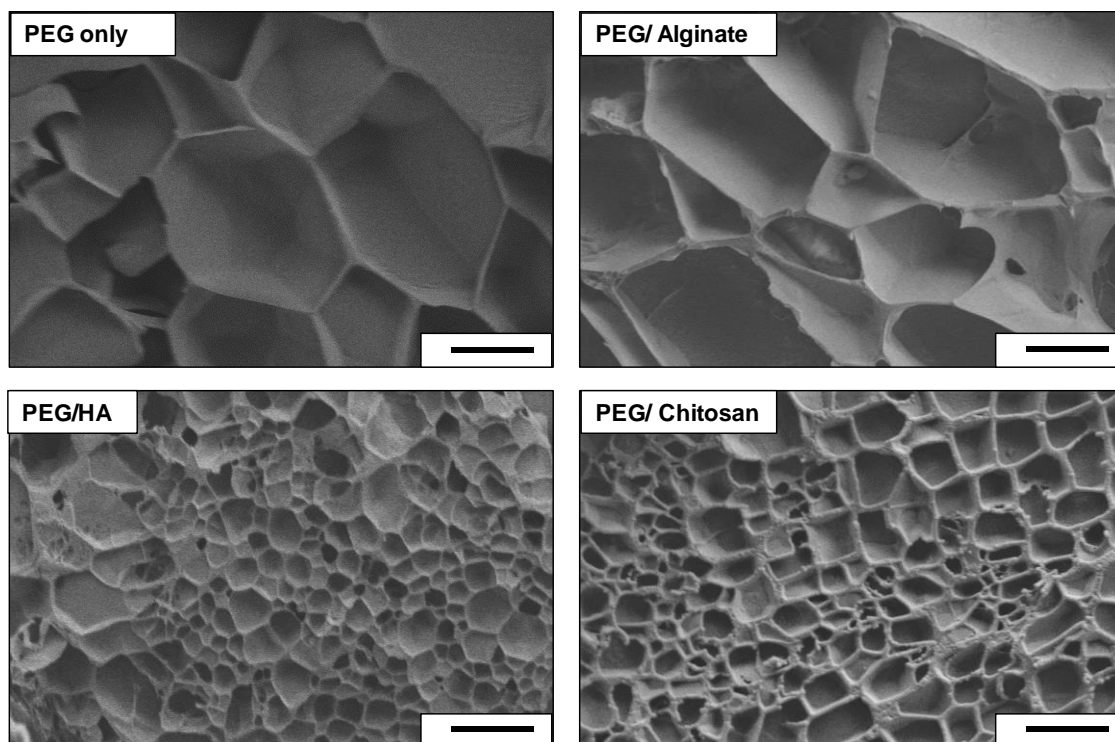


Figure 5.5. Cryo SEM images of the thiol-yne IPN hydrogels, scale bar = 10 μm .

5.2.4. Tensile characterisation of the thiol-yne IPNs

Synthesising hydrogels with good tensile properties allows them to withstand the surrounding pressure of a biological environment, thus better mimicking the behaviour of soft tissue.²⁵ To verify that our IPNs fulfil such a requirement, tensile studies were conducted, samples were formed in dog bone moulds, left to cure for 7 h, to ensure that they were fully crosslinked, and then subjected to uniaxial tensile testing. The PEG only system was able to withstand a strain of $204 \pm 42\%$ (Figure 5.6a), which is higher than initially expected as similar PEG systems prepared using radical thiol-ene chemistry only reach a strain of 150%.^{38,39} More remarkably, the thiol-yne IPNs with alginate and gelatin displayed a greater improvement in tensile properties, reaching tensile strain values up to $353 \pm 36\%$ (Figure 5.6a and 5.7). This increase in tensile performance demonstrates a facile way of improving the properties of these hydrogels by simply introducing a secondary electrostatic loose network. Interestingly, the strain at break for the PEG/Alginate IPN can be further enhanced (up to $490 \pm 88\%$, Figure 5.6b) by increasing the Ca^{2+} ion content. However, this impacts the tensile strength of the hydrogel and results in opaque hydrogels, which could make imaging encapsulated cells more difficult. In contrast, incorporating a single natural polymer (HA or heparin) into the thiol-yne hydrogels gave no significant improvement to the tensile performance ($260 \pm 49\%$ and $168 \pm 58\%$, respectively, Figure 5.6a). In this case, the single natural polymers disrupted the thiol-yne crosslinking reaction indicated by GF studies (*i.e.* GF decreased from 75 to 32 and 56% respectively, Figure 5.3), resulting in a network with more defects and dangling ends. Finally, as chitosan is only soluble in acidic conditions, the overall pH of

the system was lowered, which affected the efficiency of nucleophilic thiol-yne reaction in this system as previously mentioned (*i.e.* GF decreases from 75 to 55%, Figure 5.3). Therefore, the PEG/Chitosan system exhibited inferior properties, including a lower strain at break ($158 \pm 58\%$) than that displayed by the PEG only system.

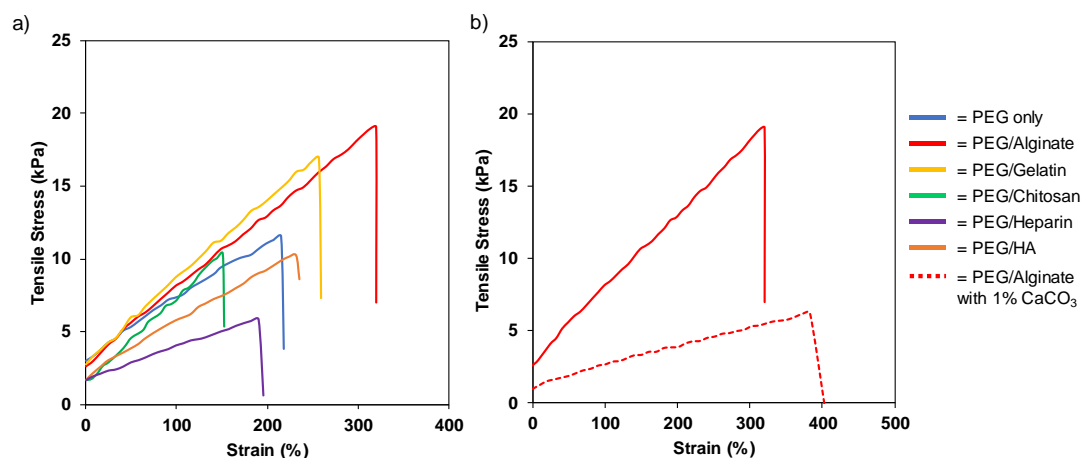


Figure 5.6. Strain-stress curves of a) the thiol-yne IPNs; and b) PEG/Alginate IPNs prepared with different CaCO₃ concentrations.

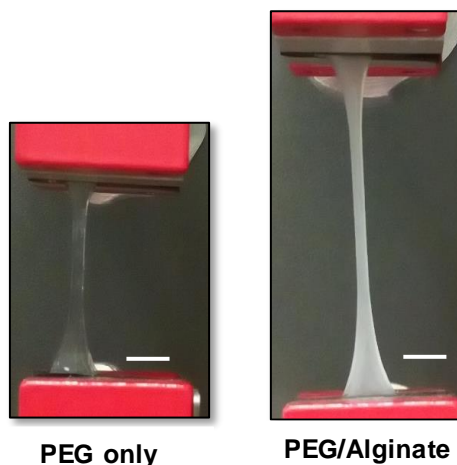


Figure 5.7. Image of the tensile testing conducted to demonstrate the improved stretchability PEG/Alginate IPN hydrogels compared to the PEG only system, scale bar = 0.5 cm.

5.2.5. Rheological Characterisation of the Thiol-yne IPNs

Through rheological studies, the reasons for such improved tensile performance could be understood, in particular for the PEG/Alginate system. The structured network of these hydrogels exhibited an elastic behaviour with G' higher than G'' and with G' almost frequency independent (Figure 5.8), which indicated that the hydrogels reach stabilisation rapidly after formation (Figure 5.2). The single dense network (PEG only) was a moderately stiff system ($G' = 5.5 \pm 0.5$ kPa at 10 rad s^{-1}); however, by incorporating a natural polymer to form an IPN, G' decreased as a result of the presence of a natural polymer reducing the stiffness of the hydrogel. For the PEG/Alginate system, G' decreased to 1.4 ± 0.03 kPa, allowing the material to become softer and have the ability to withstand higher amounts of strain (Figure 5.8a). Reducing the stiffness of these materials brought them into the intermediate range for soft biological tissue,⁴⁰ opening up an opportunity for these materials to potentially improve cell proliferation and differentiation in an applicable and relevant environment compared to the PEG only networks. The drop in G' also correlated with the larger mesh size values calculated in section 5.2.3.1. This indicated that the lower PEG content allowed longer polymer chains between crosslinked points increasing the mesh size and resulting in less rigid structures which reduced G' . This reduction in G' , combined with the electrostatic interactions between the negatively charged alginate chains and the positive calcium ions in the PEG/Alginate system, allows this IPN to exhibit overall the best improvement in tensile properties. Conversely, for the systems where a secondary natural polymer is only blended into the thiol-yne network (*i.e.* does not form electrostatic crosslinks), a decrease in G' is

also seen (*i.e.* $G' = 1.4 \pm 0.5$ and 2.1 ± 0.3 kPa for PEG/HA and PEG/Heparin respectively, Figure 5.8b); however, this has a negative effect on these systems' ability to withstand external forces because they do not possess electrostatic bonds to dissipate the external tensile strain when are broken. Instead, the sample is stretched and breaks at lower amounts of strain as the increased flexibility, indicated by G' , creates a weaker sample. The same effect is seen for the PEG/Chitosan IPN where the addition of chitosan also decreases G' values. Additionally, the reduced crosslinking efficiency of the thiol-yne reaction in this system reduces the strength of the sample, which results in a poor overall tensile performance.

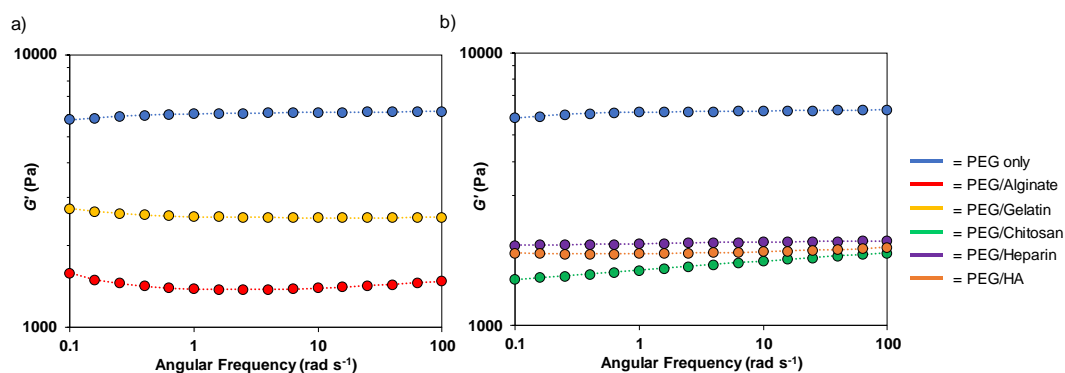


Figure 5.8. Representative rheological frequency sweeps for the thiol-yne IPNs: a) PEG/Gelatin and PEG/Alginate, which display improved tensile performance in comparison to the PEG only system; b) PEG/Chitosan, PEG/Heparin, and PEG/HA, which exhibits an inferior tensile performance in comparison to the PEG only system.

5.2.6. Compression Testing of the thiol-yne IPNs

In addition to the improved tensile properties, it is important that the robust compression strength of the original thiol-yne hydrogels (2 ± 0.5 MPa) is maintained to withstand the external compressive pressure found *in vivo*. To confirm this, the compressive stress of the thiol-yne IPN systems was attained by uniaxial compression testing; hydrogels were made in cylindrical moulds, left to cure for 7 h, and then subjected to 98% strain while the resultant stress was recorded. Indeed, PEG/Alginate and PEG/Gelatin systems displayed improved, high compressive strengths (2.3 ± 0.4 MPa and 2.4 ± 0.1 MPa, respectively, Figure 5.9) with respect to the PEG only system, which demonstrates the robust nature of the IPNs working together to form biomaterials for high load bearing environments (*e.g.* cartilage joints). However, the compressive strength of the hydrogels where chitosan, heparin, and HA were incorporated decreased to 1.8 ± 0.2 , 1.5 ± 0.2 and 1.8 ± 0.1 MPa, respectively, thus hindering their robust nature. Nevertheless, these systems still provide sufficient support as cell culture scaffolds with a similar strength to articular cartilage (1.5 MPa).⁴¹ Overall, the PEG/Alginate IPN exhibited the most improved tensile performance, having the ability to mimic the stretchability of native tissue while enhancing the robust nature of the thiol-yne hydrogels. The PEG/Alginate IPN benefits the most from the features of both the dense thiol-yne matrix and the secondary electrostatic crosslinked network, resulting in an ideal material for an ECM mimic.²⁹

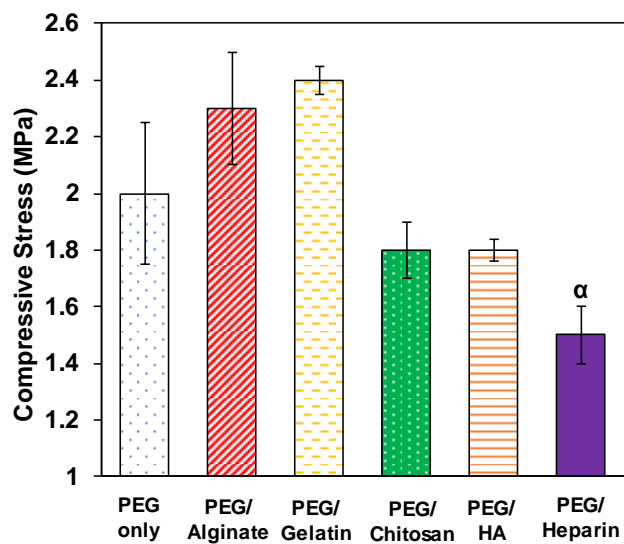


Figure 5.9. Maximum compressive stress for the thiol-yne IPNs at 98% strain, 10 replicates for each system. α = Significantly different from PEG only condition $p < 0.05$.

5.2.7. Self-healing characterisation of the thiol-yne IPNs

Material self-healing, which implies spontaneous new bond formation when the original bonds are disrupted, is driven, for instance, by non-covalent interactions (*i.e.* hydrogen bonding, disulfide exchange, metal ligand complexes).^{42, 43 44} Thus, a self-healable hydrogel that can be easily synthesised, while also possessing robust compressive strength has immense potential for regenerative medicine. Hence, to test the self-healing nature of our strong stretchable thiol-yne IPNs, dog-bone shaped samples were prepared and left to cure for 1 h before cutting. The cut pieces were then swapped with another sample and brought back together and left overnight to heal (Figure 5.10). Samples were then subjected to tensile testing at a rate of 5 mm min⁻¹, and their stress/strain curves were compared before and after the self-healing process.

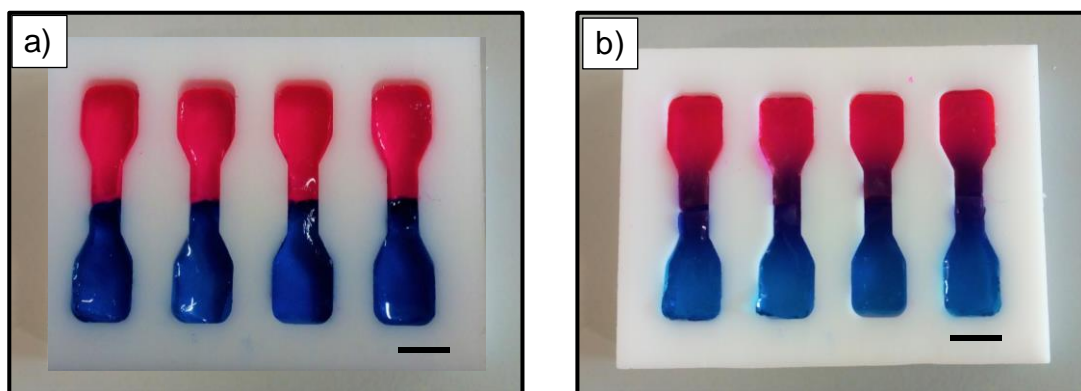


Figure 5.10. Images taken during the self-healing process. PEG/HA hydrogels were prepared in blue dye/PBS and rhodamine(pink)/PBS to highlight the self-healed site. Dog-bone shaped samples were prepared and left to cure for 1 h before cutting (a)The cut pieces were swapped with another sample and brought back together in the mould (b) and left to self-heal overnight to heal, scale bar = 0.5 cm.

As expected, the PEG/Alginate and PEG/Chitosan IPNs self-healed, forming stable hydrogels after the self-healing process as a consequence of the secondary electrostatic network forming new bonds (Figure 5.11).¹² The addition of an uncrosslinked natural polymer (*i.e.* HA or heparin) did not render self-healing properties owing to the absence of electrostatic interactions in the secondary network. These materials were softer and, although possessed adhesive properties that allowed them to hold their own weight, they were unable to self-heal (Figure 5.11) and broke at the cut site when handled (*i.e.* no self-healing had taken place, Figure 5.12).

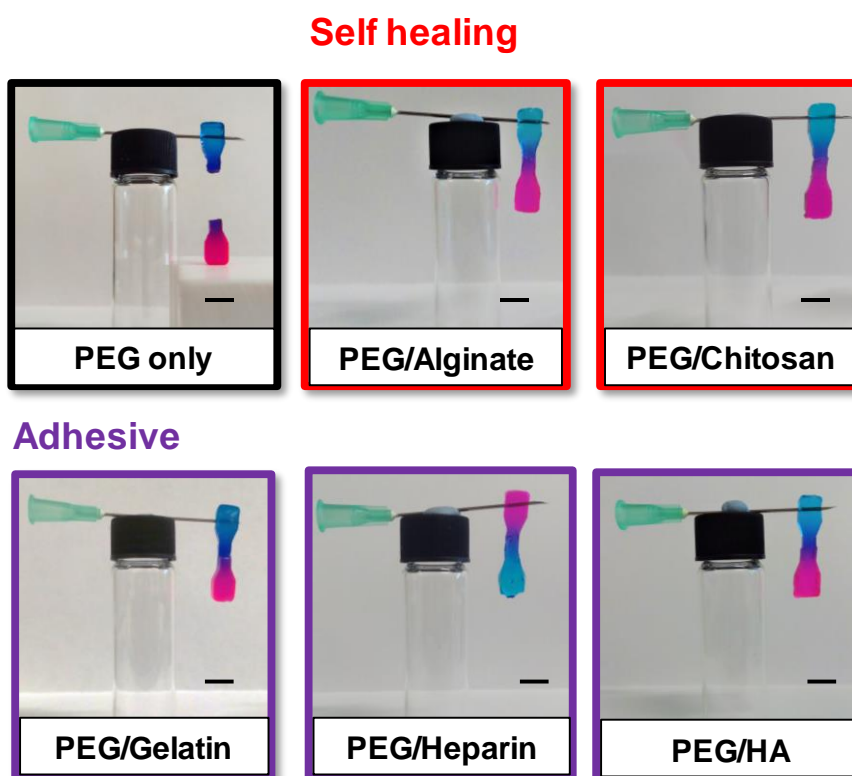


Figure 5.11. Assessment of the self-healing response of thiol-yne IPNs: PEG only hydrogels did not possess self-healing or adhesive properties, whereas PEG/Alginate and PEG/Chitosan IPNs self-healed (red boxes) and PEG/Gelatin, PEG/Heparin, and PEG/HA displayed adhesive properties (purple boxes). Hydrogels synthesised in blue dye/PBS and PBS/Rhodamine (Pink) Scale bar = 0.5 cm.

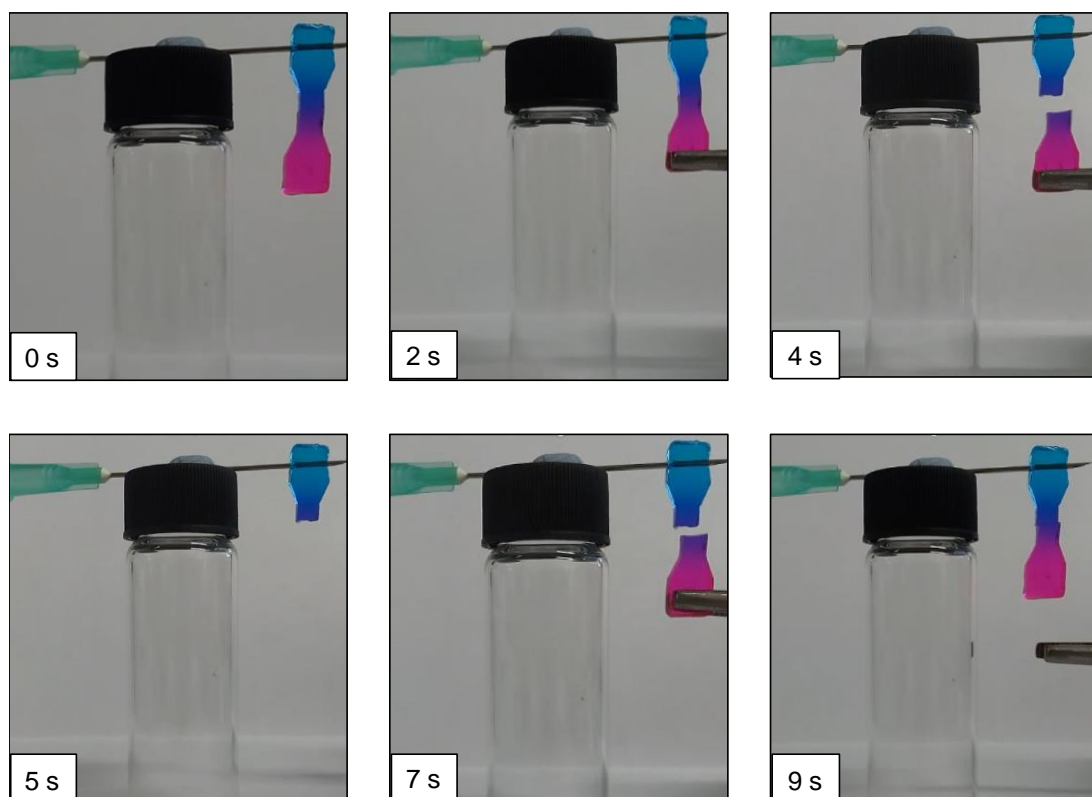


Figure 5.12. Freeze frames of the video to demonstrate the adhesive properties of the PEG/HA hydrogels.

To assess the strength of the self-healed IPNs (PEG/Alginate and PEG/Chitosan), both systems were subjected to tensile testing after the self-healing process. Interestingly, the strain at break for the self-healed PEG/Chitosan IPN was unaffected by the self-healing process (*i.e.* tensile strain not significantly different between original and self-healed sample $p < 0.05$), having the ability to recover to the same amount of strain as the original sample (157%, Figure 5.13a). This could be ascribed to the poor crosslinking efficiency, which promotes chitosan chains and GP to migrate forming more electrostatic interactions. In contrast, the self-healed PEG/Alginate hydrogels displayed poorer tensile profiles than the original samples, with strain values decreasing from $353 \pm 36\%$ to $249 \pm$

39%. The failure for both self-healing systems occurred above the healed site, thus indicating that the cut site had fully recovered and was not the weakest part of the hydrogel (Figure 5.13b). A further advantage of these systems is the simplicity of the self-healing process (RT, overnight) allowing these materials to easily recover after failure, broadening their applications in a tissue engineering setting. Although the PEG/Chitosan IPN were able to recover their initial tensile properties, the self-healed PEG/Alginate system was more robust, as shown by its ability to be twisted, stretched, and bent (Figure 5.14). Overall, the addition of a secondary electrostatic network to the thiol-yne PEG system resulted in hydrogels which were not only robust when originally made, but also retained these robust features when broken and self-healed.

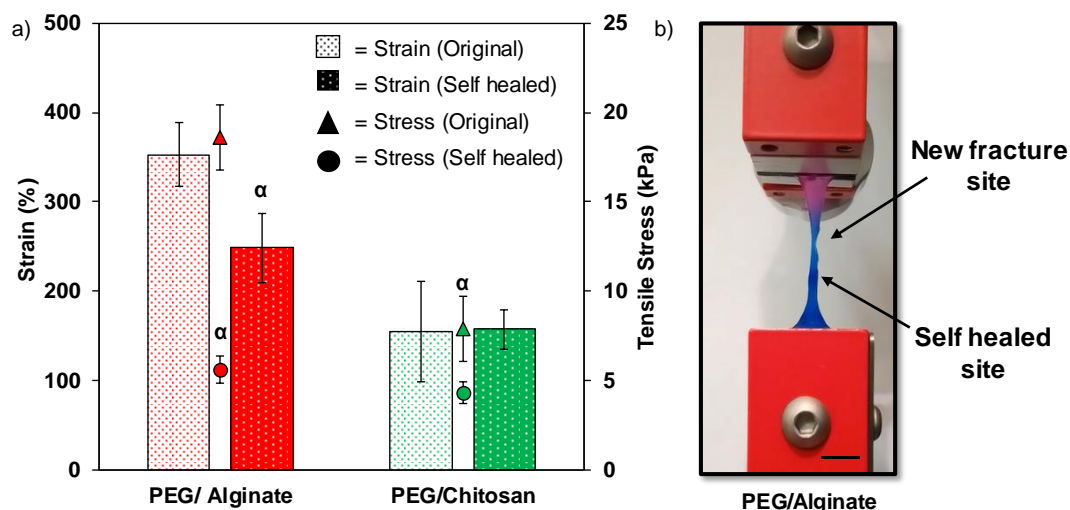


Figure 5.13. Tensile performance of self-healed thiol-yne IPNs: a) maximum tensile strain (LHS axis, bars) and maximum tensile stress (RHS axis, triangle and circle) (minimum of 5 replicates per system); b) image of PEG/Alginate breaking during tensile testing, scale bar = 0.5 cm. α = significantly different to original sample, $p < 0.05$.

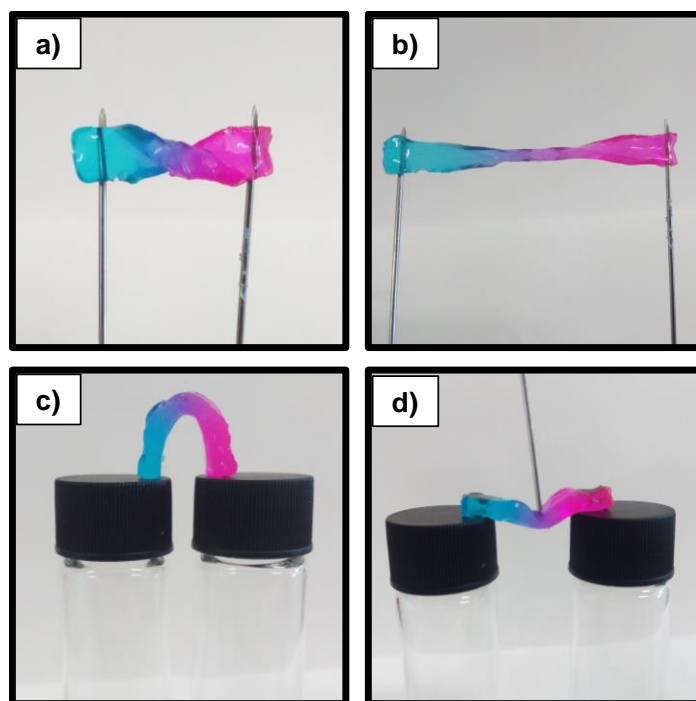


Figure 5.14. Images showing the self-healed PEG/Alginate hydrogel a) being twisted 180°; b) being twisted and stretched between two needles; c) bending on two vial caps; and d) withstanding an external force, scale bar = 0.5 cm.

5.2.8. Cytocompatibility testing of the thiol-yne IPN

Owing to the improved features acquired through the Ca^{2+} crosslinked alginate secondary network (*i.e.* stretchability and self-healing), the cytotoxicity of PEG/Alginate thiol-yne IPNs was determined and compared to that displayed by the PEG only system, as well as to PEG/HA, where the natural polymer is only blended (*i.e.* not forming a cross-linked network). Mesenchymal stem cells (MSCs) were encapsulated in a 3D configuration, and cell viability was assessed with alamarBlue® metabolic assay and live/dead fluorescent staining at different time points (*i.e.* 24, 48, and 72 h, Figure 5.15 and 5.16). After 24 h of incubation, all hydrogels displayed similar high cell viability, indicating that the thiol-yne matrices are cytocompatible, which is in good agreement with

previous studies seen in Chapter 3.⁴⁵ Moreover, the incorporation of a polysaccharide within the dense network did not affect cell viability. At longer incubation times (72 h), cell growth was not sustained for the PEG only system (Figure 5.15a), cell metabolic activity was significantly lower after 72 h in comparison to the 24 h time point, which was not observed for the other two systems. This was also confirmed by live/dead staining where cell viability decreased significantly for the PEG only system ($88 \pm 3\%$ to $77 \pm 2\%$ live cells, Figure 5.16). These differences were attributed to how cells distinctively interact with the polymeric matrices and feel their surrounding environment. Features such as the stiffness, porosity, or the presence of charged chains could all attribute to the cell metabolic activity improving the cytocompatibility of the thiol-yne IPNs.

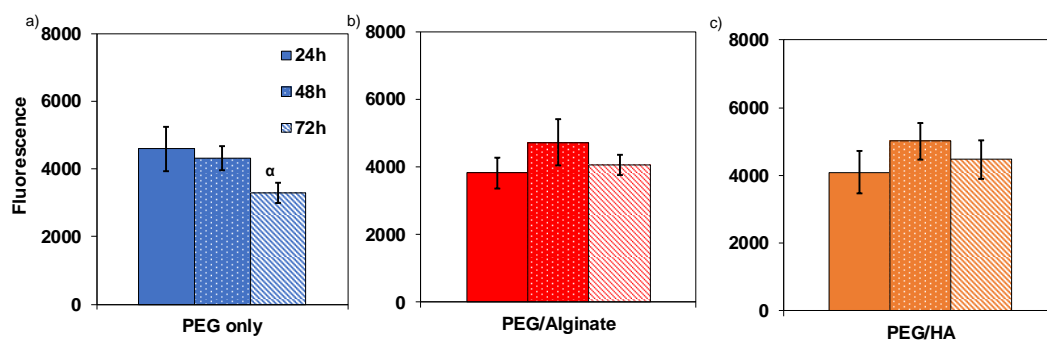


Figure 5.15. Metabolic activity of cells encapsulated in a) PEG only, b) PEG/Alginate, and c) PEG/HA hydrogels after 24, 48, and 72 h incubation times. Greek letter on bars refer to significant differences (p value < 0.05): α vs 72h.

Remarkably, cell viability after 72 h was significantly higher for PEG/Alginate hydrogels, viability increased from $87 \pm 3\%$ to $95 \pm 2\%$ live cells over a 72 h period (Figure 5.16). In contrast, no change was observed for PEG/HA ($92 \pm 2\%$ / $88 \pm 3\%$ live cells). Interestingly, the MSCs embedded in the PEG/Alginate hydrogels appeared to aggregate and form clusters, which highlights that in this environment cells are able to

move and interact with each other over time, resulting in a superior material in comparison to the PEG control system. Indeed, by applying a simple and straightforward approach, the blended PEG/Alginate thiol-yne IPNs with enhanced features act as a suitable scaffold for biomedical applications.

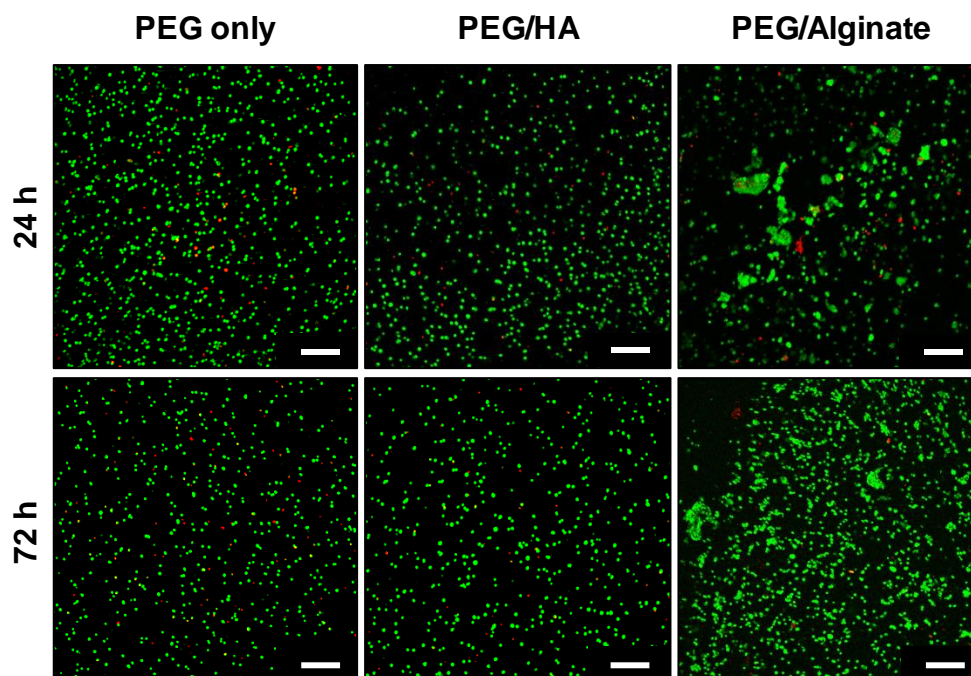


Figure 5.16. Cytocompatibility of PEG only, PEG/HA, and PEG/alginate hydrogels. Representative images of 3D encapsulated cells after 24 and 72 hours of incubation. Scale bar 200 μm .

5.3. Conclusions

The excellent features displayed by the addition of a secondary network to the thiol-yne robust networks has demonstrated a simple but effective way to improve the properties of covalent synthetic hydrogel systems. It has highlighted how two systems can work together to produce an advantageous material which possesses the beneficial properties of both systems whilst overcoming the drawbacks of both networks. The addition of alginate chains, crosslinked with calcium ions, has rendered superior hydrogels, not only stretchable and with enhanced tensile performance, but also with self-healing capabilities. Most importantly, in comparison to the PEG only system, PEG/Alginate hydrogels exhibit much higher cell viability, resulting in ideal matrices for cell growth and proliferation. This strategy, which is based on exploiting the features of a range of commercially available starting materials, still allows hydrogels to be prepared under biological relevant conditions without the need for further purification, and thus can be easily translated to a commercial setting where biomaterials that mimic the ECM are needed.

5.4. References

1. E. Caló and V. V. Khutoryanskiy, *Eur. Polym. J.*, 2015, **65**, 252-267.
2. K. Y. Lee and D. J. Mooney, *Prog. Polym. Sci.*, 2012, **37**, 106-126.
3. A. Bin Imran, K. Esaki, H. Gotoh, T. Seki, K. Ito, Y. Sakai and Y. Takeoka, *Nat. Commun.*, 2014, **5**, 5124.
4. S. Mitragotri, P. A. Burke and R. Langer, *Nat Rev Drug Discov*, 2014, **13**, 655-672.
5. Y. Lu, A. A. Aimetti, R. Langer and Z. Gu, *Nat. Rev. Mater.*, 2016, **2**, 16075.
6. B. V. Slaughter, S. S. Khurshid, O. Z. Fisher, A. Khademhosseini and N. A. Peppas, *Adv. Mater.*, 2009, **21**, 3307-3329.
7. M. E. Smithmyer, L. A. Sawicki and A. M. Kloxin, *Biomater. Sci.*, 2014, **2**, 634-650.
8. A. M. Rosales and K. S. Anseth, *Nat. Rev. Mater.*, 2016, **1**, 15012.
9. C. W. Peak, J. J. Wilker and G. Schmidt, *Colloid. Polym. Sci.*, 2013, **291**, 2031-2047.
10. Z. Gong, G. Zhang, X. Zeng, J. Li, G. Li, W. Huang, R. Sun and C. Wong, *ACS Appl. Mater. Interfaces*, 2016, **8**, 24030-24037.
11. F. Yu, X. Cao, J. Du, G. Wang and X. Chen, *ACS Appl. Mater. Interfaces*, 2015, **7**, 24023-24031.
12. D. L. Taylor and M. in het Panhuis, *Adv. Mater.*, 2016, **28**, 9060-9093.

13. V. K. Thakur and M. R. Kessler, *Polymer*, 2015, **69**, 369-383.
14. D. G. Bekas, K. Tsirka, D. Baltzis and A. S. Paipetis, *Composites, Part B*, 2016, **87**, 92-119.
15. S. K. Ghosh, *Self-healing Materials: Fundamentals, Design Strategies, and Applications*, Wiley, 2009.
16. R. J. Wojtecki, M. A. Meador and S. J. Rowan, *Nat. Mater.*, 2010, **10**, 14.
17. J. Kim and R. C. Hayward, *Trends Biotechnol.*, 2012, **30**, 426-439.
18. E. A. Appel, J. del Barrio, X. J. Loh and O. A. Scherman, *Chem. Soc. Rev.*, 2012, **41**, 6195-6214.
19. M. Zhang, D. Xu, X. Yan, J. Chen, S. Dong, B. Zheng and F. Huang, *Angew. Chem.*, 2012, **124**, 7117-7121.
20. J. Cui and A. d. Campo, *Chem. Commun.*, 2012, **48**, 9302-9304.
21. A. Phadke, C. Zhang, B. Arman, C.-C. Hsu, R. A. Mashelkar, A. K. Lele, M. J. Tauber, G. Arya and S. Varghese, *Proc. Natl. Acad. Sci. USA*, 2012, **109**, 4383-4388.
22. T. Bai, S. Liu, F. Sun, A. Sinclair, L. Zhang, Q. Shao and S. Jiang, *Biomaterials*, 2014, **35**, 3926-3933.
23. F. Luo, T. L. Sun, T. Nakajima, T. Kurokawa, Y. Zhao, K. Sato, A. B. Ihsan, X. Li, H. Guo and J. P. Gong, *Adv. Mater.*, 2015, **27**, 2722-2727.

24. E. A. Appel, M. W. Tibbitt, J. M. Greer, O. S. Fenton, K. Kreuels, D. G. Anderson and R. Langer, *ACS Macro Lett.*, 2015, **4**, 848-852.
25. N. Annabi, A. Tamayol, J. A. Uquillas, M. Akbari, L. E. Bertassoni, C. Cha, G. Camci-Unal, M. R. Dokmeci, N. A. Peppas and A. Khademhosseini, *Adv. Mater.*, 2014, **26**, 85-124.
26. Y. Li, J. Rodrigues and H. Tomas, *Chem. Soc. Rev.*, 2012, **41**, 2193-2221.
27. W. Zhao, X. Jin, Y. Cong, Y. Liu and J. Fu, *J. Chem. Technol. Biotechnol.*, 2013, **88**, 327-339.
28. T. Coviello, P. Matricardi, C. Marianecci and F. Alhaique, *J. Control. Release*, 2007, **119**, 5-24.
29. R. DeVolder and H.-J. Kong, *Wiley Interdiscip. Rev. Syst. Biol. Med.*, 2012, **4**, 351-365.
30. S. J. Bidarra, C. C. Barrias and P. L. Granja, *Acta Biomater.*, 2014, **10**, 1646-1662.
31. K. Y. Lee and D. J. Mooney, *Chem. Rev.*, 2001, **101**, 1869-1879.
32. Y. Wen and J. K. Oh, *Macromol. Rapid Commun.*, 2014, **35**, 1819-1832.
33. N. A. Peppas, J. Z. Hilt, A. Khademhosseini and R. Langer, *Adv. Mater.*, 2006, **18**, 1345-1360.
34. G. Deng, F. Li, H. Yu, F. Liu, C. Liu, W. Sun, H. Jiang and Y. Chen, *ACS Macro Lett.*, 2012, **1**, 275-279.

35. K. Ito, *Polym. J.*, 2007, **39**, 489.
36. M. C. Darnell, J.-Y. Sun, M. Mehta, C. Johnson, P. R. Arany, Z. Suo and D. J. Mooney, *Biomaterials*, 2013, **34**, 8042-8048.
37. L. J. Macdougall, V. X. Truong and A. P. Dove, *ACS Macro Lett.*, 2017, **6**, 93-97.
38. T. Yang, M. Malkoch and A. Hult, *J. Polym. Sci., Part A: Polym. Chem.*, 2013, **51**, 363-371.
39. J. Cui, M. A. Lackey, A. E. Madkour, E. M. Saffer, D. M. Griffin, S. R. Bhatia, A. J. Crosby and G. N. Tew, *Biomacromolecules*, 2012, **13**, 584-588.
40. I. Levental, P. C. Georges and P. A. Janmey, *Soft Matter*, 2007, **3**, 299-306.
41. P. Calvert, *Adv. Mater.*, 2009, **21**, 743-756.
42. A. B. W. Brochu, S. L. Craig and W. M. Reichert, *J. Biomed. Mater. Res., Part A*, 2011, **96A**, 492-506.
43. A. Pérez-San Vicente, M. Peroglio, M. Ernst, P. Casuso, I. Loinaz, H.-J. Grande, M. Alini, D. Eglin and D. Dupin, *Biomacromolecules*, 2017, **18**, 2360-2370.
44. F. R. Kersey, D. M. Loveless and S. L. Craig, *J. R. Soc., Interface*, 2007, **4**, 373-380.
45. L. J. Macdougall, M. M. Pérez-Madrigal, M. C. Arno and A. P. Dove, *Biomacromolecules*, 2017, **19**, 1378-1388.

Chapter 6.

Design of Synthetic Extracellular Matrices for Probing Breast Cancer Cell Growth Using Robust Cytocompatible Nucleophilic Thiol-yne Addition Chemistry

6.1. Introduction

Three-dimensional (3D) culture systems are of continued and growing interest for studies in tissue engineering and disease.¹⁻⁴ In particular, seminal works have demonstrated the relevance of 3D culture *in vitro* studies of breast cancer, to recapture *in vivo* breast cancer phenotypes and the importance of extracellular matrix (ECM) signalling in cancerous cell growth and metastasis.⁵⁻⁹ Traditionally, such 3D culture studies often have utilised protein matrices harvested from tissues, such as basement membrane extract¹⁰ and collagen I.^{11, 12} However, owing to the complex nature of cancer progression and many other diseases, design and deployment of well-defined synthetic mimics of the ECM provides opportunities for hypothesis testing about the effects of specific microenvironment cues, as well as systems for the screening of drug candidates, without the batch-to-batch variation of harvested materials.¹³⁻¹⁸ Synthetic biomaterials, such as hydrogels, have proven to be useful tools for mimicking key aspects of the mechanical and biochemical properties of the ECM in a variety of cell culture applications.¹⁹⁻²⁴ In recent years, there has been heightened interest in synthetic poly(ethyl glycol) (PEG) hydrogel based ECM mimics as a consequence of their controlled mechanical properties and ability to include a wide range of biochemical cues.²⁵ Furthermore, seminal studies have demonstrated how matrix degradability and integrin-binding can be key properties for many cellular processes, from cell adhesion and proliferation to motility and differentiation,^{18, 26-28} where a variety of chemistries with varied degrees of cytocompatibility and property control have been used. These studies highlight the opportunity that such well-defined materials provide for 3D cell culture and

the need for more robust and cytocompatible chemistries for the generation and modification of these systems in the presence of cells.

In the study of breast cancer, such well-defined materials have provided unique tools for multidimensional culture studies and insights into key cell-matrix interactions in different aspects of disease progression.^{25, 29, 30} These observations have confirmed that material properties are fundamental to furthering our understanding of breast cancer cell response to different microenvironments and the ability to fine tune the mechanical and biochemical properties of their culture environment.³¹⁻³⁶ Building upon these studies, opportunities remain in the establishment of new robust and accessible chemistries for the formation and modulation of matrix properties for the 3D culture of breast cancer cells and related niche cells. Of particular interest are chemistry based approaches for the formation of hydrogels in the presence of cells sensitive to chemical stimuli (*e.g.* free radicals or catalysts).³⁷⁻³⁹ The judicious choice of the crosslinking chemistry used for the formation of synthetic matrices is important for the facile encapsulation of a range of cell types and their culture over time.⁴⁰ Previous chapters have shown a complementary approach to the popular radical initiated thiol-ene chemistry by establishing the utility and versatility of nucleophilic thiol-yne addition chemistry for the encapsulation of cells within PEG hydrogels. In this chapter, the nucleophilic thiol-yne PEG hydrogels have been designed to undergo both programmed and cell-driven degradation, particularly for sensitive breast cancer cells. As previously described, the nucleophilic thiol-yne reaction allows the formation of robust cytocompatible hydrogel materials in an efficient manner without the need for an external catalyst (*e.g.* light or a metal catalyst), free radicals, or any external stimulus.⁴¹⁻⁴³ Herein, a nucleophilic thiol-yne PEG hydrogel platform has

been developed to mimic the mechanical properties of soft tissues, enabling the facile incorporation of bioactive peptides for promoting cell adhesion, while allowing fine-tuning of local and bulk network degradation. This work showcases the potential for thiol-yne PEG hydrogels to be used for the culture of breast cancer cells for probing cell-microenvironment through the encapsulation and 3D culture of a range of different breast cancer cell lines: MDA-MB-231, invasive triple negative breast cancer cells; T47D, estrogen receptor positive (ER+) breast cancer cells; and most notably MCF-7, ER+ breast cancer cells that are used extensively as a model ER+ breast cancer cell line.⁴⁴

6.2. Results and Discussion

6.2.1. Design of Nucleophilic Thiol-yne PEG Hydrogel-Based ECM Mimics

Click chemistries have shown great utility for the rapid formation of synthetic hydrogels for cell culture applications; yet, a need remains for material chemistries free of catalyst and initiator that allow the formation of well-defined synthetic mimics of the ECM using accessible precursors. Nucleophilic thiol-yne chemistry offers an opportunity to easily create a versatile cell culture platform that provides control of chemical and mechanical properties with reaction conditions relevant for the encapsulation of sensitive cells. Towards creating this cell culture platform for breast cancer cell culture, a range of PEG precursors with different architecture and molecular weights were functionalised with alkyne or thiol end groups (conversion >92%). As previously reported (Chapter 2 and 3),⁴⁵ 3-arm (1 kg mol^{-1}) PEG alkyne was synthesised using propiolic acid through a simple Fischer esterification process. Thiol-terminated PEG precursors were synthesised in a similar manner using 3-mercaptopropionic acid with 2- or 3-arm PEG precursors at 2 kg mol^{-1} , or 1 kg mol^{-1} respectively. Hydrogels were then formed at 10 wt% in either phosphate buffered saline (PBS) solution (pH 7.4) or Dulbecco's Modified Eagle Medium, (DMEM) in a 1:1 alkyne:thiol ratio. As a consequence of the highly efficient nature of the thiol-yne reaction, no further purification steps were needed, and the hydrogels were used as prepared. The same hydrogel nomenclature, used in Chapters 2 and 3, is expanded here to describe the different hydrogel systems and is dependent on the PEG precursors and peptide incorporation, each component is denoted considering the number of arms, molecular weight, and the incorporated functionality, **S** for thiol, **A** for alkyne or **P** for peptide. Hence, **3₁S** refers to the 3-arm thiol-terminated PEG precursor (1 kg mol^{-1}).

Hydrogels, formed using this chemistry, degrade by hydrolysis over time as a consequence of ester linkages used in the functionalisation of the PEG precursors. This degradation characteristics allows for cell proliferation over time, which is critical to long-term cell culture in 3D. However, if degradation occurs too rapidly, the structural support will not be maintained for the duration of the cell study. Previous chapters have shown the difference in degradation rates of the thiol-yne PEG hydrogels depending on the architecture of the PEG thiol precursors. High molecular weight 2-arm PEG thiol precursors caused the hydrogels to swell and degrade rapidly over a 3-day period. However, the nonswelling **31A31S** system was shown to rapidly form robust materials which are stable for over 30 days (Chapter 3), as a consequence of its dense crosslinked network which slows down its degradation profile in aqueous environments.⁴⁵ Yet its design lacked the incorporation of adhesion peptides, which are needed for prolonged cell culture of many adherent cell types as shown by the PEG-only system in Chapter 5. Incorporating short receptor-binding peptides inspired by the insoluble proteins present in the ECM allows the cells to interact with the network and can provide handles to maintain cell viability over long-term cell culture, promote cell proliferation, or mimic various extracellular environments.^{46, 47} In particular, the vitronectin/fibronectin mimetic adhesion sequence, RGDS (peptide sequence: Arg-Gly-Asp-Ser), has been incorporated into various synthetic matrices to impart biological activity and improve cell viability and has been shown to be relevant for promoting adhesion of breast cancer cells, including MCF-7s.^{46, 47} Therefore to improve the characteristics of the thiol-yne **31A31S** system, by inclusion of peptides, various hydrogels were synthesised, with differing alkyne:thiol end group ratios to allow for the peptide to covalently attached. As a result of the versatile

nature of the thiol-yne hydrogel system, gelation occurred even when the stoichiometry of the end groups (alkyne:thiol) deviated from 1:1 (the original system). In fact, robust hydrogel networks could be synthesised with fewer thiol end groups (20 mM less PEG thiol-functionality, Figure 6.1a), demonstrating the potential to incorporate high concentrations of bioactive functionalities into the network. The swelling profile of these hydrogels varied greatly as the alkyne:thiol ratio changed, with fewer thiol end groups, the network became less dense allowing more water to be drawn into the network, preventing the network from shrinking (<100% swelling factor (SF)). These systems all maintained their original (100% SF) over the 30-day period (Figure 6.1a). In addition, it was found that the swelling and degradation rate of the **3_{1A}3_{1S}** system could also be tuned through blending different ratios of the PEG thiol architectures (2- and 3-arm at 4 kg mol⁻¹ and 1 kg mol⁻¹ respectively). With a 50:50 ratio (2-arm:3-arm, **3_{1A}2_{4S}3_{1S}**) the hydrogel swelled to four times its original mass but maintained its structure for 15 days (Figure 6.1b) which is a remarkable improvement compared to the **3_{1A}2_{3S}** system which degraded after 3 days (Chapter 3). These swelling studies demonstrated the efficiency of the nucleophilic reaction which enabled the formation of robust structures in a tuneable way which could easily be adapted to different situations and environments.

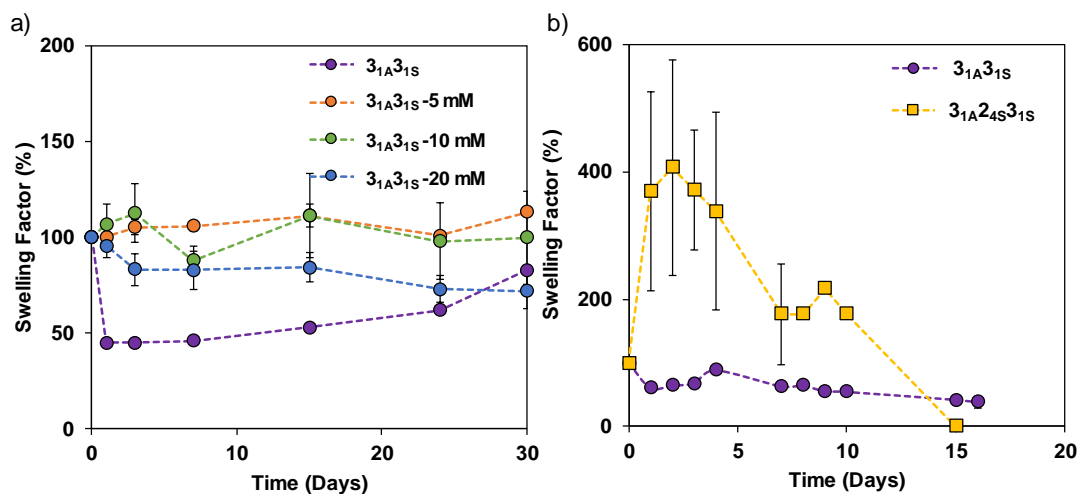


Figure 6.1. Swelling profiles of the thiol-yne PEG hydrogels, a) $3_{1A}3_{1S}$ system with reduced amounts of PEG thiol precursor (5 mM, 10 mM and 20 mM), b) $3_{1A}2_{4S}3_{1S}$ blended system. Repeated in triplicate, $SF(\%) = \frac{\text{Swollen mass}}{\text{Initial mass}} \times 100$.

For further testing, it was concluded that the stoichiometry of thiol-functional groups in the thiol-yne $3_{1A}3_{1S}$ system was reduced by 5 mM enabling available alkyne groups to react with the addition 5 mM of RGDS, while maintaining the 1:1 stoichiometric ratio of overall thiol and alkyne content within the system, $3_{1A}3_{1S}P_{RGDS}$. A thiol-functionalised pendant peptide sequence (CGRGDS) was easily incorporated into the network by covalently reacting it with available alkyne end groups within the network, in a similar manner to thiol-ene hydrogel matrices as demonstrated in the literature.⁴⁸ The inclusion of a pendant peptide increased the gelation time of the system, as the number of crosslinking sites were reduced because the RGDS did not contribute to the overall gel formation. Confirmation that the pendant RGDS was covalently incorporated in the network was carried out by monitoring the fluorescence of the hydrogels modified with a fluorescent RGDS ($3_{1A}3_{1S}P_{RGDS}$) and calculating the concentration of peptide present using a standard curve (Figure 6.2). The results demonstrated the successful incorporation of 1.8 mM peptide into the network upon the inclusion of 5 mM peptide at network

formation. This concentration is comparable to other systems incorporating bioactive peptides, in which cell attachment and interaction with the matrix was observed.⁴⁹ This further highlights the thiol-yne hydrogels ability to mimic aspects of the ECM through the facile inclusion of ECM-inspired adhesion peptides.

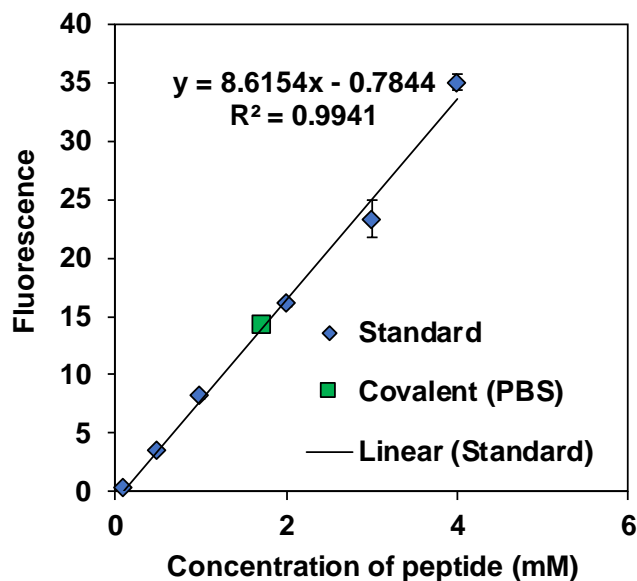


Figure 6.2. Fluorescence analysis of pendant peptide (RGDS) incorporation in the $3_{1A}3_{1S}P_{RGDS}$ hydrogel system.

To further imparted bioactivity, cells need to have space to grow and proliferate, which can be achieved in a number of ways (*e.g.* matrix degradation or stress relaxation) allowing encapsulated cells to remodel their surroundings; indeed, this remodelling process has been shown to be a key feature in the application of synthetic materials as 3D cell culture scaffolds, particularly to allow for proliferation over time.⁵⁰⁻⁵² Control over the degradability in these thiol-yne hydrogels can be obtained through various routes; 1) by incorporating a thermally-responsive segment,⁴⁵ 2) by modifying the PEG architecture (Chapter 3) and 3) through a simple blending process of different PEG thiol architectures as previously shown (Chapter 2). Optimisation reactions, utilising the blending route (3)

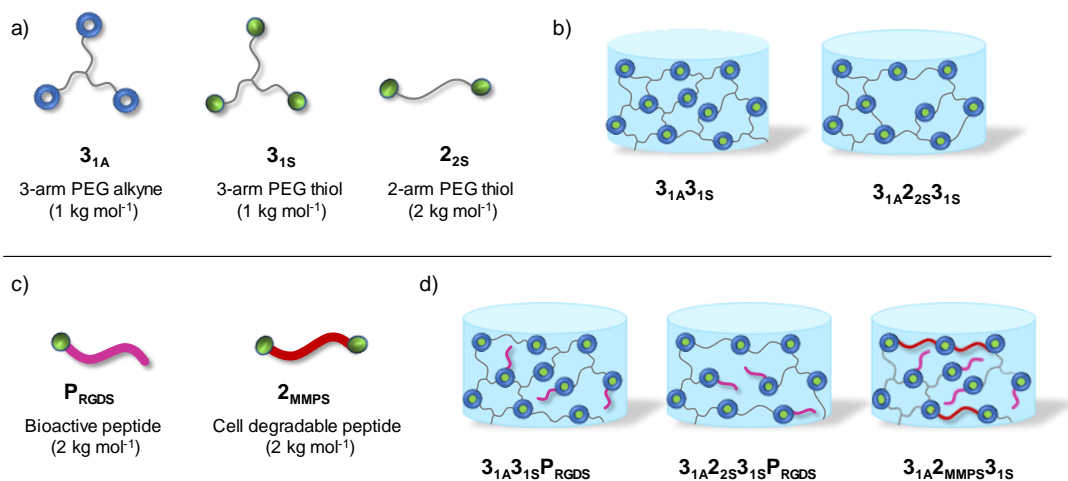
were carried out under cell culture conditions (*e.g.* in the presence of cells and in DMEM) to monitor the degradation of the blended hydrogels with time to understand the correct ratio of 2-arm:3-arm PEG thiol precursor (**2s:3s**), was required for sustained cell culture studies. A range of blended hydrogel systems were synthesised, and their degradation times monitored (Table 6.1). The blended systems with higher 3-arm PEG thiol contents resisted degradation for longer amounts of time but were also visual seen to swell. Lower contents of 3-arm PEG thiol reduced the crosslinking density of the system, which allowed water to infiltrate into the system causing the material to swell and degrade rapidly over the experimental time frame. Therefore, the blended systems, **3_{1A}2_{2s}3_{1s}** and **3_{1A}2_{2s}3_{1s}PRGDS** were synthesised for further testing, with the thiol functional groups mixed at a ratio of 10:90 **2s:3s**.

Table 6.1. Optimisation of the **3_{1A}2_{2s}3_{1s}** hydrogel system encapsulated with MDA-MB-231 cells for long term cell culture.

% 3 arm PEG thiol	% 2 arm PEG thiol	Day 3	Day 5	Day 6	Day 7
50	50	Degraded			
60	40	Degraded			
70	30	Slightly swollen	Degradation started	Degraded	
80	20	Slightly swollen	Degradation started	Degraded	
90	10	Original size	Slightly swollen	Slightly swollen	Swollen gels

3_{1A}2_{2s}3_{1s} hydrogels synthesised in serum free DMEM with the incorporation of 5 mM RGDS peptide. MDA-MB-231 cells encapsulated at a seeding density of 2,500 cells μL^{-1} . Hydrogels were visually inspected each day over a 7 day period.

Furthermore, to increase the ability of cells to interact with their synthetic environment and to increase degradability of the system, a 2-arm thiol-functionalised cell-degradable matrix metalloproteinase (MMP, GCRDVPMS↓MRGGDRCG) linker was incorporated into the network, (**3_{1A}2_{MMPS}3_{1S}**) which allows the network to be locally degraded by the cells. Similar to the above blended systems, the thiol-functional groups were mixed at a ratio of 10:90 **2_{MMPS}:3_{1S}**. For the **3_{1A}2_{MMPS}3_{1S}** system, the MMP linker was incorporated into the system by substituting the 2-arm PEG thiol precursor, as they have similar molecular weights (1.7 kg mol⁻¹ and 2 kg mol⁻¹ respectively). The **3_{1A}2_{MMPS}3_{1S}** system included 5 mM RGDS similar to the **3_{1A}3_{1S}PRGDS** and **3_{1A}2_{2S}3_{1S}PRGDS** systems to increase cell interaction with the synthetic matrix and promote cell viability. For clarity the addition of **PRGDS** has not been included in nomenclature for the **3_{1A}2_{MMPS}3_{1S}** system; however, RGDS has been incorporated throughout the testing of the **3_{1A}2_{MMPS}3_{1S}** system. Overall, five different thiol-yne hydrogel networks were synthesised (**3_{1A}3_{1S}**, **3_{1A}3_{1S}PRGDS**, **3_{1A}2_{2S}3_{1S}**, **3_{1A}2_{2S}3_{1S}PRGDS** and **3_{1A}2_{MMPS}3_{1S}**), with the aim of creating synthetic extracellular matrices incorporating different peptide motifs and tuning their degradation profiles (Scheme 6.1).



Scheme 6.1. Hydrogel formation: (a) Alkyne- and thiol-functionalised PEG architecture, (b) Hydrogel networks formed by thiol-yne chemistry at 10 wt%. Thiol and alkyne end group react upon mixing under basic conditions. Alkyne:Thiol ratio = 1:1 $3_{1A}3_{1S}$ = 3-arm PEG alkyne (3_{1A}) reacted with 3-arm PEG thiol (3_{1S}), $3_{1A}2_{2S}3_{1S}$ = 3_{1A} reacted with a mixture of 3_{1S} and 2-arm PEG thiol (2_{2S}) in a ratio of 10:90, to increase the rate of hydrogel degradation, (c) Thiol-functional bioactive peptide (P_{RGDS}) and 2-arm thiol-functional cell degradable peptide (2_{MMPS}), incorporated into the hydrogel network to enable cell adhesion and some cell-driven remodelling increase ECM characteristics, (d) Hydrogel network formation with bioactive peptides at 10 wt%. 2_{MMPS} replaced 2_{2S} in $3_{1A}2_{MMPS}3_{1S}$. Note that all $3_{1A}2_{MMPS}3_{1S}$ hydrogels also contain bioactive pendant peptide, however P_{RGDS} is not incorporated into the nomenclature.

6.2.2. Characterisation of Thiol-yne PEG Hydrogels as ECM Mimics

6.2.2.1. Swelling Kinetics of the Thiol-yne PEG Hydrogels

Initial characterisation of various network compositions was carried out through gelation time (*via* the vial tilt method) and swelling kinetic profile characterisation. All the hydrogels formed within 5 min in PBS solution; however, in DMEM, a more appropriate media for culturing cells, the networks formed much faster (less than 1 min). The increase in gelation time could be a result of the components in the DMEM which could act as a base and catalyse the reaction. The pH of the DMEM could have also increased slightly when the precursors were dissolved in DMEM compared to PBS solution. This would promote the formation of the thiolate ion which could then attack

the alkyne increasing the rate of the reaction and therefore the gelation time. As previously demonstrated, when formed in PBS solution, the **3_{1A}3_{1S}** system shrinks initially and then maintains a steady state for over 30 days, however when the network was formed with 5 mM less thiol end groups the material maintained its original size (Figure 6.1a). With the addition of RGDS to the **3_{1A}3_{1S}-5mM** system (**3_{1A}3_{1S}PRGDS**) an intermediate swelling profile was obtained, demonstrating the influence the peptide had on the swelling profile of the network and its resistant to degradation, with a robust structure maintained over 30 days (Figure 6.3a). It was important to monitor the hydrogel's swelling behaviour in realistic conditions for cell culture experiments, thus a swelling experiment was conducted in serum-free medium in the presence of cells (MDA-MB-231) and the gelation time and swelling profiles of the **3_{1A}3_{1S}PRGDS**, **3_{1A}2_{2S}3_{1S}PRGDS** and **3_{1A}2_{MMPS}3_{1S}** systems were monitored (Figure 6.3b). The gelation time for these system, increased to several minutes in the presence of cells, which could have been a result of the cells reducing the functional end group mobility and therefore increasing gelation time. However, this proved advantageous for this system, increasing the very rapid gelation time, allowing for the successful encapsulation of cells throughout the sample. The initial shrinkage of **3_{1A}3_{1S}PRGDS** was reduced compared to the original **3_{1A}3_{1S}** system, which was further observed in the blended system when a 2-arm thiol was also incorporated, **3_{1A}2_{2S}3_{1S}PRGDS** and in agreement with the previous study (Figure 6.1b). The networks start to swell and degrade rapidly which again is a result of the presence of cells during the crosslinking reaction, disrupting the efficiency of the reaction, reducing the crosslinking density in the network. This in turn allowed more water to infiltrate into the system and increased the rate of ester hydrolysis of the functional end groups, causing the hydrogels to degrade

more rapidly (7 days compared to 30 days). Nevertheless, the increase in swelling over the course of the 3D cell culture gives rise to less dense pore structures, potentially allowing for additional cell proliferation at later time points.

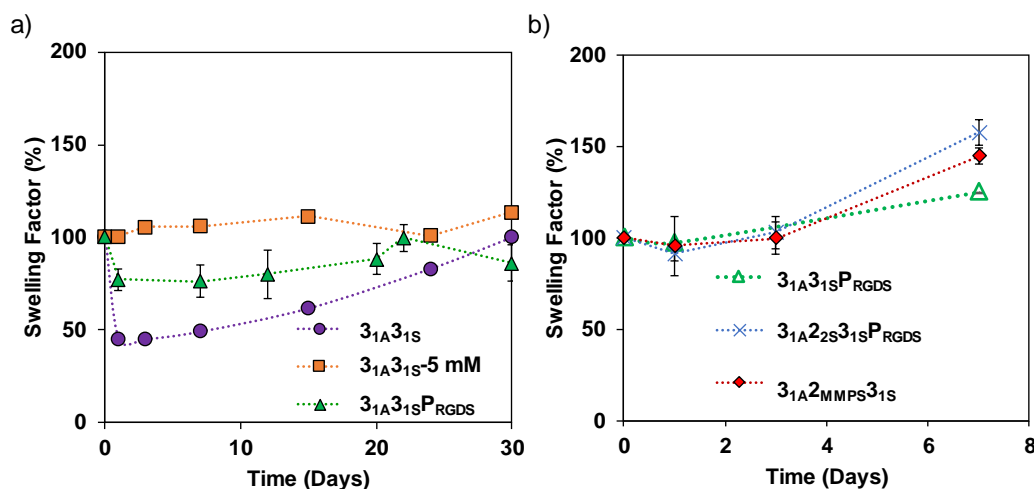


Figure 6.3. (a) Swelling characteristics of the thiol-yne hydrogels synthesised in PBS; Comparison of $3_{1A}3_{1S}$ (circle) (1:1 alkyne:thiol end groups), $3_{1A}3_{1S}$ -5mM with reduced amount of 3_{1S} (-5 mM) (square), and $3_{1A}3_{1S}PRGDS$ (triangle). (b) Comparison of the swelling characteristics of the thiol-yne hydrogels made in serum-free DMEM with the encapsulation of MCF-7 cells over 1 week; $3_{1A}3_{1S}PRGDS$ (open triangle), $3_{1A}2_{2S}3_{1S}PRGDS$ (cross), $3_{1A}2MMP3_{1S}$, 10:90 ratio of $2MMP:3_{1S}$ (diamond).

6.2.2.2. Mechanical Properties of the Thiol-yne PEG Hydrogels

Characterisation of hydrogel stiffness was carried out through rheological and compression experiments, to understand the hydrogel's mechanical properties for the development of ECM mimics. The thiol-yne hydrogels were synthesised in serum-free media to capture a more accurate representation of the hydrogel's mechanical properties. Rheological testing revealed this series of thiol-yne systems created environments with a range of storage moduli (G'), with values ranging from $G' = 10 \pm 1.3$ kPa for the original $3_{1A}3_{1S}$ system to $G' = 4 \pm 0.1$ kPa for the $3_{1A}2_{2S}3_{1S}PRGDS$ system (Figure 6.4a and b, Table 6.2). As previously mentioned gelation time increased when the hydrogels were made in

DMEM which resulted in an increase in G' from 6.7 ± 0.1 kPa for **3_{1A}3_{1S}** (synthesised in PBS solution, Chapter 3) to 10 ± 1.3 kPa for the same system synthesised in DMEM. This was a consequence of the rapid gelation time (*i.e.* 26 ± 3 s in PBS solution to <5 s in DMEM) causing functional groups to react quickly with other groups in close proximity increasing the probability of loops and entanglement formation, creating stiffer hydrogels.^{53,54} Only the **3_{1A}2_{2S}3_{1S}PRGDS** system was significantly different ($p < 0.05$) from the original **3_{1A}3_{1S}** system, as a result of the incorporation of the 2-arm PEG thiol precursor in addition to the pendant peptide incorporation (Figure 6.4a). The stiffness of the materials decreased as the crosslinking density decrease as a result of the hydrogels forming off stoichiometry reducing the number of crosslinked sites, reducing the rigidity of the hydrogel and therefore reducing G' . Furthermore, through the addition of a pendant hydrophilic peptide to the network more water is drawn into the system swelling the network, making a softer gel and as a result G' decreases. Rheological testing further confirmed the rapid gelation time of these systems in DMEM, by the rapid crossover of G' and G'' with time demonstrating the production of stable hydrogels in less than 5 min (Figure 6.4c). All the hydrogels displayed high resistance to strain, with the internal structure only breaking down at high strain values above 100% (Figure 6.4d), a similar profile to the results in Chapter 3, Figure 3.6. This demonstrates that the addition of a pendant peptide or 2-arm PEG thiol precursor had not affected the hydrogel's ability to withstand external pressures and therefore is a robust material for ECM mimics.

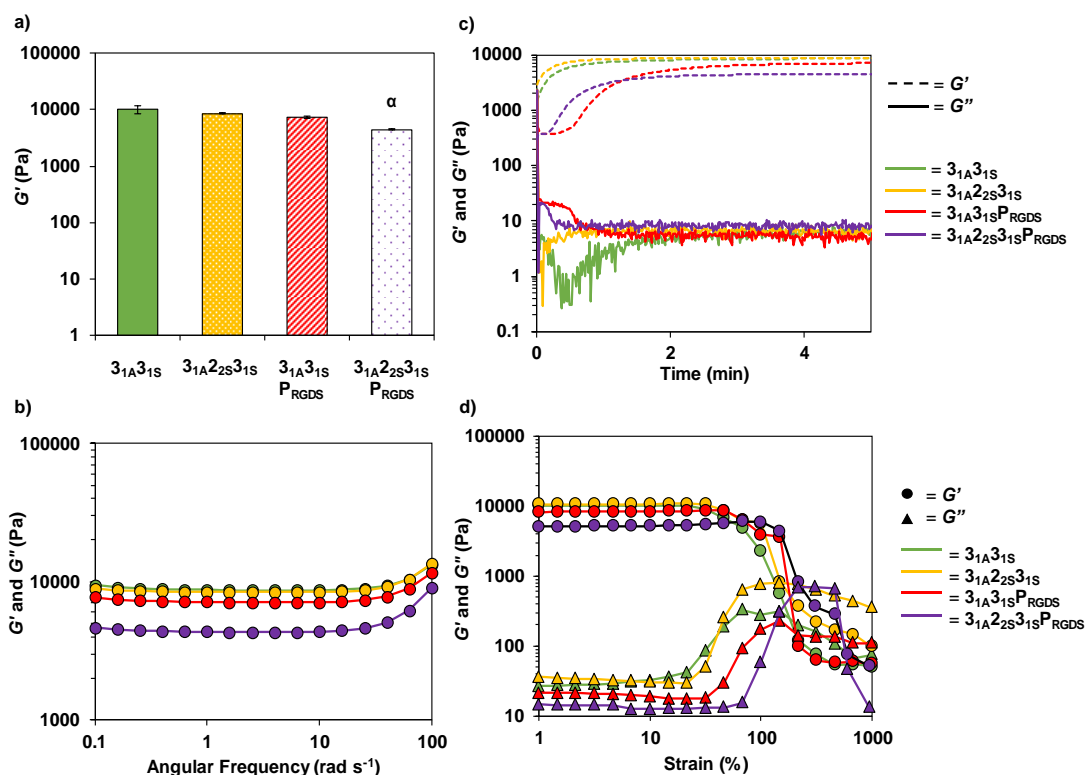


Figure 6.4. Representative rheological data for the thiol-yne hydrogels synthesised in DMEM and repeated in triplicate; a) Average G' at a constant frequency of 10 rad s^{-1} and 0.5% strain, α = Significantly different from $3_{1A}3_{1S}$ conditions, $p < 0.05$. b) Frequency sweep at a constant strain of 0.5% , c) Evolution of G' and G'' with time, d) Amplitude sweep at a constant frequency of 10 rad s^{-1} .

However, the compressive strength of these materials is not affected by the change in stoichiometry of the end groups or by the addition of RGDS to the network (no significant difference $p < 0.05$) demonstrating the robust nature of nucleophilic thiol-yne addition to form hydrogels (Figure 6.5a and Table 6.2). In addition, the Young's moduli (E), calculated from $E = 2G(1 + \nu)$ where $G = \sqrt{G'^2 + G''^2}$ and $\nu = 0.5$ (Poisson's ratio),^{55, 56} was calculated to allow for direct comparisons to be drawn between these materials and the elastic properties of different biological environments. For these materials E ranged from $30.9 \pm 0.4 \text{ kPa}$ for $3_{1A}3_{1S}$ to $13.4 \pm 0.04 \text{ kPa}$ for $3_{1A}2_{2S}3_{1S}P_{RGDS}$, (Figure 6.5b and Table 6.2) mimicking the moduli of a range of soft tissues including

different stages of breast cancer progression (e.g. low to high grade infiltrating ductal carcinoma).⁵⁷ In correlation with the rheological data (Figure 6.4), the only significantly difference in Young's modulus was for the $3_{1A}2_{2S}3_{1S}P_{RGDS}$ system as a result of the 2-arm thiol PEG precursor and the incorporation of RGDS decreasing the number of crosslinked sites in the network and therefore decreasing the modulus of the ECM scaffold.

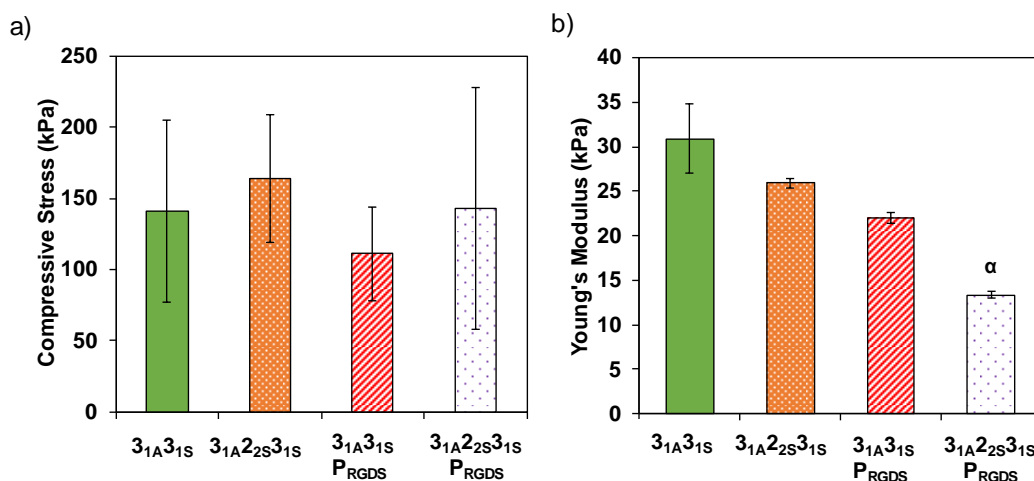


Figure 6.5. Mechanical data for the thiol-yne hydrogels synthesised in DMEM, (a) Average compression stress, 400 μ L sample size, cylindrical shape with a diameter of 9 mm and length of 4 mm. Samples cured for 1 h before testing, load cell= 50 N, data not statically different, (b) Average Young's Modulus (E) calculated from $E = 2G(1 + \nu)$ where $G = \sqrt{G'^2 + G''^2}$ and $\nu = 0.5$ (Poisson's ratio),⁵³,⁵⁴ α = Significantly different from $3_{1A}3_{1S}$ conditions, $p < 0.05$.

Table 6.2. Gelation time and mechanical properties of the thiol-yne PEG hydrogels synthesised in DMEM

Hydrogel	Gelation Time ^a (s)	G' (kPa) ^b	G'' (Pa) ^b	E (kPa) ^c	Compressive Stress (%) ^d
$3_{1A}3_{1S}$	<5	10.3 ± 1.3	10 ± 2.5	30.9 ± 3.9	141 ± 64
$3_{1A}3_{1S}P_{RGDS}$	<10	7.4 ± 0.2	17 ± 5.0	25.9 ± 0.5	164 ± 45
$3_{1A}2_{2S}3_{1S}$	15	8.6 ± 0.2	14 ± 3.4	22.0 ± 0.6	111 ± 33
$3_{1A}2_{2S}3_{1S}P_{RGDS}$	20	4.5 ± 0.1	12 ± 0.2	13.4 ± 0.04	143 ± 85

^aGelation time recorded via the vial tilt method. ^bAverage G' and G'' moduli were calculated from the frequency sweep experiments at 10 rad s^{-1} and 0.5 % strain. ^cYoung's Moduli (E) were calculated from the average rheological G' and G'' values using the equation: $E = 2G(1 + \nu)$ and $G = \sqrt{G'^2 + G''^2}$, where E = Young's Modulus, $\nu = 0.5$ (Poisson's ratio for hydrogel materials), G = shear modulus, G' = shear storage modulus and G'' = shear loss modulus.^{53, 54} ^dAverage strain from 10 samples.

6.2.3. 2D Cell Culture of Breast Cancer Cells in Hydrogel Formation-Mimetic Conditions

The use of cytocompatible chemistry is essential for the formation of 3D culture platforms that encapsulate cells within the network. As previous work has shown (Chapters 3 and 5),⁴⁵ the nucleophilic thiol-yne addition is cytocompatible with a range of cell lines, highlighting the ideal characteristics it possess as a crosslinking reaction for cell culture platforms.^{41, 42, 58} In addition, the lack of catalysts and free radicals during gel formation make it a potentially useful tool for encapsulation of sensitive cell lines. As an initial evaluation of the suitability of this chemistry for probing breast cancer cell growth, three different breast cancer cell lines were investigated: MDA-MB-231, a highly invasive, ER- breast cancer cell line; T47D, a ER+ breast cancer cell line; and MCF-7, an ER+ non-invasive tumorigenic mammary breast cancer cell line. Non-gel forming thiol-yne reaction conditions (2-dimensional, (2D)) were incubated with plated cells (96 well

plate, seeding density = 15,000 cells cm^{-2}) for each breast cancer cell line with the commonly used radically-initiated thiol-ene reaction as a comparison (Figure 6.6). For the 2D thiol-yne reaction, 3-arm PEG alkyne precursor was reacted with cysteine, a small molecule thiol, in a 1:1 alkyne:thiol ratio, using the same concentrations used to synthesise a 10 wt% hydrogel. The 2D thiol-yne precursors (PEG alkyne and cysteine) were also assessed using the concentrations of functional groups used in gel formation. These conditions and the media and PBS control conditions were incubated with the cells at 37 °C for 15 min before being removed and replaced with fresh media. For comparison, the 2D radically-initiated thiol-ene reaction utilised a 10 wt% PBS solution of PEG_{3.4k}(SH)₂ with 2-arm allyl functionalised peptide. Lithium acylphosphinate (LAP) was added as a photoinitiator and the solution was added to wells, the plates were exposed to long wavelength UV light (365 nm, 10 mW cm^{-2}) for 1 min, then the reaction condition was removed and replaced with fresh media. For 2D cell culture, cell metabolic activity was assessed using the CellTiter 96 assay, a colorimetric assay which includes a tetrazolium compound and an electron coupling reagent, phenazine ethosulfate. Metabolic activity appeared high for all conditions with the exception of the PEG alkyne condition, which showed dramatically low metabolic activity across all cell lines (Figure 6.6).

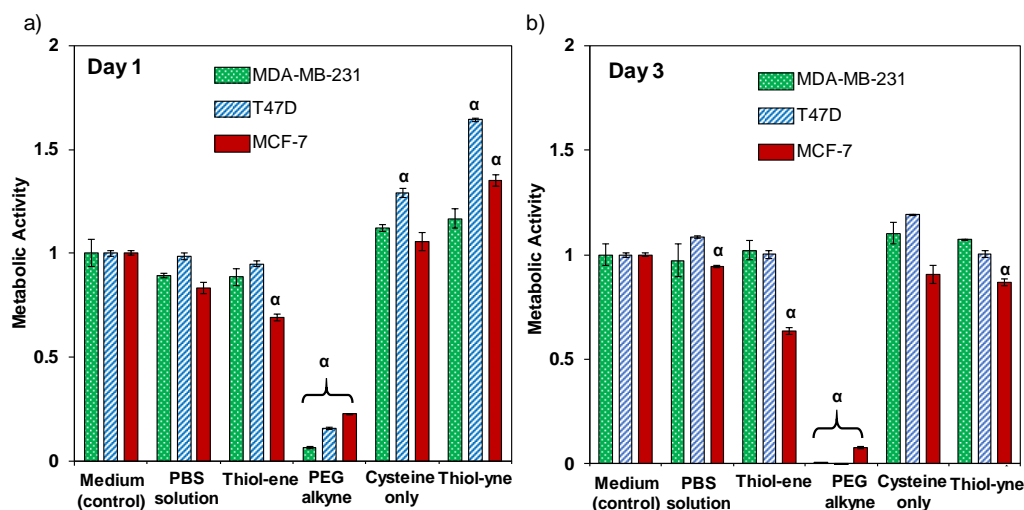


Figure 6.6. Metabolic activity of breast cancer cells in 2D hydrogel formation-mimetic environments; a) Day 1, b) Day 3. α = Significantly different from control conditions, $p < 0.05$.

This result highlighted a key characteristic of the ester-linked thiol-yne precursors. If the PEG alkyne precursor is presented to the cells in the absence of free thiols, thus preventing the thiol-yne reaction from occurring, the precursor is toxic. It was hypothesised that this was a consequence of ester hydrolysis, which cleaves the ester bond very rapidly releasing propionic acid which is very toxic, (*i.e.* $LD_{50} = 100 \text{ mg kg}^{-1}$ in rats) to the cells. To prove this hypothesis, MCF-7 cells were incubated with commercially available propionic acid (concentration kept consistent with conditions used in a 10 wt% PEG hydrogel formation). The metabolic activity of the MCF-7 cells were compared to the media and PBS only controls using the CellTiter96 assay (Figure 6.7). The results show very low metabolic activity for the propionic acid condition indicating the high toxicity of propionic acid in comparison to media and PBS alone. This highlights the cause of toxicity in the ester PEG alkyne precursor is the release of propionic acid. In comparison, the metabolic activity is recovered in the thiol-yne condition, in which a stoichiometric amount of cysteine is presented to react with the available alkynes of the

3-arm PEG alkyne. The crosslinking product of the thiol-yne reaction, the vinyl thioether, has increased stability to ester hydrolysis, and as a result does not negatively influence cell proliferation.

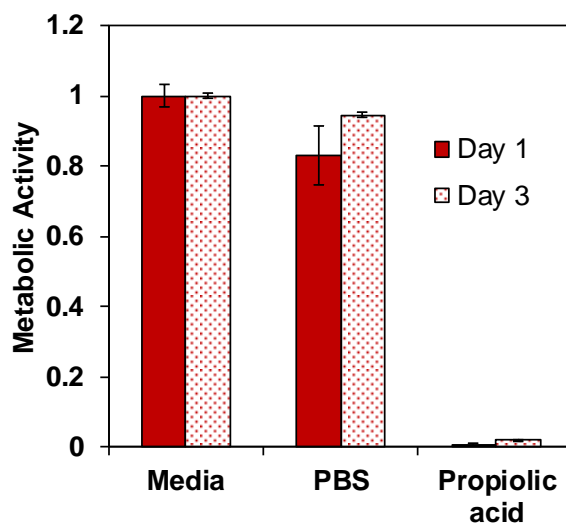


Figure 6.7. Metabolic activity of MCF-7 cells incubated with propiolic acid in 2D compared to media and PBS. After 24 h of culture, cells were exposed to each condition for 15 min. Metabolic assay was assessed by Cell-Titer 96 assay (Absorbance = 490 nm).

There was a less dramatic, yet significant, reduction in metabolic activity of MCF-7 cells for the thiol-yne treatment, for which the MDA-MB-231 and T47D cell lines showed no reduction in metabolic activity (Figure 6.6). This result suggested a sensitivity of MCF-7 cells to reaction conditions which utilise photoinitiated free radicals during the crosslinking reaction. By day 3, the MCF-7 cells also show a metabolic activity that is statistically different ($p < 0.05$) from the growth medium control for the thiol-yne hydrogel mimetic treatment, yet the metabolic activity remains high in comparison to the photoinitiated thiol-yne reaction condition mimic (86.7% and 63.5% respectively), suggesting that the thiol-yne reaction conditions may be more suitable for the encapsulation of MCF-7 cells. These initial 2D results highlighted a potential benefit of using the nucleophilic thiol-yne addition as an alternative to the commonly used radically-

initiated thiol-ene chemistry for hydrogel crosslinking in the presence of cell lines which are more sensitive to free radicals.

6.2.4. 3D Encapsulation of Breast Cancer Cells in Thiol-yne PEG Hydrogels

In vitro synthetic cell culture platforms provide well-controlled environments, which can be used to further understand the growth and behaviour of breast cancer cells. An advantage for the use of bulk hydrogel materials as 3D cell culture platforms, is the ability for cells to be easily distributed throughout the scaffold and therefore it is not necessary for cells to migrate into the material after scaffold synthesis. However, by forming the 3D culture environment in the presence of cells, it is essential for the crosslinking chemistry to be cytocompatible. Therefore, after initial cytocompatibility testing in 2D culture, the nucleophilic thiol-yne addition pathway was evaluated as a route to encapsulate breast cancer cells in 3D using alamarBlue assays and live/dead imaging. Preliminary encapsulation experiments were carried out in the **31A31S** hydrogels formed in PBS solution. This system allowed for the successful encapsulation of MDA-MB-231 and T47D cell lines at early time points (day 1 and day 3, Figure 6.8a and b), as shown by the high metabolic activity and cell viability. In contrast, the metabolic activity of MCF-7 cells in this system was low, and live/dead images show very small cell bodies suggesting unhealthy or dying cells (Figure 6.8c). It was hypothesised that these results were a result of the sensitivity of the MCF-7 cells to PBS solution for extended periods of time.

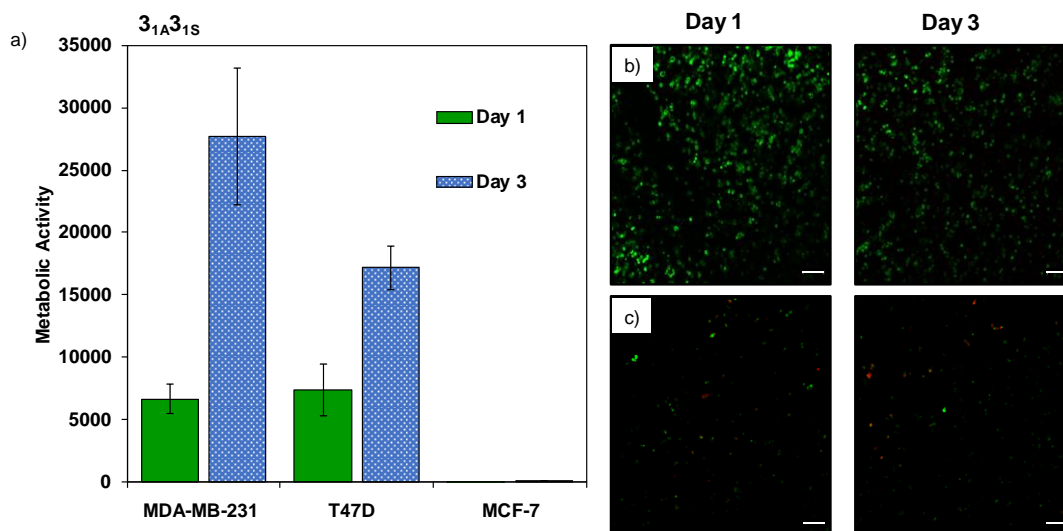
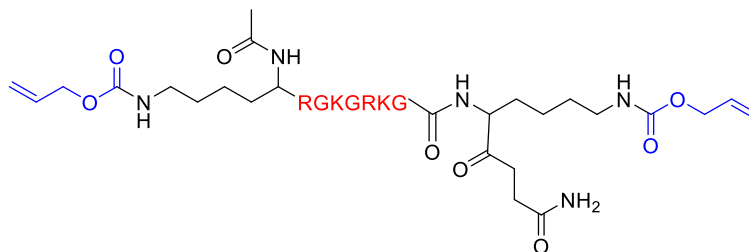


Figure 6.8. The metabolic activity of a) MDA-MB-231 and T47D (5,000 cells μL^{-1}), and MCF-7 cells, (2,500 cells μL^{-1}), encapsulated in the $3_{1A}3_{1S}$ (no RGDS) system formed in PBS solution (pH 7.4). Cell metabolic activity was assessed after 1 and 3 days of culture within the hydrogels by an alamarBlue assay, b) Live/Dead images of MDA-MB-231 cells encapsulated in $3_{1A}3_{1S}$ hydrogels (5,000 cells μL^{-1}), c) Live/Dead images of MCF-7 cells encapsulated in $3_{1A}3_{1S}$ hydrogels (2,500 cells μL^{-1}).

To test this hypothesis MCF-7 cells were encapsulated in $3_{1A}3_{1S}PRGDS$ hydrogels synthesised in serum-free DMEM (Figure 6.9). As previously observed, when these systems were synthesised in DMEM in the presence of cells the gelation time increased, allowing the solution to be pipetted into suitable moulds for future testing. To demonstrate the mild nature of the nucleophilic thiol-yne addition chemistry and to draw comparisons between different crosslinking chemistries, commonly used radically-initiated thiol-ene hydrogels were also synthesised in DMEM in the presence of MCF-7 cells. The thiol-ene PEG hydrogels were synthesised in DMEM using a 4-arm thiol-functionalised PEG precursor (20 kg mol^{-1}) reacted with stoichiometric amounts of 2-arm alloc-functionalised peptide crosslinker, (KK(alloc)GGPQIWGQGK(alloc)K), (Scheme 6.2) and 2 mM of alloc-functionalised fibronectin mimetic peptide (K(alloc)GWGRGDS) at 10 wt%.⁵⁹ In

addition, 2 mM of LAP initiator was added and the solution was exposed to 365 nm light (10 mW cm⁻²) for 1 min to allow for the polymerisation to occur.



2-arm alloc-functionalised Peptide

Scheme 6.2. Alkene functionalised 2-arm peptide used in the synthesis of thiol-ene hydrogels. Adapted from ref 59.

As the thiol-ene hydrogel systems portrays a very different swelling profile to the thiol-yne system (3.1 times more swelling), as a consequence of higher molecular weight precursors, two seeding densities were also investigated (2,500 cells μL^{-1} and 7,750 cells μL^{-1}) for the thiol-ene systems. The lower seeding density contained the same total number of cells as the thiol-yne condition, and the higher seeding density replicated the same cell density in the materials after swelling, to account for the potential effects of cell-cell interactions on cell proliferation. The thiol-ene chemistry led to significantly lower cell metabolic activity in comparison to the thiol-yne chemistry in all cases (Figure 6.9a). This is further confirmed through live/dead cell images, which showed small cells and punctate staining in the thiol-ene hydrogel system in comparison to the thiol-yne hydrogel system where the cells are much larger and uniformly brighter with few dead cells, (Figure 6.9 b and c). These results further support our initial results in 2D culture studies that suggested the sensitivity of MCF-7 cells for otherwise gentle photopolymerisation conditions, especially to the solution used to swell the matrix. This

experiment confirms the increased sensitivity MCF-7 have towards PBS solution and therefore all future hydrogels explored in this chapter were synthesised in DMEM. These results demonstrated the vast potential of the thiol-yne chemistry as a crosslinking reaction for the encapsulation of cell lines that have increased sensitivity towards the presence of free radicals. This hydrogel scaffold system provides a well-defined synthetic *in vitro* platform that enables the 3D encapsulation of MCF-7 cells, and potentially other sensitive cell lines, opening the door to future studies for better understanding of breast cancer progression and other processes in variety of tissue regeneration and disease applications.

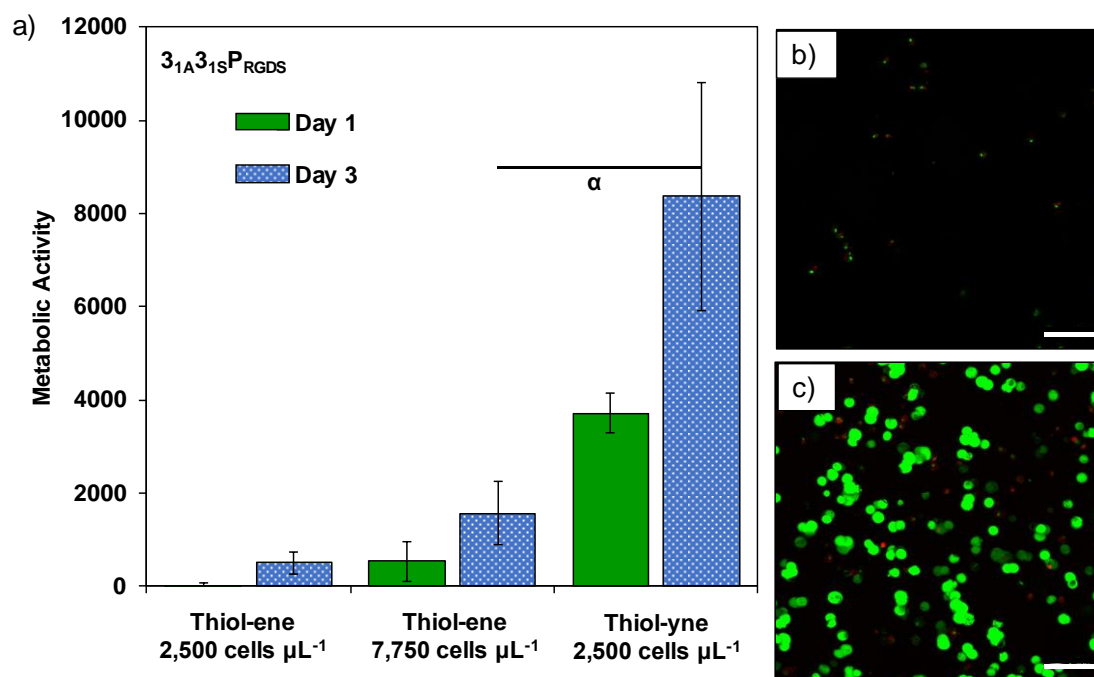


Figure 6.9. Encapsulation of MCF-7 cells in photo-initiated thiol-ene and thiol-yne ($3_{1A}3_{1S}P_{RGDS}$) hydrogels formed in serum-free medium. Cells were encapsulated in the thiol-ene gels at two different cell concentrations (2,500 and 7,750 cells μL^{-1}). a) MCF-7 cell metabolic activity was assessed after 1 and 3 days of culture within the hydrogels by an alamarBlue assay, b) Live/Dead images from Day 3 time point for the thiol-ene condition (7,750 cells μL^{-1}), c) Live/Dead images from Day 3 thiol-yne condition (2,500 cells μL^{-1}). Scale bar = 50 μm . α = data significantly different between thiol-ene and thiol-yne conditions on Day 3 $p < 0.05$.

6.2.5. MCF-7 Cell Proliferation in Degradable ECM Mimetic Thiol-yne PEG Hydrogels

Introduction of controlled network degradability is one route that can be incorporated into 3D cell culture platforms to allow cells to grow and proliferate within the structure over time. As previously stated, increased network degradability can be incorporated into the thiol-yne **31A31S** system through a blending technique by incorporating a 2-arm thiol-functionalised PEG (2 kg mol^{-1}) into the system, **31A22S31S**PRGDS. With the reduction of the 3-arm thiol precursor and the addition of the pendant adhesion peptide, the network becomes less stiff, as shown by the rheology data (decrease in G' from $10 \pm 1.3 \text{ kPa}$ to $4 \pm 0.1 \text{ kPa}$), which indicates that the structure is less dense, with increased pore size enabling the system to swell, which therefore should allow the cells to grow and proliferate. To test this phenomenon in the thiol-yne PEG hydrogels with the inclusions of peptides, longer term viability studies (10 days) were carried out with MCF-7 cells. The **31A31S**PRGDS, **31A22S31S**PRGDS and **31A2MMPS31S** system were synthesised in DMEM in the presence of MCF-7 cells (seeding density $2,500 \text{ cells } \mu\text{L}^{-1}$) and metabolic activity was assessed through alamarBlue assays and visually through live/dead imaging. The results confirmed, that over time as the systems swell and degrade, the MCF-7 cells are able to grow and proliferate indicated by the increase in metabolic activity at later time points (Figure 6.10). Confirmation was also obtained visually through live/dead images, where small MCF-7 cluster formation began at the day 3 time point and continued to day 10, in which large clusters of cells were present compared to the smaller clusters formed at the later time points in the **31A31S**PRGDS system (Figure 6.11 a and b).⁶⁰

⁶¹ Cluster formation is an expected morphology for epithelial MCF-7 cells.

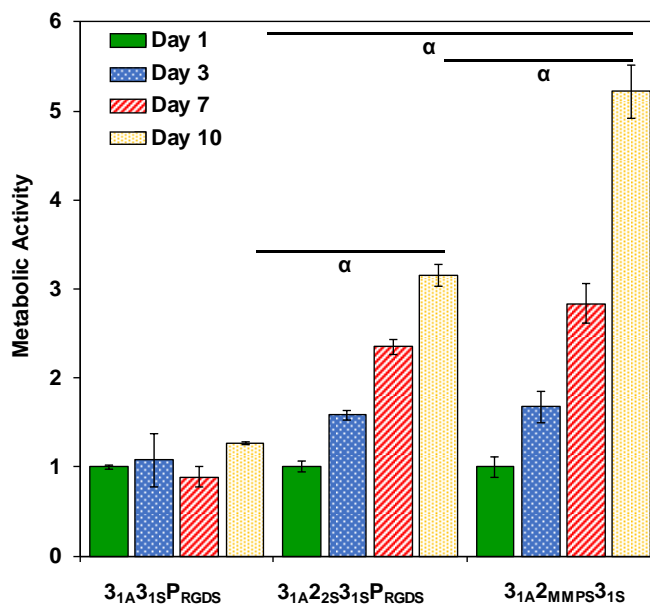


Figure 6.10. The metabolic activity of MCF-7 cells in 3D degradable thiol-yne hydrogels ($2,500 \text{ cells } \mu\text{L}^{-1}$) assessed through the alamarBlue assay at 1, 3, 7 and 10 days after encapsulation. α = Significantly different values for day 10 between all gelation conditions, $\rho < 0.05$. Within the $3_{1A}2_{2S}3_{1S}P_{RGDS}$ and $3_{1A}2_{MMPS}3_{1S}P_{RGDS}$ conditions, the metabolic activity at each day is statistically different ($\rho < 0.05$) from the previous time point. For the $3_{1A}3_{1S}P_{RGDS}$ condition, only the day 10 metabolic activity is statistically different ($\rho < 0.05$) from day 1.

This phenomenon was increased through the incorporation of a cell degradable linker, to the thiol-yne network, ($3_{1A}2_{MMPS}3_{1S}$). Incorporation of a MMP degradable peptide crosslinker imparts local degradability of the network by MMPs secreted by the cells. This system therefore has two methods of degradation: 1) ester hydrolysis from the ester bonds in the functionalised PEG precursor components that allows for bulk degradation of the hydrogel over time and 2) enzymatic hydrolysis of an MMP degradable crosslink that allows cells to locally degrade the network. In these materials, by day 10, the cell metabolic activity was greatly increased compared to the $3_{1A}2_{2S}3_{1S}P_{RGDS}$ system, (Figure 6.10) suggesting that the cells are degrading the matrix which leads to increased cell proliferation and the formation of cell clusters. Image analysis of cell cluster diameter

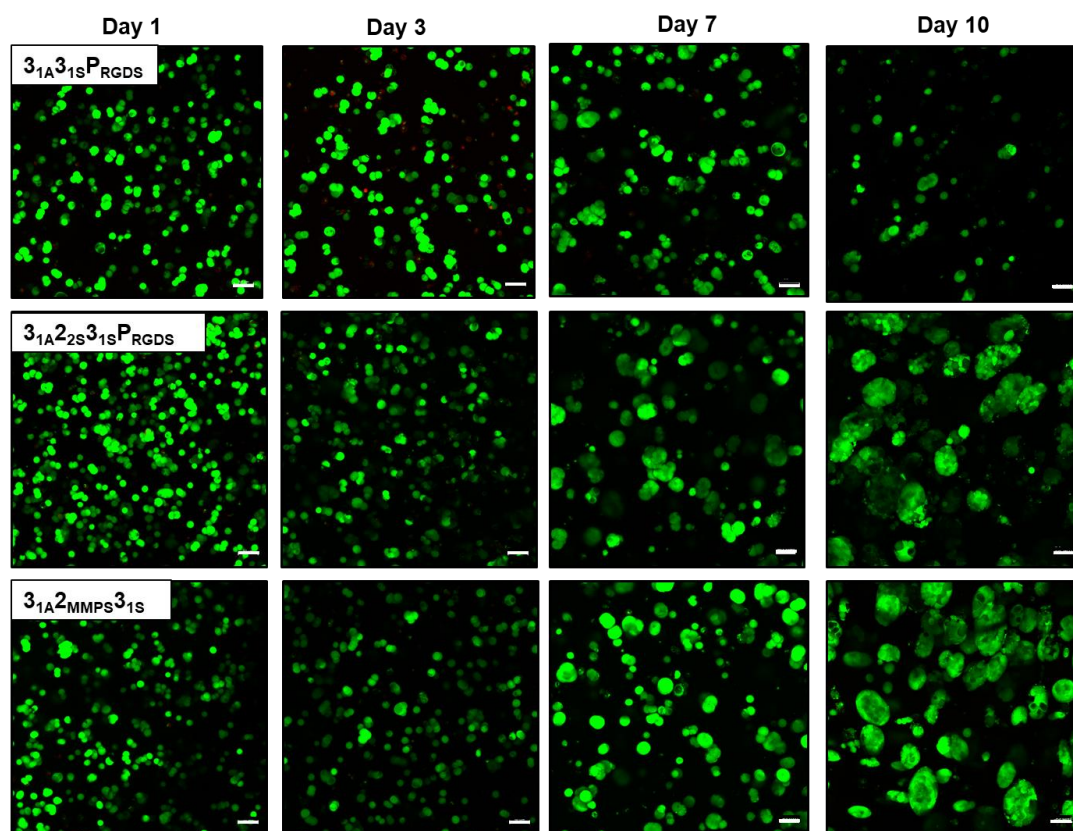


Figure 6.11. Live/Dead images of the MCF-7 cells in degradable thiol-yne hydrogels. The incorporation of **2_{2S}** and **2_{MMPS}** significantly increased cluster formation. This observation suggests, the cells ability to locally degrade the matrix increases cluster formation in these matrices.

quantitatively confirms these visual observations (Figure 6.12). The morphology of the clusters in these images is characteristic of MCF-7 cells, and similar to that typically observed in naturally-derived hydrogel systems.⁶² Forming MCF-7 cell clusters in a fully synthetic hydrogel system, demonstrates the potential of this chemistry to form a tuneable platform for controlled culture of MCF-7 cells. These synthetic hydrogels afford the opportunity to reduce batch-to-batch variability between samples and provide a ‘blank slate’ for manipulation of matrix properties in various ways depending on the application required.

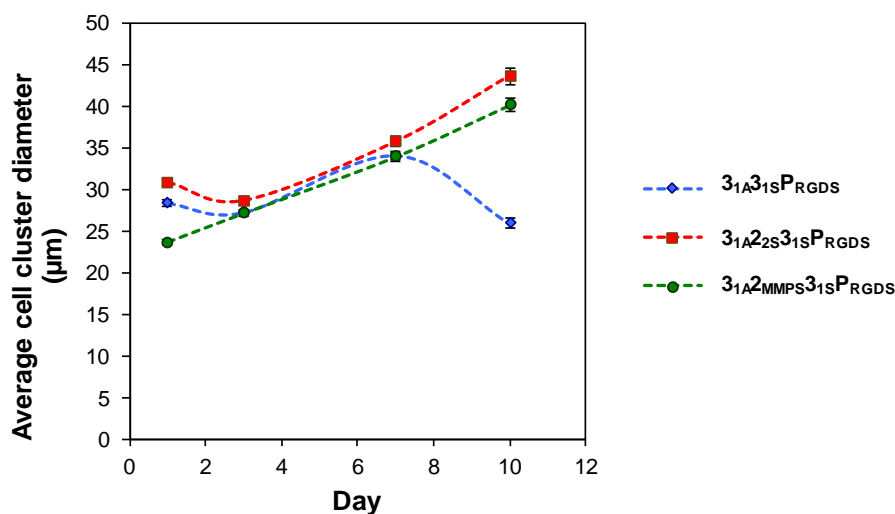


Figure 6.12. Analysis of cell cluster diameter over time for various thiol-yne hydrogel compositions over 10 days in culture. All compositions were formed in serum free media (2,500 cells μL^{-1}). Cell clusters were stained with calcein and images were taken in 200 μm stacks (interval = 5.7 μm) by confocal microscopy (LSM 810 confocal microscope; Zeiss).

The continual increase in metabolic activity over the 10-day experiment suggested that the cell clusters were forming as a consequence of proliferation, and not exclusively as a result of cell migration from a single cell encapsulation to clusters. To continue to probe the mechanism of cell cluster formation, MCF-7 cells encapsulated in thiol-yne **31A22S31S PRGDS** hydrogels were immunostained for a proliferation marker, Ki-67 (Figure 6.13). Ki-67, indicates cells that are in the active phases of the cell cycle and is associated with proliferation. Image quantification indicates that $41 \pm 6\%$ of cells on day 1 and $59 \pm 6\%$ of cells on day 3 were Ki-67 positive, values which are not statistically different ($p > 0.05$). The presence of Ki-67 suggests that, at least in part, cell clusters are growing as cells divide. Overall, this system provides a platform for observing the proliferation of cell clusters and has potential to be adapted to probe questions of cell interactions with their culture environment.

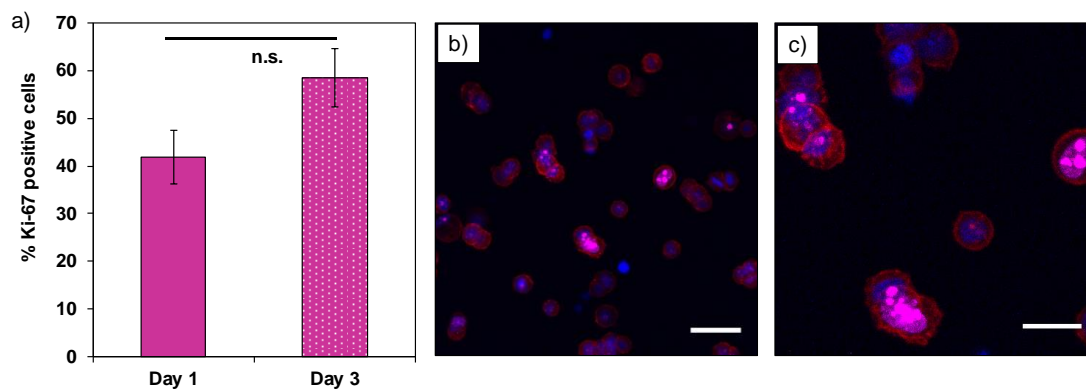


Figure 6.13. Proliferation of MCF-7 cells in 3D cell culture. MCF-7 cells were encapsulated in $3_{1A}2_{2S}3_{1S}P_{RGDS}$ hydrogels and immunostained for nuclei (blue), f-actin (red), and Ki-67 (magenta) 1 and 3 days after encapsulation; a) Image quantification on Day 1 and D3 with Ki-67 positive. These values are not statistically different ($p > 0.05$), b) Representative images shown for day 1 time point. Scale bar = 50 μm . (c) Enlarged image to highlight Ki-67 positive cells. Scale bar = 25 μm .

6.3. Conclusions

Development of well-defined matrices as tools for 3D cell culture is an ideal route to better understanding disease progression and drug evaluation for breast cancer. To synthesise these platforms, the chemistry behind the material must be capable of reliably producing controlled mechanical properties and presenting desired bioactive functionality in a predictable manner, while also encapsulating cells without impacting their viability. In this chapter, the nucleophilic thiol-yne addition reaction has been used to create synthetic PEG hydrogels as ECM mimics which can access a range of hydrogel stiffnesses, easily incorporate bioactive peptide, and furthermore demonstrate the ability to tune the network's degradability by ester hydrolysis and cell-driven degradation, to allow for cell proliferation for long-term 3D cell culture. With this system, the ability to successfully encapsulate three breast cancer cell lines, MDA-MB-231, T47D and MCF-7 has been shown. By highlighting the increased sensitivity of MCF-7 cells to radical-initiated thiol-ene crosslinking chemistry, this work has demonstrated the efficacy of network formation by nucleophilic thiol-yne chemistry in serum-free media as a potential alternative for other sensitive cell lines, clearly demonstrating the importance the chemistry behind new biomaterials has on their future success. Furthermore, a system has been created which is capable of bulk network degradability as well as local degradability mediated by MMP secretion by cells within the culture which has enabled the formation of stable MCF-7 cell clusters within 10 days of 3D culture. This work has highlighted the benefits of nucleophilic thiol-yne addition chemistry for the formation of a synthetic 3D culture platform for a sensitive breast cancer cell line, opening the door for future studies to design more complex network compositions and observe their effect on the cluster

formation and behaviour of a variety of breast cancer cell lines, including the MCF-7 cell line. This 3D cell culture platform could be used broadly to study the impact of various controlled mechanical and biochemical compositions on the cell fate and behaviour of sensitive cell lines.

6.4. References

1. D. F. Quail and J. A. Joyce, *Nat. Med.*, 2013, **19**, 1423.
2. C. R. Thoma, M. Zimmermann, I. Agarkova, J. M. Kelm and W. Krek, *Adv. Drug Delivery Rev.*, 2014, **69-70**, 29-41.
3. Y. Sasai, *Cell Stem Cell*, 2013, **12**, 520-530.
4. D. Antoni, H. Burckel, E. Josset and G. Noel, *Int. J. Mol. Sci.*, 2015, **16**, 5517.
5. C. M. Nelson and M. J. Bissell, *Annu. Rev. Cell Dev. Biol.*, 2006, **22**, 287-309.
6. G. Y. Lee, P. A. Kenny, E. H. Lee and M. J. Bissell, *Nat. Methods*, 2007, **4**, 359-365.
7. D. Barkan, H. Kleinman, J. L. Simmons, H. Asmussen, A. K. Kamaraju, M. J. Hoenorhoff, Z. Y. Liu, S. V. Costes, E. H. Cho, S. Lockett, C. Khanna, A. F. Chambers and J. E. Green, *Cancer Res.*, 2008, **68**, 6241-6250.
8. D. Barkan, L. H. El Touny, A. M. Michalowski, J. A. Smith, I. Chu, A. S. Davis, J. D. Webster, S. Hoover, R. M. Simpson, J. Gauldie and J. E. Green, *Cancer Res.*, 2010, **70**, 5706-5716.
9. S. Choi, S. Coonrod, L. Estroff and C. Fischbach, *Acta Biomater.*, 2015, **24**, 333-342.
10. G. Benton, J. George, H. K. Kleinman and I. P. Arnaoutova, *J. Cell. Physiol.*, 2009, **221**, 18-25.
11. E. L. Baker, R. T. Bonnecaze and M. H. Zamao, *Biophys. J.*, 2009, **97**, 1013-1021.

12. P. Schedin and P. J. Keely, *Cold Spring Harbor Perspect. Biol.*, 2011, **3**, a003228.
13. M. Alemany-Ribes and C. E. Semino, *Adv. Drug Delivery Rev.*, 2014, **79-80**, 40-49.
14. K. Guiro and T. L. Arinzeh, *Breast Cancer: Basic Clin. Res.*, 2015, **9**, 57-70.
15. G. P. Gupta and J. Massagué, *Cell*, 2006, **127**, 679-695.
16. S. C. Owen and M. S. Shoichet, *J. Biomed. Mater. Res., Part A*, 2010, **94A**, 1321-1331.
17. M. W. Tibbitt and K. S. Anseth, *Biotechnol. Bioeng.*, 2009, **103**, 655-663.
18. A. Villasante and G. Vunjak-Novakovic, *Expert Opin. Drug Discovery*, 2015, **10**, 257-268.
19. G. Rijal and W. Li, *Biomaterials*, 2016, **81**, 135-156.
20. M. P. Lutolf and H. M. Blau, *Adv. Mater.*, 2009, **21**, 3255-3268.
21. D. O. Freytes, L. Q. Wan and G. Vunjak-Novakovic, *J. Cell. Biochem.*, 2009, **108**, 1047-1058.
22. N. Gjorevski and C. M. Nelson, *Cytokine Growth Factor Rev.*, 2009, **20**, 459-465.
23. J. A. Rowley, G. Madlambayan and D. J. Mooney, *Biomaterials*, 1999, **20**, 45-53.
24. L. T. Saldin, M. C. Cramer, S. S. Velankar, L. J. White and S. F. Badylak, *Acta Biomater.*, 2017, **49**, 1-15.

25. M. C. Regier, S. I. Montanez-Sauri, M. P. Schwartz, W. L. Murphy, D. J. Beebe and K. E. Sung, *Biomacromolecules*, 2017, **18**, 709-718.
26. B. Trappmann, B. M. Baker, W. J. Polacheck, C. K. Choi, J. A. Burdick and C. S. Chen, *Nat. Commun.*, 2017, **8**, 371.
27. N. J. Walters and E. Gentleman, *Acta Biomater.*, 2015, **11**, 3-16.
28. S. R. Caliari and J. A. Burdick, *Nat. Methods*, 2016, **13**, 405.
29. A. E. G. Baker, R. Y. Tam and M. S. Shoichet, *Biomacromolecules*, 2017, **18**, 4373-4384.
30. F. M. Watt and W. T. S. Huck, *Nat. Rev. Mol. Cell Biol.*, 2013, **14**, 467.
31. C. S. Chen, *Trends in Cell Biology*, 2016, **26**, 798-800.
32. Y. K. Kurokawa and S. C. George, *Adv. Drug Delivery Rev.*, 2016, **96**, 225-233.
33. N. Ki-Hwan, S. T. S. Alec, L. Saifullah, K. Sunghoon and K. Deok-Ho, *J. Lab. Autom.*, 2014, **20**, 201-215.
34. E. W. Esch, A. Bahinski and D. Huh, *Nat. Rev. Drug Discovery*, 2015, **14**, 248.
35. A. Skardal, T. Shupe and A. Atala, *Drug Discovery Today*, 2016, **21**, 1399-1411.
36. N. S. Bhise, J. Ribas, V. Manoharan, Y. S. Zhang, A. Polini, S. Massa, M. R. Dokmeci and A. Khademhosseini, *J. Controlled Release*, 2014, **190**, 82-93.
37. A. V. Belikov, B. Schraven and L. Simeoni, *J. Biomed. Sci.*, 2015, **22**, 85.

38. G. W. Thorpe, C. S. Fong, N. Alic, V. J. Higgins and I. W. Dawes, *Proc. Natl. Acad. Sci. USA*, 2004, **101**, 6564-6569.
39. X. Chen, M. Song, B. Zhang and Y. Zhang, *Oxidative Medicine and Cellular Longevity*, 2016, **2016**, 10.
40. D. Seliktar, *Science*, 2012, **336**, 1124-1128.
41. V. X. Truong, K. M. Tsang and J. S. Forsythe, *Biomacromolecules*, 2017, **18**, 757-766.
42. V. X. Truong, M. P. Ablett, S. M. Richardson, J. A. Hoyland and A. P. Dove, *J. Am. Chem. Soc.*, 2015, **137**, 1618-1622.
43. X. Y. Cai, J. Z. Li, N. N. Li, J. C. Chen, E.-T. Kang and L. Q. Xu, *Biomater. Sci.*, 2016, **4**, 1663-1672.
44. H. Wang, J. Qian, Y. Zhang, W. Xu, J. Xiao and A. Suo, *Cancer Cell Int.*, 2017, **17**, 55.
45. L. J. Macdougall, M. M. Pérez-Madrigal, M. C. Arno and A. P. Dove, *Biomacromolecules*, 2017, **19**, 1378-1388.
46. S. Wang, X. Cai, L. Wang, J. Li, Q. Li, X. Zuo, J. Shi, Q. Huang and C. Fan, *Chemical Science*, 2016, **7**, 2722-2727.
47. S. P. Singh, M. P. Schwartz, J. Y. Lee, B. D. Fairbanks and K. S. Anseth, *Biomater. Sci.*, 2014, **2**, 1024-1034.
48. A. Raza, C. S. Ki and C.-C. Lin, *Biomaterials*, 2013, **34**, 5117-5127.

49. C. N. Salinas and K. S. Anseth, *J. Tissue Eng. Regener. Med.*, 2008, **2**, 296-304.
50. O. Chaudhuri, L. Gu, D. Klumpers, M. Darnell, S. A. Bencherif, J. C. Weaver, N. Huebsch, H.-p. Lee, E. Lippens, G. N. Duda and D. J. Mooney, *Nat. Mater.*, 2015, **15**, 326.
51. S. Khetan, M. Guvendiren, W. R. Legant, D. M. Cohen, C. S. Chen and J. A. Burdick, *Nat. Mater.*, 2013, **12**, 458-465.
52. Z. Gong, S. E. Szczesny, S. R. Caliari, E. E. Charrier, O. Chaudhuri, X. Cao, Y. Lin, R. L. Mauck, P. A. Janmey, J. A. Burdick and V. B. Shenoy, *Proc. Natl. Acad. Sci. USA*, 2018, **115**, E2686-E2695.
53. H. X. Zhou, J. Woo, A. M. Cok, M. Z. Wang, B. D. Olsen and J. A. Johnson, *J. A. Proc. Nat. Acad. Sci. U. S. A.*, 2012, **109**, 19119-19124.
54. K. Kawamoto, M. J. Zhong, R. Wang, B. D. Olsen and J. A. Johnson, *Macromolecules*, 2015, **48**, 8980-8988.
55. O. Chaudhuri, S. T. Koshy, C. Branco da Cunha, J.-W. Shin, C. S. Verbeke, K. H. Allison and D. J. Mooney, *Nat. Mater.*, 2014, **13**, 970.
56. S. T. Gould, N. J. Darling and K. S. Anseth, *Acta Biomater.*, 2012, **8**, 3201-3209.
57. M. S. Rehmann and A. M. Kloxin, *Soft Matter*, 2013, **9**, 6737-6746.
58. L. J. Macdougall, V. X. Truong and A. P. Dove, *ACS Macro Lett.*, 2017, **6**, 93-97.
59. L. A. Sawicki and A. M. Kloxin, *Biomater. Sci.*, 2014, **2**, 1612-1626.

60. N. Peela, F. S. Sam, W. Christenson, D. Truong, A. W. Watson, G. Mouneimne, R. Ros and M. Nikkhah, *Biomaterials*, 2016, **81**, 72-83.
61. L. J. Bray, M. Binner, A. Holzheu, J. Friedrichs, U. Freudenberg, D. W. Hutmacher and C. Werner, *Biomaterials*, 2015, **53**, 609-620.
62. M. M. Vantangoli, S. J. Madnick, S. M. Huse, P. Weston and K. Boekelheide, *PLOS ONE*, 2015, **10**, e0135426.

Chapter 7.

A Kinetic Study of the Nucleophilic Thiol-yne Addition Reaction and its Application in Hydrogel Synthesis

7.1. Introduction

The degradation and biocompatibility profile of synthetic hydrogel materials is critically important for many applications¹⁻⁴ (*e.g.* drug delivery^{5, 6} and tissue engineered scaffolds).⁷⁻⁹ Hydrogels are defined by their high water content and porous structure;^{10, 11} but also their poor mechanical properties.¹² As research into biomedical devices accelerates there is an ever-increasing need for hydrogels to be robust yet possess swelling and degradation profiles which are suitable for a given application.¹³⁻¹⁵ As shown in previous chapters, degradation of the swollen polymer networks through hydrolysis alters the swelling profile of the hydrogel. As a consequence the mechanical properties of the hydrogel suffers.¹⁶ Degradation in the network can be beneficial for cell proliferation¹⁷⁻¹⁹ or delivery of cargo;^{20, 21} however, if the process occurs too rapidly it can result in inferior materials. Therefore, the material cannot perform the required function highlighting the need to synthesise hydrogels with controlled degradation and swelling profiles is required.²²

For many biomedical applications, hydrogels need to be synthesised in the presence of cells, therefore the choice of crosslinking should be cytocompatible and able to take place under physiological conditions. As such the nucleophilic thiol-yne addition reaction is an ideal crosslinking reaction for the formation of cell laden poly(ethylene glycol) (PEG) hydrogels.²³ However, two drawbacks to the nucleophilic thiol-yne reaction have been highlighted in the previous chapters. In chapter 6 it was demonstrated that the PEG alkyne precursor was very toxic to breast cancer cells when dissolved in phosphate buffer saline (PBS) solution and not reacted. This was a result of the ester

linkage present in the PEG alkyne precursors hydrolysing and releasing propiolic acid into the culture. Propiolic acid has a LD₅₀ (lethal dose in which 50% of the test rat sample died) of 100 mg kg⁻¹,²⁴ and was shown to be the cause of the high cell death in the PEG alkyne sample. Furthermore, in Chapter 3 the swelling and degradation profile of the **31A2s** systems were shown to be inadequate for prolonged study in aqueous environments (*i.e.* the hydrogel swelled and degraded in three days)²⁵ as a result of the hydrolysis of the ester units in the polymer network. These drawbacks demonstrated that the ester linkages, formed in the functionalisation of the alkyne and thiol PEG precursors, were disadvantageous to the thiol-yne PEG hydrogel systems. Addressing these drawbacks was necessary before the materials could be considered potential biomaterial candidates.

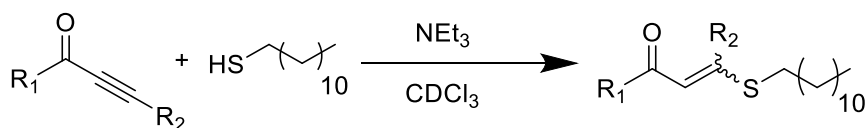
The nucleophilic thiol-yne reaction requires an activated alkyne-functional group (*i.e.* carbonyl group adjacent to the alkyne) for it to occur under mild reaction conditions (*e.g.* room temperature and PBS solution). Previous work (Chapters 2 and 3) demonstrated the use of Fischer esterification reactions for the facile synthesis of ester-alkyne functionalised PEG precursors.^{26, 27} To improve the cytocompatibility of the PEG alkyne precursor and the degradation profile of the thiol-yne hydrogels the ester-functionality needed to be replaced with a functional group less susceptible to hydrolysis. However, changing the group adjacent to the alkyne (*i.e.* the ester-functionality) would affect the rate of the nucleophilic thiol-yne reaction and therefore the properties of the resultant hydrogels. The rate of the crosslinking reaction for hydrogel synthesis needs to be carefully controlled to avoid the resultant hydrogels forming too rapidly and negatively impacting the strength of the hydrogels. Indeed, with an increased reaction rate the viscosity of the solution rapidly increases and results in the end groups being trapped and

less accessible. This reduces the precursors ability to undergo the thiol-yne reaction, thus decreasing the number of crosslinked sites and compromising the strength of the hydrogel.²⁸ In contrast, if the adjacent functional group slows down the rate of the thiol-yne reaction then the hydrogel will take longer to form or may not form at all. Consequently, this could reduce the strength of the hydrogels as the functional groups are further away from each other and thus less likely to react, reducing the number of crosslinked sites and resulting in a weaker network.²⁹ It is therefore vital that a similar rate of thiol-yne reaction is maintained when the linkage between the PEG unit and the alkyne is changed. Thus, this chapter will address the drawbacks of the ester-functional thiol-yne hydrogel system by conducting a small molecule nucleophilic thiol-yne rate study to identify an activating adjacent functional group with a similar rate of reaction to the ester-functionality. Once identified, this chemistry will be used to functionalise a PEG precursor with alkyne-functionality and the cytocompatibility of the new alkyne precursor will be assessed. Furthermore, the degradation profiles of the resultant thiol-yne hydrogels will be evaluated.

7.2. Results and Discussion

7.2.1. Nucleophilic Thiol-yne Kinetic Study

The ester-functionalised alkyne and thiol PEG precursors enabled the nucleophilic thiol-yne reaction to proceed very rapidly, whilst also forming robust hydrogels.^{26, 27, 30} However, to reduce the toxicity of the ester-functionalised PEG alkyne precursor the ester-functionality could be replaced with a functional group which is less susceptible to hydrolysis. This would also improve the degradation and swelling profile of the resultant thiol-yne hydrogel but could affect the rate of the crosslinking thiol-yne reaction and consequently the gelation time of the hydrogels. To understand this effect in more detail, a small molecule nucleophilic thiol-yne kinetic study was conducted with a series of small molecule alkynes. Each alkyne was reacted with 1-dodecanethiol (DT) in deuterated chloroform (CDCl_3) and the effect different activating or adjacent groups to the alkyne, had on the initial rate of the nucleophilic thiol-yne reaction was examined (Scheme 7.1). Ethyl propiolate, a small molecule ester alkyne, was used as the control alkyne and its rate of reaction was compared to small molecule alkynes with different functional groups (Scheme 7.1).



Scheme 7.1. Small molecule nucleophilic thiol-yne reaction scheme between an activated alkyne and 1-dodecanethiol (DT). $\text{R}_1 = \text{OCH}_2\text{CH}_3$ (ester control), C_6H_5 (aromaticity), CH_3 (ketone), OC_6H_5 (aromatic ester) or NHCH_2CH_3 and $\text{R}_2 = \text{H}$. Or $\text{R}_1 = (\text{CH}_2)_4\text{CH}_3$ (ketone) or C_6H_5 (aromaticity) and $\text{R}_2 = \text{CH}_3$.

7.2.1.1. The Effect of Activating Carbonyl Groups on the Rate of the Nucleophilic Thiol-yne Reaction

It was hypothesised that the rate of reaction would increase when the alkyne became more electron deficient (*e.g.* incorporating ketone and aryl functionality). The adjacent carbonyl groups could draw electrons away from the alkyne making it more susceptible to attack from a thiolate ion. Conversely, in the presence of an amide adjacent to the alkyne the reaction rate would reduce as fewer electrons are drawn away from the alkyne making it less susceptible to addition of a thiolate ion. Also, these adjacent functionalities are less hydrolytically cleavable than the ester linker, thus degradation that produces a toxic small molecule alkyne would not be expected. Initial kinetic studies explored the effect of the ketone and aromatic ketone functionalities; 3-butyn-2-one and phenyl-2-propyn-1-one (PPO) respectively (Figure 7.1). The carbonyl functional groups adjacent to the alkyne can pull electron density away from the alkyne, resulting in an electron deficient alkyne which should increase the rate of the thiol-yne reaction.

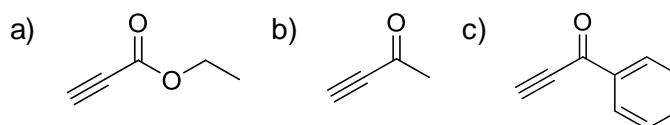


Figure 7.1 Small molecule alkynes with activating groups adjacent to the alkyne; a) ethyl propiolate (ester-functionality), b) 3-butyn-2-one (ketone-functionality), c) phenyl-2-propyn-1-one (PPO, ketone-aromaticity).

The reaction rates were determined and compared to the rate of the nucleophilic thiol-yne reaction with ethyl propiolate (control reaction). Specifically, each alkyne was reacted with DT in CDCl_3 and trimethylamine (NEt_3). These reaction conditions were chosen as they had previously shown to give high product conversion (96%) in 10 min with stereoselectivity towards the *trans* product (87%).³¹ Conversion was determined by the comparison of integrals between a stable proton environment on the alkyne starting material (e.g. the quartet at $\delta = 4.13$ ppm corresponding to the ethyl group on ethyl propiolate) and the formed alkene proton environment (e.g. a set of doublets at $\delta = 5.68$ and 5.78 ppm corresponding to the formation of the *cis* and the *trans* alkene protons respectively) (Figure 7.2). ^1H NMR spectra were recorded periodically to monitor the conversion with time (Figure 7.3).

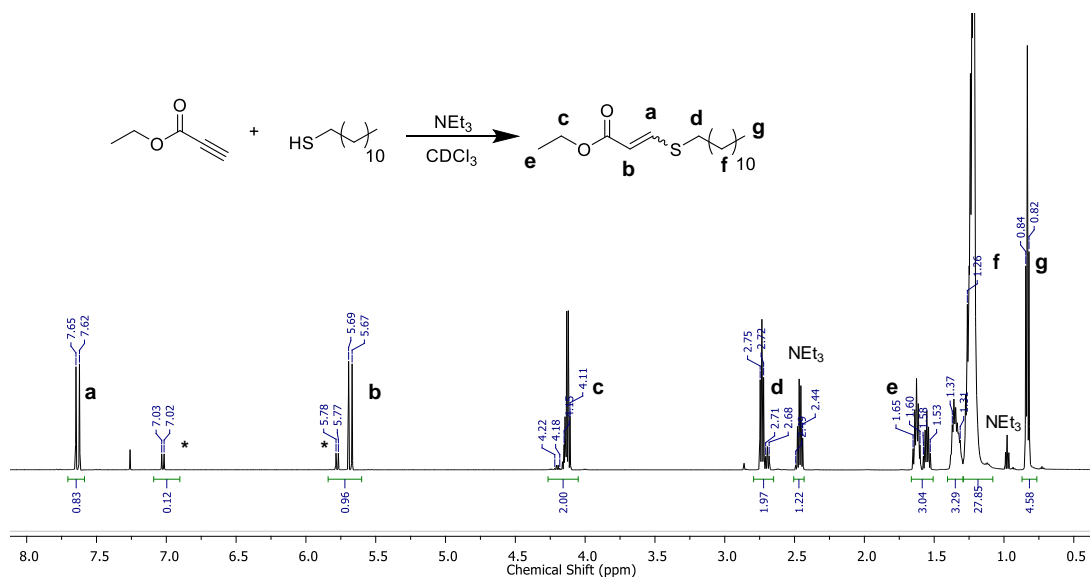


Figure 7.2. a) Reaction between ethyl propiolate (ester-functionalised alkyne) and DT and ^1H NMR spectrum of the thiol-yne reaction between ethyl propiolate and DT with NEt_3 in CDCl_3 after 60 min, *= *cis* alkene product, (298 K, CDCl_3 , 600 MHz).

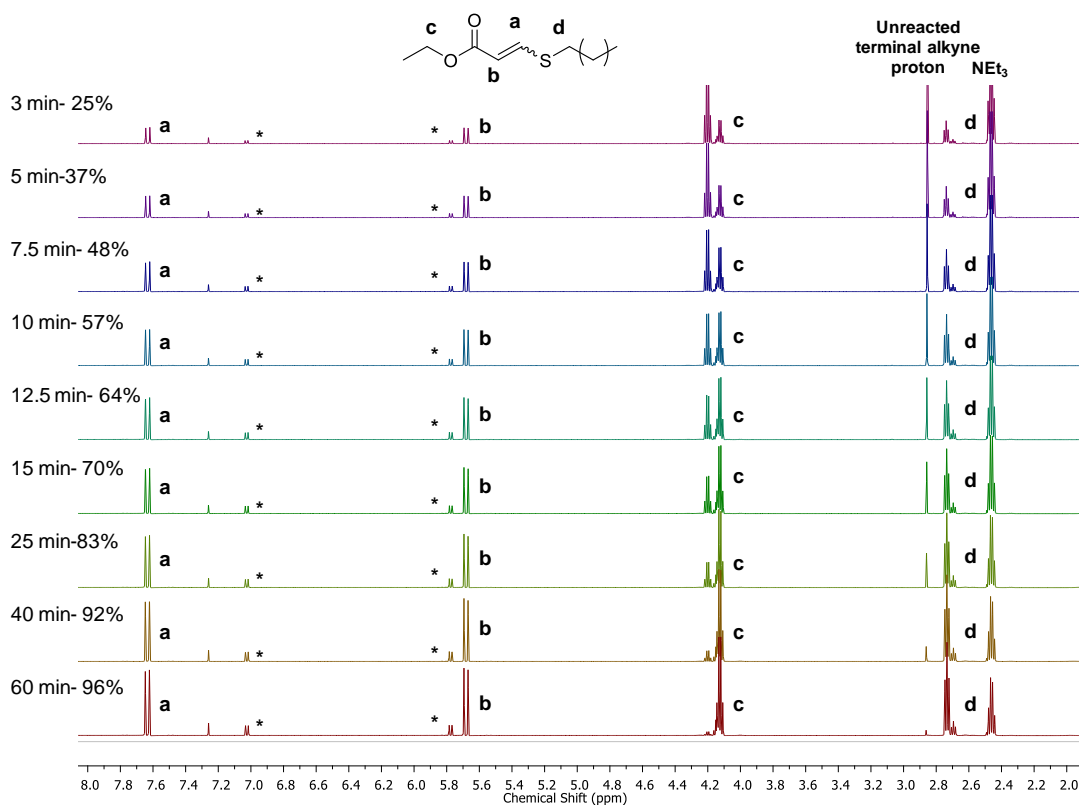


Figure 7.3. ^1H NMR spectra showing the conversion of ethyl propiolate and DT to the vinyl thioether product, * = *cis* alkene (298 K, CDCl_3 , 600 MHz).

The conversion of alkyne to vinyl thioether was determined from the ^1H NMR spectroscopic data and was used to calculate the concentration of the alkyne in the initial stages of the thiol-yne reaction. To determine the rate of the reaction first and second order rate charts were constructed, which revealed that the thiol-yne reaction fitted first order kinetics in the initial stages of the reaction. This was demonstrated by the exponential decay relationship between $[A]_t$ and time (Figure 7.4a) and a negative linear correlation between $\ln[A]_t$ and time (Figure 7.4b). The first order rate equation (Equation 7.1) was therefore used to determine the initial rate of the thiol-yne reaction.

$$\ln[A]_t = \ln[A]_0 - kt$$

Equation 7.1. First order rate equation where $\ln[A]_t$ is the concentration of alkyne at a certain time point, t , $\ln[A]_0$ is the starting concentration of alkyne and k is the rate constant for the reaction.

The rate of reaction was then calculated using the gradient of the line (e.g. $7 \pm 0.04 \times 10^{-2} \text{ min}^{-1}$ for ethyl propiolate) (Figure 7.4b) and normalised for the concentration of NEt_3 used for each study (e.g. 21 mM NEt_3 for ethyl propiolate). Using this method, the initial reaction rate for the control thiol-yne reaction between ethyl propiolate and DT was determined as $2 \times 10^{-1} \text{ s}^{-1}$.

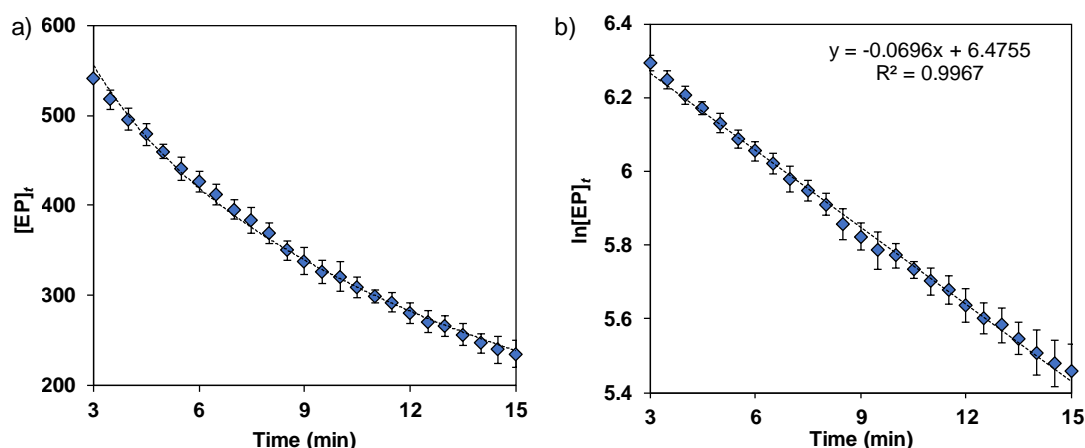


Figure 7.4. a) Plot of the concentration of ethyl propiolate (EP) with respect to time showing a logarithmic correlation; b) first order rate chart used to determine the rate constant (k) for the reaction.

The rate of the thiol-yne reactions for PPO and 3-Butyn-2-one were also determined. As expected PPO had the highest initial rate of reaction with DT at $5.02 \pm 0.6 \times 10^2 \text{ s}^{-1}$ (Table 7.1). This confirmed that the alkyne containing the aromatic ketone was more electron deficient and as a result the rate of the thiol-yne reaction increased. Interestingly, ^1H NMR spectroscopy of the thiol-yne PPO and DT products revealed the *cis* vinyl thioether to be the major product. The *trans* vinyl thioether was predicted to be the major product as the control ester reaction resulted in a 13:87 *cis:trans* ratio. Under

these non polar weakly basic conditions (NEt_3 , CDCl_3) the nucleophilic thiol-yne reaction with ester-activated alkynes (shown in Chapter 4) favours a *trans* mechanism for the formation of the vinyl thioether.³¹ However, the PPO experiment has shown that the activating functional group adjacent to the alkyne can also influence the stereochemistry of the resultant product (Figure 7.5). The attack of the alkyne by the thiol-base pair to the same side of the alkyne (*trans* mechanism) is disfavoured because the steric hindrance caused by the bulky aromatic ring, thus the thiolate ion reacts with the alkyne first (*cis* mechanism). In addition, the PPO-DT *cis* transition state is favoured as the negativity charged carbonyl oxygen is stabilised through conjugation with the aromatic ring, resulting in the *cis* isomer as the major product (Figure 7.6).

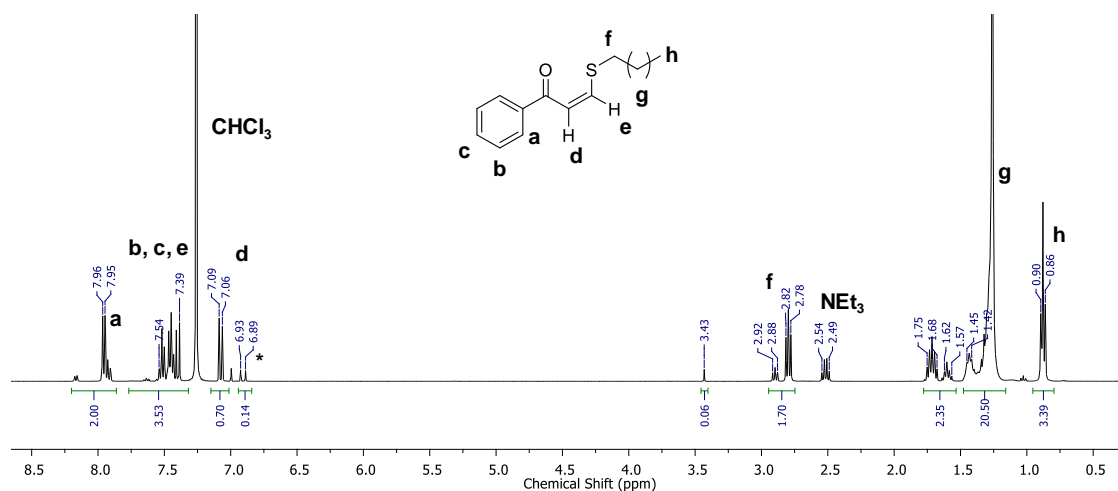


Figure 7.5. ^1H NMR spectrum of the nucleophilic thiol-yne reaction between phenyl-2-propyn-1-one and DT in the presence of NEt_3 and CDCl_3 , * = *trans* isomer, (298 K, CDCl_3 , 300 MHz).

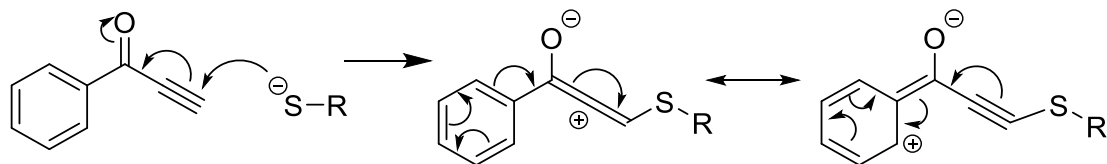
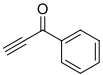
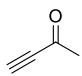
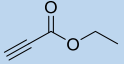


Figure 7.6. Resonance structures of PPO reacting with DT through the favoured *cis* transition state showing charge stabilisation through the aromatic ring.

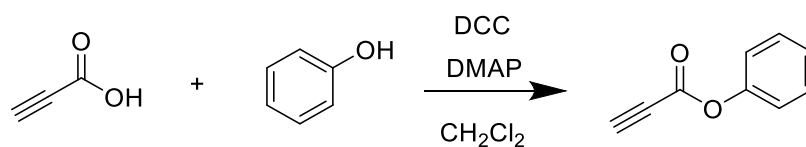
Subsequently, 3-butyn-2-one was used to investigate the effect of removing aromaticity on the rate of reaction with a ketone-activated alkyne. When using 3-butyn-2-one the normalised initial rate of the thiol-yne reaction decreased compared to PPO to $2.5 \pm 0.05 \text{ s}^{-1}$ (Table 7.1). The reaction rate was lower than observed for PPO because the removal of the aryl group makes the alkyne in 3-butyn-2-one less activated and therefore less susceptible to attack. However, the rate of reaction was still faster when compared to the control reaction with the ester-containing ethyl propiolate. The ketone (3-butyn-2-one) has a stronger inductive effect than the ester (ethyl propiolate) and as a result greater electron density is pulled away from the alkyne making it more susceptible to attack. The stereochemistry for the resultant vinyl thioether product was 27:72 *cis:trans*, revealing the amount of *cis* product had increased slightly compared to the control reaction with the ester-containing ethyl propiolate (13:87 *cis:trans*). However, the *trans* product was still favoured demonstrating the ketone has little effect on the overall resulting stereochemistry. This ratio also confirmed there was no correlation observed between the rate of the thiol-yne reaction and the stereochemistry of the resultant product. Overall, as hypothesised, both functional groups increased the rate of the thiol-yne reaction dramatically when compared to the original ester-alkyne chemistry. Thus, it was postulated that the elevated rate would be too rapid for hydrogel synthesis and would result in hydrogels with inferior mechanical properties.

Table 7.1. Effect of the functional group adjacent to the alkyne on rate of the nucleophilic thiol-yne reaction with DT (1.2 eq) with NEt_3 in CDCl_3 .

Alkyne	Structure	Functional group	$[\text{NEt}_3]$ (mM)	Rate (s^{-1})	Normalised rate ($\text{s}^{-1} \text{mM}^{-1}$)	Relative rate ^a	<i>cis:trans</i> ratio
Phenyl-2-propyn-1-one (PPO)		Aromatic ketone	0.0005	0.24 ± 0.03	502 ± 63	1	83:17
3-Butyn-2-one		Ketone	0.1	0.24 ± 0.005	2.5 ± 0.05	201	27:72
Ethyl propiolate		Ester	21	4.2 ± 2	0.2 ± 0.1	2516	13:87

^aRelative to phenyl-2-propyn-1-one

To investigate the reactivity of an aryl ester alkyne in the nucleophilic thiol-yne reaction, phenyl propiolate, was synthesised according to a previous literature procedure (Scheme 7.2).³² Propiolic acid was coupled to phenol (1.1 eq.) through a *N,N'*-dicyclohexylcarbodiimide (DCC, 1.0 eq.) coupling reaction with 4-dimethylaminopyridine (DMAP, 0.1 eq) in CH_2Cl_2 . After purification *via* column chromatography and vacuum distillation the desired product was achieved with a 57% yield and characterised by ^1H NMR, ^{13}C NMR and FT-IR spectroscopy (Figure 7.7).



Scheme 7.2. Reaction scheme for the synthesis of phenyl propiolate.

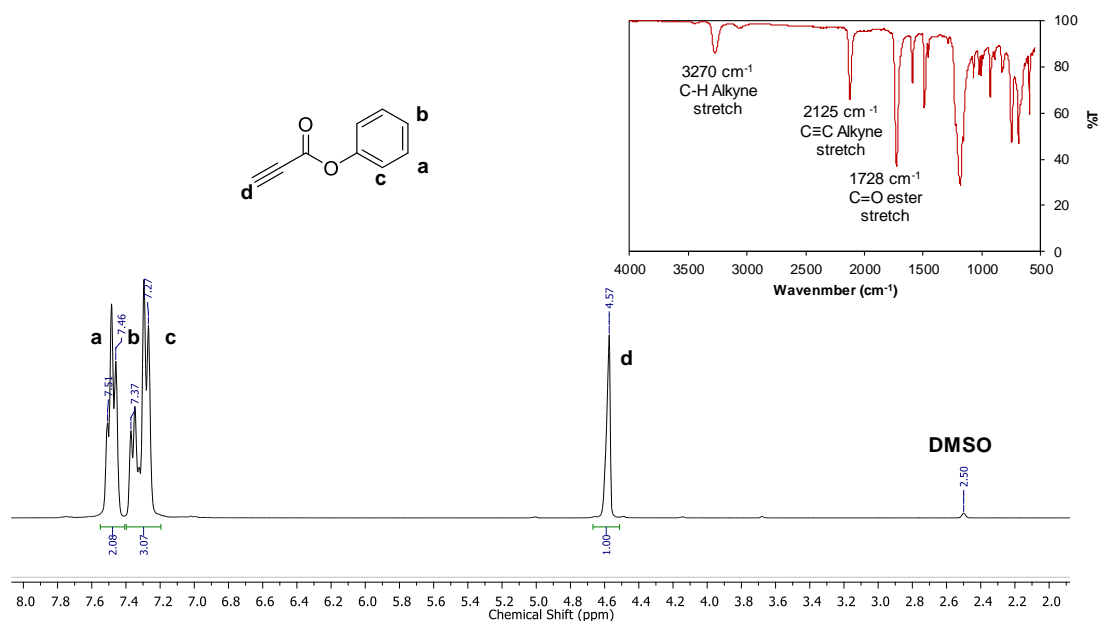
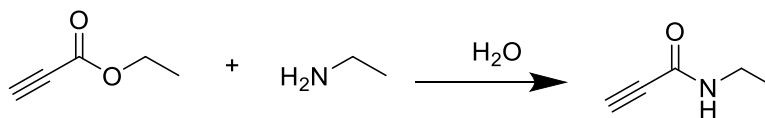


Figure 7.7 ^1H NMR spectrum of phenyl propiolate (298 K, $(\text{CD}_3)_2\text{SO}$, 300 MHz) with insert showing the FT-IR spectrum of phenyl propiolate.

By retaining the ester-functionality, with phenyl propiolate, the effect of aromaticity on the initial rate of the thiol-yne reaction and stereochemistry of the vinyl thioether could be observed. The initial rate of reaction increased by less than one order of magnitude to $9.3 \pm 0.07 \times 10^{-1} \text{ s}^{-1}$ (Table 7.2) when compared to the control reaction with the ester-containing ethyl propiolate. This demonstrated that the alkyne was slightly more electron deficient in phenyl propiolate as a result of the aromatic ester pulling electrons away from the alkyne and making it more susceptible to the addition of a thiolate ion. Through analysis of the vinyl thioether product, it was also evident that the presence of the aryl group adjacent to the ester group resulted in greater stereoselectivity for the *trans* product (6:94 *cis:trans* ratio). As the aromatic ring was further away from the alkyne in phenyl propiolate it no longer contributed to steric hindrance, as observed with phenyl-2-propyn-1-one, enabling the thiol-base pair to attack the alkyne from the same side. Furthermore, the increased electron density from the aromatic ring did not stabilise the

cis transition state and therefore the formation of the *cis* product was not favoured. As the rate of the reaction was similar to the control with ethyl propiolate it was postulated that the gelation time for the resultant hydrogels would be similar to the ester-functionalised hydrogels. However, despite being in agreement with literature values, the DCC coupling reaction used to synthesise the aromatic ester-functionality was low yielding (57%).³² It is likely that the reaction to functionalise the PEG precursor with the aryl ester would therefore also be low yielding. This would result in only a small number of functionalised polymer end groups on the PEG precursor chains, causing the number of crosslinks in the hydrogel formation to reduce and subsequently this would reduce the quality of the resultant hydrogels. Therefore, the aryl ester was not considered as an ideal candidate to replace the ester thiol-yne PEG hydrogels.

To optimise the rate of the thiol-yne reaction the kinetic study was expanded to investigate the effect of an amide functional group on the reactivity of an adjacent alkyne. A small molecule amide-alkyne, ethyl propiolamide, was synthesised and the rate of the thiol-yne reaction with DT determined. Ethyl propiolamide was synthesised using a modified literature procedure,³³ ethylamine (1.05 eq., 66-70 wt% H₂O) was reacted with ethyl propiolate (1 eq.) in the presence of H₂O (Scheme 7.3). The product was purified *via* vacuum distillation and characterised by ¹H NMR, ¹³C NMR and FT-IR spectroscopy (Figure 7.8 and 7.9).



Scheme 7.3. Reaction scheme for the synthesis of ethyl propiolamide.

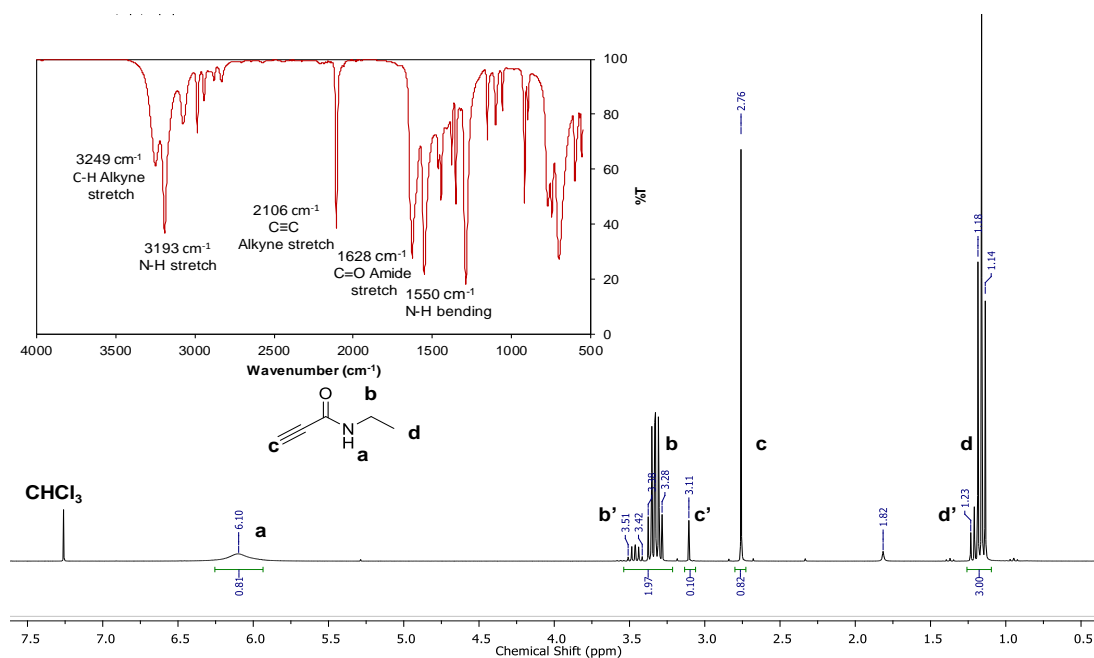


Figure 7.8. ^1H NMR spectrum for ethyl propiolamide (298 K, CDCl_3 , 300 MHz) with insert showing the FT-IR spectrum for ethyl propiolamide.

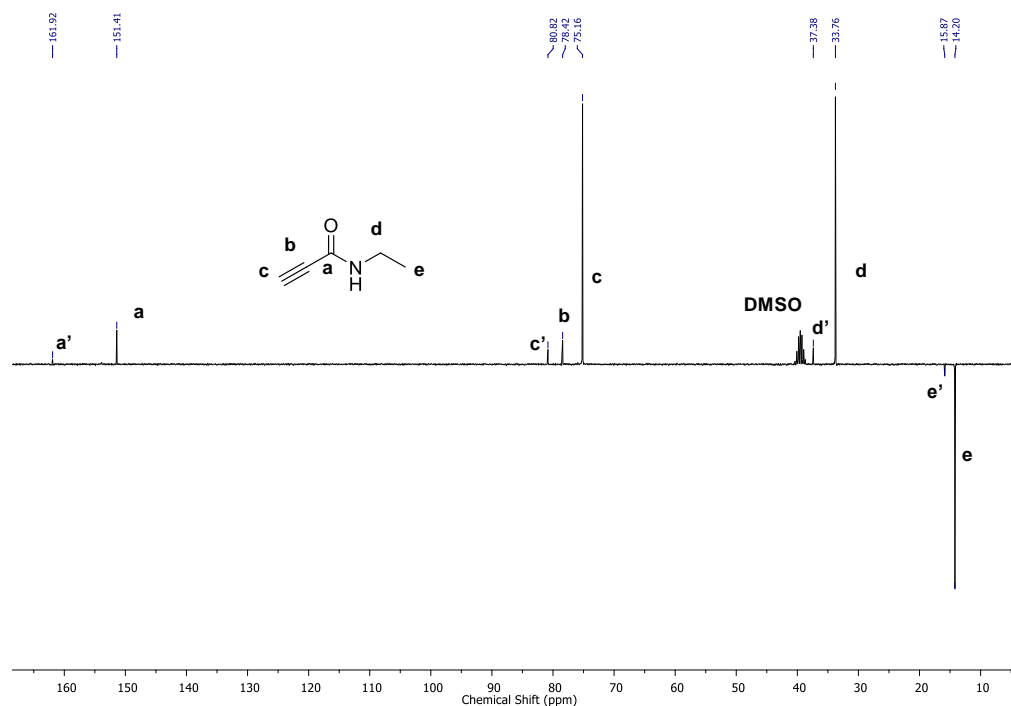


Figure 7.9. ^{13}C NMR spectrum for ethyl propiolamide (298 K, $(\text{CD}_3)_2\text{SO}$, 300 MHz).

However, despite repeated purification techniques, impurities were still present in the ^1H NMR and ^{13}C NMR spectra. It was postulated that the additional signals could be attributed to the formation of strong hydrogen bonds between the molecules (Figure 7.10).³⁴ To prove this, the product was dissolved in deuterated *N,N*-dimethylformamide (DMF) and the sample was characterised at elevated temperatures with ^1H NMR spectroscopy. However, no difference in the intensity of the shifts was observed between 303 and 333 K (Figure 7.11). Further characterisation through high resolution electron spray ionisation mass spectrometry (ESI-MS) and elemental analysis confirmed that the amide alkyne product was successfully synthesised with high purity (Figure 7.12). Thus, it was concluded that the additional peaks in the ^1H NMR and ^{13}C NMR spectra were a result of hydrogen bonding. This demonstrated the high strength of the hydrogen bonding between amide-alkynes in combination with interactions between terminal alkynes.

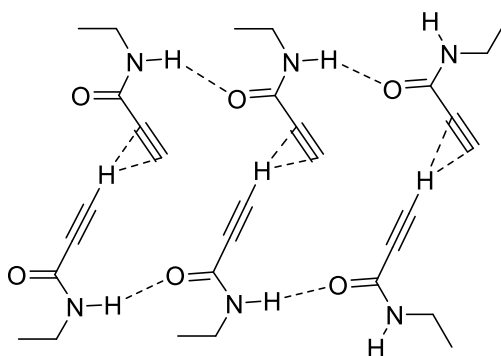


Figure 7.10. Postulated hydrogen bonding between ethyl propiolamide molecules.

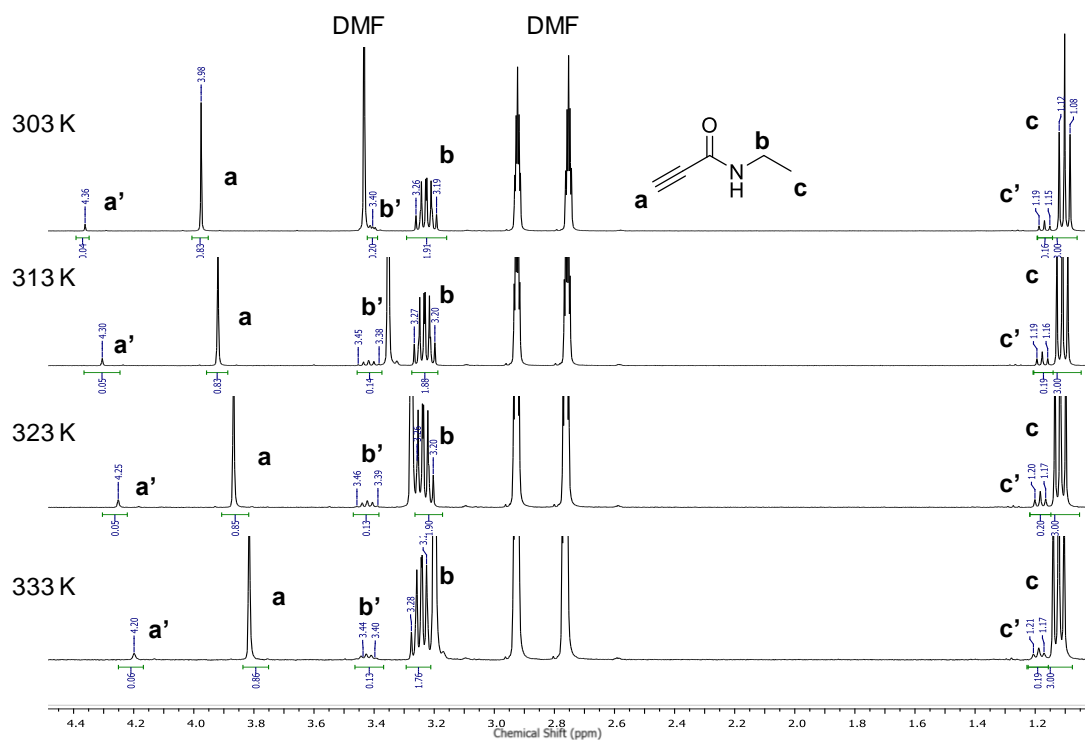


Figure 7.11. ¹H NMR spectra of ethyl propiolamide in deuterated DMF with increasing temperature (303–333 K, 400 MHz).

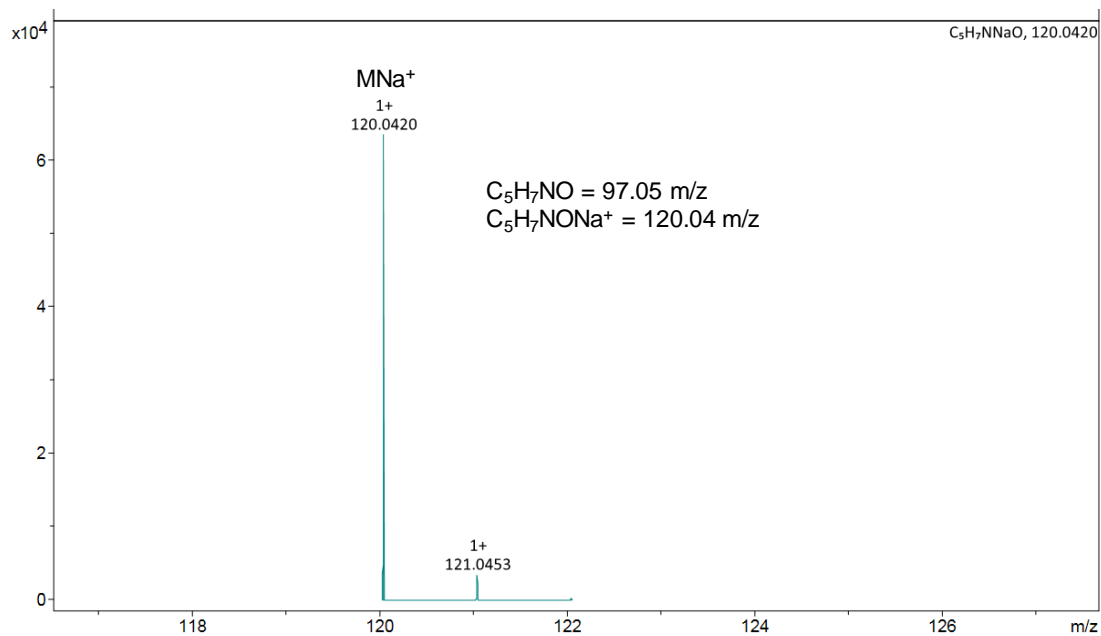


Figure 7.12. High resolution ESI-MS of ethylpropiolamide. Confirmation of small molecule purity.

The amide functionality dramatically decreased the normalised initial rate of the thiol-yne reaction to $5.5 \pm 0.4 \times 10^{-4} \text{ s}^{-1}$ (Table 7.2). The positive mesomeric effects of the amide prevented the formation of an electron deficient alkyne and therefore the alkyne was not as susceptible to attack by a thiolate ion as the ester-alkyne. Interestingly, equal ratios of the vinyl thioether isomers were formed in the reaction (50:50 *cis:trans*). This change in stereochemistry could have been a result of the amide which increased the stability of the carbocation and resulted in an increased amount of *cis* isomer (Figure 7.13). Overall, the amide-alkyne functionality is a potential replacement for the ester-alkyne, however a slower rate of reaction may be beneficial in the synthesis of the hydrogels to favour the formation of perfect network formation and decrease the formation of loops.

Table 7.2. Effect of the functional group adjacent to the alkyne on rate of the nucleophilic thiol-yne reaction.

Alkyne	Structure	Functional group	[NEt ₃] (mM)	Rate (s ⁻¹)	Normalised rate (s ⁻¹ mM ⁻¹)	Relative rate ^a	<i>cis:trans</i> ratio
Phenyl propiolate		Aromatic ester	1.33	1.2 ± 0.1	0.9 ± 0.07	539	6:94
Ethyl propiolate		Ester	21	4.2 ± 2	0.2 ± 0.1	2516	13:87
Ethylpropiolamide		Amide	94	0.05 ± 0.003	$5.5 \pm 0.4 \times 10^{-4}$	907497	50:50

^aRelative to phenyl-2-propyn-1-one

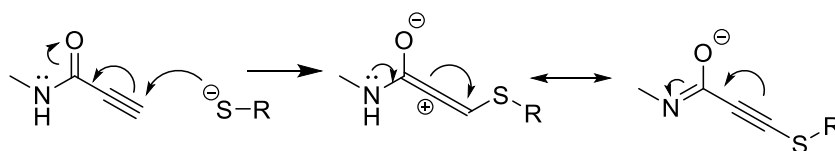


Figure 7.13. Resonance structure of ethyl propiolamide *cis* transition state after attack of a thiolate ion demonstrating the increased stabilisation through amide resonance structures.

7.2.1.2 The Effect of Methyl-Terminated Alkynes on the Rate of the Nucleophilic Thiol-yne Click Reaction

An alternative route to reduce the toxicity of the PEG alkyne precursor is to substitute the terminal acidic alkyne-proton, present in the current chemistry, with a terminal methyl group. Propiolic acid, the hydrolysis product from the ester chemistry PEG alkyne precursor, is a small, very toxic molecule. However, its analogue 2-butynoic acid (*i.e.* a methyl-terminated alkyne carboxylic acid) is less hazardous.³⁵ Therefore, the rate of the thiol-yne reaction with ethyl butynoate (*i.e.* a methyl-terminated ester-alkyne) (Figure 7.14) was determined in order to explore the initial rate of the reaction with a methyl-terminated alkyne.

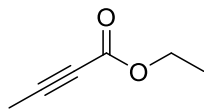
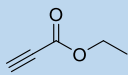
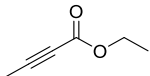


Figure 7.14. Structure of ethyl butynoate.

The initial rate of the thiol-yne reaction with ethyl butynoate was calculated as $1.8 \pm 0.2 \times 10^{-5} \text{ s}^{-1}$, four orders of magnitude lower than the proton-terminated alkyne, ethyl propiolate (Table 7.3). It was thought this result was a consequence of the methyl group increasing the electron density around the alkyne and thus reducing the susceptibility of the alkyne to attack by a thiolate ion. In addition, the increased steric hindrance introduced by the methyl group may have reduced the accessibility of the alkyne to the thiolate ion. The addition of a methyl group also impacted the stereochemistry of the resultant vinyl thioether product. The methyl group disfavoured the thiol-base pair from attacking the same side of the alkyne (*E* mechanism) and therefore the *Z* mechanism was favoured (68:32 *Z:E* ratio). *Z* and *E* nomenclature have been used here as the four substituents on

the alkene bond are different. If a methyl-terminated alkyne was incorporated into the PEG alkyne precursor the gelation time of the hydrogel would increase, impacting the properties of the resultant hydrogels and potentially reduce the toxicity of the hydrolysed PEG alkyne precursor.

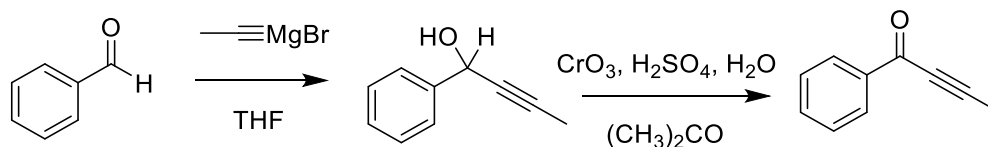
Table 7.3. Effect of a methyl-terminated alkyne on rate of the nucleophilic thiol-yne reaction.

Alkyne	Structure	Functional group	[NEt ₃] (mM)	Rate (s ⁻¹)	Normalised rate (s ⁻¹ mM ⁻¹)	Relative rate ^a	Z:E ratio
Ethyl propiolate		Ester	21	4.2 ± 2	0.2 ± 0.1	2516	13:87
Ethyl butynoate		Ester + terminal methyl	1000	0.018 ± 0.002	1.8 ± 0.24 × 10 ⁻⁵	27861953	68:32

^aRelative to phenyl-2-propyn-1-one

To increase the rate of the thiol-yne reaction using methyl-terminated alkynes; the nucleophilic thiol-yne kinetic study was expanded to include small molecules with methyl-terminated alkynes and ketone or aryl functionality. This enabled fine tuning of the thiol-yne reaction before translation to hydrogel synthesis. In addition, it is postulated that these functionalities, if introduced to hydrogel synthesis, would reduce the toxicity of the PEG alkyne precursor and improve the resultant degradation and swelling profiles of the hydrogels. 1-Phenyl but-2-yn-1-one, an aromatic ketone with a methyl-terminated alkyne, was synthesised using a previously modified procedure (Scheme 7.4).³⁶ Briefly, benzaldehyde was reacted with propynyl magnesium bromide to form an intermediate aromatic alkyne-alcohol. The intermediate was subsequently oxidised under Jones' oxidation conditions to give the resultant ketone product. The product was purified *via*

column chromatography and vacuum distillation to yield a colourless oil which was characterised by ^1H NMR, ^{13}C NMR and FT-IR spectroscopy (Figure 7.15).



Scheme 7.4. Synthetic route utilised for the synthesis of 1-phenyl but-2-yn-1-one.³⁶

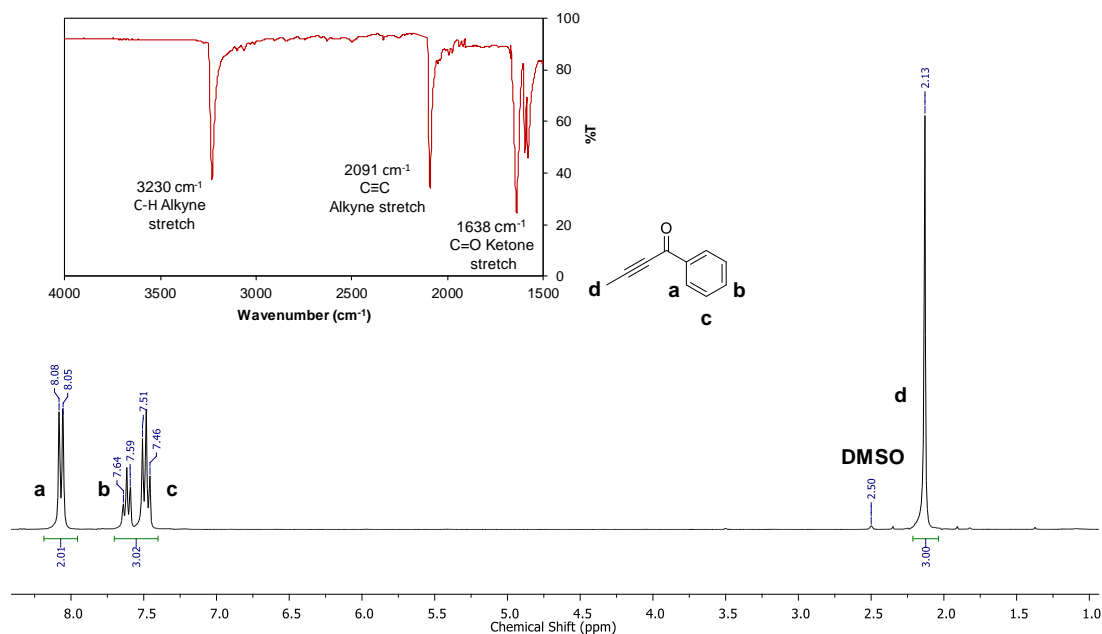
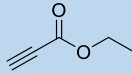
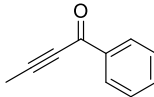
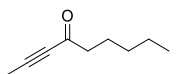


Figure 7.15. ^1H NMR spectrum for 1-phenyl but-2-yn-1-one (298 K, CDCl_3 , 300 MHz) with insert showing the FT-IR spectrum for 1-phenyl but-2-yn-1-one.

The initial rate of the thiol-yne reaction with 1-phenyl but-2-yn-1-one was calculated as $2.6 \pm 0.008 \times 10^{-4} \text{ s}^{-1}$, much slower than the rate of the ester-alkyne (ethyl propiolate) (Table 7.4). This result was surprising as the adjacent aromatic ketone was expected to make the alkyne more electron deficient as shown with PPO (Section 7.2.1.1). However, this study highlighted the influence the terminal-alkyne group has on the reactivity of the ketone alkyne in combination with an aromatic ring. The methyl group

increased the electron density around the alkyne and as a consequence increased the rate of the thiol-yne reaction compared to the ester-alkyne with a terminal proton. Furthermore, the bulky planar aromatic ring, coupled with a ketone reduced the bond rotation in the molecule and further hindered the thiolate ion from attacking making the reaction much less favourable and therefore presents a slow initial reaction rate compared to the ester-alkyne. This also impacted the stereochemistry of the vinyl thioether product as attack on the same side of the alkyne by a thiol-base hydrogen bonded pair was therefore not favoured, even when the conditions for *E* isomer formation were employed (NEt₃, CHCl₃). This result was confirmed by ¹H NMR spectroscopy which revealed that formation of the *Z* vinyl thioether was favoured in the reaction (68:32 *Z*:*E* ratio) (Figure 7.16).

Table 7.4. Effect of the adjacent functional group on rate of the nucleophilic thiol-yne reaction

Name	Structure	Functional group	[NEt ₃] (mM)	Rate (s ⁻¹)	Normalised rate (s ⁻¹ mM ⁻¹)	Relative rate ^a	<i>Z</i> : <i>E</i> ratio
Ethyl propiolate		Ester	21	4.2 ± 2	0.2 ± 0.1	2516	13:87
1-phenyl but-2-yn-1-one		Aromatic ketone + terminal methyl	839	0.02 ± 0.007	2.6 ± 0.08 × 10 ⁻⁴	1901951	68:32
Non-2-yn-4-one		Ketone + terminal methyl	87	0.02 ± 0.002	2.1 ± 0.2 × 10 ⁻⁴	2451916	55:45

^aRelative to phenyl-2-propyn-1-one

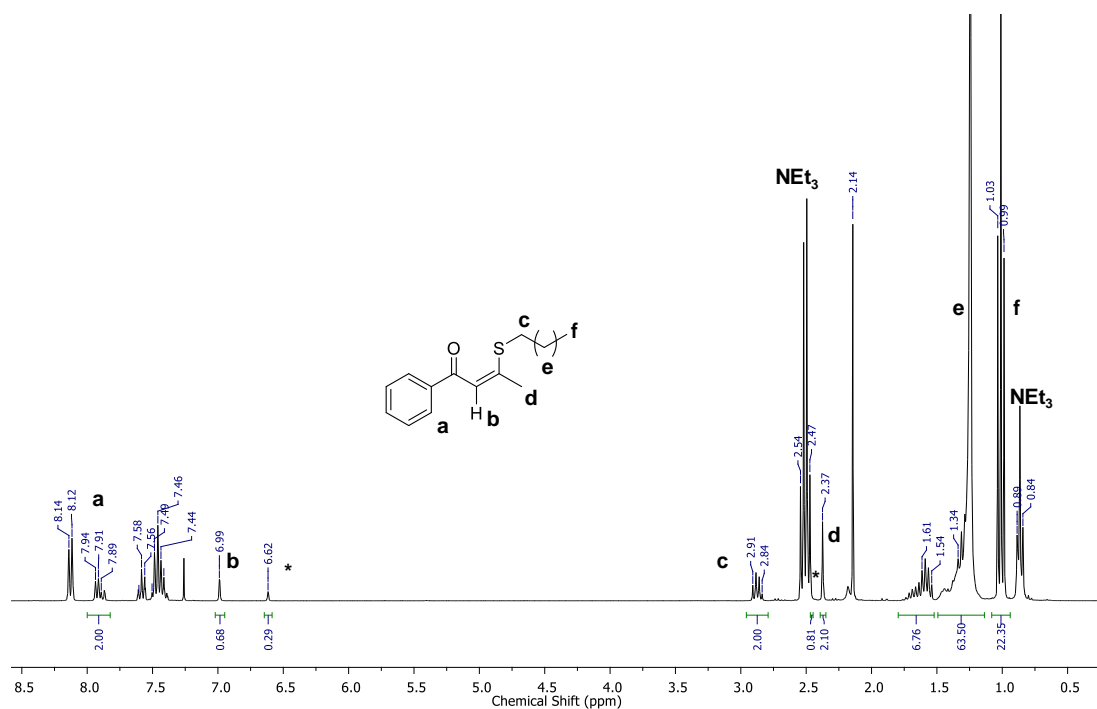
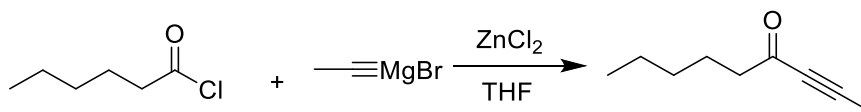


Figure 7.16. The thiol-yne product of 1-Phenyl but-2-yn-1-one with DT in the presence of NEt₃ in CDCl₃, *=Z isomer, (298 K, CDCl₃, 400 MHz).

To reduce the steric hindrance in an attempt to increase the rate of the thiol-yne reaction with a methyl-terminated alkyne, an alkyl ketone with a methyl-terminated alkyne, non-2-yn-4-one was synthesised (Scheme 7.5). Hexanoyl chloride was reacted with propynyl magnesium bromide to form the required alkyl ketone alkyne and purified by column chromatograph and vacuum distillation. The product was characterised by ¹H NMR, ¹³C NMR and FT-IR spectroscopy (Figure 7.17).



Scheme 7.5. Reaction scheme for the synthesis of Non-2-yn-4-one.

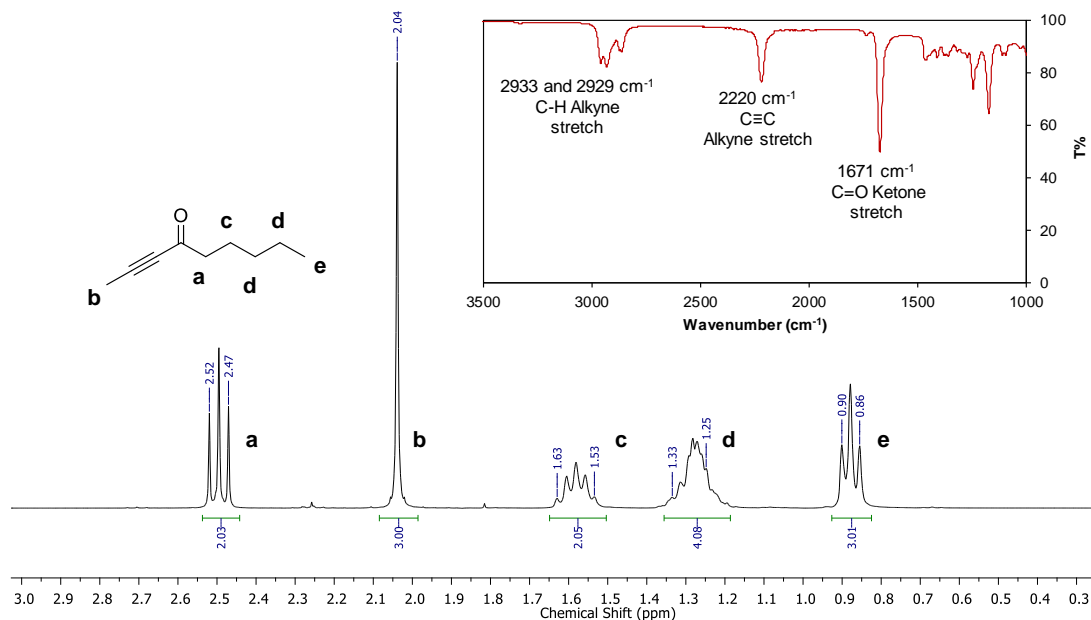


Figure 7.17. ¹H NMR spectrum of Non-2-yn-4-one (298 K, (CH₃)₂SO, 300 MHz) with insert showing the FT-IR spectrum of non-2-yn-4-one.

However, when reacted with DT, the alkyl ketone with methyl-terminated alkyne (non-2-yn-4-one) the initial rate of the thiol-yne reaction, $2.1 \pm 0.2 \times 10^{-4} \text{ s}^{-1}$ was a similar rate to 1-phenyl but-2-yn-1-one and much slower than ester-alkyne (ethyl propiolate). Yet the formation of the *Z* isomer was reduced (55:45 *Z:E* ratio). This result reflected the significant role steric hindrance plays in the rate of the reaction and the stereochemistry of the resultant product. For hydrogel synthesis, it is postulated that the rate reducing methyl-terminated alkyne would reduce the rate of an alkyl ketone PEG precursor in a thiol-yne reaction enabling easier production and handling of the hydrogels compared to the current ester-alkyne hydrogels. In addition, it would be easier to synthesise onto a PEG chain than the aromatic ketone. Therefore, it was a suitable candidate for the synthesis of thiol-yne PEG hydrogels with improved degradation properties using precursors that should be less cytotoxic (section 7.2.2).

Overall, the thiol-yne kinetic study has shown that the presence of different functional groups adjacent to the alkyne significantly influenced the rate of the nucleophilic thiol-yne reaction (Figure 7.18) and the stereochemistry of the resultant vinyl thioether product. This study was fundamental to understanding how to synthesise thiol-yne hydrogels with improved degradation and swelling profiles without impacting their robust mechanical properties.

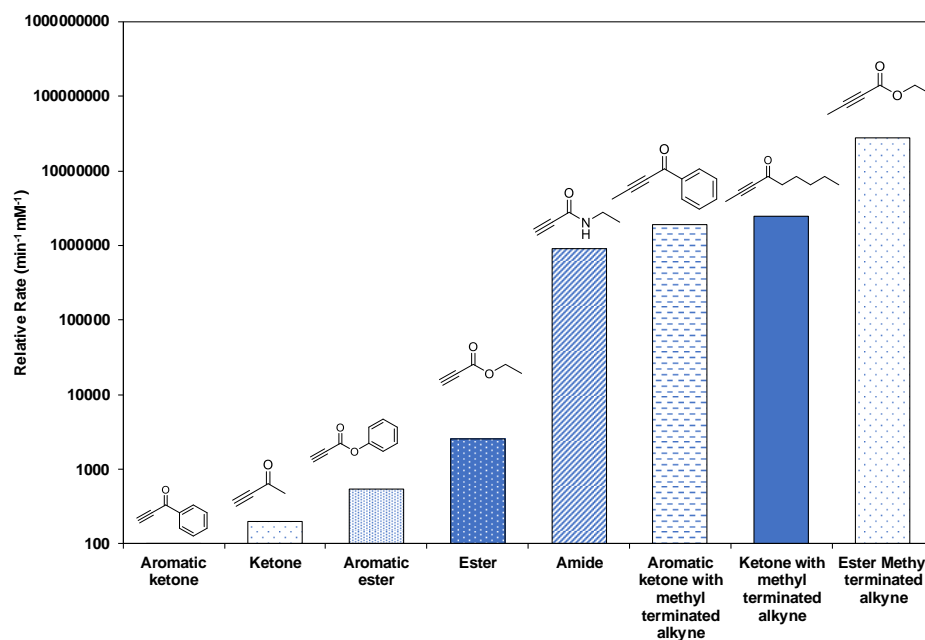


Figure 7.18. Relative rates of nucleophilic thiol-yne reaction with a range of small molecule alkynes reacted with DT in the presences of NEt₃ in CDCl₃.

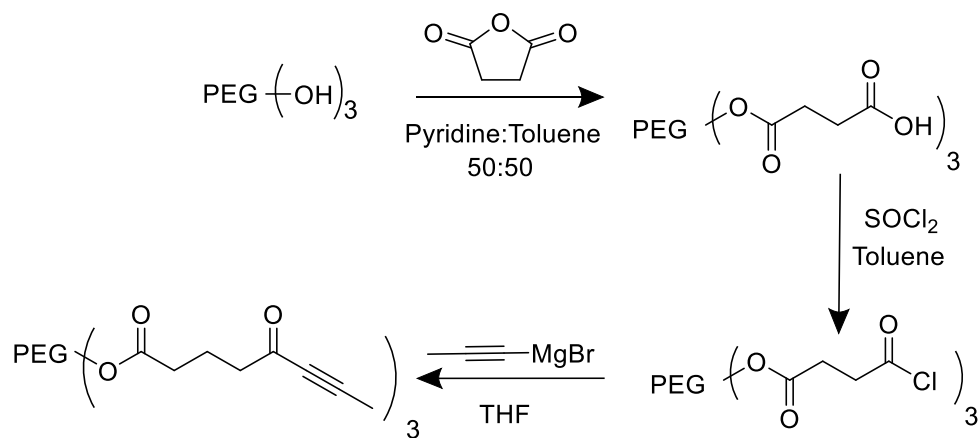
7.2.2. Methyl-Terminated Alkyne Ketone PEG Thiol-yne Hydrogels

The thiol-yne kinetic study demonstrated that the rate of the thiol-yne reaction could be easily tuned through modification of the activating group adjacent to the alkyne or through the substitution of the terminal alkyne-proton with a methyl group. The alkyl ketone with a methyl-terminated alkyne, non-2-yn-4-one, was found to incorporate the ideal functionality to tune the rate of the reaction to a similar value as was observed for

the original ester chemistry. Therefore, it was selected as a potential candidate for the synthesis of thiol-yne hydrogels from a less toxic PEG alkyne precursor with improved degradation and swelling profiles.

7.2.2.1. *Synthesis of Methyl-Terminated Alkyne PEG Ketone Precursor via a Succinic Anhydride Grignard Reaction*

To synthesise a methyl-terminated alkyne with ketone functionality, glycerol ethoxylate (3-arm PEG, 1 kg mol^{-1}) was functionalised with succinic anhydride to form a PEG functionalised carboxylic acid following a previous reported procedure.³⁷ The 3-arm PEG carboxylic acid was converted to an acyl chloride using thionyl chloride (SOCl_2) and a subsequent Grignard reaction was carried out with propynyl magnesium bromide to form the desired ketone alkyne functionality (Scheme 7.6). The product was purified by column chromatograph and dialysis to remove any unreacted PEG and undesired product colouration. The product was characterised by ^1H NMR, FT-IR spectroscopy and SEC analysis (Figure 7.19 and 7.20).



Scheme 7.6. Synthetic route utilised to synthesise a ketone-functional 3-arm PEG (1 kg mol^{-1}) with a methyl-terminated alkyne.

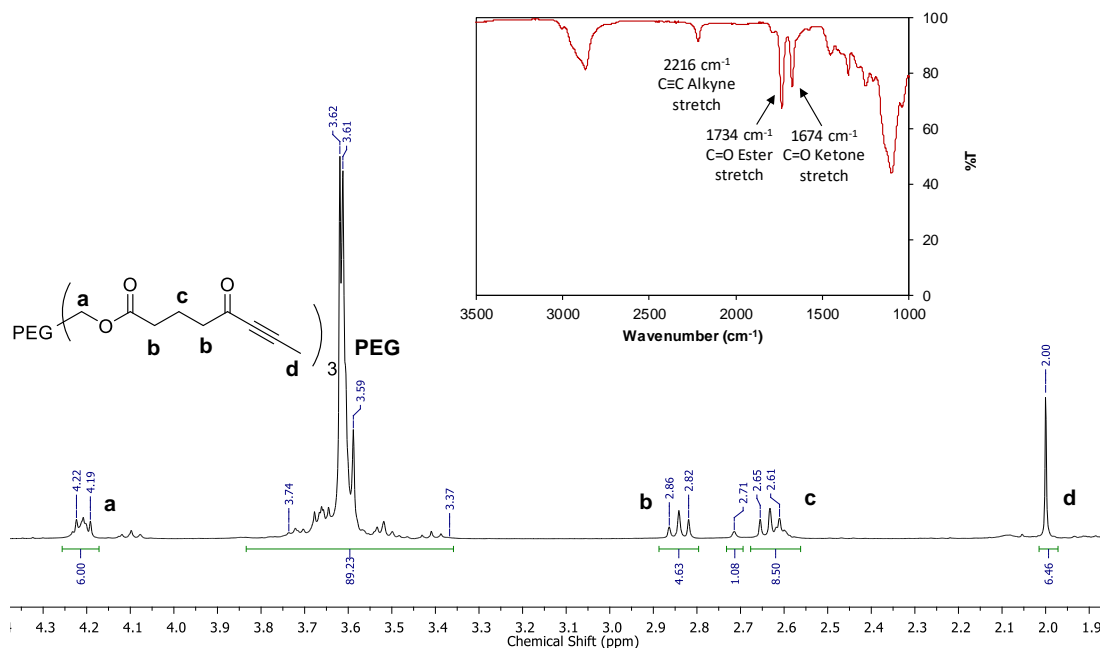


Figure 7.19. ^1H NMR of the ketone-functional 3-arm PEG with a methyl-terminated alkyne, (298 K, CDCl_3 , 300 MHz) with insert showing the FT-IR of the ketone-functional 3-arm PEG with a methyl-terminated alkyne.

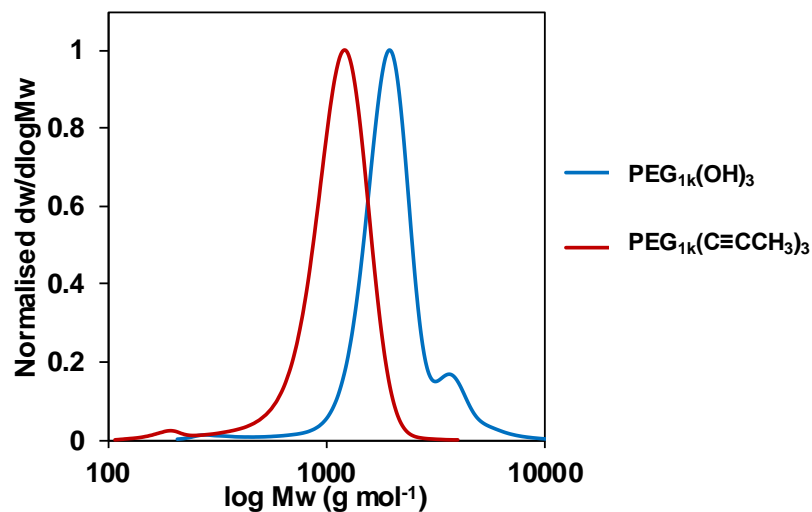
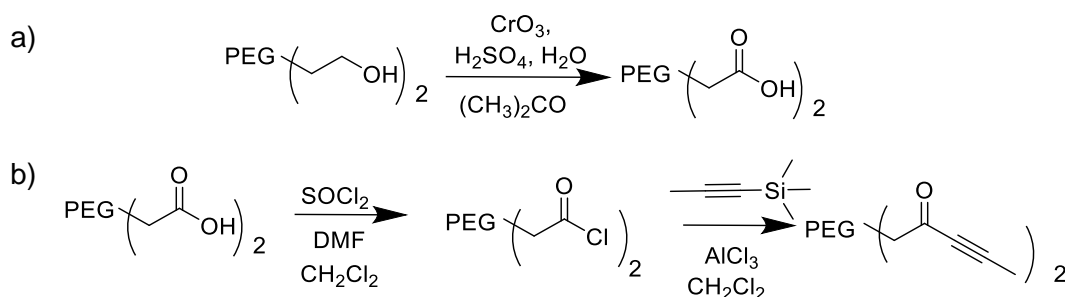


Figure 7.20. SEC analysis of the ketone-functional 3-arm PEG with a methyl-terminated alkyne (1 kg mol^{-1}). Molecular weight was determined against polystyrene standards using CHCl_3 (0.5% NEt_3) as the eluent.

Once synthesised, the purified ketone-functional PEG with a methyl-terminated alkyne was used as an alkyne precursor to form thiol-yne hydrogels with a 4-arm PEG thiol, synthesised previously (Chapter 3, Section 3.2.1). The alkyne:thiol ratio was kept at 1:1 and the polymer content was maintained at 10 wt% PBS solution. Gelation occurred in 30 min (measured *via* vial tilt method) which was longer than the ester thiol-yne PEG hydrogel synthesis (gel time = 10 min). The increase in gelation time could have been caused by the low purity of the ketone-functional PEG with methyl-terminated alkyne. Although the alkyne precursor was purified by column chromatography and dialysis, the ^1H NMR spectra revealed additional signals in the spectrum which indicated that additional PEG environments were present in the product (Figure 7.19). These impurities may have contributed to the increased gelation time as fewer crosslinking groups were available, therefore resulting in inferior materials. Moreover, the synthetic route chosen formed an ester linkage which would have been subjected to hydrolysis if the thiol-yne hydrogel were immersed in an aqueous environment. It is therefore postulated that the hydrogels would still have increased degradation and swelling rates. Therefore, the ketone hydrogels synthesised following this method would be inadequate for the desired biomaterial application. This highlighted the need of a synthetic route for the ketone synthesis which would avoid ester formation and reduce the number of side reactions occurring in the ketone synthesis.

7.2.2.2. Synthesis of Methyl-Terminated Alkyne PEG ketone Precursor via Friedel-Crafts Acylation

The new synthetic scheme chosen oxidised the hydroxyl groups on a 2-arm PEG (2 kg mol⁻¹) to form a 2-arm PEG carboxylic acid and avoided the formation of any ester linkage (Scheme 7.7a). The resultant PEG carboxylic acid was subsequently converted to ketone through a Friedel Crafts acylation with 1-(trimethylsilyl)propyne following a previously reported procedure (Scheme 7.7b).³⁸ The crude product was characterised by ¹H NMR and FT-IR spectroscopy (Figure 7.21) which revealed low conversion to the desired product (14% conversion calculated using the singlet at $\delta = 1.81$ ppm).



Scheme 7.7. Synthetic route to form the ketone-functional PEG with a methyl-terminated alkyne; a) Jones' oxidation to form PEG carboxylic acid, b) Thionyl chloride acylation followed by a Friedel-Crafts acylation reaction to form the PEG ketone-functionality.

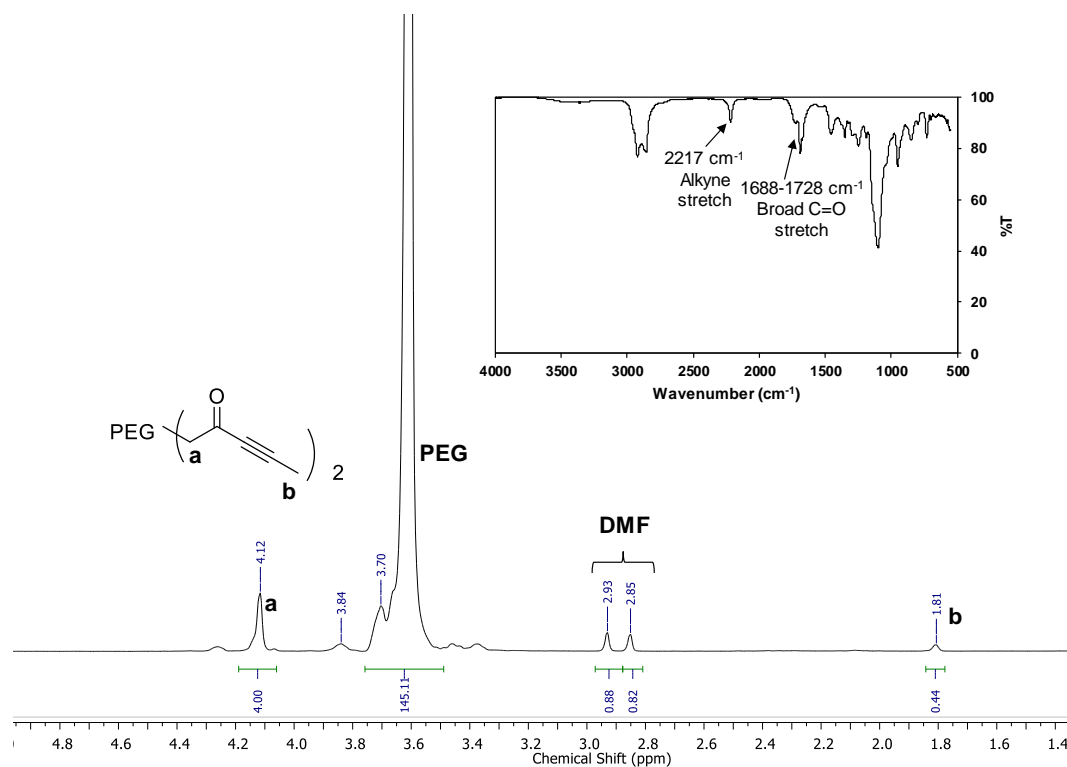
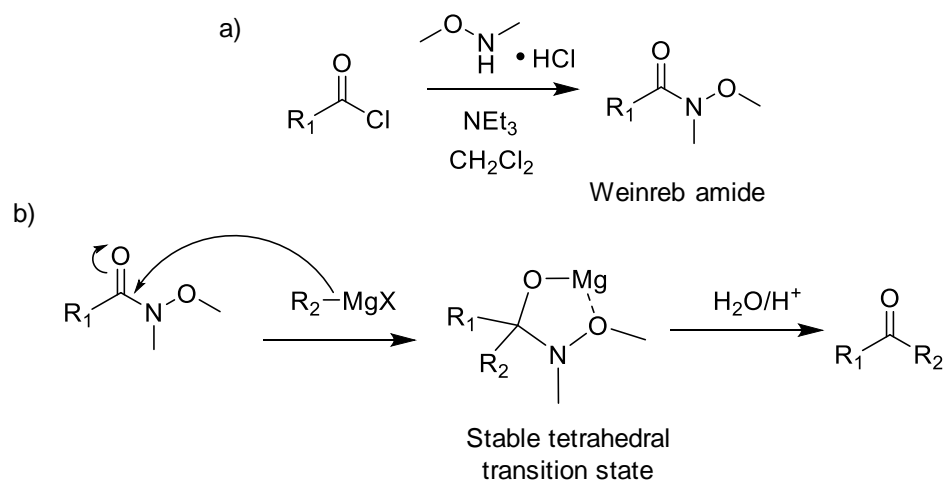


Figure 7.21. ¹H NMR spectrum for the ketone-functional PEG with a methyl-terminated alkyne synthesised through Friedel-Crafts acylation, (298 K, CDCl₃, 300 MHz) with insert showing the FT-IR spectrum for the ketone-functional PEG with a methyl-terminated alkyne.

It was hypothesised that the low conversion was a result of the relatively high molecular weight of the polymer starting material (2 kg mol⁻¹). Although the synthetic procedure was modified to accommodate the PEG precursor, the route was not effective in forming highly functionalised materials. Furthermore, removal of unreacted PEG proved to be very difficult as the polarity and solubility of the functionalised PEG was very similar to the PEG precursor. Therefore, this synthetic route was also not a viable option to functionalise PEG with a ketone functional group. A new synthetic route that allowed a higher conversion to be obtained was necessary.

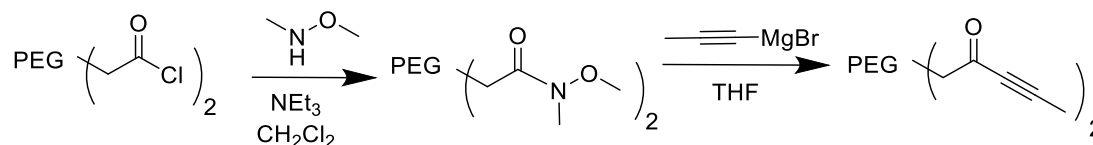
7.2.2.3. Synthesis of Methyl-Terminated Alkyne PEG Ketone Precursor through a Weinreb Amide Synthetic Route

A synthetic route was designed to utilise an intermediate Weinreb amide in order to increase the conversion of PEG hydroxyl groups to methyl-terminated alkynes through a ketone linker. The use of a Weinreb amide intermediate as a precursor for a Grignard reaction is well known in the literature for being high yielding in the synthesis of small molecules (*i.e.* 84-96% yields).³⁹ This is a result of the formation of a favoured tetrahedral intermediate between the Weinreb amide and the organometallic Grignard reagent (Scheme 7.8). In addition, the mechanism of the reaction is less sensitive to moisture and hence ideal for the functionalisation of PEG which is inherently hydroscopic. Furthermore, as the intermediate transition state is favoured, the number of side reactions are reduced which in turn increases the conversion to the desired product.



Scheme 7.8. a) Synthesis of a Weinreb amide; b) mechanism for the selective formation of a ketone from a Weinreb amide and Grignard reagent, R = alkyl group.

As a result, the functionalised 2-arm PEG acyl chloride, synthesised *via* the same route previously stated (section 7.2.3.2, Scheme 7.7b), was reacted with *N,O*-dimethylhydroxylamine hydrochloride in the presence of NEt_3 and CH_2Cl_2 to form a 2-arm PEG Weinreb amide. The PEG Weinreb amide was subsequently reacted with propynyl magnesium bromide in a Grignard reaction to form the ketone-functionality (Scheme 7.9). The intermediate reaction steps were characterised by ^1H NMR, ^{13}C NMR, FT-IR spectroscopy and SEC analysis in order to confirm that each step went to a high conversion.



Scheme 7.9. Synthetic route to synthesise a methyl-terminated alkyne ketone-functionalised PEG precursor *via* a Weinreb amide.

Analysis of the $\text{PEG}_{2k}(\text{COOH})_2$ confirmed the presence of a carboxylic acid functionality in the intermediate product (Figure 7.22). Analysis of the acyl chloride reaction showed a small signal at 4.02 ppm in the ^1H NMR spectrum for $\text{PEG}_{2k}(\text{COCl})_2$ suggesting that a residual amount of $\text{PEG}_{2k}(\text{COOH})_2$ was present (Figure 7.23). However, its presence could be attributed to the instability of acyl chlorides where a small amount of the product could have degraded as the sample was exposed to moisture during analysis. As such, the $\text{PEG}_{2k}(\text{COCl})_2$ was reacted *in situ* to form the PEG Weinreb amide under anhydrous conditions, to increase the conversion to the Weinreb amide.

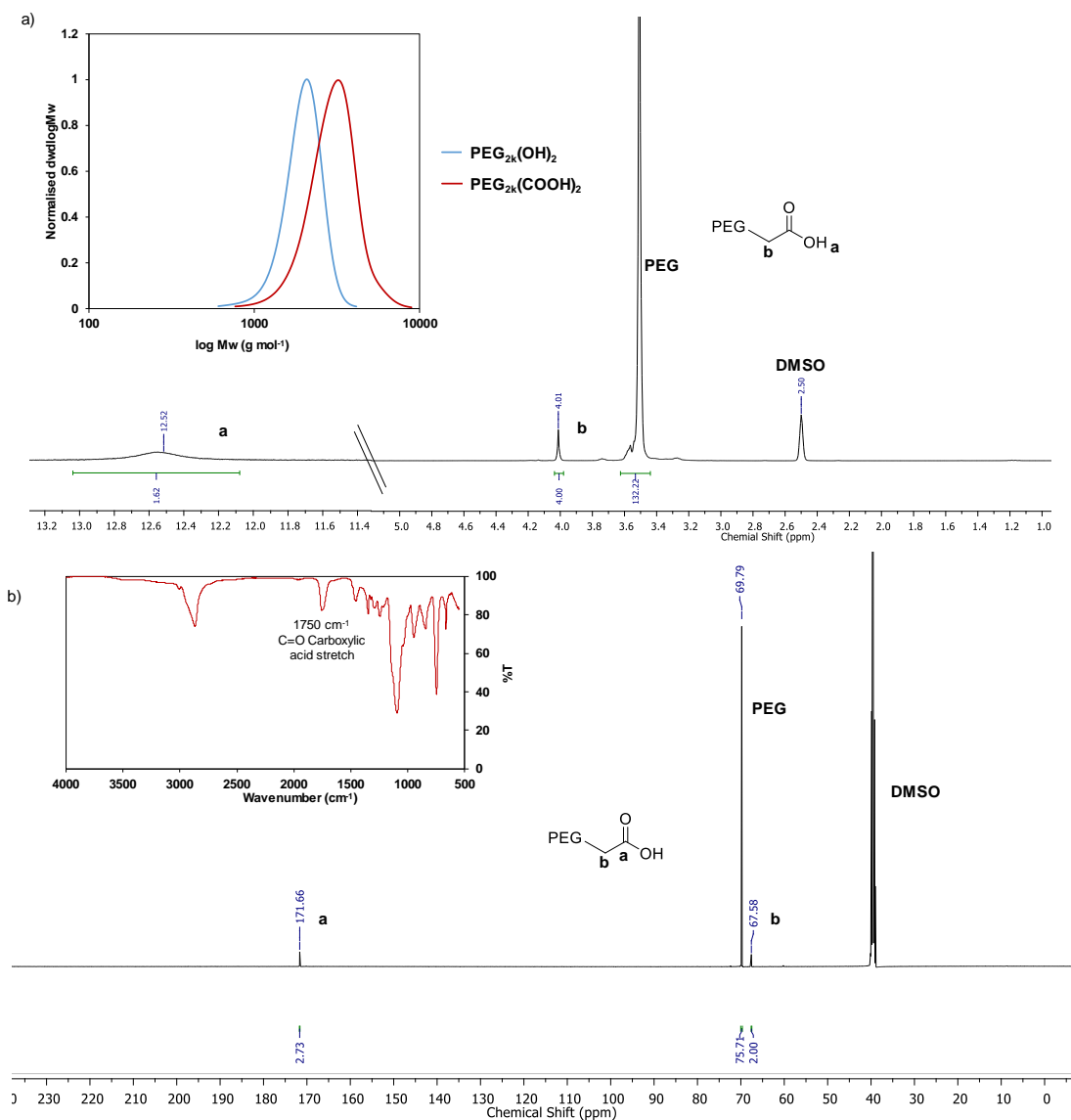


Figure 7.22. ¹H NMR spectrum of 2-arm PEG_{2k}(COOH)₂ functionalised through Jones oxidation, (298 K, (CH₃)₂SO), 300 MHz) with insert showing the SEC analysis of 2-arm PEG(COOH) (2 kg mol⁻¹) Molecular weight was determined against PEG standards using H₂O: CH₃OH (80:20 ratio) as the eluent; b) quantitative ¹³C NMR spectrum of 2-arm PEG_{2k}(COOH)₂ with insert showing the FT-IR spectrum of 2-arm PEG_{2k}(COOH)₂, (298 K, (CH₃)₂SO), 500 MHz).

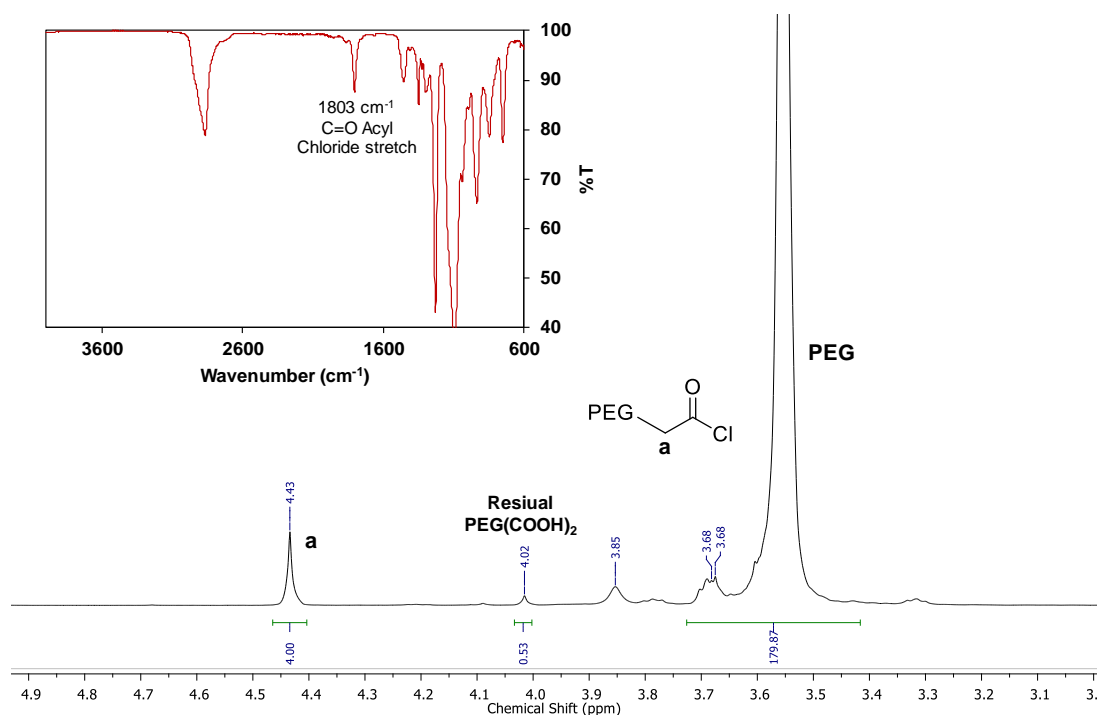


Figure 7.23. ^1H NMR spectrum for 2-arm $\text{PEG}_{2k}(\text{COCl})_2$, (298 K, CDCl_3 , 300 MHz), with Insert showing the FT-IR spectrum of 2-arm $\text{PEG}_{2k}(\text{COOH})_2$.

Characterisation of the PEG Weinreb amide confirmed a high conversion to the desired product (>99% by ^1H NMR spectroscopy) (Figure 7.24). However, a small amount of $\text{PEG}_{2k}(\text{COOH})_2$ was detected in the FT-IR spectrum (1750 cm^{-1}) in addition to two carbonyl shifts in the ^{13}C NMR spectrum ($\delta = 171$ and 107 ppm) which suggested that $\text{PEG}_{2k}(\text{COOH})_2$ was also present. However, analysis by quantitative ^{13}C NMR spectroscopy showed only a low amount of $\text{PEG}_{2k}(\text{COOH})_2$ was present (16%). Attempts to remove this impurity or to convert it to the desired product were unsuccessful. Consequently, the impure PEG Weinreb amide was used in the next step to synthesise the PEG ketone.

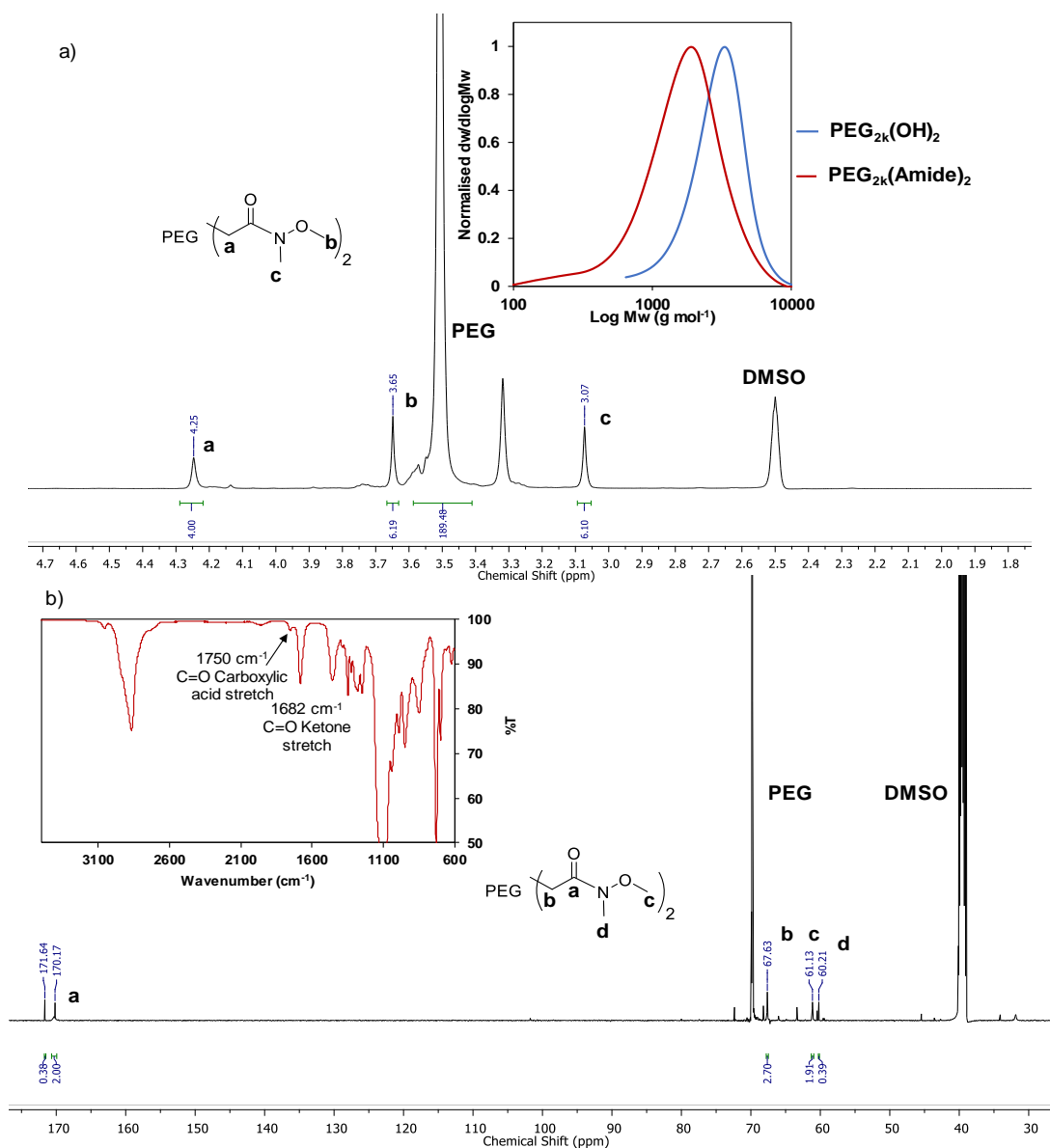


Figure 7.24. ^1H NMR spectrum of 2-arm PEG Weinreb amide, (298 K, $(\text{CH}_3)_2\text{SO}$), 300 MHz), with insert showing SEC analysis of 2-arm PEG Weinreb amide (2 kg mol^{-1}) Molecular weight determined against PEG standards using $\text{H}_2\text{O}:\text{CH}_3\text{OH}$ (80:20 ratio) as eluent, b) Quantitative ^{13}C NMR spectrum of 2-arm PEG Weinreb amide, (298 K, $(\text{CH}_3)_2\text{SO}$), 500 MHz), with insert showing FT-IR spectrum of 2-arm PEG Weinreb amide.

The final step of the synthesis required the formation of a methyl-terminated alkyne PEG with ketone-functionality. A Grignard reaction was carried out between propynyl magnesium bromide and the functionalised PEG Weinreb amide under anhydrous conditions and the resultant product characterised by ^1H NMR, ^{13}C NMR, FT-

IR spectroscopy and SEC analysis (^1H NMR indicated >99% conversion) (Figure 7.25 and 7.26). Impurities were detected in the final product identified by a singlet at $\delta = 1.8$ ppm in the ^1H NMR and a high molecular weight shoulder in the SEC analysis. Furthermore, the quantitative ^{13}C NMR spectrum revealed numerous additional signals which suggested further impurities were also present in the final product. Additional purification was carried out including column chromatography and dialysis however they were unsuccessful but confirmed the impurities to be different PEG populations because of their similar polarity and molecular weight. Thus, the impure product was used in preliminary attempts to make hydrogels.

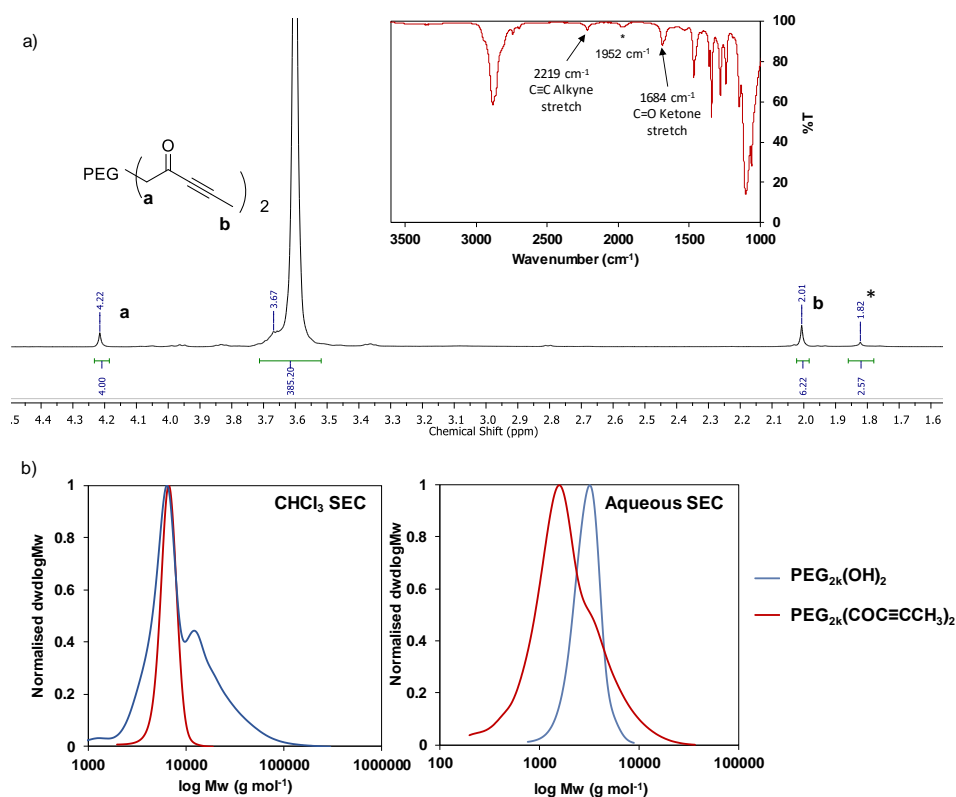


Figure 7.25. a) ^1H NMR spectrum of the methyl-terminated PEG ketone, (298 K, CDCl_3 , 300 MHz) with Insert showing the FT-IR spectrum of the methyl-terminated PEG ketone, *= impurity, b) SEC analysis of the methyl-terminated PEG ketone (2 kg mol^{-1}) by CHCl_3 SEC (LHS) Molecular weight was determined against polystyrene standards using CHCl_3 (0.5% NEt_3) as the eluent, and aqueous SEC analysis (RHS) molecular weight was determined against PEG standards using $\text{H}_2\text{O}:\text{CH}_3\text{OH}$ (80:20 ratio) as the eluent.

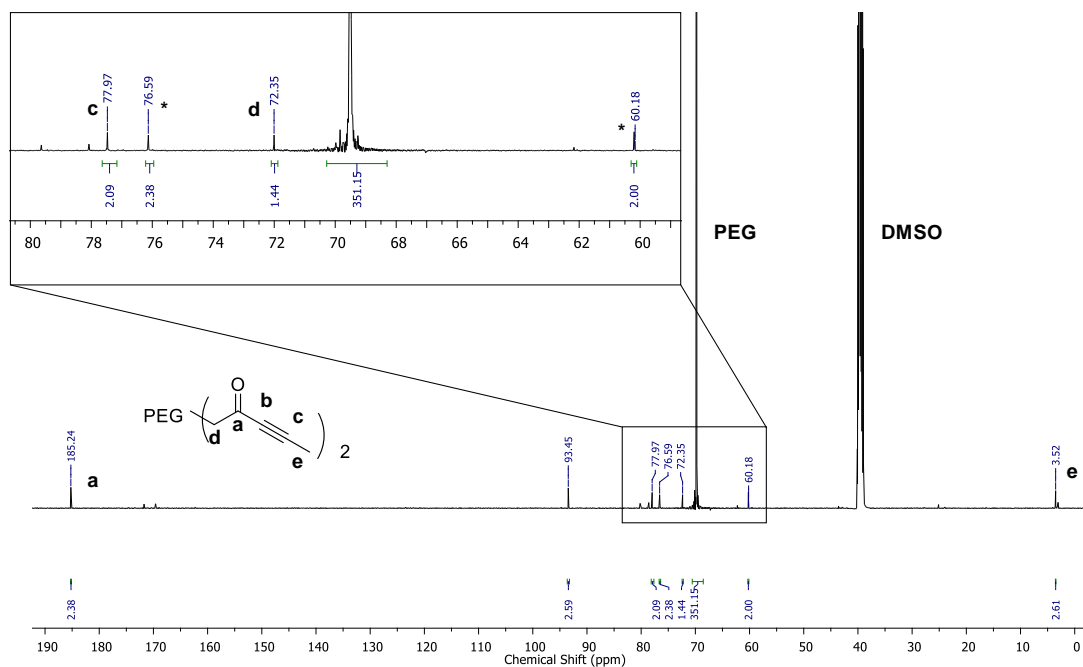


Figure 7.26. Quantitative ^{13}C NMR spectrum of the methyl-terminated PEG ketone precursor, *= impurities, (298 K, $(\text{CH}_3)_2\text{SO}$, 500 MHz).

7.2.2.4 Synthesis and Characterisation of Thiol-yne PEG Hydrogels Synthesised using a Methyl-Terminate Alkyne PEG Ketone.

Thiol-yne hydrogels were synthesised with the methyl-terminated alkyne PEG ketone precursor (2 kg mol^{-1}) with a 3-arm PEG thiol precursor (1 kg mol^{-1}), previously characterised (Chapter 3, Section 3.2.1). The precursors were made at 10 and 20 wt% polymer content with a 1:1 alkyne:thiol ratio; however, no gelation occurred. ^1H NMR and FT-IR spectroscopy of the solution revealed the reaction had occurred, indicated by the ^1H NMR signals at $\delta = 6.78$ and 2.63 ppm corresponding to the vinyl proton and methyl group respectively. The FT-IR spectrum revealed the disappearance of the alkyne stretch at 2218 cm^{-1} and the presence of an alkene stretch at 1538 cm^{-1} which confirmed the formation of a vinyl thioether (Figure 7.27 and 7.28). However, no gelation or

increased viscosity of the solution was observed as there was insufficient crosslinking points for network formation.

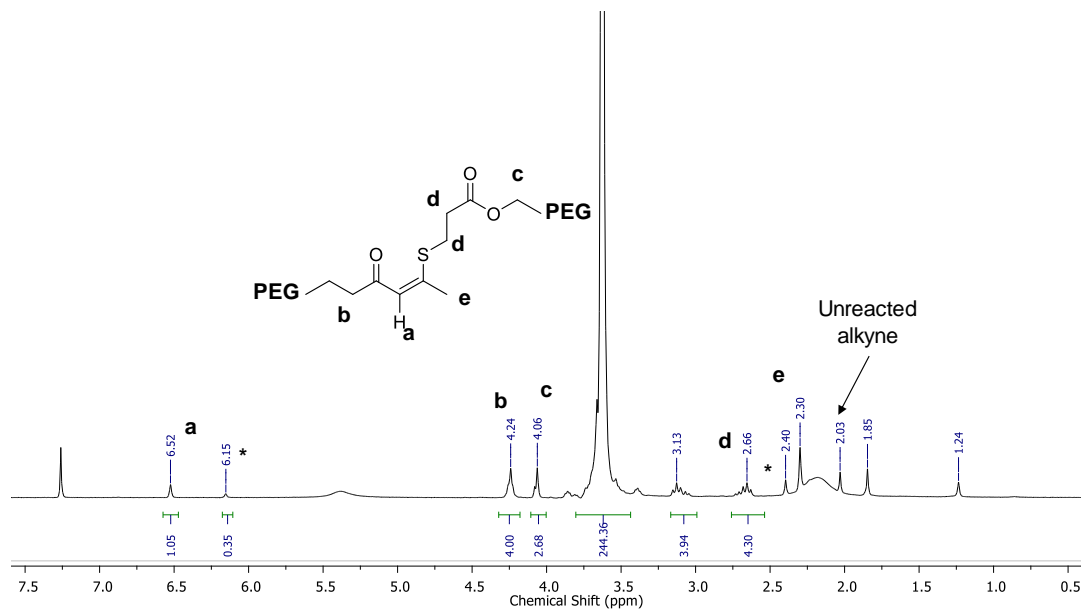


Figure 7.27. ^1H NMR spectrum of the methyl-terminated alkyne PEG ketone precursor reacting with 3-arm PEG thiol in PBS solution at 10 wt%, *= *E* isomer, (298 K, CDCl_3 , 300 MHz).

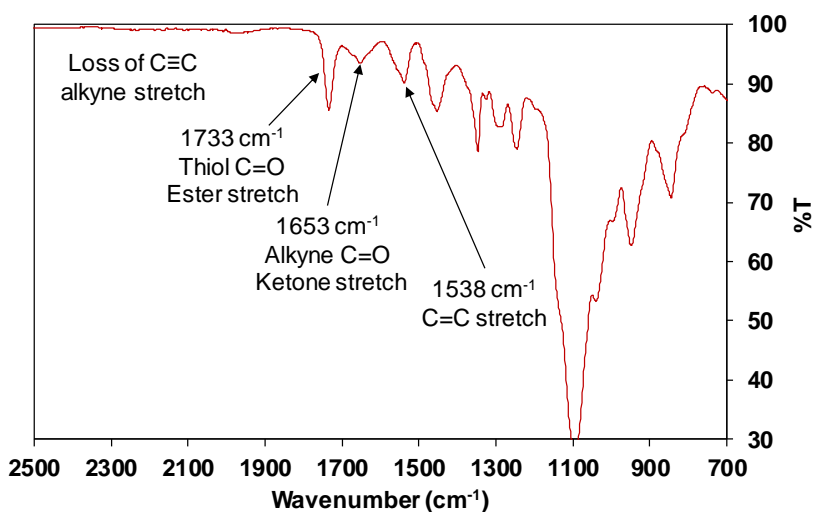


Figure 7.28. FT-IR spectrum of the vinyl thioether PEG product when the methyl-terminated alkyne PEG ketone was reacted with 4-arm PEG thiol in PBS solution (1:1 ratio, 10 wt%).

This experiment highlighted that very high functionalisation and purity of the PEG precursors was necessary for the hydrogel synthesis. Additionally, the synthetic route

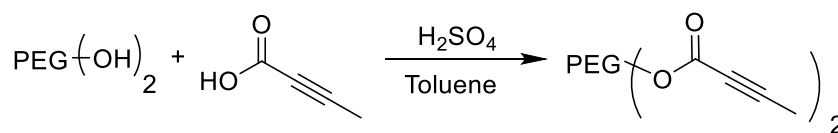
chosen was moisture sensitive and contained multiple steps. As a result, the final product synthesised was unable to form hydrogels. Another synthetic route to form a PEG alkyne precursor with improved characteristics was therefore explored.

7.2.3. Methyl-Terminated Alkyne Ester-PEG Thiol-yne Hydrogels

In the small molecule thiol-yne kinetic study the substitution of a methyl group on the terminal alkyne was found to decrease the rate of the thiol-yne reaction (Section 7.2.1.2). Therefore, as the methyl-terminated alkyne PEG ketone precursor did not form hydrogels (Section 7.3.2.4), the formation of ester-functional thiol-yne hydrogels with methyl-terminated alkynes was investigated.

7.2.3.1. Synthesis of Methyl-Terminated Alkyne Ester-PEG Precursors

Through simple Fischer esterification reactions, similar to previous PEG functionalisation reactions (Chapters 2, Section 2.2.1), 2-arm PEG (1 kg mol^{-1}) was reacted with butynoic acid (Scheme 7.10) to synthesise a methyl-terminated alkyne ester PEG precursor. The product was fully characterised by ^1H NMR, ^{13}C NMR spectroscopy and SEC analysis (Figure 7.28).



Scheme 7.10. Fischer esterification reaction to functionalise PEG with butynoic acid to form an ester-activated methyl-terminated alkyne.

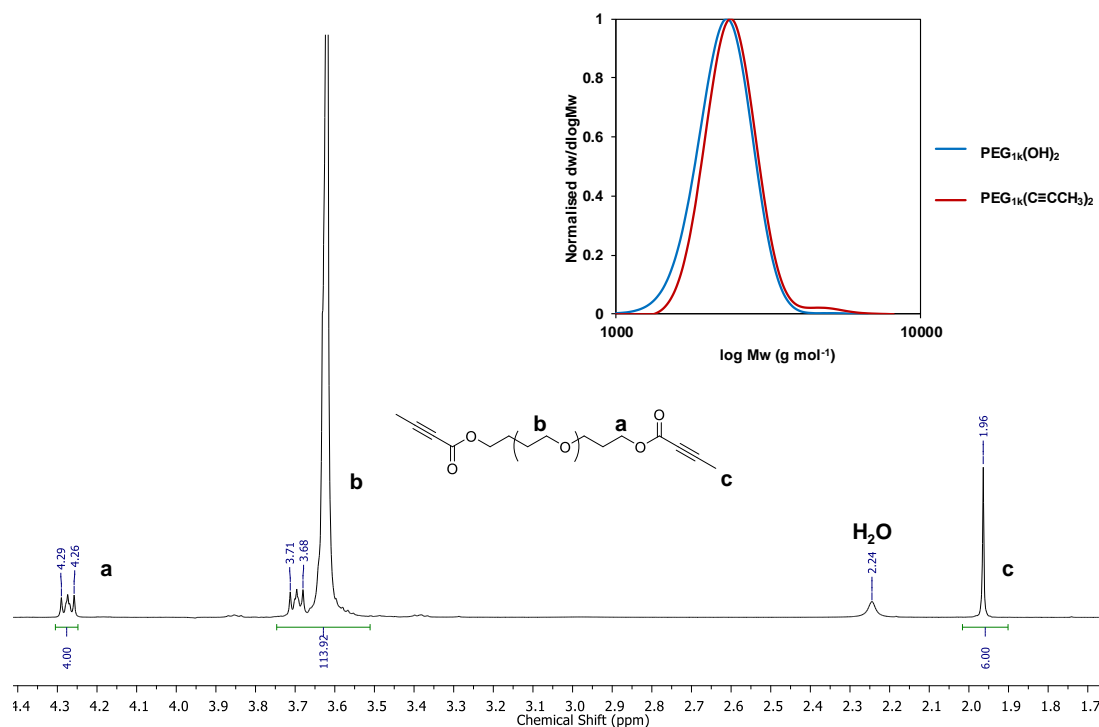


Figure 7.29. ¹H NMR spectrum of 2-arm ester-PEG functionalised with methyl-terminated alkyne end groups, (298 K, CDCl₃, 300MHz) with insert showing a SEC chromatogram of 2-arm PEG methyl-terminated alkyne precursors (1 kg mol⁻¹). Molecular weight was determined against PMMA using DMF (5 mM NH₄BF₄) as the eluent.

7.2.3.2. Characterisation of Methyl-Terminated Alkyne Thiol-yne PEG Hydrogels

Once synthesised, the 2-arm ester-functionalised PEG methyl-terminated alkyne was investigated as an alkyne precursor for the synthesis of thiol-yne PEG hydrogels. Two hydrogel systems, utilising 3- or 4-arm PEG thiol architectures (1 and 2 kg mol⁻¹ respectively) were synthesised as described Chapter 3, Section 3.2.1 to give **2_{1A}3_{1S}** and **2_{1A}4_{2S}** hydrogels (nomenclature explained in Chapter 2, Section 2.2.2). The methyl-terminated PEG alkyne was dissolved in PBS solution (pH 7.4) (10 wt%) and reacted in a 1:1 molar ratio with either the 3-arm PEG thiol (1 kg mol⁻¹) or 4-arm PEG thiol (2 kg mol⁻¹) dissolved to 10 wt% in PBS solution (final concentration = 10 wt%). Unfortunately,

no gelation occurred after 24 h with either of the PEG thiol precursors. Gelation time was reduced by increasing the pH of the solution using a Trizma® buffer solution (pH 8). At 20 wt% the **2_{1A}4_{2S}** hydrogel formed in 25 min and could be repeatedly compressed (up to 10 times) with an average maximum compressive stress of 1.2 ± 0.05 MPa at 95% strain (Figure 7.29). It was postulated that the increased gelation time, caused by the reduced reactivity of the alkyne, allowed mobility of PEG precursors before the solution became too viscous and restricted the movement of chain ends.¹³ As a result, more crosslinking sites were formed and a more ‘perfect’ network was created with fewer ‘dangling chain ends’ and defects which enabled the hydrated polymer network to withstand repeated compression.⁴⁰⁻⁴²

Although this system formed robust hydrogels, higher concentrations of polymer were required (*i.e.* 20 wt% vs. 10 wt%). This is a major drawback as high polymer contents would hinder the flow of nutrients and oxygen in and out of the hydrated network making these hydrogels unsuitable as tissue scaffold applications.^{10, 43} This work highlighted the

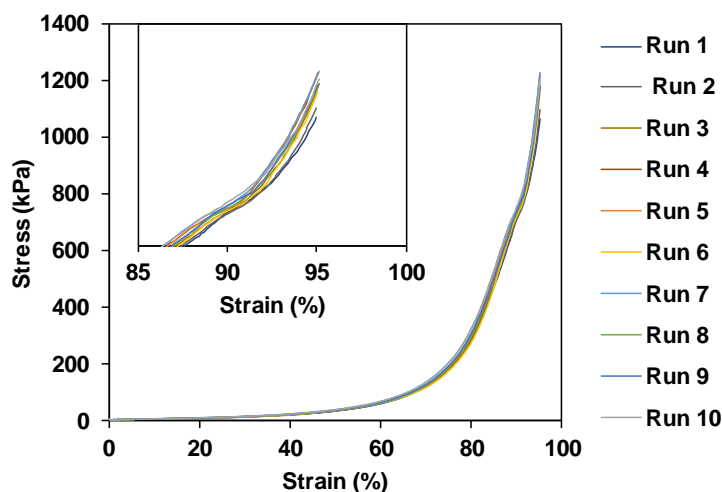


Figure 7.30. Representative stress/strain chart of a **2_{1A}4_{2S}** hydrogel (20 wt%, trizma buffer) to demonstrate repeated compressive strength with insert showing an expanded view of the high strain values and demonstrating little hysteresis occurred with repeated compression.

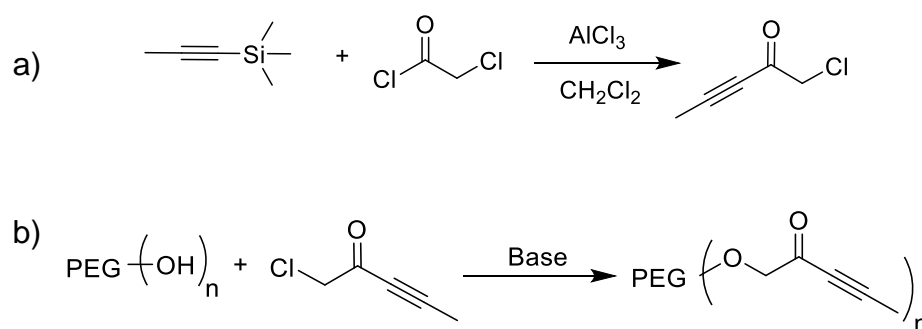
affect the methyl-terminated alkyne ester-functionalised PEG precursor had on the synthesis of robust hydrogels. The increase in pH and polymer content was necessary for the synthesis of these thiol-yne hydrogels however they are not ideal reaction conditions for encapsulating cells inside these materials. To overcome this, new synthetic routes need to utilise a functional linker which is not susceptible to hydrolysis and thus allowing the use of a proton-terminated alkyne. This would enable a proton-terminated alkyne to be used facilitating fast gelation times under milder conditions.

7.3. Conclusions

The crosslinking chemistry used to form hydrogel materials can dictate many of the characteristics of the resultant hydrogel. Improving hydrogel characteristics can lie within the chemistry used to synthesise the material. In this chapter, the rate of the nucleophilic thiol-yne reaction has been studied with different small molecule alkynes in an attempt to improve the swelling and degradation profiles of the ester-functionalised thiol-yne PEG hydrogels. The rate of the reaction increased when the activating group, adjacent to the alkyne, drew electrons away from the triple bond (*e.g.* ketones or aromaticity) and therefore made it more reactive to a thiolate ion. Interestingly, the adjacent functional groups also dictated the stereochemistry of the resultant thiol-yne products through stabilisation of the intermediate transition states and the resultant accessibility of the alkyne. The addition of a methyl group to the terminated alkyne resulted in the alkyne being less susceptible to attack from a thiolate ion and therefore reduced the rate of the thiol-yne reaction. Through this study, the methyl-terminated alkyne activated by an adjacent alkyl ketone was found to be a suitable replacement to the ester chemistry currently used to synthesise thiol-yne hydrogels. However, although different synthetic routes were attempted, the synthesis of a pure PEG ketone with a methyl-terminated alkyne was unsuccessful. The routes selected prevented the formation of hydrogels with improved characteristics and highlighted the requirements for functionalisation reactions with high conversion to be implemented in the precursor synthesis. Through a successful esterification reaction with 2-butyric acid, methyl-terminated alkynes were synthesised and formed robust hydrogels; however, the elevated

pH conditions and increased polymer contents required were not ideal for the synthesis of new biomaterials.

Hydrogels synthesised using a PEG alkyne precursor with ketone functionality had great potential to improve the degradation and swelling properties of thiol-yne hydrogels as well as improve the toxicity of the PEG alkyne precursor. Further studies in this area should explore new synthetic routes without the need for anhydrous conditions and multiply step reactions. One route which could be utilised to form the required ketone PEG precursor is a Williamson ether reaction. Firstly, a small molecule, 1-chloropent-3-yn-2-one could be synthesised as it has both a methyl-terminated alkyne and ketone functionality.⁴⁴ Once purified, 1-chloropent-3-yn-2-one could be reacted with the hydroxyl group on the PEG chain to create the methyl-terminated alkyne PEG ketone precursor.⁴⁵



Scheme 7.11. New synthetic route for the synthesis of a methyl-terminated alkyne PEG with ketone-functionality, a) synthesis of 1-chloropent-3-yn-2-one, b) Williamson ether reaction to functionalise a PEG hydroxyl group.

7.4. References

1. T. R. Hoare and D. S. Kohane, *Polymer*, 2008, **49**, 1993-2007.
2. C.-C. Lin and A. T. Metters, *Adv. Drug Delivery Rev.*, 2006, **58**, 1379-1408.
3. P. van de Wetering, A. T. Metters, R. G. Schoenmakers and J. A. Hubbell, *J. Control. Release*, 2005, **102**, 619-627.
4. Y. Jiang, J. Chen, C. Deng, E. J. Suuronen and Z. Zhong, *Biomaterials*, 2014, **35**, 4969-4985.
5. K. R. Kamath and K. Park, *Adv. Drug Delivery Rev.*, 1993, **11**, 59-84.
6. J. Li and D. J. Mooney, *Nat. Rev. Mater.*, 2016, **1**, 16071.
7. J. Yu, F. Chen, X. Wang, N. Dong, C. Lu, G. Yang and Z. Chen, *Polym. Degrad. Stab.*, 2016, **133**, 312-320.
8. M. A. Daniele, A. A. Adams, J. Naciri, S. H. North and F. S. Ligler, *Biomaterials*, 2014, **35**, 1845-1856.
9. K. Y. Lee and D. J. Mooney, *Chem. Rev.*, 2001, **101**, 1869-1879.
10. A. S. Hoffman, *Adv. Drug Delivery Rev.*, 2002, **54**, 3-12.
11. N. A. Peppas, J. Z. Hilt, A. Khademhosseini and R. Langer, *Adv. Mater.*, 2006, **18**, 1345-1360.
12. J.-Y. Sun, X. Zhao, W. R. K. Illeperuma, O. Chaudhuri, K. H. Oh, D. J. Mooney, J. J. Vlassak and Z. Suo, *Nature*, 2012, **489**, 133-136.

13. J. L. Drury and D. J. Mooney, *Biomaterials*, 2003, **24**, 4337-4351.
14. S. P. Zustiak and J. B. Leach, *Biomacromolecules*, 2010, **11**, 1348-1357.
15. N. A. Peppas, P. Bures, W. Leobandung and H. Ichikawa, *Eur. J. Pharm. Biopharm.*, 2000, **50**, 27-46.
16. K. S. Anseth, C. N. Bowman and L. Brannon-Peppas, *Biomaterials*, 1996, **17**, 1647-1657.
17. O. Chaudhuri, L. Gu, D. Klumpers, M. Darnell, S. A. Bencherif, J. C. Weaver, N. Huebsch, H.-p. Lee, E. Lippens, G. N. Duda and D. J. Mooney, *Nat. Mater.*, 2015, **15**, 326.
18. S. Khetan, M. Guvendiren, W. R. Legant, D. M. Cohen, C. S. Chen and J. A. Burdick, *Nat. Mater.*, 2013, **12**, 458-465.
19. Z. Gong, S. E. Szczesny, S. R. Caliri, E. E. Charrier, O. Chaudhuri, X. Cao, Y. Lin, R. L. Mauck, P. A. Janmey, J. A. Burdick and V. B. Shenoy, *Proc. Natl. Acad. Sci. USA*, 2018, **115**, E2686-E2695.
20. J. Li, E. Weber, S. Guth-Gundel, M. Schuleit, A. Kuttler, C. Halleux, N. Accart, A. Doelemeyer, A. Basler, B. Tigani, K. Wuersch, M. Fornaro, M. Kneissel, A. Stafford, B. R. Freedman and D. J. Mooney, *Adv. Healthcare Mater.*, 2018, DOI: doi:10.1002/adhm.201701393.
21. P. M. Kharkar, A. M. Kloxin and K. L. Kiick, *J. Mater. Chem. B*, 2014, **2**, 5511-5521.

22. E. S. Place, J. H. George, C. K. Williams and M. M. Stevens, *Chem. Soc. Rev.*, 2009, **38**, 1139-1151.
23. X. Y. Cai, J. Z. Li, N. N. Li, J. C. Chen, E.-T. Kang and L. Q. Xu, *Biomater. Sci.*, 2016, **4**, 1663-1672.
24. *Propiolic acid*; MSDS No. P51400 [Online]; Sigma Aldrich: Feb 22, 2013. <http://www.sigmaaldrich.com/catalog/substance/propiolicacid> (accessed Jul 26, 2016).
25. L. J. Macdougall, M. M. Pérez-Madrigal, M. C. Arno and A. P. Dove, *Biomacromolecules*, 2017, **19**, 1378-1388.
26. L. J. Macdougall, V. X. Truong and A. P. Dove, *ACS Macro Lett.*, 2017, **6**, 93-97.
27. V. X. Truong, M. P. Ablett, S. M. Richardson, J. A. Hoyland and A. P. Dove, *J. Am. Chem. Soc.*, 2015, **137**, 1618-1622.
28. C. K. Kuo and P. X. Ma, *Biomaterials*, 2001, **22**, 511-521.
29. J. L. Drury, R. G. Dennis and D. J. Mooney, *Biomaterials*, 2004, **25**, 3187-3199.
30. V. X. Truong, K. M. Tsang and J. S. Forsythe, *Biomacromolecules*, 2017, **18**, 757-766.
31. V. X. Truong and A. P. Dove, *Angew. Chem., Int. Ed.*, 2013, **52**, 4132-4136.
32. E. Bialecka-Florjańczyk, *Synth. Commun.*, 2000, **30**, 4417-4424.
33. W. D. Crow and N. J. Leonard, *J. Org. Chem.*, 1965, **30**, 2660-2665.

34. T. Steiner, E. B. Starikov, A. M. Amado and J. J. C. Teixeira-Dias, *J. Chem. Soc., Perkin Trans. 2*, 1995, 1321-1326.
35. *2-Butynoic acid*;, SDS No. 303666 [Online]; Sigma Aldrich: Dec 21, 2015. <https://www.sigmaaldrich.com/catalog/product/aldrich/303666> (accessed 5 April 2018).
36. M. T. Herrero, I. Tellitu, E. Domínguez, S. Hernández, I. Moreno and R. SanMartín, *Tetrahedron*, 2002, **58**, 8581-8589.
37. M. Malhotra, C. Tomaro-Duchesneau and S. Prakash, *Biomaterials*, 2013, **34**, 1270-1280.
38. E. C. Schwartz, 2010, WO 2010/039531 A1.
39. S. Nahm and S. M. Weinreb, *Tetrahedron Lett.*, 1981, **22**, 3815-3818.
40. H. X. Zhou, J. Woo, A. M. Cok, M. Z. Wang, B. D. Olsen and J. A. Johnson, *J. A. Proc. Nat. Acad. Sci. U. S. A.*, 2012, **109**, 19119-19124.
41. H. X. Zhou, E. M. Schon, M. Z. Wang, M. J. Glassman, J. Liu, M. J. Zhong, D. D. Diaz, B. D. Olsen and J. A. Johnson, *J. Am. Chem. Soc.*, 2014, **136**, 9464-9470.
42. K. Kawamoto, M. J. Zhong, R. Wang, B. D. Olsen and J. A. Johnson, *Macromolecules*, 2015, **48**, 8980-8988.
43. Y. Zhang, D. An, Y. Pardo, A. Chiu, W. Song, Q. Liu, F. Zhou, S. P. McDonough and M. Ma, *Acta Biomater.*, 2017, **53**, 100-108.

44. K. C. Collins, K. Tsuchikama, C. A. Lowery, J. Zhu and K. D. Janda, *Tetrahedron*, 2016, **72**, 3593-3598.
45. F. A. Loiseau, K. K. Hii and A. M. Hill, *J. Org. Chem.*, 2004, **69**, 639-647.

Chapter 8.

Conclusions and Future Work

8.1. Conclusions

This thesis has established the nucleophilic thiol-yne reaction as a suitable crosslinking approach for the development of robust hydrogel materials with superior performance, ideal for biomedical purposes. In particular, the optimisation of poly(ethylene glycol) (PEG) precursors (Chapter 2 and 3) and the unique stereochemical control over vinyl thioether bond (Chapter 4) has reflected the versatility of this crosslinking reaction. Through the addition of natural polymers (Chapter 5) or peptides (Chapter 6) to the thiol-yne networks has demonstrated their cytocompatible nature with a range of different cell lines. These 3D scaffolds were robust structures which could support the culture of cells and also possess controlled degradation. In addition, this thesis has explored the kinetics of the nucleophilic thiol-yne addition reaction with an aim to further improve the properties of the thiol-yne PEG hydrogels (Chapter 7). Overall, this work reflects the potential of the nucleophilic thiol-yne reaction to obtain materials for a wide range of applications.

In the context of the thiol-yne reaction, adjusting the properties of the PEG precursors, such as their molecular weight, architecture, or concentration, has proven a useful strategy to produce hydrogels with finely tuned properties and, most importantly, high cytocompatibility. More specifically, a series of alkyne- and thiol-functionalised PEG precursors have been synthesised and crosslinked to form a series of nucleophilic thiol-yne hydrogels. These hydrogels have exhibited excellent features and have performed as robust materials to mimic the properties of the extracellular matrix (ECM). These 3D polymeric networks were synthesised under biologically relevant conditions (*i.e.* phosphate buffered saline (PBS) solution at pH 7.4 and room temperature) without

the need of an external catalysis and with no additional purification steps. Through a simple blending process, this efficient procedure allowed controlled and predictable mechanical properties to be achieved. Additionally, the gelation time, pore size and compressive strength of the thiol-yne hydrogels were able to be tuned through this route, thus reflecting the versatile nature of these materials. The characteristics of the developed hydrogels mimicked a range of different biological environments, highlighting the adaptable nature of this material.

To control the swelling nature of a hydrogel in aqueous environments is a favourable characteristic to maintain the structure of a hydrogel over time. To achieve this control with the thiol-yne hydrogels the number of functional groups per precursor was increased. The molecular weight of the precursors was maintained and as a result, the number of hydrophobic crosslinked points in the network increased. This achieved a more densely crosslinked structure, which did not swell when immersed in aqueous conditions. Consequently, these materials displayed enhanced compressive strength over longer periods. Therefore, the nonswellable hydrogels provided a structure which was able to withstand external pressure while preventing water uptake, ideal properties for applying these materials as tissue engineering scaffolds.

From an organic chemistry perspective and to further explore the advantages of the nucleophilic reaction, the stereochemistry of the vinyl thioether bond was tuned. Accordingly, the mechanical performance of the resultant thiol-yne PEG hydrogels changed. Interestingly, the range of storage moduli (G') achieved with these stereocontrolled materials was larger than reports in the literature for other hydrogel

systems. This demonstrated a huge potential for these 3D hydrogel networks for tissue engineering purposes, such as stem cell differentiation. This method, to control the mechanical properties of hydrogels, revealed the important role stereochemistry can play in material synthesis. Optimisation of the synthetic route is still required to enable the encapsulation of cells within these materials.

By applying a different strategy, which consisted of the formation of interpenetrating networks (IPNs), the properties of the thiol-yne PEG hydrogels were also improved. In this case, the addition of a non-covalent crosslinked secondary network to the dense thiol-yne matrix rendered the robust hydrogels, not only stretchable and with improved tensile performance, but also self-healing, capability that took place at room temperature without external stimuli. Most importantly, the IPN hydrogels sustained cell growth over time, allowing cells to move and interact with each other, a vital design feature of scaffolds for tissue regeneration. Hence this strategy, which presented an effective approach to improve the performance of covalently crosslinked synthetic hydrogels, demonstrated that exceptional properties could again be achieved by a simple blending concept if carefully designed. Ultimately, this platform, if translated to similar systems, has the potential to produce new biomaterials with enhanced features.

Knowledge on the nucleophilic thiol-yne reaction for the synthesis of hydrogels was further expanded through the incorporation of bioactive peptides and encapsulate breast cancer cells to the network. Most importantly, such platforms were found to be less toxic to cells in comparison to the radical-initiated thiol-ene reaction. This demonstrated that chemistry plays a crucial role when designing biomaterials to ensure their success.

Another essential aspect of hydrogel design is the importance of tuning the networks degradation profiles. Through covalently attaching thiol-functionalised cell degradable linkers into the thiol-yne PEG hydrogels, the scaffolds could degrade through ester hydrolysis and cell-driven degradation which had a direct impact on long-term cell proliferation. This highlights the great potential thiol-yne chemistry has to study the effect of various controlled mechanical and biochemical cues on the fate and behaviour of cell lines that have increased sensitivity to other mild crosslinking chemistries.

With a similar aim, of improving the properties of the thiol-yne PEG hydrogels, the nucleophilic thiol-yne reaction was studied in depth to evaluate the effect different adjacent functional groups had on the rate of the thiol-yne reaction. As expected, the change in electron density around the alkyne influenced the rate of the thiol-yne reaction. Potential functional groups were highlighted which could be incorporated into the PEG alkyne precursors to improve the properties of the hydrogels. However, when these functionalities were translated to PEG precursors, inferior thiol-yne hydrogels formed, as a consequence of insufficient functionalisation of PEG precursors. Further studies are therefore required to improve the synthetic routes to these PEG alkynes. Once established, these precursors have the potential to form hydrogels with improved swelling, degradation and cytotoxicity properties.

Overall, the nucleophilic thiol-yne chemistry is unparalleled as a synthetic route to form biomaterials. This thesis highlights the key benefits of the nucleophilic thiol-yne reaction and has revealed its potential to form truly tailored, dynamic biomaterials.

8.2. Future work

This thesis discloses the remarkable qualities of the nucleophilic thiol-yne reaction, however there are still many areas of material synthesis where the addition of thiols to alkynes holds huge potential. Firstly, this work has only addressed the use of alkyne- and thiol-functionalised poly(ethylene glycol) (PEG) precursors for preparing robust hydrogels. Hence, as highlighted in the introduction, there is a vast library of polymers suitable to be functionalised with both activated alkyne and thiol end groups to form thiol-yne hydrogels under physiological conditions with additional features. In the area of polymer synthesis, expanding the composition and molecular weight of the polymer precursor could further develop the range of mechanical properties displayed by these hydrogel materials and as a consequence increase the number of relevant applications.

In addition, to fully understand the effect stereochemistry has on cell behaviour, the synthesis of stereocontrolled thiol-yne systems requires improved cytocompatible synthetic routes, which will allow for cell encapsulation. Currently, the polarity of the solvent used to dictate the stereochemistry of the vinyl thioether bond, formed during gelation, requires a range of organic solvents. Therefore, the presence of toxic organic solvents prevents the *in situ* encapsulation of cells during hydrogel formation, restricting their use as extracellular matrix (ECM) mimics. Future work in this area should build upon the knowledge described in Chapter 7, which demonstrated that adjacent functional groups can also dictate stereochemistry, to synthesise stereocontrolled hydrogels in water. This change would allow cell encapsulation within the hydrogel during gelation.

However, the functionalisation reactions to create these PEG precursors needs to be optimised.

With enhanced degradation and swelling rates, the thiol-yne hydrogel materials allow for cell encapsulation and culture over longer periods since the polymer networks retain their robust structure and mechanical integrity. This work has shown the ability of the thiol-yne hydrogels to encapsulate a diverse range of cell lines and adhesive peptides. However, to further mimic the complex ECM matrix, these systems need to incorporate other important biological molecules that influence and stimulate cells during culture, such as growth factors. Hence, if this requirement was achieved, while also incorporating self-healing and improved tensile properties, the thiol-yne chemistry has the potential to form truly dynamic, versatile biomaterials.

Chapter 9.
Experimental

9.1. Materials

4-arm PEG-tetrahydroxyl (molar mass 2 kg mol⁻¹) was purchased from JenKem Technology, USA. Hyaluronic acid (Sodium salt, low molecular weight 40-50 kg mol⁻¹) (Chapter 5) was purchased from Carbosynth. All other solvents and reagents were purchased from Sigma Aldrich, Alfa Aesar or Fisher Scientific and used without purification.

9.2. General Considerations

9.2.1. Small Molecule Characterisation

¹H and ¹³C NMR spectra were recorded on a Bruker Avance III HD 300 MHz, 400 MHz or 500 MHz spectrometer at 298 K. Chemical shifts were reported as δ in parts per million (ppm) and referenced to the chemical shift of the residual solvent resonances (CDCl₃: ¹H δ = 7.26 ppm, ¹³C δ = 77.16 ppm; (CD₃)₂CO: ¹H δ = 2.05 ppm, ¹³C δ = 29.8 and 206.26 ppm, D₂O: ¹H δ = 4.79 ppm; (CD₃)₂SO: ¹H δ = 2.50 ppm, ¹³C δ = 39.52 ppm; C₃D₇NO: ¹H δ = 2.75, 2.92 and 8.03 ppm, ¹³C δ = 29.76, 34.89 and 163.15 ppm).

High resolution mass spectra (HRMS) were collected using an Agilent 6130B single Quad (ESI).

Elemental analysis was performed in duplicate by Warwick Analytical Services.

Fourier Transform Infrared (FT-IR) spectra were recorded using a Perkin-Elmer Spectrum 100 FT-IR spectrometer. For each spectrum 16 scans from 600 to 4,000 cm⁻¹ were recorded with a correction for background absorbance.

9.2.2. Polymer Characterisation

Size exclusion chromatography (SEC) was used to determine the molar masses and molar mass distributions (dispersities, D_M) of the functionalised polymers. SEC conducted in chloroform (CHCl_3) (0.5% NEt_3) used a Varian PL-SEC 50 system equipped with $2 \times$ PLgel 5 μM MIXED-D columns in series and a differential refractive index (RI) detector at a flow rate 1.0 mL min^{-1} . The system was calibrated against a Varian Polymer Laboratories Easi-Vial poly(styrene) (PS) standard and analysed by the software package Cirrus v3.3.

SEC conducted in *N, N*-dimethyl formamide (DMF) (5 mM NH_4BF_4) used a Varian PL-SEC 50 system equipped with $2 \times$ PLgel 5 μM MIXED-C + guard columns in series and a differential refractive index (RI) detector at a flow rate of 1.0 mL min^{-1} . The systems were calibrated against Varian Polymer Laboratories Easi-Vial linear poly(methyl methacrylate) (PMMA) standards and analysed by the software package Cirrus v3.3.

SEC conducted under aqueous conditions used an Agilent PL50 instrument equipped with differential refractive index (DRI) detector. The system was equipped with $2 \times$ Aquagel H columns (300 x 7.5 mm) and an Aquagel 5 μm guard column. The eluent was Water:Methanol ($\text{H}_2\text{O}:\text{MeOH}$) (80:20). Samples were run at 1.0 mL min^{-1} at $35 \text{ }^\circ\text{C}$. Poly(ethylene oxide) standards (Agilent EasyVials) were used for calibration. Analyte samples were filtered through a membrane with $0.45 \mu\text{m}$ pore size before injection. Respectively, experimental molar mass (M_n) and dispersity (D_M) values of synthesised polymers were determined by conventional calibration using Agilent SEC software.

9.2.3. General Characterisation Techniques for Hydrogels

9.2.3.1. Gel Fraction and Equilibrium Water Content (EWC)

To determine the gel fraction hydrogels were lyophilised and weights (W_g) recorded. The hydrogels were then allowed to swell for in deionised water for 3 days with frequent changes in water to extract unreacted polymers. The hydrogels were then lyophilised and weights (W_r) were recorded again. All measurements were repeated in triplicate. The gel fraction was expressed as:

$$\text{Gel Fraction (\%)} = \frac{W_r}{W_g} \times 100 \%$$

To determine the equilibrium water content (EWC) the prepared hydrogels were allowed to swell in phosphate buffer saline (PBS) solution for 1 day to reach swelling equilibrium. The surface water was then removed with soft tissue paper and the weights recorded (W_s). The hydrogels were then lyophilised, and the weights recorded (W_d). All measurements were repeated in triplicate. The equilibrium water content was expressed as:

$$\text{EWC (\%)} = \frac{W_s - W_d}{W_s} \times 100 \%$$

9.2.3.2. Mesh Size Calculations

Flory-Rehner calculations were used to determine each thiol-yne PEG hydrogel mesh size.^{1, 2} The swelling ratio based on the hydrogel mass (Q_M) was calculated for each hydrogel:

$$Q_M = \frac{M_S}{M_D}$$

where M_S is the hydrogel mass after swelling and M_D is the dry hydrogel mass. The volume swelling ratio (Q_V) was then calculate using Q_M :

$$Q_V = 1 + \frac{\rho_p}{\rho_s} (Q_M - 1)$$

where ρ_p is the density of the dry hydrogel (1.12 g cm^{-3} for PEG)¹ and ρ_s is the density of the solvent (1 g cm^{-3} for H₂O). The swelling calculations were then used to determine hydrogel mesh size (ξ). First, the molecular weight between cross-links (M_C) was calculated:

$$\frac{1}{\bar{M}_C} = \frac{2}{\bar{M}_n} - \frac{\bar{v}_1(\ln(1-v_2)+v_2+\chi_1v_2^2)}{v_2^{1/3}-\frac{v_2}{2}}$$

where \bar{M}_n is the number-average molecular weight of the un-crosslinked hydrogel (the molecular weight of the polymer), V_1 is the molar volume of the solvent ($18 \text{ cm}^3 \text{ mol}^{-1}$ for water), v_2 is the polymer volume fraction in the equilibrium swollen hydrogel, which is equal to the reciprocal of Q_V , \bar{v}_1 is the specific volume of the polymer (ρ_p/ρ_s), and χ_1 is the polymer-solvent interaction parameter (0.426 for PEG-H₂O^{3,4} and assumed constant for these hydrogels because χ_1 has been found to be nearly independent of PEG v_2 for $v_2=0.04$ to 0.2).⁵

Mesh size was then determined,² the root-mean-square end-to-end distance of the polymer chain in the unperturbed state ($(\bar{r}_0^2)^{1/2}$) was calculated:

$$(\bar{r}_0^2)^{1/2} = lC_n^{1/2}n^{1/2}$$

where l is the average bond length (0.146 nm), C_n is the characteristic ratio of the polymer (typically 4.0 for PEG)¹ and n is the number of bonds in the cross-link:

$$n = 2 \frac{\overline{M}_C}{M_r}$$

where M_r is the molecular weight of the repeat unit (44 for PEG). Mesh size was then calculated for each thiol-yne hydrogel:

$$\xi = v_2^{-1/3} (\overline{r}_0^2)^{1/2}$$

All measurements were repeated in triplicate.

9.2.3.3. Swelling and Degradation Procedure

Hydrogels were fabricated and left to cure for 1 h at room temperature. The prepared hydrogels were then placed in PBS solution pH 7.4 and incubated at 37 °C in an orbital shaker-incubator (Model ES-20, Grant Instruments (Cambridge) Ltd.) with a shaking speed of 80 rpm. The PBS solution was replaced regularly to remove unreacted PEG precursors and to prevent the build-up of solute concentration. At pre-set time intervals, the hydrogels were removed, gently blotted dry and the weight was recorded. The swelling factor (SF) and degradation was monitored by the percentage of weight of the hydrogel at each time point (t) compared to the weight before submersion which is defined as:

$$\text{Swelling Factor (\%)} = \frac{W_t}{W_0} \times 100\%$$

where W_t is the weight measured at specific time point, t , and W_0 is the initial wet weight before immersed (after 1 h).

9.2.3.4. Cryogenic Scanning Electron Microscopy

Cryogenic scanning electron microscopy (cryo SEM) was performed on ZEISS SUPRA 55-VP equipped with cold stage and sample preparation chamber.

In a typical procedure, a hydrogel sample was formed *in situ* on a stub and the top layer was sliced off. The stub was placed in a pre-frozen stub adaptor and frozen in liquid nitrogen (-195 °C) which was obtained by placing the sample in liquid nitrogen under vacuum. The stub was then transferred to the cold stage (at -125 °C) of the preparation chamber connecting to the SEM chamber. The frozen sample was surface fractured and sublimated at -95 °C for 15 min to reveal the cross-sectional surface. The temperature was then brought down to -125 °C and the sample was sputter coated with platinum before being transferred under vacuum into the SEM chamber, which was kept at -186 °C for imaging. The accelerating voltage was set at 2 kV to avoid burning the sample.

9.2.4. Mechanical Characterisation of Hydrogels

9.2.4.1. Rheological Testing

Rheological testing was carried out using an Anton Parr MCR 302 rheometer equipped with parallel plate configuration with a diameter of 50 mm unless otherwise stated. A Peltier system was used to maintain the temperature at 20 °C throughout the study. Data was analysed using RheoCompass software.

9.2.4.1.1. The Evolution of Storage (G') and Loss (G'') Moduli as a Function of Time Measurements

In a typical rheological test, PEG_{1k}(SH)₂ (56.8 mg, 4.83×10^{-3} mmol) and PEG_{2k}(C≡CH)₄ (53.3 mg, 2.41×10^{-3} mmol) were dissolved in separate solutions of 500 μ L PBS pH 7.4. The two solutions were drawn up in a 1 mL syringe and injected on to the lower plate, at 20 °C. The upper plate was immediately lowered to a plate separation of 0.5 mm and the experiment started. A frequency of 5 Hz and a strain of 5% was applied to minimise interference with the gelation process and keep the measurement within the linear viscoelastic region. The normal force was also kept constant at 0 N. The gelation kinetics was characterised by the evolution of storage moduli (G') and loss moduli (G'') as a function of time. The gel point was determined by the cross-over between the G' and G'' which indicates transformation of material from liquid to solid state. A point was recorded each second until the G' and G'' plateaued. The frequency and amplitude sweeps were carried out on the gel formed from this experiment. All measurements were repeated in triplicate and the average G' and G'' were calculated for the gelation process.

9.2.4.1.2. Frequency Sweep Measurements

The frequency sweep applied a constant strain of 0.5% and the angular frequency was ramped logarithmically from 100 rad s⁻¹ to 0.1 rad s⁻¹. The normal force was kept constant at 0 N throughout the test and 5 points were taken each decade. All measurements were repeated in triplicate and the average G' and G'' were calculated over the frequency range.

9.2.4.1.3. Amplitude Sweep Measurements

The amplitude sweep applied a constant frequency of 10 rad s^{-1} and the strain was ramped logarithmically from 0.01% to 1000%. The normal force was kept constant at 0 N and 6 points were recorded for each decade. All measurements were repeated in triplicate and the average G' and G'' were calculated at increasing amounts of strain.

9.2.4.1.4. Young's Modulus Calculations from Rheological data (Chapter 6)

Young's Moduli were calculated from the average rheological G' and G'' values using the equation:⁶

$$E = 2G(1 + \nu) \text{ and } G = \sqrt{G'^2 + G''^2}$$

where E = Young's Modulus, $\nu = 0.5$ (Poisson's ratio for hydrogel materials),⁷ G = shear modulus, G' = shear storage modulus and G'' = shear loss modulus.

9.2.4.2. Uniaxial Mechanical Testing

All uniaxial tensile testing was performed on a Testometric M100-1CT universal mechanical testing instrument fitted with a load cell of 1 kN. Data was analysed using Wintest analysis software.

9.2.4.2.1. Compression Testing

In a typical procedure for compression testing, hydrogel samples were prepared in a 2 mL syringe to give a cylindrical shape with a diameter of 9 mm and length of 4 mm. Samples were left to cure for 1 h after forming, to ensure the crosslinking reaction was complete before testing. A preload force of 0.1 N was set and each test was carried out at a

compression velocity of 5 mm min^{-1} . Each hydrogel was subject to 95% strain in order to determine the ultimate compressive stress and strain. All compression tests were repeated 10 times and an average of the data was taken to find the ultimate compressive stress and strain. Compressive Young's modulus was calculated from the initial 10% of the stress/strain curve which is defined as:

$$\text{Young's Modulus} = \frac{\text{Difference in Stress}}{\text{Difference in Strain}}$$

9.2.4.2.2. Tensile Testing

All uniaxial tensile testing was performed on a Testometric M100-1CT universal mechanical testing instrument fitted with a load cell of 1 kN. Hydrogel samples were prepared in dog bone moulds (250 μL per sample, dimensions $L = 7 \text{ mm}$, $W = 3 \text{ mm}$, $D = 2 \text{ mm}$), sealed and left to cure for 7 h. Each hydrogel was then removed and clamped into the tensile holders and subjected to a rate of elongation of 5 mm min^{-1} until the sample failed. All tensile tests were repeated at least 10 times and an average of the data was taken to find the ultimate tensile stress and strain.

9.3. Experimental Procedures for Alkyne- and Thiol-Functionalised PEG Precursors

9.3.1. Synthesis of 4-Arm Alkyne-Functionalised PEG (2 kg mol^{-1})

4-arm alkyne-functionalised PEG was synthesised using a modified literature procedure.⁸ 4-arm PEG_{2k}OH (molar mass 2 kg mol^{-1} , 4 g, 2 mmol) was mixed with toluene (75 mL) and benzene (75 mL) with 2 drops of concentrated H_2SO_4 . The solution was heated to 80°C with stirring to obtain a clear homogenous solution. To this solution, propiolic acid

(1.12 g, 16 mmol) was added and the solution was heated to reflux under Dean-Stark conditions. After no more water was collected in the condenser (*ca.* 20 h) the solution was allowed to cool to room temperature and toluene was evaporated on a rotary evaporator. The resultant oil was dissolved in CH_2Cl_2 (20 mL) and washed with saturated NaHCO_3 solution (10 mL) and brine (10 mL). The organic phase was dried (MgSO_4) and concentrated. The resultant oil was dissolved in ethanol (EtOH) and stirred with charcoal (*ca.* 0.1 g) for 30 min at 40 °C. The solution was filtered through Celite[®] 545 and solvent was evaporated to collect product as clear to slight yellow oil (Yield 2.7 g, 61%). ^1H NMR ($(\text{CD}_3)_2\text{CO}$, 400 MHz): δ 4.33 (t, 2H, $^3J_{\text{HH}} = 8$ Hz, $\text{CH}_2\text{CH}_2\text{OCOCH}_2$), 3.90 (s, 1H, $\text{CH}\equiv\text{CCOO}$), 3.72-3.74 (m, 45H, $\text{OCH}_2\text{CH}_2\text{O}$), 3.6 (s, 2H, CCH_2O) ppm. ^1H NMR spectroscopy indicated *ca.* 93% conversion of the hydroxyl group to propiolate group. SEC (DMF): $M_n = 5.9 \text{ kg mol}^{-1}$ ($D_M = 1.08$).

9.3.2. Synthesis of 3-Arm Alkyne-Functionalised PEG (1 kg mol^{-1})

In a similar procedure stated in section 9.3.1, Glycerol ethoxylate (molar mass 1 kg mol^{-1} , 10 g, 10 mmol) was esterified with propiolic acid (4.2 g, 60 mmol). (Yield 8.1 g, 70%). ^1H NMR ($(\text{CD}_3)_2\text{CO}$, 400 MHz): δ 4.33 (t, 2H, $^3J_{\text{HH}} = 8$ Hz, $\text{CH}_2\text{CH}_2\text{OCOCH}_2$), 3.89 (s, 1H, $\text{CH}\equiv\text{CCOO}$), 3.71-3.74 (m, 30H, $\text{OCH}_2\text{CH}_2\text{O}$), 3.58 (s, 2H, CCH_2O) ppm. ^1H NMR spectroscopy indicated *ca.* 92% conversion of the hydroxyl group to propiolate group. SEC (DMF): $M_n = 3.3 \text{ kg mol}^{-1}$ ($D_M = 1.04$).

9.3.3. Synthesis of 2-Arm Alkyne-Functionalised PEG (1 kg mol^{-1})

In a similar procedure stated in section 9.3.1, 2-arm PEG_{1k}OH (molar mass 1 kg mol^{-1} , 10 g, 10 mmol) was esterified with propiolic acid (2.8 g, 40 mmol) to yield a white solid.

(Yield 8.5 g, 77%). ^1H NMR ($(\text{CD}_3)_2\text{CO}$, 400 MHz): δ 4.33 (t, 2H, $^3J_{\text{HH}} = 9$ Hz, $\text{CH}_2\text{CH}_2\text{OCOCH}_2$), 3.88 (s, 1H, $\text{CH}\equiv\text{CCOO}$), 3.72-3.74 (m, 45H, $\text{OCH}_2\text{CH}_2\text{O}$), 3.58 (s, 2H, CCH_2O) ppm. ^1H NMR spectroscopy indicated *ca.* 89% conversion of the hydroxyl group to propiolate group. SEC (DMF): $M_n = 3.0$ kg mol $^{-1}$ ($\mathcal{D}_M = 1.05$).

9.3.4. Synthesis of 3-Arm-Thiol-Functionalised PEG (1 kg mol $^{-1}$)

In a similar procedure stated in section 9.3.1, glycerol ethoxylate (molar mass 1 kg mol $^{-1}$, 10 g, 10 mmol) was esterified with 3-mercaptopropionic acid (4.2 g, 60 mmol) to yield a colourless oil. (Yield 9.4 g, 74%). ^1H NMR (CDCl_3 , 400 MHz): δ 4.21 (t, 2H, $^3J_{\text{HH}} = 8$, CH_2OCO), 3.58-3.64 (m, 30H, $\text{OCH}_2\text{CH}_2\text{O}$), 2.72 (q, 2H, $^3J_{\text{HH}} = 12$, $\text{OCCH}_2\text{CH}_2\text{SH}$), 2.63 (t, 2H, $^3J_{\text{HH}} = 12$, $\text{OCCH}_2\text{CH}_2\text{SH}$), 1.64 (t, 1H, $^3J_{\text{HH}} = 20$, SH) ppm. ^1H NMR spectroscopy indicated *ca.* 96% conversion of the hydroxyl group to mercaptopropionate group. SEC (CHCl_3): $M_n = 1.3$ kg mol $^{-1}$ ($\mathcal{D}_M = 1.08$).

9.3.5. Synthesis of 4-Arm Thiol-Functionalised PEG (2 kg mol $^{-1}$)

In a similar procedure stated in section 9.3.1, 4-arm PEG $_{2k}$ OH (molar mass 2 kg mol $^{-1}$, 10 g, 5 mmol) was esterified with 3-mercaptopropionic acid (4.2 g, 40 mmol) to yield a colourless oil. (Yield 9.1 g, 77%). ^1H NMR (CDCl_3 , 400 MHz): δ 4.23 (t, 2H, $^3J_{\text{HH}} = 12$, CH_2OCO), 3.42-3.60 (m, 45H, $\text{OCH}_2\text{CH}_2\text{O}$), 2.74 (q, 2H, $^3J_{\text{HH}} = 20$, $\text{OCCH}_2\text{CH}_2\text{SH}$), 2.65 (t, 2H, $^3J_{\text{HH}} = 12$, $\text{OCCH}_2\text{CH}_2\text{SH}$), 1.59 (t, 1H, $^3J_{\text{HH}} = 16$, SH) ppm. ^1H NMR spectroscopy indicated *ca.* >99% conversion of the hydroxyl group to mercaptopropionate group. SEC (CHCl_3): $M_n = 1.9$ kg mol $^{-1}$ ($\mathcal{D}_M = 1.06$).

9.3.6. Synthesis of 2-Arm Thiol-Functionalised PEG (1 kg mol⁻¹)

In a similar procedure stated in section 9.3.1, 2-arm PEG_{1k}OH (molar mass 1 kg mol⁻¹, 10 g, 10 mmol) was esterified with 3-mercaptopropionic acid (4.2 g, 60 mmol) to yield a white solid. (Yield 9.4 g, 80%). ¹H NMR (CDCl₃, 400 MHz): δ 4.26 (t, 2H, ³J_{HH} = 8, CH₂OCO), 3.63-3.68 (m, 45H, OCH₂CH₂O), 2.77 (q, 2H, ³J_{HH} = 12 Hz, OCCH₂CH₂SH), 2.68 (t, 2H, ³J_{HH} = 12 Hz, OCCH₂CH₂SH), 1.67 (t, 1H, ³J_{HH} = 8 Hz, SH) ppm. ¹H NMR spectroscopy indicated *ca.* 96% conversion of the hydroxyl group to mercaptopropionate group. SEC (CHCl₃): M_n = 1.1 kg mol⁻¹ (Đ_M = 1.24).

9.3.7. Synthesis of 2-Arm Thiol-Functionalised PEG (2 kg mol⁻¹)

In a typical esterification stated in 9.3.1, 2-arm PEG_{2k}OH (molar mass 2 kg mol⁻¹, 10 g, 5 mmol) was esterified using 3 mercaptopropionic acid (4.2 g, 40 mmol). (Yield 9.2 g, 85%). ¹H NMR (CDCl₃, 400 MHz): δ 4.27 (t, 2H, ³J_{HH} = 8 Hz, CH₂OCO), 3.64-3.69 (m, 90H, OCH₂CH₂O), 2.78 (q, 2H, ³J_{HH} = 12 Hz, OCCH₂CH₂SH), 2.69 (t, 2H, ³J_{HH} = 12 Hz, OCCH₂CH₂SH), 1.68 (t, 1H, ³J_{HH} = 8 Hz, SH) ppm. ¹H NMR spectroscopy indicated *ca.* >99% conversion of the hydroxyl group to mercaptopropionate group. SEC (CHCl₃): M_n = 2.7 kg mol⁻¹ (Đ_M = 1.26).

9.3.8. Synthesis of 2-Arm Thiol-Functionalised PEG (3 kg mol⁻¹)

In a typical esterification stated in 9.3.1, 2-arm PEG_{3k}OH (molar mass 3 kg mol⁻¹, 10 g, 3.3 mmol) was esterified using 3 mercaptopropionic acid (4.2 g, 40 mmol). (Yield 9.3 g, 88%). ¹H NMR (CDCl₃, 400 MHz): δ 4.27 (t, 2H, ³J_{HH} = 8 Hz, CH₂OCO), 3.60-3.67 (m, 136H, OCH₂CH₂O), 2.75 (q, 2H, ³J_{HH} = 12 Hz, OCCH₂CH₂SH), 2.65 (t, 2H, ³J_{HH} = 12 Hz, OCCH₂CH₂SH), 1.65 (t, 1H, ³J_{HH} = 8 Hz, SH) ppm. ¹H NMR spectroscopy indicated

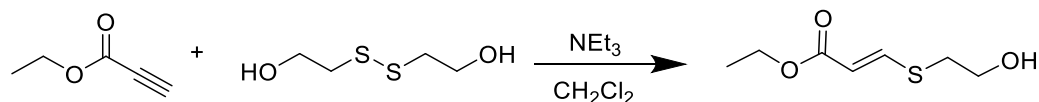
ca. >84% conversion of the hydroxyl group to mercaptopropionate group. SEC (CHCl_3): $M_n = 8.7 \text{ kg mol}^{-1}$ ($D_M = 1.10$).

9.3.9. Synthesis of 2-Arm Thiol-Functionalised PEG (4 kg mol^{-1})

In a typical esterification stated in 9.3.1, 2-arm PEG_{4k}OH (molar mass 4 kg mol^{-1} , 10 g, 2.5 mmol) was esterified using 3 mercaptopropionic acid (4.2 g, 40 mmol). (Yield 8.7 g, 83%). $^1\text{H NMR}$ (CDCl_3 , 400 MHz): δ 4.28 (t, 2H, $^3J_{\text{HH}} = 8 \text{ Hz}$, CH_2OCO), 3.63-3.8 (m, 181H, $\text{OCH}_2\text{CH}_2\text{O}$), 2.78 (q, 2H, $^3J_{\text{HH}} = 12 \text{ Hz}$, $\text{OCCH}_2\text{CH}_2\text{SH}$), 2.68 (t, 2H, $^3J_{\text{HH}} = 12 \text{ Hz}$, $\text{OCCH}_2\text{CH}_2\text{SH}$), 1.67 (t, 1H, $^3J_{\text{HH}} = 8 \text{ Hz}$, SH) ppm. $^1\text{H NMR}$ spectroscopy indicated ca. >99% conversion of the hydroxyl group to mercaptopropionate group. SEC (CHCl_3): $M_n = 6.9 \text{ kg mol}^{-1}$ ($D_M = 1.10$).

9.4. Experimental Procedures for Chapter 2

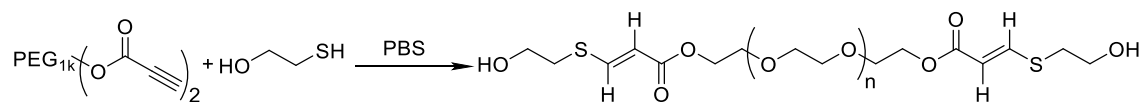
9.4.1. Control Thiol-yne Reaction between Ethyl Propiolate and 2-Hydroxyethyl Disulfide



2-Hydroxyethyl disulfide (78.6 mg, 0.5 mmol) was dissolved in dichloromethane (CH_2Cl_2) (19 mL). Ethyl propiolate (100 mg, 1 mmol) was added dropwise followed by triethylamine (NEt_3) (5.15 mg 0.05 mmol) dissolved in CH_2Cl_2 (1 mL) and the solution was stirred at room temperature. After 4 h the solvent and NEt_3 was removed *in vacuo* to yield a clear solution (89.6 mg, yield quantitative). Characterisation data were in accordance with that previously reported.⁹ $^1\text{H NMR}$ (CDCl_3 , 400 MHz): δ 7.58 (d, 1H, $^3J_{\text{HH}} = 12$, $\text{HC}=\text{CHS trans}$), 5.25 (d, 1H, $^3J_{\text{HH}} = 12 \text{ Hz}$, $\text{HC}=\text{CHS trans}$), 4.17 (q, 2H, $^3J_{\text{HH}} = 8 \text{ Hz}$, $\text{CH}_3\text{CH}_2\text{OCO}$), 4.10 (t, 2H, $^3J_{\text{HH}} = 8 \text{ Hz}$, $\text{SCH}_2\text{CH}_2\text{OH}$), 2.98 (t, 2H, $^3J_{\text{HH}} = 8 \text{ Hz}$,

SCH_2CH_2OH), 1.27(q, 3H, $^3J_{HH} = 8$ Hz, CH_3CH_2OCO) ppm. FT-IR max/cm $^{-1}$: 3171 (OH), 2926 (CH), 1701 (C=O), 1706 (C=O), 1581 (C=C), 907 (CO), 731 (C=CH).

9.4.2. Control Thiol-yne Reaction between $PEG_{1k}(C\equiv CH)_2$ and 2-Mercaptoethanol



$PEG_{1k}(C\equiv CH)_2$ (1 kg mol^{-1} , 100 mg, 0.1 mmol) and 3-Mercaptoethanol (28 μL , 0.4 mmol) were dissolved in deuterated PBS solution (pH 7.4) (500 μL) separately. 3-Mercaptoethanol solution was added dropwise to the PEG solution and stirred at room temperature. After 30 min an aliquot of the reaction mixture was removed and analysed by ^1H NMR spectroscopy. ^1H NMR (D_2O , 400 MHz): δ 7.94 (d, 1H, $^3J_{HH} = 16$, $HC=CHS$ *trans*), 7.52 (d, 1H, $^3J_{HH} = 8$, $HC=CHS$ *cis*), 6.04 (d, 1H, $^3J_{HH} = 12$ Hz, $HC=CHS$ *cis*), 4.36 (q, 2H, $^3J_{HH} = 8$ Hz, CH_2CH_2OCO), 3.85 (m, 45H, OCH_2CH_2O), 3.07 (t, 2H, $^3J_{HH} = 8$ Hz, SCH_2CH_2OH), 2.74-2.71 (t, $^3J_{HH} = 8$ Hz, SCH_2CH_2OH) ppm. FT-IR max/cm $^{-1}$: 3335 (OH), 2874 (CH), 1710 (C=O), 1640 (C=C). SEC (DMF): $M_n = 3.0\text{ kg mol}^{-1}$ ($\mathcal{D}_M = 1.05$).

9.4.3. General Procedure for the Fabrication of PEG Hydrogels by Nucleophilic Thiol-yne Addition

A 1:1 molar ratio of alkyne group to thiol group was used for all gellations by thiol-yne chemistry, the precursor content was kept at 10 wt%. In a typical procedure for making a PEG hydrogel, $PEG_{1k}(SH)_2$ (22.9 mg, 1.95×10^{-3} mmol) was dissolved in 200 μL PBS pH 7.4 solution. A separate solution of $PEG_{2k}(C\equiv CH)_4$ (21.5 mg, 9.74×10^{-3} mmol) in

200 μ L PBS pH 7.4 solution. The two solutions were mixed together on a vortex mixer for 5 s. The mixture was then injected into a mould suitable for the chosen analysis.

9.4.4. General Procedure for the Blended Thiol-yne Hydrogels

For the synthesis of blended thiol-yne hydrogels, the experimental procedure in section 9.4.3 was followed and a 1:1 molar ratio of alkyne group to thiol group was maintained. Different molar ratio of each thiol at different molecular weights were used to tune the properties of the hydrogels. The precursors were diluted with PBS and the thiol precursor were mixed together before being mixed with the diluted alkyne precursor. The mixture was then injected into a mould suitable for the chosen analysis.

9.5. Experimental Procedure for Chapter 3

9.5.1. Preparation of Nonswelling Thiol-yne Hydrogels

Thiol-yne hydrogels were prepared as stated in section 9.4.3 with a 1:1 ratio (alkyne:thiol) in PBS solution. Nonswelling hydrogels were synthesised using 3- or 4-arm PEG thiol precursors (1 or 2 kg mol⁻¹ respectively) as the thiol component.

9.5.2. Characterisation and Mechanical Testing of the Nonswelling Thiol-yne Hydrogels

Once synthesised the nonswelling hydrogels were characterised following the procedure in section 9.2.3 and 9.2.4. All experiments conducted in a minimum of triplicate.

9.5.3. Cytocompatibility Studies and 3D Cell Encapsulation

MC3T3-E1 were purchased from Public Health England and cultured as advised by supplier in MEM- α medium with addition of 10% FBS and 1% penicillin/streptomycin.

9.5.3.1. Cytocompatibility Studies (2D culture)

For the cytocompatibility studies, hydrogels were prepared in culture medium in 24-wells cell culture inserts with a 0.4 μm pore PET membrane, as described in the previous section, in a total volume of 200 μL . After 30 min incubation at 37 $^{\circ}\text{C}$, 100,000 cells suspended in 20 μL of medium were seeded on top of the hydrogel, and the material was incubated for 2 h before addition of fresh medium on top and around the hydrogel. Bio viability was assessed using a PrestoBlue viability assay. Fluorescence was measured using a BioTek plate reader ($\lambda_{\text{Ex.}} = 530 \text{ nm}$, $\lambda_{\text{Em.}} = 590 \text{ nm}$).

9.5.3.2. Cell Encapsulation Studies (3D culture)

Evaluation of cell viability during 3D cell encapsulation experiments was carried out using a Zeiss LSM 880 confocal fluorescence microscope. Staining for live cells (Calcein, $\lambda_{\text{Ex}} = 495 \text{ nm}$, $\lambda_{\text{Em}} = 515 \text{ nm}$) was excited with a 488 nm laser, while staining for dead cells (Ethidium homodimer, $\lambda_{\text{Ex.}} = 528 \text{ nm}$, $\lambda_{\text{Em.}} = 617 \text{ nm}$) was excited with a 514 nm laser. Z-stacks with an average thickness of 400 μm were collected from different zones of the samples and maximum intensity projections were obtained from each Z-stack. Images were processed using Zen (blue edition) and ImageJ software.

For 3D encapsulation studies, 500,000 cells per gel were suspended with the alkyne precursor, followed by addition of the thiol precursor prior mixing to obtain a 200 μL hydrogel. Cells were incubated up to 72 h, after which they were stained with calcein for live cells ($\lambda_{\text{Ex.}} = 495$, $\lambda_{\text{Em.}} = 515$) and ethidium homodimer for dead cells ($\lambda_{\text{Ex.}} = 528$, $\lambda_{\text{Em.}} = 617$) and imaged using a confocal fluorescence microscope. Experiments were performed in triplicate.

9.6. Experimental Procedures for Chapter 4

9.6.1. Fabrication of Stereocontrolled Thiol-yne Organogels

In a similar procedure as stated in section 9.4.3. thiol-yne gels were fabricated in a range of solvents to ascertain the correct polarity needed to target a range of different *cis:trans* ratios. A 1:1 molar ratio of alkyne group to thiol group was used for all gels and the precursor content was kept at 10 wt%. In a typical procedure for synthesising stereocontrolled thiol-yne PEG organogels (polymer network in an organic solvent) a stock solution of the required solvent system was made with NEt_3 ($0.7\text{--}34 \mu\text{L mL}^{-1}$). $\text{PEG}_{2k}(\text{SH})_4$ (20.8 mg, 8.83×10^{-3} mmol) and $\text{PEG}_{2k}(\text{C}\equiv\text{CH})_4$ (19.5 mg, 8.83×10^{-3} mmol) were separately dissolved in 200 μL of the stock solution. Subsequently, the PEG alkyne solution was added to the PEG thiol solution and the solution was mixed together on a vortex mixer for 5 s. The solution was then injected into a 2 mL syringe mould, sealed and left to cure for 1 h. Solvent and NEt_3 were then removed *in vacuo* and the samples were sliced into thin discs for analysis *via* FT-IR spectroscopy. All conditions were synthesised in triplicate for FT-IR analysis and sliced into 2 discs (12 measurements per condition). The stereochemistry was determined by normalising the *cis* C=C bending signal area at 802 cm^{-1} with the C-H stretch at 2866 cm^{-1} . As previous studies demonstrated, using H_2O as the solvent with a PEG precursor (section 9.6.2), resulted in a product with 94% *cis* content. Therefore, the *cis* content was determined by dividing the normalised peak area by the area measured for the 100% water sample (94% *cis*).

9.6.1.1. $4_{2A}4_{2S}$ Thiol-yne Gel Synthesised with CHCl_3

The **4_{2A}4_{2S}** gel was synthesis following the procedure in section 9.6.1. The stock solution was made with CHCl₃ (100%) with NEt₃ (34 μL mL⁻¹). FT-IR max/cm⁻¹: 2865 (CH), 1709 (C=O), 1706 (C=O), 1582 (C=C), 1094 (CO). FT-IR indicated 10% *cis* content (90% *trans*) in the gel in comparison to 94% H₂O gel (23% *cis* by ¹H NMR spectroscopy).

9.6.1.2. **4_{2A}4_{2S}** Thiol-yne Gel Synthesised with Acetone:CHCl₃ (60:40)

The **4_{2A}4_{2S}** gel was synthesis following the procedure in section 9.6.1. The stock solution was made with Acetone:CHCl₃ (60:40) with NEt₃ (20 μL mL⁻¹). FT-IR max/cm⁻¹: 2865 (CH), 1709 (C=O), 1706 (C=O), 1582 (C=C), 1094 (CO). FT-IR indicated 23% *cis* content (77% *trans*) in the gel in comparison to 94% H₂O gel (36% *cis* by ¹H NMR spectroscopy).

9.6.1.3. **4_{2A}4_{2S}** Thiol-yne Gel Synthesised with Acetone:H₂O (90:10)

The **4_{2A}4_{2S}** gel was synthesis following the procedure in section 9.6.1. The stock solution was made with Acetone:H₂O (90:10) with NEt₃ (10 μL mL⁻¹). FT-IR max/cm⁻¹: 2865 (CH), 1734 (C=O), 1706 (C=O), 1582 (C=C), 1094 (CO), 802 (C=C *cis*). FT-IR indicated 51% *cis* content (49% *trans*) in the gel in comparison to 94% H₂O gel (66% *cis* by ¹H NMR spectroscopy).

9.6.1.4. **4_{2A}4_{2S}** Thiol-yne Gel Synthesised with Acetone: H₂O (65:35)

The **4_{2A}4_{2S}** gel was synthesis following the procedure in section 9.6.1. The stock solution was made with Acetone:H₂O (65:35) with NEt₃ (1.7 μL mL⁻¹). FT-IR max/cm⁻¹: 2865 (CH), 1734 (C=O), 1706 (C=O), 1573 (C=C), 1094 (CO), 802 (C=C *cis*). FT-IR indicated

82% *cis* content (18% *trans*) in the gel in comparison to 94% H₂O gel (91% *cis* by ¹H NMR spectroscopy).

9.6.1.5. **4_{2A}4_{2S}** Thiol-yne Gel Synthesised with H₂O

The **4_{2A}4_{2S}** gel was synthesis following the procedure in section 9.6.1. The stock solution was made with H₂O (100%) with NEt₃ (0.7 μL mL⁻¹). FT-IR max/cm⁻¹: 2865 (CH), 1734 (C=C), 1706 (C=C), 1573 (C=C), 1094 (CO), 802 (C=C *cis*). 94% *cis* content assumed from ¹H NMR spectroscopy of small molecule reaction (93% *cis* by ¹H NMR spectroscopy of PEG reaction).

9.6.2. Synthesis of Methyl-Ether Alkyne-Functionalised PEG (550 g mol⁻¹)

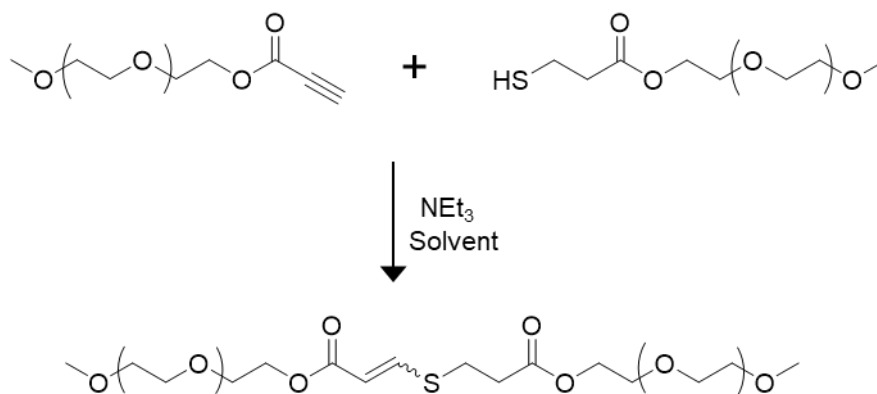
In a similar procedure stated in section 9.3.1, methyl ether PEG₅₅₀(OH) (molar mass 550 g mol⁻¹, 10 g, 18 mmol) was esterified with propiolic acid (5.1 g, 72 mmol) to yield a waxy solid. (Yield 9 g, 83%). ¹H NMR ((CD₃)₂CO, 400 MHz): δ 4.31 (t, 2H, ³J_{HH} = 9 Hz, CH₂CH₂OCOCH₂), 3.88 (s, 1H, CH≡CCOO), 3.44-3.73 (m, 50H, OCH₂CH₂O), 3.28 (s, 3H, CH₃O) ppm. ¹³C NMR ((CD₃)₂CO, 400 MHz): δ 153.1 (C=O), 77.7 (C≡CH), 72.43 (C≡CH), 71.0 (OCH₂CH₂O), 68.9 (CH₂OCO), 65.8 (CH₂CH₂OCO), 58.7 (CH₃O) ppm. FT-IR max/cm⁻¹ 2869 (CH), 2112 (C≡C), 1714 (C=O), 1101 (CO). SEC (CHCl₃): M_n = 1.1 kg mol⁻¹ (Đ_M = 1.11). ¹H NMR spectroscopy indicated *ca.* 93% conversion of the hydroxyl group to propiolate group.

9.6.3. Synthesis of Methyl-Ether Thiol-Functionalised PEG (550 g mol⁻¹)

In a similar procedure stated in section 9.3.1, methyl ether PEG₅₅₀(OH) (molar mass 550 g mol⁻¹, 10 g, 18 mmol) was esterified with 3 mercaptopropionic acid (7.6 g, 72 mmol). (Yield 9.8 g, 85%). ¹H NMR (CDCl₃, 300 MHz): δ 3.88 (t, 2H, ³J_{HH} = 8 Hz, CH₂OCO),

3.16-3.33 (m, 50H, OCH₂CH₂O), 2.99 (s, 3H, CH₃O), 2.38 (q, 2H, ³J_{HH} = 12 Hz, OCCH₂CH₂SH), 2.33 (t, 2H, ³J_{HH} = 12 Hz, OCCH₂CH₂SH), 1.44 (t, 1H, ³J_{HH} = 8 Hz, SH) ppm. ¹³C NMR ((CD₃)₂CO, 400 MHz): δ 170.4 (C=O), 71.0 (CH₂OCH₃), 69.6 (OCH₂CH₂O), 68.0 (CH₂OCO), 62.7 (CH₂CH₂OCO), 57.9 (CH₃O), 37.4 (COCH₂CH₂SH), 18.7 (COCH₂CH₂SH) ppm. FT-IR max/cm⁻¹ 2869 (CH), 1734 (C=O), 1101 (CO). SEC (CHCl₃): M_n = 1 kg mol⁻¹ (D_M = 1.15). ¹H NMR spectroscopy indicated *ca.* >99% conversion of the hydroxyl group to mercaptopropionate group.

9.6.4. General Experimental Procedure for the Nucleophilic Thiol-yne Reaction between Monofunctionalised Alkyne and Thiol PEG Precursors



Using the solvent system established in Section 9.6.1. to target different *cis* contents, a solution of mono functionalised PEG₅₅₀(SH), (53 mg, 0.08 mmol) in the required solvent (0.5 mL) and NEt₃ (0.16 mmol) was added dropwise to a stirring solution of mono-functionalised PEG₅₅₀(C≡CH), (50 mg, 0.08 mmol) in the required solvent (0.5 mL). The solution was allowed to stir at room temperature for 1 h then the solvent system was removed *in vacuo* (101 mg, all yields quantitative). Characterisation data were in accordance with that previously reported.¹⁰

9.6.4.1. Model PEG Thiol-yne Reaction in CHCl_3

Following the general procedure established in section 9.6.4, the solvent system was made with CHCl_3 (3 mL) to control the stereochemistry of the vinyl thioether bond. ^1H NMR (CDCl_3 , 300 MHz): δ 7.42 (d, 1H, $^3J_{\text{HH}} = 15$ Hz, $\text{OCOCH}=\text{CHS}$ *trans*), 6.95 (d, 1H, $^3J_{\text{HH}} = 12$ Hz, $\text{OCOCH}=\text{CHS}$ *cis*), 5.65 (d, 1H, $^3J_{\text{HH}} = 12$ Hz, $\text{OCOCH}=\text{CHS}$ *cis*), 5.55 (d, 1H, $^3J_{\text{HH}} = 15$ Hz $\text{OCOCH}=\text{CHS}$ *trans*), 4.00-4.06 (m, 2H, $\text{OCH}_2\text{CH}_2\text{OCO}$), 3.25-3.61 (m, 50H, $\text{OCH}_2\text{CH}_2\text{O}$), 3.11 (s, 3H, CH_3O) 2.42-2.51 (m, 4H, $\text{COCH}_2\text{CH}_2\text{SH}$) ppm. FT-IR max/cm^{-1} 2870 (CH), 1737 (C=O), 1709 (C=O), 1101 (CO). ^1H NMR spectroscopy indicated *ca.* 23% *cis* isomer selectivity.

9.6.4.2. Model PEG Thiol-yne Reaction in Acetone: CHCl_3 (60:40)

Following the general procedure established in section 9.6.4, the solvent system was made with Acetone: CHCl_3 (60:40) (3 mL) to control the stereochemistry of the vinyl thioether bond. ^1H NMR (CDCl_3 , 300 MHz): δ 7.43 (d, 1H, $^3J_{\text{HH}} = 15$ Hz, $\text{OCOCH}=\text{CHS}$ *trans*), 6.97 (d, 1H, $^3J_{\text{HH}} = 12$ Hz, $\text{OCOCH}=\text{CHS}$ *cis*), 5.68 (d, 1H, $^3J_{\text{HH}} = 12$ Hz, $\text{OCOCH}=\text{CHS}$ *cis*), 5.58 (d, 1H, $^3J_{\text{HH}} = 15$ Hz $\text{OCOCH}=\text{CHS}$ *trans*), 4.03-4.04 (m, 2H, $\text{OCH}_2\text{CH}_2\text{OCO}$), 3.30-3.48 (m, 50H, $\text{OCH}_2\text{CH}_2\text{O}$), 3.14 (s, 3H, CH_3O) 2.43-2.58 (m, 4H, $\text{COCH}_2\text{CH}_2\text{SH}$) ppm. FT-IR max/cm^{-1} 2868 (CH), 1734 (C=O), 1704 (C=O), 1099 (CO). ^1H NMR spectroscopy indicated *ca.* 36% *cis* isomer selectivity.

9.6.4.3. Model PEG Thiol-yne Reaction in Acetone: H_2O (90:10)

Following the general procedure established in section 9.6.4, the solvent system was made with Acetone: H_2O (90:10) (3 mL) to control the stereochemistry of the vinyl thioether bond. ^1H NMR (CDCl_3 , 300 MHz): δ 7.42 (d, 1H, $^3J_{\text{HH}} = 15$ Hz, $\text{OCOCH}=\text{CHS}$ *trans*),

6.95 (d, 1H, $^3J_{\text{HH}} = 12$ Hz, $\text{OCOCH}=\text{CHS}$ *cis*), 5.66 (d, 1H, $^3J_{\text{HH}} = 12$ Hz, $\text{OCOCH}=\text{CHS}$ *cis*), 5.56 (d, 1H, $^3J_{\text{HH}} = 15$ Hz $\text{OCOCH}=\text{CHS}$ *trans*), 4.00-4.02 (m, 2H, $\text{OCH}_2\text{CH}_2\text{OCO}$), 3.27-3.64 (m, 50H, $\text{OCH}_2\text{CH}_2\text{O}$), 3.12 (s, 3H, CH_3O) 2.40-2.88 (m, 4H, $\text{COCH}_2\text{CH}_2\text{SH}$) ppm. FT-IR max/cm $^{-1}$ 2866 (CH), 1735 (C=O), 1704 (C=O), 1099 (CO), 805 (C=C *cis*). ^1H NMR spectroscopy indicated *ca.* 66% *cis* isomer selectivity.

9.6.4.4. Model PEG Thiol-yne Reaction in Acetone:H $_2\text{O}$ (65:35)

Following the general procedure established in section 9.6.4, the solvent system was created with Acetone:H $_2\text{O}$ (65:35) (3 mL) to control the stereochemistry of the vinyl thioether bond. ^1H NMR (CDCl_3 , 300 MHz): δ 7.42 (d, 1H, $^3J_{\text{HH}} = 15$ Hz, $\text{OCOCH}=\text{CHS}$ *trans*), 6.95 (d, 1H, $^3J_{\text{HH}} = 12$ Hz, $\text{OCOCH}=\text{CHS}$ *cis*), 5.66 (d, 1H, $^3J_{\text{HH}} = 12$ Hz, $\text{OCOCH}=\text{CHS}$ *cis*), 5.56 (d, 1H, $^3J_{\text{HH}} = 15$ Hz $\text{OCOCH}=\text{CHS}$ *trans*), 4.00-4.01 (m, 2H, $\text{OCH}_2\text{CH}_2\text{OCO}$), 3.29-3.62 (m, 50H, $\text{OCH}_2\text{CH}_2\text{O}$), 3.12 (s, 3H, CH_3O) 2.43-2.82 (m, 4H, $\text{COCH}_2\text{CH}_2\text{SH}$ pm. FT-IR max/cm $^{-1}$ 2867 (CH), 1734 (C=O), 1700 (C=O), 1100 (CO), 802 (C=C *cis*). ^1H NMR spectroscopy indicated *ca.* 91% *cis* isomer selectivity.

9.6.4.5. Model PEG Thiol-yne Reaction in H $_2\text{O}$ (100%)

Following the general procedure established in section 9.6.4, the solvent system was made with H $_2\text{O}$ (100%) and NEt_3 as a catalyst (1 mL) to control the stereochemistry of the vinyl thioether bond. ^1H NMR (CDCl_3 , 300 MHz): δ 7.73 (d, 1H, $^3J_{\text{HH}} = 15$ Hz, $\text{OCOCH}=\text{CHS}$ *trans*), 7.43 (d, 1H, $^3J_{\text{HH}} = 12$ Hz, $\text{OCOCH}=\text{CHS}$ *cis*), 5.86 (m, 2H, $\text{OCOCH}=\text{CHS}$), 4.19-4.21 (m, 2H, $\text{OCH}_2\text{CH}_2\text{OCO}$), 3.44-3.79 (m, 50H, $\text{OCH}_2\text{CH}_2\text{O}$), 3.28 (s, 3H, CH_3O) 2.64-2.77 (m, 4H, $\text{COCH}_2\text{CH}_2\text{SH}$) ppm. FT-IR max/cm $^{-1}$ 2868 (CH), 1735 (C=O), 1700

(C=O), 1099 (CO), 805 (C=C *cis*). ^1H NMR spectroscopy indicated *ca.* 93% *cis* isomer selectivity.

9.6.5. Characterisation of the Stereocontrolled Thiol-yne PEG Hydrogels

Once the solvent systems were determined to target different *cis:trans* ratios of the PEG thiol-yne organogels, the samples were converted into hydrogels through a solvent switch process. The organogels were synthesised as stated in section 9.6.1, sealed and left to cure for 1 h. The samples were then immersed in acetone with frequent solvent changes. After 5 days, water was gradually introduced into the organogels to form hydrogels. Once the hydrogels had started to swell (2 days) it was determined that the solvent exchange was complete. After this process, the dimensions of the hydrogels were measured to confirm that they were the same size and swelling factor. The samples were then ready to fully characterise through swelling kinetics, rheology and compression studies. All characterisation of the hydrogels was carried out after the 7-day solvent exchange process, apart from the gel fraction study carried out straight after the 1 h curing process.

9.6.6. Rheological Characterisation of the Stereocontrolled Hydrogels

After the 7-day solvent switch process the hydrogel were subjected to oscillatory amplitude sweep experiments. The sample was tested using a parallel plate configuration with a sandblasted bottom plate to reduce the slippage of the sample. The upper plate had a similar diameter to the hydrogel sample (8 mm) to reduce the drag on the sample. The normal force was kept constant at 0.04 N to ensure there was contact between the sample and plates and to confirm the sample did not dehydrate during testing. Measurements were recorded as stated in 9.2.4.1.3.

9.7. Experimental Procedure for Chapter 5

9.7.1. PEG/Natural Polymer Hydrogel Fabrication

For the incorporation of a natural polymer into the thiol-yne PEG system the natural polymers were mixed in solution with a single PEG precursor before gelation. Once synthesised they were characterised as stated in section 9.2.3 and 9.2.4.

9.7.1.1. Fabrication of PEG/Alginate Interpenetrating Networks (IPNs)

Sodium alginate (199.1 g mol^{-1} , 21 mg, 0.11 mmol) in PBS (917 μL) was heated to $70 \text{ }^\circ\text{C}$ and stirred for 20 min to dissolve then left to cool to room temperature. In separate vials $\text{PEG}_{2k}(\text{C}\equiv\text{CH})_4$ (32.6 mg, 1.48×10^{-2} mmol) was dissolved in PBS (509 μL) and CaCO_3 (5.3 mg, 5.27×10^{-2} mmol) was dissolved in PBS (51 μL). The alginate, CaCO_3 and PEG alkyne were then added together and vortexed. The $\text{PEG}_{4k}(\text{SH})_2$ (129.7 mg, 2.95×10^{-2} mmol) dissolved in PBS (509 μL) was then mixed with $\text{D-}(+)\text{-Glucono-1,5-lactone}$ (GDL) (18.8 mg, 0.11 mmol) dissolved in PBS (51 μL). The PEG thiol/GDL vial was then added to the PEG alkyne/ Alginate/ CaCO_3 vial and mixed together on a vortex mixer for 10 s. The mixture was then injected into a mould suitable for the chosen analysis.

9.7.1.2. Fabrication of PEG/Chitosan IPNs

Chitosan (low molecular weight) (20.7 mg, 0.1 mmol) was dissolved in 0.1 M HCl (1 mL) and added to $\text{PEG}_{2k}(\text{C}\equiv\text{CH})_4$ (32.6 mg, 1.48×10^{-2} mmol) dissolved in PBS (334 μL) and mixed. $\text{PEG}_{4k}(\text{SH})_2$ (127.8 mg, 2.91×10^{-2} mmol) was dissolved in PBS (334 μL) and added to glycerol phosphate (GP) (103.5 mg, 5 wt%) in PBS (334 μL). The two solutions were then mixed together on a vortex mixer for 10 s. The mixture was then injected into a mould suitable for the chosen analysis.

9.7.1.3. Fabrication of PEG/Gelatin Hydrogels

Gelatin (from porcine skin) (21 mg, 0.1 mmol) in PBS (1 mL) was heated to 70 °C for 20 min to dissolve. The solution was allowed to cool slightly and added to PEG_{2k}(C≡CH)₄ (32.6 mg, 1.48×10^{-2} mmol) dissolved in PBS (509 μL) and mixed. The Gelatin/PEG alkyne solution was then added to PEG_{4k}(SH)₂ (129.7 mg, 2.95×10^{-2} mmol) dissolved in PBS (509 μL) mixed together on a vortex mixer for 10 s. The mixture was then injected into a mould suitable for the chosen analysis.

9.7.1.4. Fabrication of PEG/Hyaluronic Acid Hydrogels

Hyaluronic acid (HA) (Sodium salt, low molecular weight 40- 50 kg mol⁻¹) (20.7 mg, 1 wt%) was dissolved in PBS (1 mL) and added to PEG_{2k}(C≡CH)₄ (32.1 mg, 1.46×10^{-2} mmol) dissolved in PBS (502 μL) and mixed. The HA/PEG alkyne solution was then added to the PEG_{4k}(SH)₂ (127.8 mg, 2.91×10^{-2} mmol) dissolved in PBS (502 μL) mixed together on a vortex mixer for 10 s. The mixture was then injected into a mould suitable for the chosen analysis.

9.7.1.5. Fabrication of PEG/Heparin Hydrogels

Heparin (sodium salt) (20.7 mg, 1wt%) was dissolved in PBS (1 mL) and added to PEG_{2k}(C≡CH)₄ (32.1 mg, 1.46×10^{-2} mmol) dissolved in PBS (502 μL) and mixed. The HA/PEG alkyne solution was then added to the PEG_{4k}(SH)₂ (127.8 mg, 2.91×10^{-2} mmol) dissolved in PBS (502 μL) mixed together on a vortex mixer for 10 s. The mixture was then injected into a mould suitable for the chosen analysis.

9.7.2. *Cytocompatibility Studies and 3D Cell Encapsulation Studies*

The Y201 hTERT-immortalised human clonal mesenchymal stem cell (MSC) line (a kind gift from Prof Paul Genever, University of York) was cultured in MEM- α medium supplemented with 10% v/v FCS, 1% penicillin/streptomycin, 10 μ M Asc-2-phos, and 5 mL Glutamax.

9.7.2.1. *Cell Metabolic Activity (3D culture)*

For 3D cell encapsulation, hydrogels (n=4) were prepared in PBS in 24-well cell culture inserts with a 0.4 μ m pore PET membrane. Specifically, 400,000 cells per hydrogel were suspended with the thiol-terminated PEG precursor solution, followed by addition of the alkyne and mixing. Then, 100 μ L of the solution was added into the inserts and let to gel. After 10 min, fresh media was added on top (100 μ L) and around the hydrogel (900 μ L), and cells were incubated up to 3 days. Cell viability was assessed using alamarBlue® viability assay at different time points (*i.e.* 24, 48, and 72 h) according to the manufacturer's recommendations. Fluorescence was measured using a BioTek FLx800 plate reader ($\lambda_{\text{Ex.}}$ = 540 nm, $\lambda_{\text{Em.}}$ = 590 nm).

9.7.2.2. *Cell Viability Assay (3D culture)*

Cell viability was also assessed on day 1 (24 h) and day 3 (72 h) using Live/Dead™ Viability/Cytotoxicity Kit (Invitrogen), including calcein AM for live cells ($\lambda_{\text{Ex.}}$ = 495, $\lambda_{\text{Em.}}$ = 515) and ethidium homodimer for dead cells ($\lambda_{\text{Ex.}}$ = 528, $\lambda_{\text{Em.}}$ = 617). The staining solution was prepared by adding 0.5 μ L of calcein AM and 2 μ L of ethidium homodimer to 1 mL of PBS. On the day of assay, hydrogels were washed with PBS, and the staining solution was added around (350 μ L) and on top (150 μ L) of the gels, which were then

incubated for 30 min. Fluorescence imaging in three-dimensions (3D) was conducted with a Leica SP5 Inverted microscope. Z-stacks with an average thickness of 200 μm were collected from different zones of each sample, and the images were processed using ImageJ software (1.51u).

9.8. Experimental Procedure for Chapter 6

9.8.1. Synthesis of Hydrogel Precursors

9.8.1.1. Thiol-Functionalised Peptide Synthesis

Both the pendant adhesion peptide (CGRGDS) and MMP-degradable crosslinking peptide (GCRDVPMS↓MRGGDRCG) were synthesised using standard solid phase peptide synthesis (SPPS) on MBHA rink amide resin (Novabiochem) on a peptide synthesiser (Protein Technologies PS3) using Fmoc-protected amino acids (ChemPep), deprotected with 20% piperidine in DMF and activated with *O*-(Benzotriazole-1-yl)-*N,N,N',N'*-tetramethyluronium hexafluorophosphate (HBTU) at 4 \times excess. Peptide was cleaved from resin with a cleavage solution containing 95% v/v trifluoroacetic acid (TFA), 2.5 v/v triisopropylsilane (TIPS), 2.5% v/v water, and 5% w/v dithiothreitol (DTT) to prevent disulfide formation. The cleavage solution containing the peptide product was precipitated into cold ether, then pelleted by centrifugation (4400 rpm, 4 $^{\circ}\text{C}$, 5 min). Decanted for a total of three ether washes and then dried overnight. Peptides were purified by high-performance liquid chromatography (HPLC; XBridge BEH C18 OBD 5 μm column; Waters, Milford, MA) with a linear water-acetonitrile gradient and molecular weight was verified by electrospray ionisation mass spectrometry.

9.8.1.2. Synthesis of Thiol-ene Hydrogel Precursors

Thiol-ene gel precursors, including PEG_{20k}(SH)₄, macromer, alloc-functionalised peptides (K(alloc)GWGRGDS and KK(alloc)GGPQIWGQGK(alloc)K), and lithium acylphosphinate (LAP) were synthesised according to the previously published protocol.^{11, 12}

9.8.2. Hydrogel Fabrication

9.8.2.1. Thiol-yne Hydrogel Synthesis

Hydrogels were fabricated in a similar procedure as stated in 9.4.3. In a typical procedure for making a thiol-yne PEG gel, PEG_{1k}(SH)₃ (7.9 mg, 6.23×10^{-6} mmol) was dissolved in 75 μ L PBS solution (pH 7.4) solution or Dulbecco's Modified Eagle Medium (DMEM). A separate solution of PEG_{1k}(C \equiv CH)₃ (7.2 mg, 6.23×10^{-6} mmol) in 75 μ L PBS (pH 7.4) or DMEM. The two solutions were mixed together on a vortex mixer for 5 s. 20 μ L of hydrogel solution was then pipetted into a 1 mL syringe mold and left to cure.

9.8.2.2. Thiol-ene Hydrogel Synthesis

A solution of 10 wt% PEG_{20k}(SH)₄, a stoichiometric amount of alloc-functionalised crosslinker (KK(alloc)GGPQIWGQGK(alloc)K) and 2 mM of alloc-functionalised fibronectin mimetic peptide (K(alloc)GWGRGDS) and 2 mM LAP were combined in DMEM. 20 μ L of the hydrogel solution was then pipetted into a 1 mL syringe mould and polymerised by exposure to 365 nm light (10 mW cm^{-2}) for 1 min.

9.8.3. Validation of Pendant Peptide Incorporation.

Standard solutions of thiol-functional fluorescent peptide in PBS were prepared at various concentrations (0.1, 0.5, 1, 2, 3, 4 mM). Thiol-yne hydrogels were formed following the procedure stated in section 9.4.3 then soaked in the standard fluorescent peptide solutions overnight. Thiol-yne hydrogels were synthesised with 5 mM thiol-functionalised fluorescent peptide and swollen in PBS or phenol red free media overnight. Images of fluorescence were captured with a LSM 810 confocal microscope (Zeiss), with a 488 nm laser. Fluorescence of each image was quantified in ImageJ. Fluorescence of standards were graphed by concentration and fit linearly. The linear fit equation was used to determine the concentration of fluorescent peptide covalently incorporated into the gels.

9.8.4 Mechanical Characterisation of the Thiol-yne PEG Hydrogels

Compression testing was conducted as stated in section 9.2.4.1.3 with hydrogels synthesised in DMEM.

9.8.4.1. Rheological Characterisation of the Thiol-yne PEG Hydrogels

Rheological characterisation was carried as stated in section 9.2.4.1.1 with hydrogel precursors dissolved in DMEM and formed *in situ* between the rheometer plates. Average G' and G'' were calculated as a constant frequency of 10 rad s^{-1} and 0.5% strain. The Young's Moduli (described in Section 9.2.4.1.4) were calculated from these values.

9.8.5. 2D cell Metabolic Activity and 3D Cell Encapsulation

The MDA-MB-231, T47D, and MCF-7 cell lines were used in this chapter. MDA-MB-231 and T47D cell lines were maintained in Dulbecco's Modified Eagle Medium (DMEM; Corning 10-013-CV) supplemented with 10 vol% fetal bovine serum (FBS), 1

vol% Glutamax and 1 vol% penicillin/streptomycin (PS). The MCF-7 cell line was maintained in DMEM supplemented with 5 vol% FBS and 1 vol% PS.

9.8.5.1. Cell Encapsulation in 3D Thiol-yne and Radically-Initiated Thiol-ene Hydrogels

Trypsin (0.25% Trypsin / 0.1% EDTA) was added to cells, and incubated at 37 °C, until all the cells detached (~3 min), the solution was then quenched with culture medium. Cells were centrifuged (1,000 rpm, 5 min) and resuspended in serum-free DMEM. Cells were mixed with hydrogel precursor solution, and polymerisations proceeded as noted for hydrogel fabrication. For thiol-yne chemistry, it is critical that cells be mixed with the thiol-containing gel precursor first to limit exposure to any potential hydrolysis products of PEG alkyne before polymerisation.

9.8.5.2. Cell metabolic activity (2D culture)

For 2D cell culture, cell metabolic activity was assessed using the CellTiter 96 assay, a colorimetric assay which includes a tetrazolium compound and an electron coupling reagent, phenazine ethosulfate. On day -1, cells were seeded in a 96-well plate (n=3) at a concentration of 15,000 cells cm⁻². On day 0, cells were exposed to the desired treatments. For each treatment, 50 µL of solution was added to each well and incubated at room temperature for 15 min. The only treatment that was not incubated for 15 min was the radically-initiated thiol-ene treatment. Treatments included: Medium (control), PBS solution, thiol-ene, PEG alkyne, cysteine only, and thiol-yne. The thiol-ene treatment mimicked thiol-ene gelation conditions and included a 10 wt% solution of PEG_{3.4k}(SH)₂, 2-allyl functionalised peptide, and LAP in PBS, which was added to wells, then exposed to long wavelength UV light (365 nm, 10 mW cm⁻²) for 1 min. The PEG alkyne treatment

included a solution of PEG_{1k}(C≡CH)₃ in PBS (concentration equivalent for making 10 wt% gels). The cysteine only treatment was a solution of cysteine in PBS (concentration equivalent to the number of thiol groups present in 10 wt% thiol-yne PEG gel formation). The thiol-yne treatment mimicked thiol-yne gelation conditions by incorporating concentrations of PEG_{1k}(C≡CH)₃ and thiol (cysteine) required to form a 10 wt% thiol-yne PEG hydrogel in PBS. Once the treatment was removed, 100 μL of fresh culture media were added to each well. The media were exchanged after 1 h. Metabolic activity of the cells was assessed on day 1 and day 3. For day 3 samples, the 100 μL of media were changed on day 2. The metabolic activity was assessed according to the manufacturer's instructions. Briefly, 20 μL of CellTiter 96 solution was added to each well; the plates were incubated for 4 h; and then the absorbance was measured on a plate reader at 490 nm.

9.8.5.3. Cell metabolic activity (3D culture)

For 3D cell culture, cell metabolic activity was assessed using the alamarBlue assay. On day 0, cells were encapsulated in gels (n=4) and placed in 48-well plates with 500 μL of media. Metabolic activity was assessed on day 1, day 3, and day 7. Metabolic activity of the cells was assessed according to the manufacturer's instructions. Briefly, alamarBlue reagent was diluted 1:10 in phenol red free media, then media were removed from each well, and 500 μL of diluted alamarBlue solution added to each well. Well plates were incubated for 4 h, then the fluorescence was measured on a plate reader (Ex = 560, Em = 590). Media were replaced on the gels, since the same gels were measured at each time point.

9.8.5.4. Cell viability assay (3D culture)

Cell viability for 3D cell culture was assessed using a Live/Dead Assay Kit, including calcein AM and ethidium homodimer. Working solution was prepared by adding 0.5 μL of calcein AM and 2 μL of ethidium homodimer to 1 mL of PBS. On day 0, cells were encapsulated in gels ($n=3$) and placed in 48-well plates with 500 μL of media. Cell viability was assessed on day 1, day 3, day 7, and day 10. On the day of assay, media were removed, and 500 μL of working solution was added. Thiol-yne gels were incubated for 30 min and thiol-ene gels were incubated for 10 min, to account for differences in diffusion due to variation in matrix densities between the two systems. Fluorescence imaging in 3D was captured with a LSM 810 confocal microscope (Zeiss). Staining for live cells (Calcein, $\lambda_{\text{Ex.}} = 495 \text{ nm}$, $\lambda_{\text{Em.}} = 515 \text{ nm}$) was excited with a 488 nm laser, while staining for dead cells (Ethidium homodimer, $\lambda_{\text{Ex.}} = 528 \text{ nm}$, $\lambda_{\text{Em.}} = 617 \text{ nm}$) was excited with a 514 nm laser. Z-stacks with an average thickness of 200 μm were collected from three different x-y zones of each sample and orthogonal projections were obtained from each Z-stack. Images were processed using ImageJ software.

Analysis of cell cluster diameter was carried out using confocal microscopy and images processed using Volocity (Perkin Elmer). All compositions were formed in serum free media (2,500 cells μL^{-1}). Cell clusters were stained with calcein and images were taken in 200 μm stacks (interval = 5.7 μm) by confocal microscopy (LSM 810 confocal microscope; Zeiss). Images were then processed using Volocity (Perkin Elmer), the diameter of cell clusters stained with calcein was analyzed using the longest axis measurement function in Volocity. Analysis with Volocity included use of the following

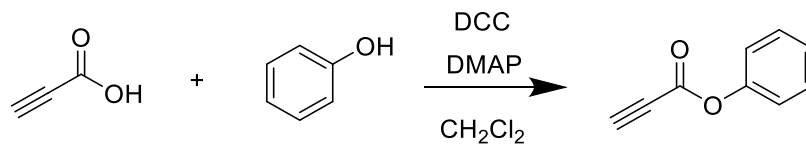
functions: find objects, close, fill holes in objects, remove noise from objects, separate touching objects, and exclude objects by size (objects $<1500 \mu\text{m}^3$).

9.8.5.5. Immunostaining of Cells in 3D Culture

Hydrogels containing cells were rinsed with PBS (2×5 min, 37°C) and then fixed with 4% paraformaldehyde (15 min, room temperature). Gels were washed with PBS (1×5 min, room temperature), and then with a solution of 3% bovine serum albumin (BSA) and 0.05% Triton-X in PBS (2×5 min, room temperature). Cells were permeabilised and blocked by incubating with a solution of 5% BSA and 0.1% Triton-X in PBS (1 h, room temperature). Ki-67 samples were stained by incubating with solution of $2 \mu\text{g mL}^{-1}$ Anti-Ki-67 antibody (abcam), 5% BSA, and 0.1% Triton-X in PBS (4°C , overnight). Gels were washed with a solution of 3% BSA and 0.05% Triton-X in PBS (3×30 min, room temperature). Secondary antibody was added by incubating in a solution of goat anti-mouse AF647 (Invitrogen), phalloidinTRITC, 5% BSA, and 0.1% Triton-X in PBS (4°C , overnight). Gels were washed with 3% BSA and 0.05% Triton-X in PBS (3×30 min, room temperature). Gels were incubated with DAPI solution (700 nM DAPI in PBS, 1 h, room temperature). Gels were washed with PBS (3×30 min, room temperature) and imaged immediately with a LSM 810 confocal microscope (Zeiss). FIJI was used for image processing and quantification of Ki-67 positive cells.

9.9. Experimental Procedure for Chapter 7

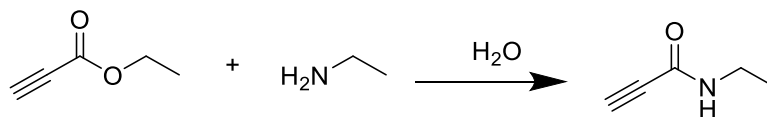
9.9.1. Synthesis of Phenyl Propiolate



Phenyl propiolate was synthesised using a modified literature procedure.^{13, 14} Phenol (5 g, 0.05 mol) and propionic acid (4.1 g, 0.055 mol) were dissolved in CH₂Cl₂ (10 mL) and cooled to 0 °C. A solution of *N,N'*-dicyclohexylcarbodiimide (DCC, 10.3 g, 0.05 mol) and 4-dimethylaminopyridine (DMAP, 0.6 g, 0.005 mol), in CH₂Cl₂ (10 mL), was added dropwise, keeping the temperature of the reaction mixture under 5 °C. The mixture was stirred for 4 h. The precipitate was filtered off and the solution was washed with H₂O. The organic layers were combined, dried over MgSO₄ and the volatile parts were removed under reduced pressure. The product was purified by column chromatography and vacuumed distilled to yield white crystals (4.2 g, 57%). Product characterisation data was in line with that previously reported.^{13, 14}

¹H NMR (((CD₃)₂SO), 298 K, 300 MHz): δ 7.49 (t, 2H, ³J_{HH} = 15 Hz, ArCH), 7.32 (m, 3H, ArCH), 4.57 (s, 1H, C≡CH) ppm. ¹³C NMR (((CD₃)₂SO), 298 K, 300 MHz): δ 151.04 (CHCO), 149.71 (OCO C≡CH), 129.74 (CHCH₂CH₂C), 126.65 (CHCH₂CH₂C), 121.47 (CHCH₂CH₂C), 80.67 (C≡CH), 74.32 (C≡CH) ppm. IR max/cm⁻¹ 2120 (C≡CH), 1728 (CO) cm⁻¹. HRMS (ESI-MS +ve): m/z 147.0441 (M⁺, 99%), 148.0474 (5). Anal. Calcd for C₉H₇O₂: C 73.9; H 4.1%. Found: C 73.6; H 4.0%.

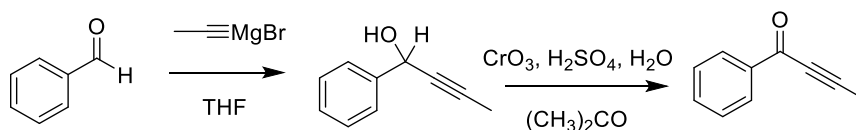
9.9.2. Synthesis of Ethyl Propiolamide



Ethyl propiolamide was synthesised using a modified literature procedure.¹⁵ Ethyl amine (4.7 g, 0.105 mol, 66-70 wt% H₂O) was diluted in H₂O (30 mL) and cooled to 0 °C. Ethyl propiolate (9.81 g, 0.1 mol) was added dropwise and the mixture was stirred for 30 min. Acetic acid (2 mL) was added followed by brine. The product was then extracted in ethyl acetate (EtOAc) (3 × 20 mL). The organic layers were combined, dried over MgSO₄ and concentrated. The product was then distilled to yield white crystals (4.9 g, 51%). Product characterisation data was in line with that previously reported.¹⁵

¹H NMR ((CDCl₃), 298 K, 300 MHz): δ 3.32 (q, 2H, ²J_{HH} = 27 Hz, CH₂), 2.76 (s, 1H, C≡CH), 1.15 (t, 3H, ²J_{HH} = 15 Hz, CH₃) ppm. ¹³C NMR ((CDCl₃, 298 K, 300 MHz): δ 152.25 (C(=O)NH), 79.25 (C≡CH), 73.00 (C≡CH), 34.90 (HNCH₂CH₃), 14.48 (HNCH₂CH₃) ppm. IR max/cm⁻¹ 3193 (NH), 2106 (C≡CH), 1628 (CO), 1550 (NH) cm⁻¹. HRMS (ESI-MS +ve): m/z 120.0420 (MNa⁺, 100%). Anal. Calcd for C₅H₇NO: C 61.8; H 7.3; N 14.4%. Found: C 61.4; H 7.3; N 14.3%.

9.9.3. Synthesis of 1-Phenylbut-2-yn-1-one

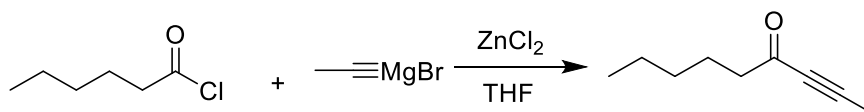


1-Phenylbut-2-yn-1-one was synthesised using a modified literature procedure.¹⁶ 1-Propynylmagnesium bromide (100 mL, 0.5M in THF, 0.05 mol) was added to a solution of benzaldehyde (4.82g, 0.045 mol) in THF (200 mL) at 0 °C. The mixture was stirred

overnight then cooled to $-10\text{ }^{\circ}\text{C}$ and sat. aq. NH_4Cl (100 mL) was added. The precipitate was filtered off and the aqueous layer was extracted with EtOAc ($3 \times 100\text{ mL}$) to yield an orange oil. To increase the yield the organic phase was concentrated and purified by column chromatography to yield the intermediate alcohol. The intermediate alcohol was diluted in acetone (2 mL) and cooled to $0\text{ }^{\circ}\text{C}$. Jones' reagent (chromic acid (CrO_3 (670 mg), H_2SO_4 (580 μL) and H_2O (1.25 mL))) was added dropwise until a green colour change was maintained (*ca.* 15 min). 2-Propanol (1 mL) was added and sat. NaHCO_3 solution was added until the pH was neutral. The solution was filtered and washed with brine (20 mL). The product was extracted into Et_2O ($3 \times 100\text{ mL}$), dried and concentrated to yield an orange oil (5.4 g, 83%). The product was purified by column chromatography then distilled to give a colourless liquid. Product characterisation data was in line with that previously reported.¹⁶

^1H NMR ($(\text{CD}_3)_2\text{SO}$), 298 K, 300 MHz): δ 8.07 (d, 2H, $^3J_{\text{HH}} = 9\text{ Hz}$, ArCH), 7.64-7.46 (m, 3H, ArCH), 2.13 (s, 1H, $\text{C}\equiv\text{CCH}_3$) ppm. ^{13}C NMR ($(\text{CD}_3)_2\text{SO}$), 298 K, 300 MHz): δ 177.04 (CCO), 136.30 (CHCCO), 133.92 (ArCH), 128.92 (ArCH), 128.54 (ArCH), 93.34 ($\text{C}\equiv\text{CCH}_3$), 78.47 ($\text{C}\equiv\text{CCH}_3$), 3.42 ($\text{C}\equiv\text{CCH}_3$) ppm. IR $\text{max}/\text{cm}^{-1}$ 2203 ($\text{C}\equiv\text{CCH}_3$), 2242 ($\text{C}\equiv\text{CCH}_3$), 1640 (CO) cm^{-1} . HRMS (ESI-MS +ve): m/z 167.0467 (MNa^+ 100%). Anal. Calcd for $\text{C}_{10}\text{H}_8\text{O}$: C 83.3; H 5.6%. Found C 81.6; H 5.6%.

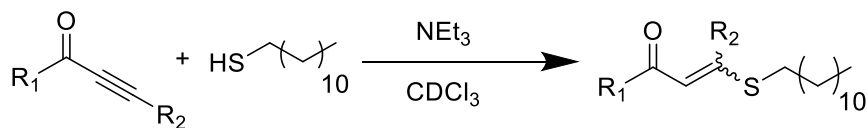
9.9.4. Synthesis of Non-2-yn-4-one



To a slurry of ZnCl_2 (14.6 g 0.107 mol) in THF (100 mL) was added 1-propynylmagnesium bromide (100 mL, 0.5 M in THF, 0.05 mol) at 0 °C with stirring. After stirring for 15 min hexanoyl chloride (5.2 mL, 0.037 mol) was added. The reaction was warmed to room temperature and stirred for 2 h. The reaction was then cooled to -10 °C and sat. aq. NH_4Cl was added. The layers were separated, and the aq. layer was extracted with Et_2O (3×100 mL) and washed with sat. aq. NH_4Cl , H_2O and brine (100 mL) then dried and concentrated to yield a small amount of product. The organic layer was then concentrated and purified by column chromatography to yield the crude product (3.2 g, 63%). The product was purified by vacuum distillation to yield a colourless oil.

^1H NMR ((CDCl_3) , 298 K, 300 MHz): δ 2.50 (t, 2H, $^3J_{\text{HH}} = 12$ Hz, COCH_2), 2.04 (s, 3H, $\text{C}\equiv\text{CCH}_3$), 1.58 (dd, 2H, COCH_2), 1.25-1.33 (m, 6H, $\text{CH}_2\text{CH}_2\text{CH}_2$), 0.88 (t, 3H, CH_3) ppm. ^{13}C NMR ((CDCl_3) , 298 K, 300 MHz): δ 187.11 (CO), 88.79 (COCH_2), 79.60 (COCH_2CH_2), 44.20 (COCH_2 CH_2CH_2), 30.62 ($\text{CH}_2\text{CH}_2\text{CH}_2\text{CH}_2\text{CH}_3$), 23.15 ($\text{CH}_2\text{CH}_2\text{CH}_2\text{CH}_2\text{CH}_3$), 21.88 ($\text{COC}\equiv\text{CCH}_3$), 12.23 ($\text{COC}\equiv\text{CCH}_3$), 3.08 ($\text{COC}\equiv\text{CCH}_3$), ppm. IR max/ cm^{-1} 2215 ($\text{C}\equiv\text{CCH}_3$), 1671 (CO) cm^{-1} . HRMS (ESI-MS +ve): m/z 167.0937 (MNa^+ 100%). Anal. Calcd for $\text{C}_9\text{H}_{14}\text{O}$: C 78.2; H 10.2%. Found C 77.5; H 10.2%.

9.9.5. General Experimental Procedure for the Nucleophilic Thiol-yne Kinetic Study



R₁ = OCH₂CH₃ (ester control), C₆H₅ (aromaticity), CH₃ (ketone), OC₆H₅ (aromatic ester) or NHCH₂CH₃ and R₂ = H. Or R₁ = (CH₂)₄CH₃ (ketone) or C₆H₅ (aromaticity) and R₂ = CH₃.

In a typical reaction NEt₃ (0.005-10 eq) and 1-dodecanethiol (DT) (1.2 eq) were dissolved in deuterated chloroform (CDCl₃) (1 mL) and stirred. The small molecule alkyne (1 eq) was added and the reaction was mixed on a vortex mixer (5 s) before an aliquot of the reaction mixture was transferred to an NMR spectroscopy tube. ¹H NMR spectra were recorded at appropriate time points and the reaction was repeated in triplicate for each alkyne. ¹H NMR spectroscopy characterisation was taken *in situ*. Conversion was determined by the comparison of integrals between a stable proton environment on the alkyne starting material *e.g.* the quartet at δ = 4.13 ppm (corresponding to the ethyl group on ethyl propiolate), and the formed alkene proton environment *e.g.* a set of doublets at δ = 5.68 and 5.78 ppm (the formation of the *cis* and the *trans* alkene protons). The initial rate of the reaction was then determined using first order kinetics taking the natural log of the total concentration of starting alkyne, ln[A]₀ divided by the concentration of alkyne at *t*, [A]_{*t*}. A rate graph was then constructed plotting ln[A]_{*t*} against time, to calculate the rate from the gradient of the line. The rate calculated was then normalised by the concentration of NEt₃ used for each study.

9.9.5.1 Thiol-yne Kinetic Study for Ethyl Propiolate (EP) with DT

Following the general procedure stated in section 9.9.5. NEt₃ (0.03 eq) was added to a solution of DT (24.2 mg, 1.2 mmol) in CDCl₃ (0.5 mL). EP (9.8 mg, 1 mmol) in CDCl₃ (0.5 mL) was added to the DT/NEt₃ solution, vortexed and an aliquot was transferred to an NMR spectroscopy tube. ¹H NMR spectra were recorded at 30 s intervals for 1 h and repeated in triplicate. ¹H NMR spectroscopy taken after 1 h *in situ* (91% conversion): ¹H NMR (CDCl₃, 600 MHz): δ 7.64 (d, 1H, ³J_{HH} = 18 Hz, OCOCH=CHSCH₂ *trans*), 7.03 (d, 1H, ³J_{HH} = 6 Hz, OCOCH=CHSCH₂ *cis*), 5.78 (d, 1H, ³J_{HH} = 6 Hz OCOCH=CHSCH₂ *cis*), 5.68 (d, 1H, ³J_{HH} = 18 Hz, OCOCH=CHSCH₂ *trans*), 4.13 (q, 2H, ³J_{HH} = 8 Hz, CH₃CH₂OCO), 2.74 (t, 2H, ³J_{HH} = 9 Hz, CHSCH₂CH₂), 1.63 (t, 3H, ³J_{HH} = 8 Hz, CH₃CH₂OCO), 1.10-1.37 (m, 20H, CH₂CH₂CH₂), 0.84 (t, 3H, ³J_{HH} = 8 Hz, CH₃CH₂) ppm. ¹H NMR spectroscopy indicated *ca.* 83% *cis* isomer selectivity.

9.9.5.2. Thiol-yne Kinetic Study for Phenyl-2-propyn-1-one (PPO) with DT

Following the general procedure stated in section 9.9.5. NEt₃ (0.005 eq) was added to a solution of DT (24.6 mg, 1.2 mmol) in CDCl₃ (0.5 mL). PPO (13 mg, 1 mmol) in CDCl₃ (0.5 mL) was added to the DT/NEt₃ solution, vortexed and an aliquot was transferred to an NMR spectroscopy tube. ¹H NMR spectra were recorded at 2 min intervals for 45 min and repeated in triplicate. ¹H NMR spectroscopy taken after 45 min *in situ* (17% conversion): ¹H NMR (CDCl₃, 400 MHz): δ 7.96 (d, 2H, ³J_{HH} = 12 Hz, ArCH), 7.39-7.54 (m, 4H, ArCH and COCH=CHSCH₂), 7.08 (d, 1H, ³J_{HH} = 12 Hz, COCH=CHSCH₂ *cis*), 5.68 (d, 1H, ³J_{HH} = 16 Hz COCH=CHSCH₂ *trans*), 2.80 (t, 2H, ³J_{HH} = 8 Hz,

CHSCH₂CH₂), 1.26-1.75 (m, 20H, CH₂CH₂CH₂), 0.88 (t, 3H, ³J_{HH} = 8 Hz, CH₃CH₂) ppm.

¹H NMR spectroscopy indicated *ca.* 14% *cis* isomer selectivity.

9.9.5.3. Thiol-yne Kinetic Study for 3-Butyn-2-one with DT

Following the general procedure stated in section 9.9.5. NEt₃ (0.001 eq) was added to a solution of DT (24.6 mg, 1.2 mmol) in CDCl₃ (0.5 mL). 3-Butyn-2-one (6.8 mg, 1 mmol) in CDCl₃ (0.5 mL) was added to the DT/NEt₃ solution, vortexed and an aliquot was transferred to an NMR spectroscopy tube. ¹H NMR spectra were recorded at 2 min intervals for 47 min and repeated in triplicate. ¹H NMR spectroscopy taken after 47 min *in situ* (17% conversion): ¹H NMR (CDCl₃, 400 MHz): δ 7.61 (d, 1H, ³J_{HH} = 16 Hz, COCH=CHSCH₂ *trans*), 7.06 (d, 1H, ³J_{HH} = 8 Hz, COCH=CHSCH₂ *cis*), 6.30 (d, 1H, ³J_{HH} = 8 Hz, COCH=CHSCH₂ *cis*), 6.10 (d, 1H, ³J_{HH} = 16 Hz, COCH=CHSCH₂ *trans*), 2.21 (s, 3H, CH₃CO), 1.26-1.64 (m, 20H, CH₂CH₂CH₂), 0.88 (t, 3H, ³J_{HH} = 8 Hz, CH₃CH₂) ppm. ¹H NMR spectroscopy indicated *ca.* 72% *cis* isomer selectivity.

9.9.5.4. Thiol-yne Kinetic Study for Phenyl Propiolate with DT

Following the general procedure stated in section 9.9.5. NEt₃ (0.1 eq) was added to a solution of DT (24.6 mg, 1.2 mmol) in CDCl₃ (0.5 mL). Phenyl propiolate (14.6 mg, 1 mmol) in CDCl₃ (0.5 mL) was added to the DT/NEt₃ solution, vortexed and an aliquot was transferred to an NMR spectroscopy tube. ¹H NMR spectra was recorded at 2 min intervals for 45 min and repeated in triplicate. ¹H NMR spectroscopy taken after 43 min *in situ* (58% conversion): ¹H NMR (CDCl₃, 400 MHz): δ 7.94(d, 2H, ³J_{HH} = 12 Hz, ArCH), 7.13-7.45 (m, 4H, ArCH and OCOCH=CHSCH₂), 6.08 (d, 1H, ³J_{HH} = 8 Hz, OCOCH=CHSCH₂ *cis*), 5.95 (d, 1H, ³J_{HH} = 16 Hz, OCOCH=CHSCH₂ *trans*), 2.88 (t, 2H,

$^3J_{\text{HH}} = 9$ Hz, $\text{CHSCH}_2\text{CH}_2$), 1.29-1.78 (m, 20Hz, $\text{CH}_2\text{CH}_2\text{CH}_2$), 0.91 (t, 3H, $^3J_{\text{HH}} = 8$ Hz, CH_3CH_2) ppm. ^1H NMR spectroscopy indicated *ca.* 94% *cis* isomer selectivity.

9.9.5.5. Thiol-yne Kinetic Study for Ethyl Propiolamide with DT

Following the general procedure stated in section 9.9.5. NEt_3 (1 eq) was added to a solution of DT (24.6 mg, 1.2 mmol) in CDCl_3 (0.5 mL). Ethyl propiolamide (9.7 mg, 1 mmol) in CDCl_3 (0.5 mL) was added to the DT/ NEt_3 solution, vortexed and an aliquot was transferred to an NMR spectroscopy tube. ^1H NMR spectra was recorded at 1 h intervals for 14 h and repeated in triplicate. ^1H NMR spectroscopy taken after 14 h *in situ* (52% conversion): ^1H NMR (CDCl_3 , 400 MHz): δ 7.54 (d, 1H, $^3J_{\text{HH}} = 16$ Hz, $\text{NHCOCH}=\text{CHSCH}_2$ *trans*), 6.79 (d, 1H, $^3J_{\text{HH}} = 8$ Hz, $\text{NHCOCH}=\text{CHSCH}_2$ *cis*), 5.72 (d, 1H, $^3J_{\text{HH}} = 8$ Hz $\text{NHCOCH}=\text{CHSCH}_2$ *cis*), 5.69 (d, 1H, $^3J_{\text{HH}} = 16$ Hz, $\text{NHCOCH}=\text{CHSCH}_2$ *trans*), 3.33 (q, 2H, $^3J_{\text{HH}} = 8$ Hz, $\text{CH}_3\text{CH}_2\text{NHCO}$), 2.74 (t, 2H, $^3J_{\text{HH}} = 9$ Hz, $\text{CHSCH}_2\text{CH}_2$), 1.24-1.66 (m, 20H, $\text{CH}_2\text{CH}_2\text{CH}_2$), 0.84 (t, 3H, $^3J_{\text{HH}} = 8$ Hz, CH_3CH_2) ppm. ^1H NMR spectroscopy indicated *ca.* 50% *cis* isomer selectivity.

9.9.5.6. Thiol-yne Kinetic Study for Ethyl Butynoate with DT

Following the general procedure stated in section 9.9.5. NEt_3 (1 eq) was added to a solution of DT (246 mg, 1.2 mmol) in CDCl_3 (0.25 mL). Ethyl butynoate (115 mg, 1 mmol) in CDCl_3 (0.25 mL) was added to the DT/ NEt_3 solution, vortexed and transferred to an NMR spectroscopy tube. ^1H NMR spectra were recorded at 1 h intervals for 14 h and repeated in triplicate. ^1H NMR spectroscopy taken after 14 h *in situ* (21% conversion): ^1H NMR (CDCl_3 , 400 MHz): δ 5.47 (s, 1H, $\text{C}=\text{CHCO}$ *E* isomer), 5.20 (s, 1H, $\text{C}=\text{CHCO}$ *Z* isomer), 3.88 (q, 2H, $^3J_{\text{HH}} = 8$ Hz, $\text{CH}_3\text{CH}_2\text{OCO}$), 2.56 (t, 2H, $^3J_{\text{HH}} = 8$ Hz,

CHSCH₂CH₂), 1.93 (s, 3H, CH₃C=CH *E* isomer), 1.69 (s, 3H, CH₃C=CH *Z* isomer), 1.00-1.40 (m, 20H, CH₂CH₂CH₂), 0.61 (t, 3H, ³J_{HH} = 8 Hz, CH₃CH₂) ppm. ¹H NMR spectroscopy indicated *ca.* 32% *cis* isomer selectivity.

9.9.5.7. Thiol-yne Kinetic Study for 1-Phenylbut-2-yn-1-one with DT

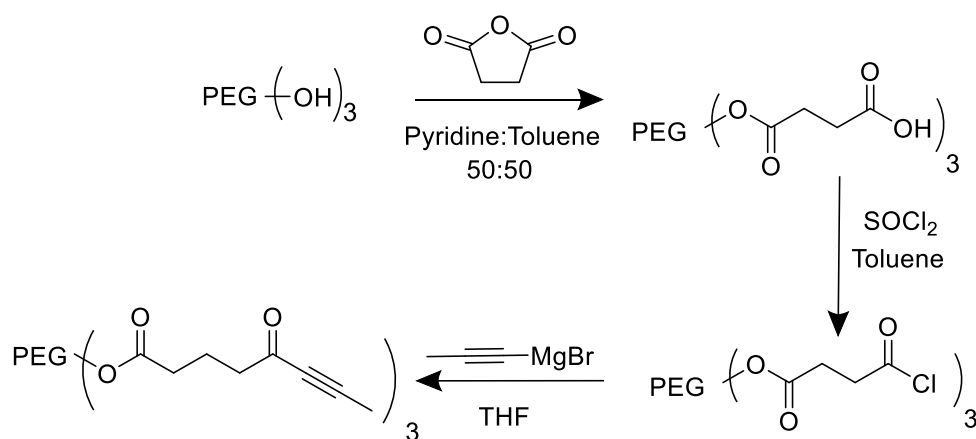
Following the general procedure stated in section 9.9.5. NEt₃ (10 eq) was added to a solution of DT (24.6 mg, 1.2 mmol) in CDCl₃ (0.5 mL). 1-Phenylbut-2-yn-1-one (14.4 mg, 1 mmol) in CDCl₃ (0.5 mL) was added to the DT/NEt₃ solution, vortexed and an aliquot was transferred to an NMR spectroscopy tube. ¹H NMR spectra was recorded at 4 min intervals for 1 h and repeated in triplicate. ¹H NMR spectroscopy taken after 1 h *in situ* (22% conversion): ¹H NMR (CDCl₃, 400 MHz): δ 8.13(d, 2H, ³J_{HH} = 12 Hz, ArCH), 7.92 (m, 1H, ArCH), 7.44-7.58 (m, 2H, ArCH), 6.99 (s, 1H, COCH=CCH₃S *E* isomer), 6.62 (s, 1H, COCH=CCH₃S *Z* isomer), 2.88 (t, 2H, ³J_{HH} = 9 Hz, CHSCH₂CH₂), 2.47 (s, 3H, COCH=CCH₃S *Z* isomer), 2.37 (s, 3H, COCH=CCH₃S *E* isomer), 1.24-1.61 (m, 20H, CH₂CH₂CH₂), 0.92 (t, 3H, ³J_{HH} = 8 Hz, CH₃CH₂) ppm. ¹H NMR spectroscopy indicated *ca.* 32% *cis* isomer selectivity.

9.9.5.8. Thiol-yne Kinetic Study for Non-2-yn-4-one with DT

Following the general procedure stated in section 9.9.5. NEt₃ (8.2 eq) was added to a solution of DT (24.6 mg, 1.2 mmol) in CDCl₃ (0.5 mL). Non-2-yn-4-one (13.8 mg, 1 mmol) in CDCl₃ (0.5 mL) was added to the DT/NEt₃ solution, vortexed and an aliquot was transferred to an NMR spectroscopy tube. ¹H NMR spectra was recorded at 1 h intervals for 16 h and repeated in triplicate. ¹H NMR spectroscopy taken after 16 h *in situ* (24% conversion): ¹H NMR (CDCl₃, 400 MHz): δ 6.16 (s, 1H, COCH=CCH₃S *E* isomer),

5.84 (s, 1H, COCH=CCH₃S *Z* isomer), 2.73-2.77 (m, 2H, CHSCH₂CH₂), 2.58-2.64 (m, 6H, COCH₂CH₂CH₂CH₃), 2.16 (s, 3H, COCH=CCH₃S *E* isomer), 1.19-1.62 (m, 20H, CH₂CH₂CH₂), 0.82 (t, 3H, ³J_{HH} = 8 Hz, CH₃CH₂) ppm. ¹H NMR spectroscopy indicated *ca.* 45% *cis* isomer selectivity.

9.9.6. Synthesis of Methyl-Terminated Alkyne PEG Ketone Precursor via Succinic Anhydride Grignard Reaction



9.9.6.1. Functionalisation of 3-arm PEG_{1k}(OH)₃ with Succinic Anhydride¹⁷

3-arm PEG_{1k}(COOH)₃ was synthesised using a modified literature procedure.¹⁷ Glycerol ethoxylate (3-arm PEG_{1k}OH, molar mass 1 kg mol⁻¹, 10 g, 10 mmol) was dissolved in toluene (150 mL). A stirred solution of succinic anhydride (6 eq) in pyridine (50 mL) was added via cannula transfer. The solution was heated to reflux and maintained for 7 h. The solution was then concentrated and dissolved in CHCl₃, centrifuged and filtered, this was repeated three times followed by precipitation into diethyl ether (Et₂O). The product was then dissolved in CH₂Cl₂ and charcoal (*ca.* 0.1 g) was added. The solution was stirred for 1 hr then filtered through Celite[®] 545 and MgSO₄ then concentrated. The product was then purified by column chromatography to yield a yellow oil (8.5 g, 65%).

^1H NMR ((CDCl_3), 298 K, 300 MHz): δ 5.64 (s, 1H, OH), 4.20 (t, 2H, $^3J_{\text{HH}} = 9$ Hz, $\text{CH}_2\text{CH}_2\text{OCOCH}_2$), 3.51-3.68 (m, 30H, $\text{CH}_2\text{CH}_2\text{O}$), 2.59 (s, 2H, $\text{CH}_2\text{CH}_2\text{COOH}$) ppm. ^{13}C NMR ((CDCl_3 , 298 K, 300 MHz): δ 174.88 (COOH), 172.35 (OCOCH₂), 70.43 ($\text{CH}_2\text{CH}_2\text{O}$), 69.00 (OCH₂CH₂OCO), 63.81 (OCH₂CH₂OCO), 29.25 ($\text{CH}_2\text{CH}_2\text{COOH}$), 29.01 ($\text{CH}_2\text{CH}_2\text{COOH}$) ppm. FT-IR max/cm⁻¹ 1732 (CO). SEC (CHCl_3) $M_w = 1.1$ kg mol⁻¹ ($D_M = 1.03$).

9.9.6.2. Functionalisation of 3-arm PEG_{1k}(COOH)₃ with Thionyl Chloride

3-arm PEG_{1k}(COOH)₃ (8 g, 1 eq) was dissolved in toluene (20 mL). Thionyl chloride (4 mL, 6 eq) was added *via* a cannular transfer. The reaction was then heated to 40 °C and left overnight then degassed to remove residual SOCl₂ and toluene. The crude product was then used *in situ* to synthesise 3-arm PEG_{1k}(COC≡CCH₃)₃.

^1H NMR ((CDCl_3), 298 K, 300 MHz): δ 4.23 (t, 2H, $^3J_{\text{HH}} = 9$ Hz, $\text{CH}_2\text{CH}_2\text{OCOCH}_2$), 3.52-3.72 (m, 30H, $\text{CH}_2\text{CH}_2\text{O}$), 3.20(t, 2H, $^3J_{\text{HH}} = 9$ Hz, $\text{CH}_2\text{CH}_2\text{COCl}$), 2.69 (t, 2H, $^3J_{\text{HH}} = 9$ Hz, $\text{CH}_2\text{CH}_2\text{COCl}$) ppm. FT-IR max/cm⁻¹ 1789 (C=O), 1732 (C=OCl).

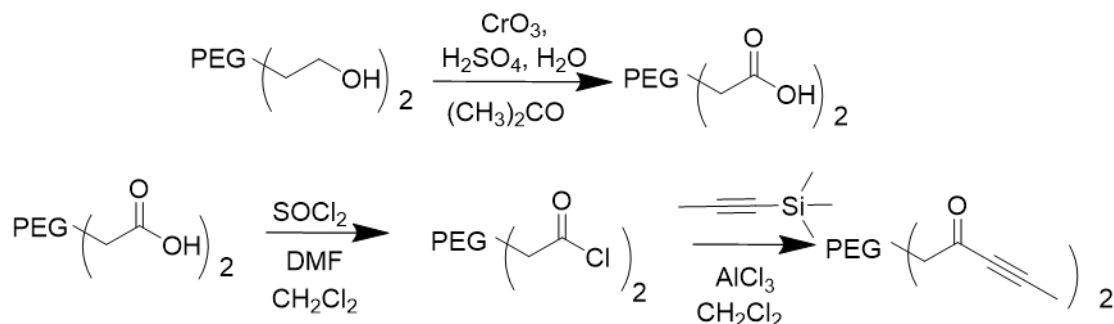
9.9.6.3. Functionalisation of 3-arm PEG_{1k}(COC≡CCH₃)₃

3-arm PEG_{1k}(COCl)₃ was reacted *in situ* following the same procedure used for the synthesis of non-2-yn-4-one (section 9.9.5). To a slurry of ZnCl₂ (6.4 g 8 eq) in THF (50 mL) was added 1-propynylmagnesium bromide (94 mL, 0.5 M in THF, 8 eq) at 0 °C with stirring. After stirring for 15 min 3-arm PEG_{1k}(COCl)₃ (8 g, 1 eq) was added. The reaction was warmed to room temperature and stirred for 2 h. The reaction was then cooled to -10 °C and sat. aq. NH₄Cl was added and the solution was filtered. The layers were separated and the aq. layer was extracted into Et₂O (3 × 100 mL). This layer was then dried and

concentrated to yield a small amount of product. The organic phase (THF) was concentrated and purified by column chromatography to yield an increased amount of product. The product was dissolved in CH_2Cl_2 and charcoal (*ca.* 0.1 g) was added to the solution. The reaction was then stirred overnight then filtered through Celite[®] 545 and concentrated. The product was then dissolved in H_2O then dialysed for 3 days in H_2O to yield the product as yellow oil (4.3 g 50%).

^1H NMR ((CDCl_3) , 298 K, 300 MHz): δ 4.21 (t, 2H, $^3J_{\text{HH}} = 9$ Hz, $\text{CH}_2\text{CH}_2\text{OCOCH}_2$), 3.37-3.74 (m, 30H, $\text{OCH}_2\text{CH}_2\text{O}$), 2.84 (t, 2H, $^3J_{\text{HH}} = 9$ Hz, $\text{CH}_2\text{CH}_2\text{CO}$), 2.63 (t, 2H, $^3J_{\text{HH}} = 9$ Hz, $\text{CH}_2\text{CH}_2\text{CO}$), 2.00 (s, 3H, $\text{C}\equiv\text{CCH}_3$) ppm. SEC (CHCl_3) $M_w = 2.2$ kg mol^{-1} ($D_M = 1.20$).

9.9.7. Synthesis of Methyl-Terminated Alkyne PEG ketone Precursor through a Friedel-Crafts Acylation



9.9.7.1. Oxidation of PEG_{2k}(OH)₂ using Jones' Reagent

PEG_{2k}(OH)₂ (molar mass 2 kg mol^{-1} , 5 g, 2.5 mmol) was dissolved in acetone ($(\text{CH}_3)_2\text{CO}$) (60 mL) and Jones' reagent was added dropwise, with the temperature kept below 35 °C, until a green colour change was maintained (*ca.* 15 min). Jones' reagent was made as followed; H_2O (6 mL) was added to CrO_3 (2 g) at 0 °C followed by H_2SO_4 (2 mL)

dropwise. The reaction was left to stir at 0 °C for 30 min then warmed to room temperature and left overnight. 2-Propanol (4 mL) was added to the reaction and was stirred for 1 h, then filtered and concentrated. The product was extracted into CHCl_3 and dried (MgSO_4) to yield a waxy white solid (4.8 g, 93%).

^1H NMR ($(\text{CD}_3)_2\text{SO}$), 298 K, 300 MHz): δ 12.52 (s, OH), 4.01 (t, 4H, CH_2COOH), 3.64 (m, 90H, $\text{OCH}_2\text{CH}_2\text{O}$) ppm. ^{13}C NMR ($(\text{CD}_3)_2\text{SO}$), 298 K, 300 MHz): δ 171.66 (C=O), 69.79 ($\text{OCH}_2\text{CH}_2\text{O}$), 67.58 (CH_2COOH) ppm. SEC ($\text{H}_2\text{O}:\text{MeOH}$) $M_n = 2.7 \text{ kg mol}^{-1}$ ($D_M = 1.13$). FT-IR max/ cm^{-1} 1750 (C=O).

9.9.7.2. Functionalisation of $\text{PEG}_{2k}(\text{COOH})_2$ with Thionyl Chloride

$\text{PEG}_{2k}(\text{COOH})_2$ (500 mg, 0.25 mmol) was dissolved in CH_2Cl_2 (anhydrous, 10 mL) with DMF (2 drops). Thionyl chloride (distilled, 1 mL) was added *via* a cannular transfer. The reaction was then refluxed and monitored *via* FT-IR for full conversion to acyl chloride. The reaction was then concentrated and the crude product was used *in situ* in the synthesis of $\text{PEG}_{2k}(\text{COC}\equiv\text{CCH}_3)_2$.

^1H NMR ($(\text{CD}_3)_2\text{SO}$), 298 K, 300 MHz): δ 4.43 (t, 4H, CH_2COCl), 3.50-3.69 (m, 90H, $\text{OCH}_2\text{CH}_2\text{O}$), ppm. FT-IR max cm^{-1} 1803 (C=OCl).

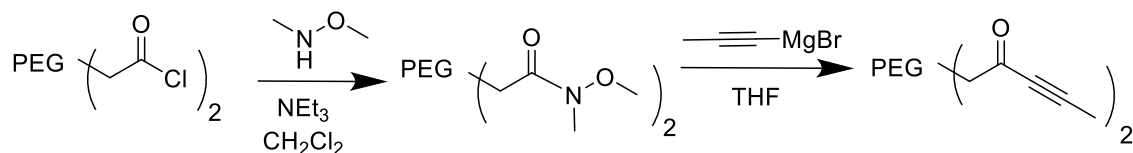
9.9.7.3. Functionalisation of $\text{PEG}_{2k}(\text{COCl})_2$ via Friedel-Crafts Acylation

$\text{PEG}_{2k}(\text{COCl})_2$ was reacted *in situ*, CH_2Cl_2 (anhydrous, 10 mL) was added to the reaction mixture and the reaction was cooled to 0 °C. 1-(Trimethylsilyl) propyne (1 mL, 0.7 mmol) was added and stirred for 10 min before AlCl_3 (0.9 g, 0.7 mmol) was added and the reaction was stirred at room temperature overnight. 1 M HCl (2 mL) was slowly added to reaction

followed by H₂O (5 mL) and the reaction was stirred before extracted into CH₂Cl₂ (3 × 5 mL). The organic layer was dried (MgSO₄) and concentrated to yield a brown oil (200 mg, 38%).

¹H NMR ((CDCl₃), 298 K, 300 MHz): δ 4.10-4.18 (m, 6H, CH₂CH₂COC≡CCH₃), 3.50-3.74 (m, 90H, OCH₂CH₂O), 1.81 (s, 3H, C≡CCH₃) ppm. ¹³C NMR ((CDCl₃), 298 K, 300 MHz): δ 171.76 (C=O acid), 162.40 (C=O ketone) ppm. FT-IR max/cm⁻¹ 2217 (C≡C), 1688 (C=O ketone), 1728 (C=O acid).

9.9.8. Synthesis of Methyl-Terminated Alkyne PEG Ketone Precursor through a Weinreb Amide Synthetic Route



9.9.8.1. Synthesis of 2-arm PEG (2 kg mol⁻¹) Weinreb Amide

PEG_{2k}(COCl)₂ was synthesised as described in section 9.9.7.1 and 9.9.7.2 in a Schlenk flask under N₂ and reacted *in situ* to form the PEG Weinreb amide intermediate. PEG_{2k}(COCl)₂ (15 g, 7.5 mmol) was dissolved in CH₂Cl₂ (anhydrous, 50 mL) and *N,O*-dimethylhydroxylamine hydrochloride (dried over P₂O₅, 2 g, 45 mmol) was added. The reaction was cooled to 0 °C and NEt₃ (dried over CaH, 3 g, 30 mmol) was added dropwise. The reaction was stirred at room temperature overnight under N₂ then aq. NaHCO₃ sat. was added. The organic layer was washed with NaHCO₃ (3 × 10 mL) and brine (3 × 10 mL) then dried (MgSO₄) and concentrated. The residual oil was precipitated into ice cold Et₂O and dried to yield a waxy white oil (14.3 g, 89%).

^1H NMR ($(\text{CD}_3)_2\text{SO}$), 298 K, 300 MHz): δ 4.20-4.30 (m, 2H, $\text{CH}_2\text{CONCH}_3\text{OCH}_3$), 3.68 (s, 3H, $\text{CH}_2\text{CONCH}_3\text{OCH}_3$), 3.41-3.62 (m, 90H, $\text{OCH}_2\text{CH}_2\text{O}$), 3.07 (s, 3H, $\text{CH}_2\text{CONCH}_3\text{OCH}_3$) ppm. ^{13}C NMR ($(\text{CD}_3)_2\text{SO}$), 298 K, 300 MHz): δ 170.17 (C=O), 69.79 ($\text{OCH}_2\text{CH}_2\text{O}$), 67.63 ($\text{CH}_2\text{CONCH}_3\text{OCH}_3$), 61.13 ($\text{CH}_2\text{CONCH}_3\text{OCH}_3$), 60.21 ($\text{CH}_2\text{CONCH}_3\text{OCH}_3$) ppm. SEC ($\text{H}_2\text{O}:\text{MeOH}$) $M_n = 1.2 \text{ kg mol}^{-1}$ ($D_M = 1.60$). FT-IR max/ cm^{-1} 1682 (NHC=O).

9.9.8.2. *Synthesis of Methyl-Terminated Alkyne 2-arm PEG ketone (2 kg mol^{-1}) from a Weinreb Amide*

2-arm PEG Weinreb amide (2 kg mol^{-1}), (14 g, 0.65 mmol) synthesised in section 9.9.8.1, was dissolved in THF (anhydrous, 200 mL) in a Schlenk flask under N_2 . The reaction was cooled to $0 \text{ }^\circ\text{C}$ and propynyl magnesium bromide (90 mL, 0.5 M, 45 mmol) was added *via* cannular transfer. The reaction was heated to $40 \text{ }^\circ\text{C}$ and left stirring overnight. The reaction was then cooled to $0 \text{ }^\circ\text{C}$ and ice cold 1 M HCl (100 mL) was slowly added to the reaction. The reaction was then extracted into CH_2Cl_2 ($3 \times 100 \text{ mL}$) dried (MgSO_4) and concentrated. The resultant oil was precipitated into ice cold Et_2O twice and the product was collected as a pale yellow powder (9 g, 66%).

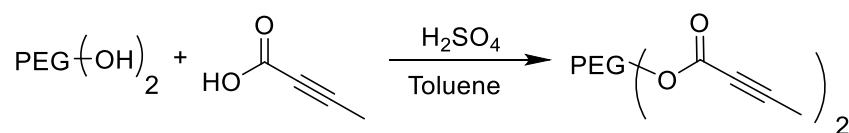
^1H NMR (CDCl_3), 298 K, 300 MHz): δ 4.20-4.25 (m, 2H, $\text{CH}_2\text{COC}\equiv\text{CCH}_3$), 3.51-3.67 (m, 90H, $\text{OCH}_2\text{CH}_2\text{O}$), 2.01 (s, 3H, $\text{C}\equiv\text{CCH}_3$) ppm. ^{13}C NMR ($(\text{CD}_3)_2\text{SO}$), 298 K, 500 MHz): δ 185.24 (C=O), 93.45 ($\text{CH}_2\text{COC}\equiv\text{CCH}_3$), 77.97 ($\text{CH}_2\text{COC}\equiv\text{CCH}_3$), 72.35 ($\text{CH}_2\text{COC}\equiv\text{CCH}_3$), 69.79 ($\text{OCH}_2\text{CH}_2\text{O}$), 3.52 ($\text{CH}_2\text{COC}\equiv\text{CCH}_3$) ppm. SEC ($\text{H}_2\text{O}:\text{MeOH}$) $M_n = 1.4 \text{ kg mol}^{-1}$ ($D_M = 1.90$). FT-IR max/ cm^{-1} 2219 (C \equiv C) 1684 (C=O ketone).

9.9.9. *Synthesis and Characterisation of Thiol-yne PEG Hydrogels Fabricated from a Methyl Terminate Alkyne PEG Ketone.*

Thiol-yne hydrogels were synthesised with the methyl-terminated alkyne PEG ketone precursor (2 kg mol^{-1}) with a 3-arm PEG thiol precursor (1 kg mol^{-1}) in PBS solution at pH 7.4 following the general procedure stated in section 9.4.3. The alkyne:thiol ratio remained constant at 1:1 ratio throughout testing and the polymer content varied between 10-20 wt%. No gelation occurred and the 20 wt% solution was analysed by ^1H NMR and FT-IR spectroscopy.

^1H NMR (CDCl_3), 298 K, 300 MHz): δ 6.52 (s, 1H, $\text{COCH}=\text{CCH}_3\text{S}$, *E* isomer), 6.15 (s, 1H, $\text{COCH}=\text{CCH}_3\text{S}$, *Z* isomer), 4.24 (s, 2H, $\text{CH}_2\text{COC}=\text{CCH}_3\text{S}$), 4.06 (s, 2H, $\text{CH}_2\text{OCOCH}_2\text{CH}_2\text{S}$), 3.51-3.67 (m, 120H, $\text{OCH}_2\text{CH}_2\text{O}$), 2.63-2.69 (m, 4H, $\text{SCH}_2\text{CH}_2\text{CO}$), 2.40 (s, 3H, $\text{CH}_2\text{COC}=\text{CCH}_3\text{S}$, *Z* isomer), 2.30 (s, 3H, $\text{CH}_2\text{COC}=\text{CCH}_3\text{S}$, *E* isomer), 2.03 (s, 3H, $\text{C}\equiv\text{CCH}_3$) ppm. FT-IR max/cm^{-1} 1733 (C=O ester), 1653 (C=O ketone), 1538 (C=C).

9.9.10. *Synthesis of 2-arm PEG ester methyl terminate alkyne*



In a similar procedure stated in section 9.3.1, 2-arm PEG_{1k}OH (molar mass 1 kg mol^{-1} , 5 g, 5 mol) was esterified with butynoic acid (1.7 g, 20 mmol) to yield a white solid. (Yield 4.8 g, 84%). ^1H NMR (CDCl_3), 300 MHz): δ 4.26-4.29 (t, 2H, $^3J_{\text{HH}} = 9 \text{ Hz}$, $\text{CH}_2\text{CH}_2\text{OCOCH}_2$), 3.52-3.71 (m, 45H, $\text{OCH}_2\text{CH}_2\text{O}$), 1.96 (s, 3H, $\text{COC}\equiv\text{CCH}_3$) ppm. ^{13}C NMR (CDCl_3 , 298 K, 300 MHz): δ 162.44 (CCOC), 70.64 ($\text{OCH}_2\text{CH}_2\text{O}$), 68.79

($C\equiv CCH_3$), 64.82 ($C\equiv CCH_3$), 3.89 ($C\equiv CCH_3$) ppm. 1H NMR spectroscopy indicated *ca.* >99% conversion of the hydroxyl group to butyniolate group. SEC (DMF): $M_n = 2.7$ kg mol $^{-1}$ ($D_M = 1.04$).

9.9.11. Synthesis and Characterisation of Thiol-yne PEG Hydrogels Fabricated using a Methyl-Terminate Alkyne PEG Ester

Thiol-yne hydrogels were synthesised with the methyl-terminated alkyne PEG ketone precursor (2 kg mol $^{-1}$) with a 3-arm PEG thiol precursor (1 kg mol $^{-1}$) or 4-arm PEG thiol precursor (2 kg mol $^{-1}$) following the general procedure stated in section 9.4.3. To optimise the gelation process the polymer content was increased to 20 wt% (1:1 alkyne:thiol ratio maintained). To decrease the gelation time the precursors were also dissolved in Trizma® buffer solution (pH 8) to increase the pH of the solution to favour the nucleophilic thiol-yne reaction. Once formed the hydrogels were characterised *via* compression testing as previously described in section 9.2.4.1.3.

9.10. References

1. S. P. Zustiak and J. B. Leach, *Biomacromolecules*, 2010, **11**, 1348-1357.
2. T. Canal and N. A. Peppas, *J. Biomed. Mater. Res.*, 1989, **23**, 1183-1193.
3. S. Lu and K. S. Anseth, *Macromolecules*, 2000, **33**, 2509-2515.
4. J. Baier Leach, K. A. Bivens, C. W. Patrick Jr and C. E. Schmidt, *Biotechnol. Bioeng.*, 2003, **82**, 578-589.
5. E. W. Merrill, K. A. Dennison and C. Sung, *Biomaterials*, 1993, **14**, 1117-1126.
6. O. Chaudhuri, S. T. Koshy, C. Branco da Cunha, J.-W. Shin, C. S. Verbeke, K. H. Allison and D. J. Mooney, *Nat. Mater.*, 2014, **13**, 970.
7. S. T. Gould, N. J. Darling and K. S. Anseth, *Acta Biomater.*, 2012, **8**, 3201-3209.
8. V. X. Truong, M. P. Ablett, S. M. Richardson, J. A. Hoyland and A. P. Dove, *J. Am. Chem. Soc.*, 2015, **137**, 1618-1622.
9. T. C. Owen, *Bioorg. Chem.*, 2008, **36**, 156-160.
10. V. X. Truong and A. P. Dove, *Angew. Chem., Int. Ed.*, 2013, **52**, 4132-4136.
11. L. A. Sawicki and A. M. Kloxin, *Biomater. Sci.*, 2014, **2**, 1612-1626.
12. L. A. Sawicki and A. M. Kloxin, *J. Visualized Exp.*, 2016, 54462.
13. P. V. Ramachandran, M. T. Rudd and M. V. R. Reddy, *Tetrahedron Lett.*, 2005, **46**, 2547-2549.
14. E. Bialecka-Florjańczyk, *Synth. Comm.*, 2000, **30**, 4417-4424.

15. W. D. Crow and N. J. Leonard, *J. Org. Chem.*, 1965, **30**, 2660-2665.
16. M. T. Herrero, I. Tellitu, E. Domínguez, S. Hernández, I. Moreno and R. SanMartín, *Tetrahedron*, 2002, **58**, 8581-8589.
17. M. Malhotra, C. Tomaro-Duchesneau and S. Prakash, *Biomaterials*, 2013, **34**, 1270-1280.